GROUNDWATER RECHARGE ESTIMATION IN ETHIOPIA

Yohannes Degu Dawana

A Thesis Submitted to the School of Earth Sciences

Presented in Partial Fulfillment of the Requirements for the Degree of Doctor of Philosophy (Hydrogeology)

Addis Ababa University

Addis Ababa, Ethiopia

December 2020

ABSTRACT

Understanding the rate of groundwater recharge is crucial to studies of water availability, wellhead protection, contaminant transport, ground-water and surface-water interactions, effects of urbanization, and aquifer vulnerability to contamination. The aim of this study was to determine the rate of groundwater recharge in the study area at long term monthly temporal and 250-meter spatial resolutions by applying the WetSpass-M model, recursive digital filter base flow separation, and chloride mass balance methods, and by developing a groundwater conceptual model before implementing the recharge estimation methods.

The multi criteria decision analysis (MCDA) combined the rainfall, soil texture, land use/land cover (LULC), lithology, lineament density, drainage density, and slope factors in the GIS environment to develop a conceptual model of groundwater recharge to the study area and evaluate the appropriateness of the recharge estimation methods selected for the estimation. The WetSpass-M model requires the land use/land cover (LULC), slope, soil texture, depth to groundwater, and climatological variables (rainfall, temperature, potential evapotranspiration, and wind speed) for the estimation of physically distributed groundwater recharge in the study area. The base flow separation, on the other hand, used river flow data on 18 river gauge stations located at the outlets of the major rivers of the study area. The chloride mass balance method requires precipitation amount, chloride concentration in rainfall, chloride concentration in groundwater as input datasets.

The MCDA result showed that both the spatial and temporal characteristics of the groundwater recharge potential in the study area was highly controlled by the rainfall characteristics in the study area. Similarly, the highest estimations of WetSpass-M and base flow separation methods were observed in months and areas that receive the highest rainfall.

Accordingly, the long term average estimation to the rainy months in the study area (June to September) by WetSpass-M model was found to be 10.5 mm, 18 mm, 15.7 mm and 10 mm, but by the base flow separation method, it was 3 mm, 5.5 mm, 10.9 mm, and 14.2 mm. Some particular areas such as Goro in the western part of the study area, due to their higher and extended rainfall characteristics, receive higher amount of groundwater recharge almost throughout the year. In Goro, groundwater recharge reached up to 400 mm/yr which was around 20% of the average rainfall in that particular location. The long term annual average groundwater recharge in the study area from WetSpass-M, Base flow separation, and chloride

mass balance were found to be 73 mm (81 BCM), 63 mm (40 BCM), 65 mm (72 BCM) respectively.

The outputs of this study, due to its finer spatial and temporal resolution, can be very useful to better understand the characteristics of rate of both the spatial and temporal groundwater recharge in the country as well as to studies related to groundwater management, contamination susceptibility, landslide, and subsidence.

ACKNOWLEDGEMENT

First of all, I would like to thank and praise the almighty GOD for HE HIMSELF is the KNOWLEDGE and WISDOM.

I would like to thank the Addis Ababa Science and Technology University for granting me this PhD scholarship.

I would like to express my sincere gratitude to my advisor Dr. Seifu Kebede for his continuous guidance, comment, and instruction all the way from providing the title of my PhD research up to the final stage of the research. Besides my advisor, I would like to thank the rest of my thesis committee: Prof. Tenalem Ayenew, Dr. Surya Baghavane, and Dr. Dessie Nedaw, Dr. Tilahun Azagegn for their insightful comments and encouragement, but also for the hard question which incented me to widen my research from various perspectives.

I would like to express my heart felt gratitude to Dr. Tibebu Kasawmar, Dr. Behailu Berhanu, Dr. Tadesse, Dr. Mersha Alemu, Mr. Abebayehu, Mrs. Yehualashet Tadesse, Mr. Assefa Eyassu for their useful comments, discussion, encouragement, and help.

I would like to acknowledge the Geological Survey of Ethiopia, the Ministry of Water, Irrigation, and Electricity and the National Meteorological Agency for providing me all relevant data for my research as per my request. I would specifically like to acknowledge Mrs. Tenaye of the Geological Survey of Ethiopia for her invaluable cooperation.

Last but not least, I would like to express my deepest gratitude to my parents, brothers, sisters, my wife (Mrs. Gadisse Retta), children (Fnotebrhan, Kalehiywot, Brhanemeskel, and Hana), ‘kidanwiyan’ brothers and ‘kidanawiyat’ sisters, and friends Dr. Ibrahim Mama and Dr. Ermias Teferi for their help, support, and love.

DEDICATED TO

[ኪዳናዊ] KIDANAWI ERMIAS KEBEDE ABAYNESH,

NIBURE-ID,

the true Ethiopian patriot and a testimony to the true Ethiopianhood

CONTENTS

FIGURES

TABLES

ACRONYMS

AET	Actual evapotranspiration
AfSIS	Africa Soil Information Service
ANS	Arabian-Nubian Shield
BFI	Base flow index
BGS	British Geological Survey
DEM	Digital Elevation Model
EMA	Ethiopian Mapping Agency
FAO	World Food Organization
GIS	Geographic Information System
GRACE	Gravity Recovery and Climate Experiment
GSE	Geological Survey of Ethiopia
GW	Groundwater
HWSD	Harmonized World Soil Database
I	Interception
ITCZ	Inter Tropical Convergence Zone
MCM	Million Cubic Meter
MER	Main Ethiopian Rift
mm	millimeter
mm/yr	millimeter per year
LAI	Leaf Area Index
LULC	Land use/land cover
MCDA	Multi Criteria Decision Analysis
MoWIE	Ministry of Water, Irrigation and Energy
MoWR	Ministry of Water Resources
NASA	National Aeronautics and Space Administration
NASA LP DAAC	NASA Land Processes Distributed Active Archive Center
NASA USDA SMAP	NASA USDA Soil Moisture Active Passive
NNW	North-North-East

NNE-SSW	North-North-East South-South-West
NMA	National Meteorological Agency
N-S	North-South
P	Precipitation
PET	Potential Evapotranspiration
q	Specific discharge
R	Groundwater recharge
RSCZ	Red Sea Convergence Zone
SSE	South-South-East
STJ	Subtropical Jet
SJ	Somali Jet
SRTM	Shuttle Radar Topography Mission
TEJ	Tropical Easterly Jet
RAP	River analysis package
RCD	Regional Consecutive Dryness level
USDA	United States of Department of Agriculture
USGS	United States Geological Survey
USGS EROS	USGS Earth Resources Observation Systems
WetSpass-M	Water and Energy Transfer between Soil, Plants, and Atmosphere under quasi Steady State (Monthly)
WLRC	Water and Land Resource Center

CHAPTER ONE

1. BACKGROUND

1.1. Introduction

Understanding the rate of groundwater recharge is crucial to studies of water availability, wellhead protection, contaminant transport, ground-water and surface-water interactions, effects of urbanization, and aquifer vulnerability to contamination (Scanlon *et al*., 2002). Groundwater provides more than 90% of the water supply for domestic and industrial uses in Ethiopia (Kebede, Hailu, Crane, Ó Dochartaigh and Bellwood-Howard, 2018). Because groundwater is the safest, the most easily accessible, and the most resistant water resource to climatic variations, it is the major source of fresh water globally (Simmers, 1990; Clarke *et al*., 1996). The dependency on the resource is even increasing due to population growth and the advancement of aridity (Simmers, 1990). Globally, it is estimated that 1.3 billion people use groundwater for different purposes (Clarke *et al*., 1996).

Even though groundwater accounts for 97% of the whole fresh water globally (Nace, 1967; Shiklomanov and Rodda, 2003), if it is extracted at a higher rate than its replenishing rate, groundwater levels can be declined, the amount of water in streams and lakes can be reduced, landslides and subsidence can be triggered (Morris *et al*., 2003), and ultimately, the ecosystems that depend on it can permanently be damaged. Therefore, groundwater utilization requires careful and efficient ways of groundwater management practices.

Nevertheless, groundwater recharge is one of the hydrologic components that are inaccessible for direct measurement so that it is among the least understood processes in the hydrologic cycle. On top of that, due to the spatial and temporal variabilities of the factors that control groundwater recharge in an area (such as lithology, lineaments, slope, land use/land cover [LULC], soil and rainfall), its magnitude varies in space and time. Therefore, a lot of groundwater recharge

estimation methods, that differ each other in several aspects, have been developed (Lerner *et al*., 1990; Simmers, 1997; Scanlon *et al*., 2002b; Healy and Scanlon, 2010).

Furthermore, estimated values may incorporate uncertainty due to the inherent characteristic of estimation methods, and there is no a standard way to quantify the amount of error associated in an estimation. Healy and Scanlon (2010) identified several sources of uncertainties in groundwater recharge estimation methods: Incorrect groundwater recharge conceptual model, improper application of groundwater recharge estimation methods and measurement errors. It is from the incorrect conceptual model that the most serious error associate to recharge estimations. An incorrect groundwater recharge conceptual model to an area can lead to a selection of inappropriate groundwater recharge estimation techniques and result meaningless estimates. Improper application of an estimation method can result from lack of understanding of the method or poor representation of the spatial and temporal variabilities of the input data. Thus, minimizing the errors arising from these sources can be considered as a reasonable approach to obtain realistic recharge estimates to an area.

In the study area, there are limited national scale studies on groundwater recharge estimation. WAPCOS (1990) implemented multiple methods to estimate the annual groundwater recharge in the study area. Chernet (1993) also estimated the annual groundwater recharge in the study area by using base flow separation method. Kebede (2013), on the other hand, compiled the annual recharge estimations in basin master plan projects and different literatures. However, in the study area, the groundwater recharge rate at distributed spatial discretization and monthly temporal step has never been studied. Additionally, a development of conceptual model of groundwater recharge has never guided groundwater recharge estimations in the study area.

Thus, this paper estimates the long-term monthly groundwater recharge by using the WetSpass-M model and digital recursive base flow separation methods and the long-term annual groundwater recharge by using chloride mass balance. Prior to the recharge estimation, a conceptual model of groundwater recharge is developed to identify the most important factors that control groundwater recharge in the study area as well as evaluate the consistency between the assumptions of the estimation methods and the conceptual model developed to the study area. The recharge estimation is performed at a spatial resolution of 250 m and temporal resolution of long term monthly average. The outputs of this study can be very useful to better understand the characteristics of the rate of

groundwater recharge in the country both spatially and temporally as well as to studies related to groundwater management, contamination susceptibility, landslide, and subsidence.

1.2. Previous studies

There are limited number of studies on groundwater recharge estimation in the study area at national scale, unlike the numerous studies at catchment levels. WAPCOS (1990) estimated that the exploitable annual groundwater recharge in the study area is 2.6 billion m^3. This figure represents 10% of the total recharge in the country. Chernet (1993) estimated the groundwater recharge of the study area by using base flow separation method, and he found that the annual average groundwater recharge in the country ranges between 0 and 400 mm. According to the global estimations of Döll and Fiedler (2008), on the other hand, the annual average groundwater recharge in the study area ranges between 0 and 250 mm. Kebede (2013) compiled all the groundwater recharge estimations in basin master plan projects and research papers; consequently, he found that the annual average groundwater recharge in the country is 39 mm. Apart from national scale estimations, there are various research papers that estimated groundwater recharge at catchment scales: By using WetSpass model (Kahsay *et al*., 2019; Tilahun and Merkel, 2009; Yenehun *et al*., 2017; Gebru and Tesfahunegn, 2019; Dereje and Nedaw, 2019; Gebreyohannes *et al*., 2013; Gebremeskel and Kebede, 2017; Meresa and Taye, 2018), by using environmental isotopes, soil-water balance and chloride mass balance (Demlie *et al*., 2007; Demlie, 2015), by using base flow separation (Abiy *et al*., 2016; Yimam et al., 2019), and by using multiple approaches (Berehanu *et al*., 2017).

1.3. Research Questions

Water consumption in the study area is increasing due to fast population, irrigation, and industrial growth (FAO, 2016). Since groundwater has higher contribution for consumption purposes in the study area, its existing and planned usage are needed to be evaluated to assess if it is being used and planned environmentally friendly, which is achieved by an efficient and successful groundwater management system. Thus, groundwater management is a huge task and holistic

approach. One of the tasks is to determine the rate of groundwater recharge in an area, which is an important step to understand groundwater systems and determine a safe yield in an area.

Accurate recharge estimations are crucial inputs for efficient groundwater management system in an area. According to the findings in several researches (Lerner et al., 1990; Simmers, 1997; Scanlon et al., 2002b; Healy and Scanlon, 2010), recharge estimations approach to real recharge rates in an area when uncertainties in estimations are minimized. Thus, this study seeks to determine the real amount of groundwater recharge in the study area by implementing methods that can minimize uncertainties in estimations. The methods implemented are as follows:

1) *Implementing multiple groundwater recharge estimation methods in the study area.* Different estimation methods, due to the difference in their conceptual frameworks, input datasets and so forth, produce different results that can be considered as different aspects of the groundwater recharge characteristics in the study area. This in turn could lead to better understanding of the rate of groundwater recharge in the study area.
2) *Developing a conceptual model of groundwater recharge to the study area*. The major source of uncertainty in an estimation arises from the inconsistency between the conceptual model of groundwater recharge and the assumptions inherent to the estimation methods applied in the area (Healy and Scanlon, 2010). Therefore, a conceptual model of groundwater recharge was developed to the study area, and a comparison was carried out between the model and the assumptions of the estimation methods to guide and evaluate the output of the groundwater recharge estimations.
3) *Setting finer spatial and temporal resolutions in the estimation methods to achieve a better representation of the study area.* Lack of a better representation of a study area is identified as one the major sources of uncertainty in recharge estimations (Healy and Scanlon, 2010). Thus, this study selected a temporal resolution of long term monthly average and a spatial resolution of 250-meters. From the monthly recharge outputs, it is possible to obtain seasonal and annual recharge rates in the study area. On the other hand, the 250-meter cell recharge values provide detailed view of the rate of groundwater recharge characteristics in the study area.

1.4. Objectives

1.4.1. Main Objective

The main objective of this study is to estimate the long term average monthly groundwater recharge in Ethiopia by using multiple groundwater recharge estimation methods: the WetSpass-M model, recursive digital filter base flow separation method, chloride mass balance method.

1.4.2. Specific objectives

- To develop a conceptual model of groundwater recharge for the study area showing the groundwater recharge potential both in the spatial and temporal domain.
- To estimate the long term monthly average groundwater recharge in the study area by using the WetSpass-M, recursive digital filtering base flow separation method, and chloride mass balance method.
- To compare the outputs of the estimation methods for the purpose of understanding groundwater recharge characteristics in the study area.

1.5. General methodology

The study implemented multiple recharge estimation methods requiring different input datasets, producing different outputs, and being organized in such a way that treating the research question logically (Figure 1.1).

The initial step of the study dealt with developing a conceptual model of groundwater recharge for the study area. The model development required the identification and integration of the input factors that control groundwater recharge in the study area for the purpose of modelling groundwater recharge in the study area: Rainfall, land use/land cover (LULC), soil texture, lithology, lineament density, slope, drainage density. Then, the conceptual model was used to select the groundwater recharge estimation methods appropriate for the study area based on the degree of consistency between the conceptual model and the assumptions inherent to the estimation methods.

In the next step of the study, the groundwater recharge of the study area was estimated by using the estimation methods selected in the previous process. The selected methods (the WetSpass-M model, recursive digital filtering base flow separation method, and chloride mass balance method) differ in their conceptual framework, data requirement, and the hydrological zones where they are applied. The WetSpass-M model, because of its conceptual framework of the water balance equation, is applied on the surface of the earth so that it estimates not only groundwater recharge in an area but also actual evapotranspiration and surface runoff. It requires land use and land cover (LULC), soil texture, slope, groundwater depth and meteorological datasets (rainfall, temperature, potential evapotranspiration and wind speed) as model inputs. The recursive digital filter base flow separation method, on the other hand, requires the river flow time series data. The chloride mass balance method requires precipitation amount, chloride concentration in precipitation, and chloride concentration in groundwater as input datasets.

Lastly, the outputs of the estimation methods were compared each other to understand the characteristics of the rate of groundwater recharge in the study area.

1.6. Significance of the research

The study area is wide and has complex topographical, geological, hydrological and meteorological setting (Billi, 2015). Therefore, there are many studies that address the different issues in the study area. Similarly, this study would have a lot of significance to the issues related to the groundwater resource in the study area. Some of the significances of the study are mentioned as follows.

In the study area, there are limited number of studies on estimating groundwater recharge at national scale, and on top of that, there is a huge gap among the estimated values. In fact, huge variation is the inherent characteristics of estimated values since there are several uncertainties involved in the estimation process. Therefore, a lot of researches that differ in their methodologies have to be conducted in the study area to determine the real amount of groundwater recharge in the study area. Accordingly, the outputs of this research are believed to have enormous contribution to determine the real amount of groundwater recharge rate in the study area.

Ethiopia is dubbed as 'the water tower of east Africa' because of its enormous water resource potential and its large international rivers (Abbay, Tekeze, Baro, Mereb, Omo, Genale and Wabishebelle) that originate at the central part of the country and flow out to neighboring countries following elevation gradient. On the other hand, the country has been affected by recurrent drought and have not met the water needs of its urban and rural population (Berhanu, Seleshi and Melesse, 2014). The reason for this paradox can be attributed to the limited understanding of the water resource of the country which includes its diurnal, seasonal, and annual characteristics as well as its dynamics to climate changes. Groundwater resource quantification in an area requires the determination of groundwater recharge. Therefore, this study could contribute a lot to the studies that aim to quantify the groundwater resource in the study area.

Currently, groundwater is the dominant source of water for all the water requirements in the study area (Kebede, Hailu, Crane, Ó Dochartaigh and Bellwood-Howard, 2018). This reality necessitates the implementation of an efficient and scientific groundwater management practices in the study area. Otherwise, groundwater systems could be disturbed, and the living things that depend on the system could eventually be damaged. Among the immediate consequences of the mismanagement of a groundwater system are the lowering of water table, reduction of water in streams and lakes, deterioration of groundwater quality, landslide, and subsidence (Morris *et al*., 2003). Although documentation on the effects of groundwater mismanagement is scarce in the study area, the drying of the Haromaya lake in 2005 can be considered as an example in this regard. Therefore, since groundwater recharge estimation is one of the requirement in efficient groundwater management practices, this study could bring a great contribution to groundwater management practices in the study area.

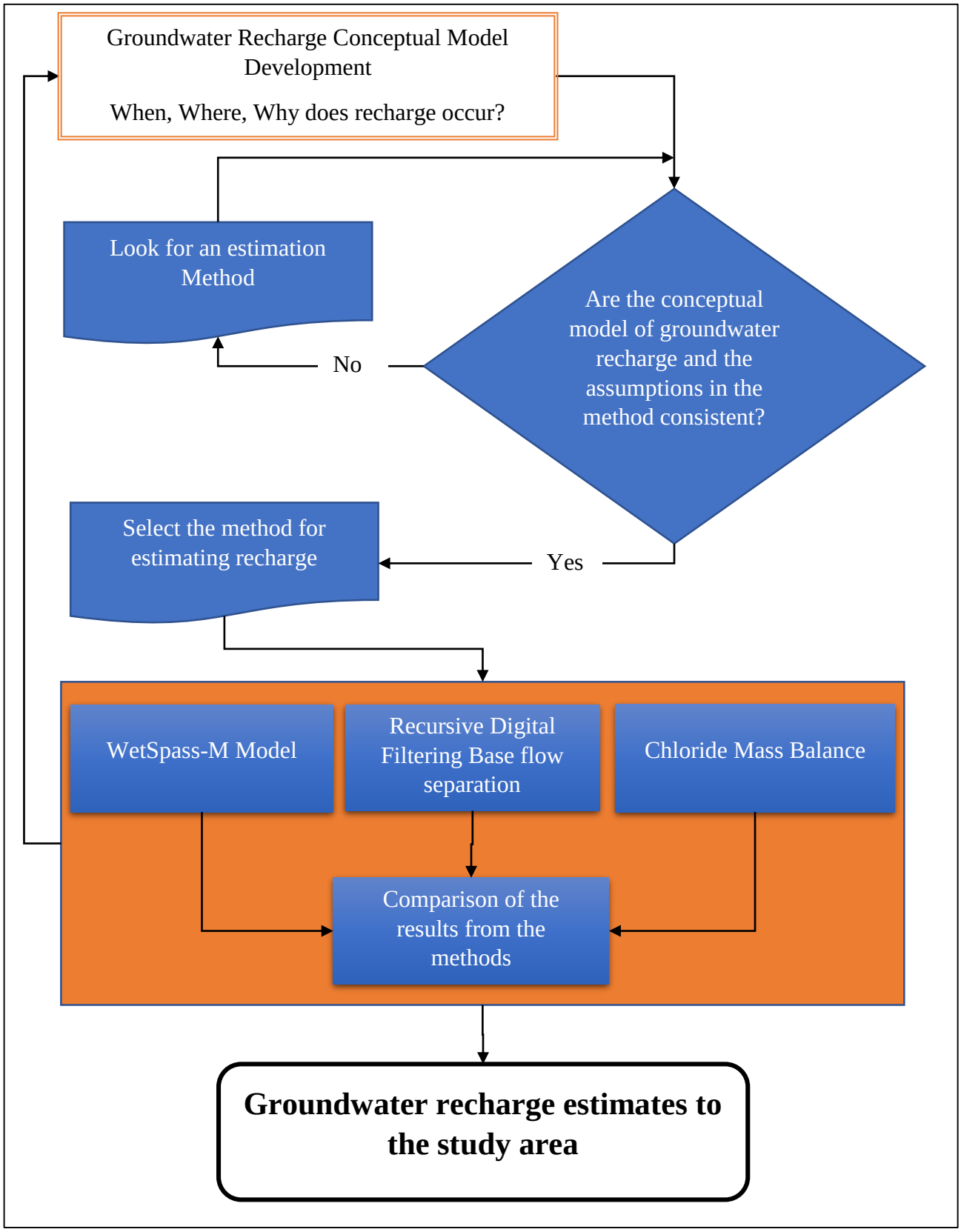

Figure 1.1: The methodology flowchart.

CHAPTER TWO

2. DESCRIPTION OF THE STUDY AREA

2.1. Location and Physiography

Ethiopia is a landlocked country in the horn of Africa, located within 3 to 15-degree latitude and 36 to 48-degree longitude, and neighbored by Eritrea to the north, Djibouti and Somalia to the east, Kenya and Somalia to the south, and Sudan and South Sudan to the west. Being 1,127,000 Km^2, it is the 10^{th} widest country in Africa. The 2007 population census counted the population size to be 73.9 million, and projected to be 94 million by 2017.

Overviewing Ethiopia's physiography shows that it is a country with a wide elevation range having the lowest elevation in Afar (-155 m.b.s.l. at Lake Asale) and the highest elevation in Semein Gonder (4620 m.a.s.l. at Ras Dejen). The topography of the country exhibits various geomorphical features: Large highlands and shield volcanoes, vast plains, and long, deep gorges, and canyons (Figure 2.1). The central part of the country is an elevated, flat-topped highland dissected by the great rift system stretched from Jordan to Mozambique through Red Sea, Ethiopia, Kenya, and Tanzania covering a total distance of around 6000 km. The part of the highland to the west of the Rift system is named western highland, and the other side is named southeastern highland which is by far smaller than the western highland (Figure 2.1). The highlands occupy 45% of the country's surface area and have an elevation range between 1000 to 4620 meters. Additionally, the highlands, hosting 90% of the country's population, comprise the country's high mountains such as Mount Ras Dejen (4620 m) and Mount Tulu Dimtu (4383 m), mountain chains such as the Seimen mountains and the Bale mountains, and deep gorges such as the Blue Nile gorge and the Mekele gorge. The rift segment in Ethiopia is 900 km long and 50 to 100 km wide. It generally slopes from south to north and is dotted at its middle section by volcano systems (e.g. Ziquala, 2989m; Boset, 2447m; Fentale, 2007m), and by volcano tectonic lakes (Ziway, Shala, Langano, Abijata, Awassa, Abaya and Chamo). The northern part of the Ethiopian rift system, having different names (the Afar depression, Afar triangle, and Denakil depression) consists of the lowest

elevation in the country. The height is also the lowest in Africa and the second lowest point in the world next to the dead sea (Billi, 2015). The peripheral part of the country is a low land that extends from the highlands to the neighboring countries in a gradational slope.

2.2. Climate

The climate of Ethiopia is controlled by the seasonal migration of the Intertropical Convergence Zone (ITCZ) and the associated atmospheric circulations: The Subtropical Jet (STJ), Red Sea Convergence Zone (RSCZ), Tropical Easterly Jet (TEJ), and Somali Jet (SJ) (Beltrando and Camberlin 1993; NMA 1996). The diverse physiographical composition and marked contrast in elevation between areas are also important factors in controlling the climate of the country, especially in determining local variations (Fazzini, Bisci and Billi, 2015; Berhanu, Seleshi and Melesse, 2014). As a result, the country exhibits a wide range of climate types: From equatorial

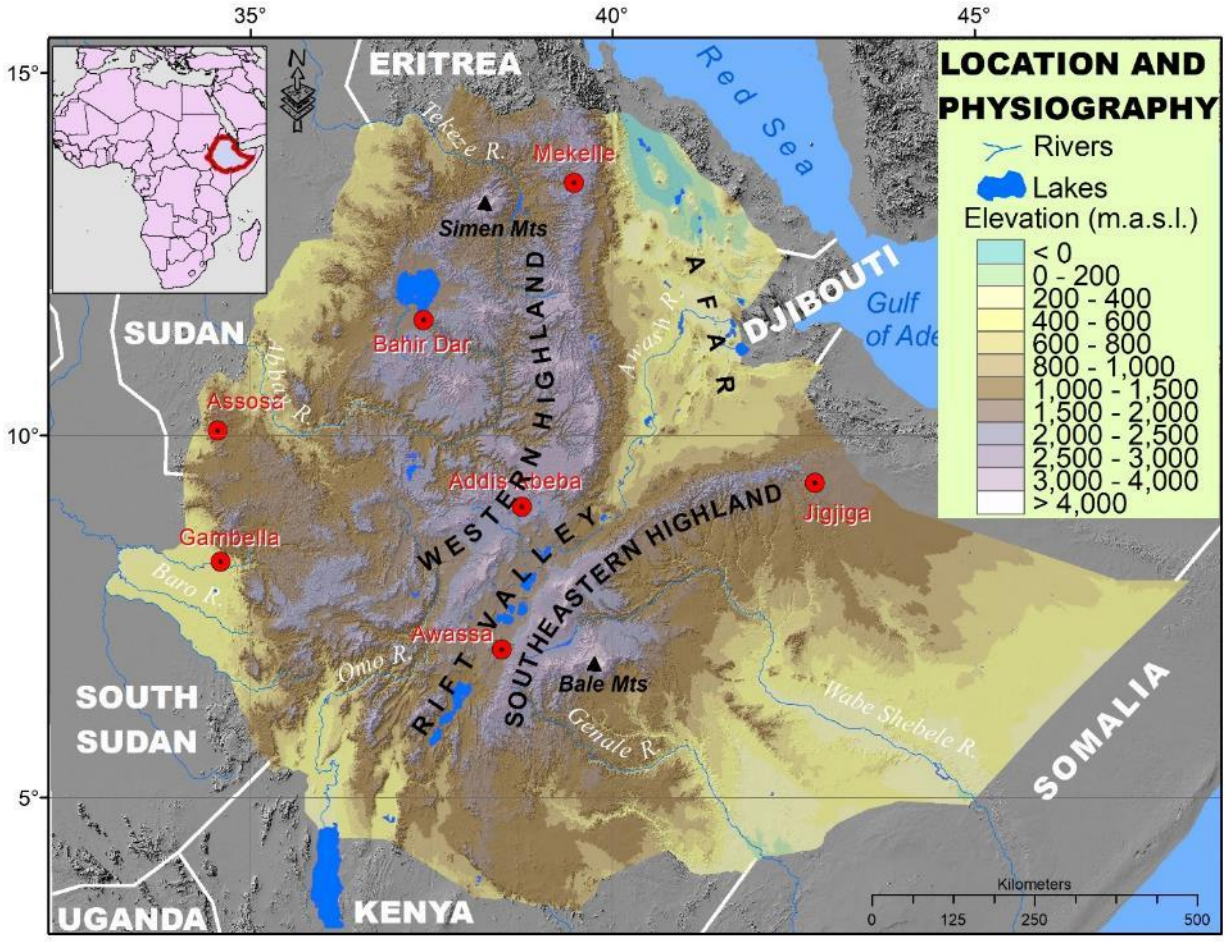

Figure 2.1: Location and physiography of the study area. (Data Source*: NASA SRTM*)

desert to hot and cool steppe, from tropical savannah and rain forest to warm temperate, and from hot lowland to cool highlands (Abiye, 2006). Moreover, due to the latitudinal effect, rainfall decreases and temperature increases as moving from south to north of the country (Fazzini, Bisci and Billi, 2015).

2.2.1. Rainfall

The rainfall pattern in Ethiopia is controlled by the intensity, position and circulation of the multi-weather systems that include the Intertropical Convergence Zone (ITCZ), Subtropical Jet (STJ), Red Sea Convergence Zone (RSCZ), and Tropical Easterly Jet (TEJ) and Somali Jet (SJ) (Beltrando and Camberlin 1993; NMA 1996; Fazzini, Bisci and Billi, 2015; Berhanu, Seleshi and Melesse, 2014). The country's diverse topographical composition and wide elevation range further define the local rainfall variation in the study area.

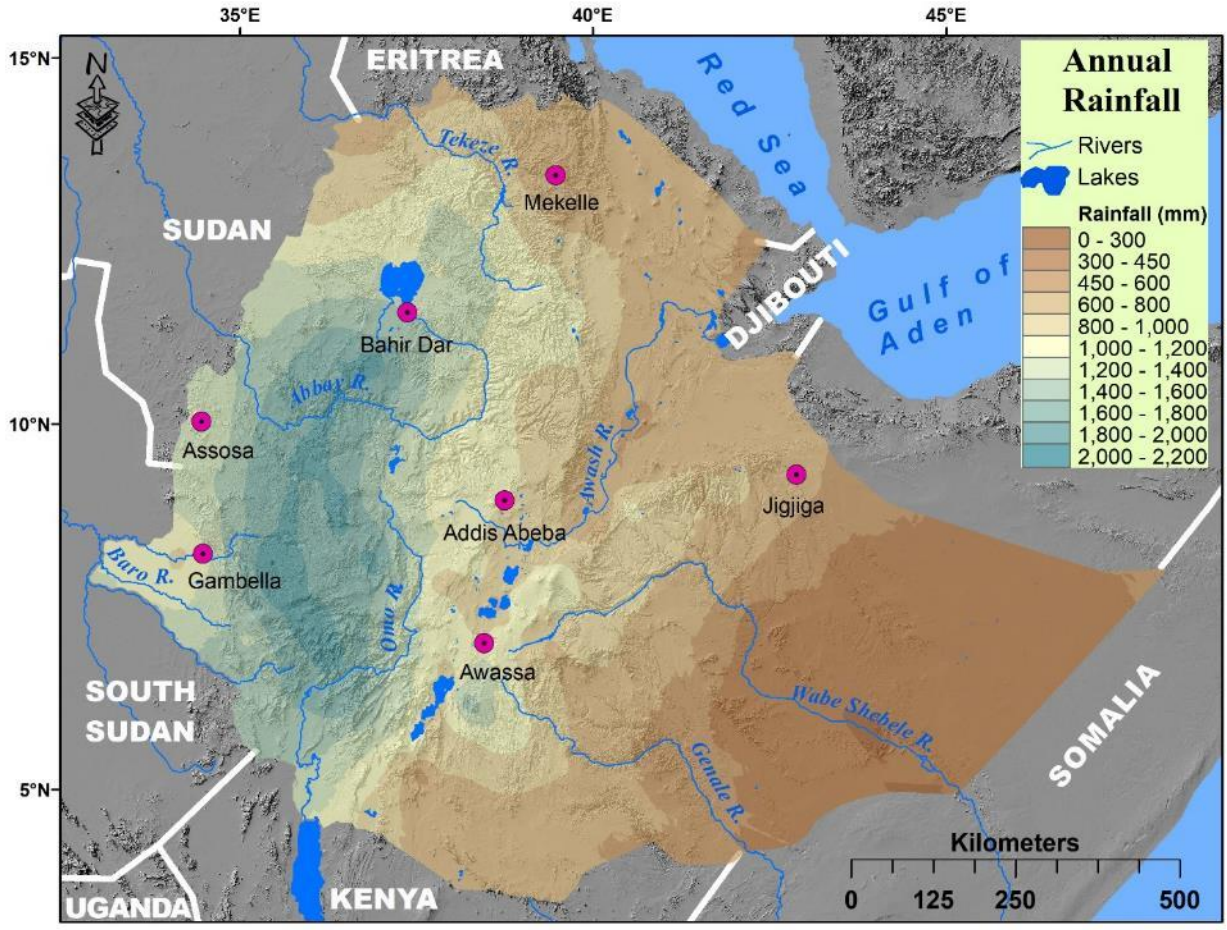

Figure 2.2: Annual rainfall distribution in the study area. (Data source: *NMA and FAO)*

Analyzing the mean annual rainfall distribution in the country shows that there is a distinctive spatial rainfall pattern. The east, the southeast, and the northeast parts of the country receive low mean annual rainfall (as low as 200 mm), and in the Afar depression, it can reach up to 50 mm (Fazzini, Bisci and Billi, 2015; Berhanu, Seleshi and Melesse, 2014). On the other hand, the central part of the country and the west highland receive mean annual rainfall of 1200 mm, and some specific areas in the western part of the country such as Goro receives more than 2000 mm (Fazzini, Bisci and Billi, 2015; Berhanu, Seleshi and Melesse, 2014) (Figure 2.2).

The temporal rainfall pattern in the country is an imprint of the multi-system weather circulations. When the circulation zone is ascending from southwest to northwest of the country during mid-June to mid-September, which is the main rainy season in the study area (called 'kiremt' locally), provides high rainfall (yielding up to 350 mm per month in the wettest regions) to large portion of the study area that includes central, northern and western part of the country (McSweeney et al. 2010, Berhanu, Seleshi and Melesse, 2014). As the circulation zone migrates to the southern part of the country, during October and November, it provides low rainfall (around 100 mm per month) to the south and southeastern parts of the country. When the zone reaches to its southern extreme position in the study area, during March to May, it provides 100 – 200 mm rainfall to the south and southeastern parts, and little rainfall to the central and northern parts of the country (McSweeney et al. 2010, Berhanu, Seleshi and Melesse, 2014).

The summer rain provides 50% of the annual rainfall in the study area, and of that, the 80 up to 85% of the rainfall falls on the highlands. Furthermore, the summer rainfall describes 50% of the spatial rainfall variability in the country whereas the spring describes 31% (Billi, 2015).

2.2.2. Temperature

The dominant factor that determines temperature pattern in the country is the topographic variation. Thus, the highland and the lowland areas in the country shows significant difference in their temperature. However, the temperature readings at each station are consistent throughout the year, and it is among the countries that have the most equilibrate and pleasant temperature setting in the African continent, except at the Denakil depression, which is an area with extremely high temperature, 34.7^{o}C usually and up to 45.7^{o}C at times (Pedgley, 1967; Fazzini, Bisci and Billi, 2015) (Figure 2.3).

The general setting of the temperature distribution in the country shows that the lowest mean temperature (14.2 ^{o}C) is recorded in the highlands where elevations are over 2300 up to 2600 m a.s.l., irrespective of geographic location (Fazzini, Bisci and Billi, 2015) (Figure 2.3). The lowest temperature, however, can go as low as to 8 ^{o}C, and a few days of frost is a common experience in the highlands. One of the lowest temperature record is obtained in the Bale Mountains which is usually around – 7 ^{o}C. Higher mean temperature is recorded in the rift valley and the lowlands in the peripheral part of the country. In the rift, temperature increases as moving from south to north, attaining the maximum in Denakil depression. However, in the elevation range between 1000 and 1500, mean annual temperature is in the range of 20 – 25 ^{o}C (Fazzini, Bisci and Billi, 2015).

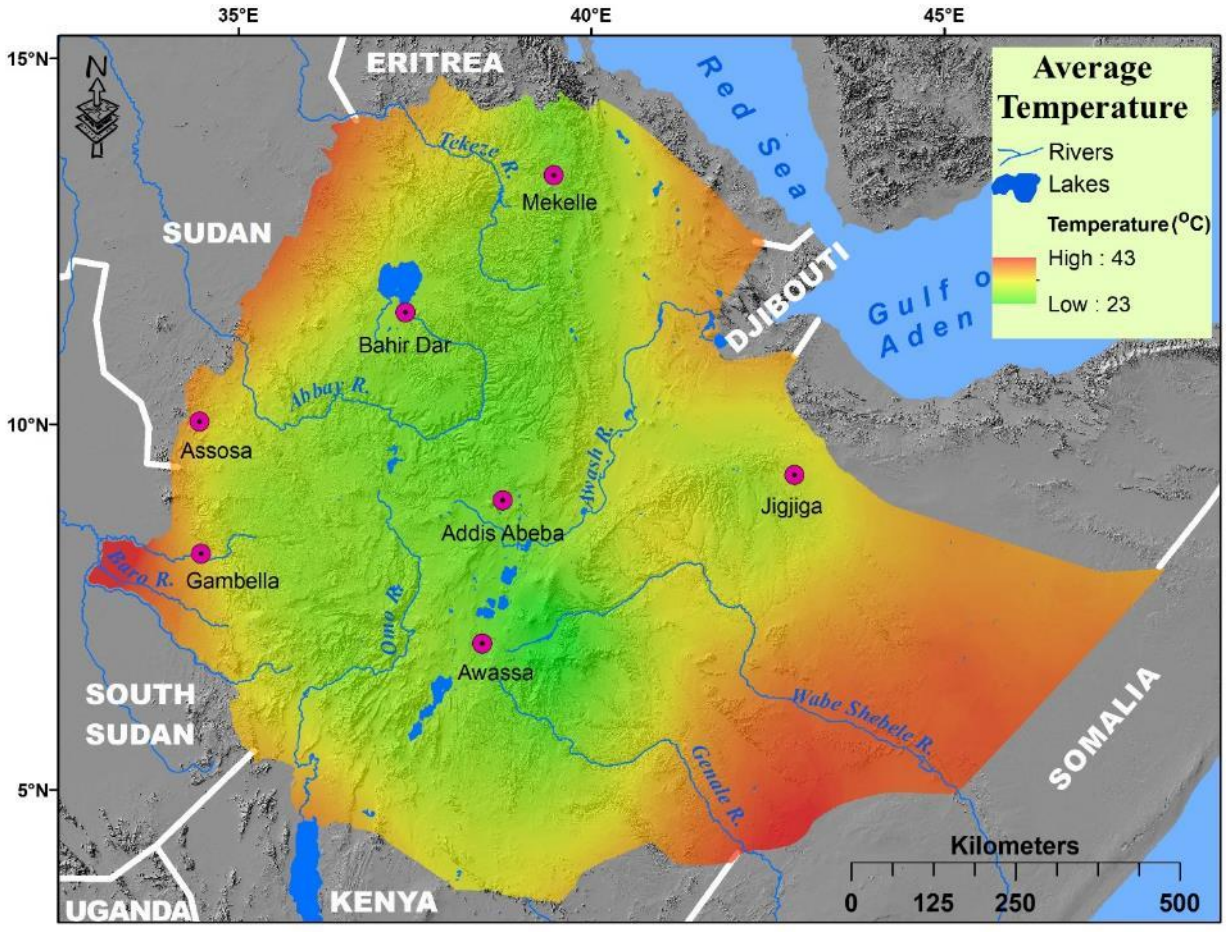

Figure 2.3: Average temperature distribution in the study area. (Data source: *NMA and FAO)*

2.2.3. Wind Speed and Humidity

Since the horn of Africa is not a cyclone-genetic area, the country is characterized by nearly uniform wind speed (Billi, 2015). The spatial variability of the wind speed is also the result of the complex physiography of the country (Figure 2.4). Similarly, humidity is controlled by the position of ICTZ and physiography of the country, and it is tightly correlated with the distribution of rainfall in the country (Billi, 2015).

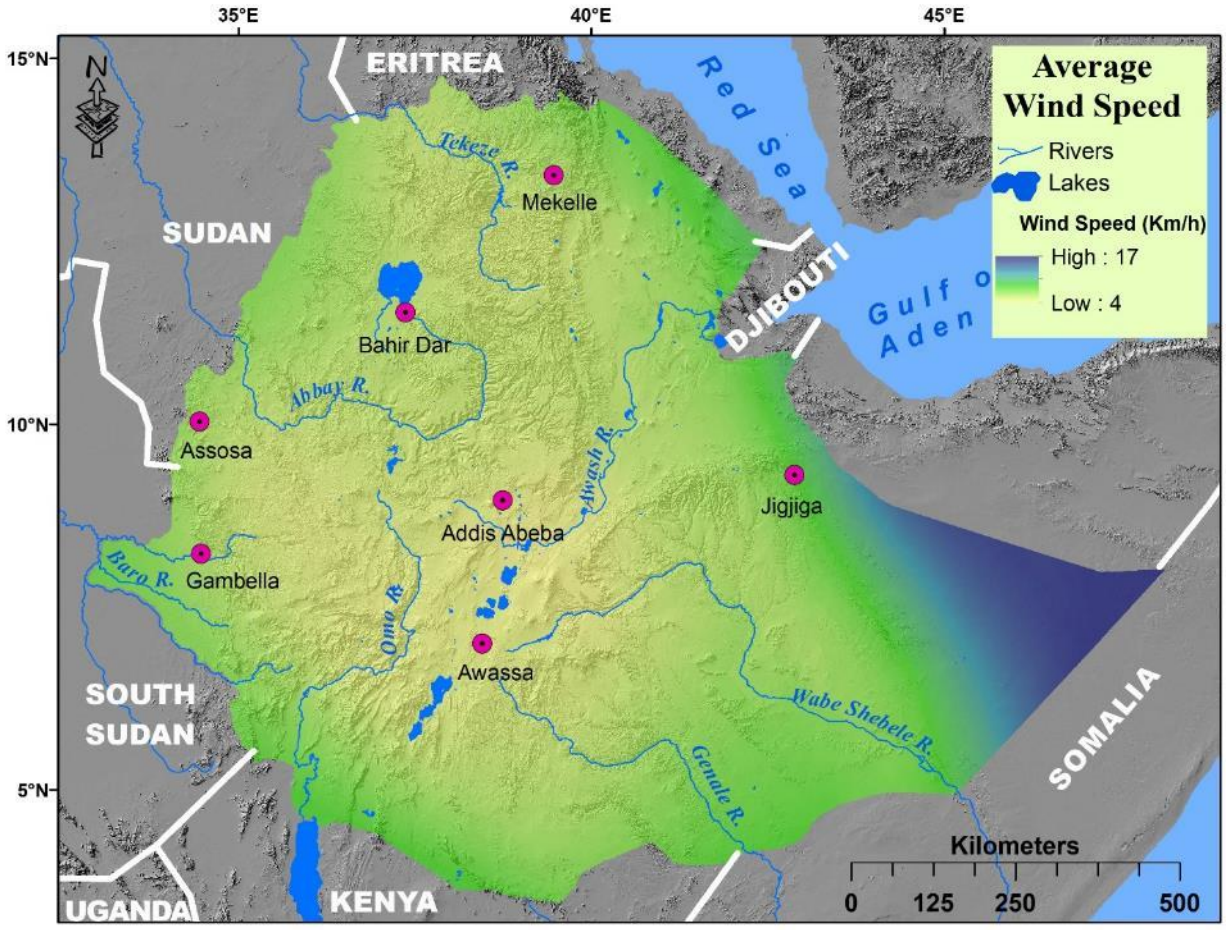

Figure 2.4: Average wind speed distribution in the study area. (Data source: *NMA and FAO)*

2.3. Geology (Geologic history, stratigraphy, formations)

Ethiopian landmass constitutes complex formations of igneous, sedimentary, and metamorphic rocks and unconsolidated sediments which are formed by the geological events and processes since Precambrian (Figure 2.5). The major geologic events that happened in Ethiopia are orogeny in Precambrian, peneplanation, glaciation and continental breakup in Paleozoic, cyclic marine transgression and regression in Mesozoic, huge continental flood basalt eruption and formation of rift valley in Cenozoic, and pluvial-interpluvial sediment accumulation in Quaternary (Figure 2.6).

2.3.1. The Precambrian basement complex (Metamorphic rocks)

The metamorphic rock formations of the study area are formed by the orogeny process that collided the West and East Gondwana by closing the Mozambique ocean to form the N–S elongated mega-collisional structure, the East African Orogen, stretched from Israel to Madagascar in Precambrian (Stern, 1994). It resulted two distinctive types of metamorphic formations: The Arabian-Nubian Shield (ANS) and the Mozambique belt. The Arabian-Nubian shield is a zone of dominantly low-grade volcano-sedimentary rocks overlain by metasediments (stromatolitic carbonates and diamictites) associated with "Snowball" (Beyth *et al*., 2003). It is dominantly exposed in the northern part of the country. The Mozambique belt is a zone of dominantly of amphibolite and granulite facies and gneiss terranes, and it is dominantly exposed in the southern and western part of the country. The metamorphic rock formations form the foundation of the Ethiopian landmass and underwent denudation for considerable geologic time (Coltorti *et al*., 2007).

2.3.2. The Paleozoic Sedimentary Rocks

The next units in the Ethiopian litho-stratigraphy are the lower Enticho Sandstone of the Ordovician to Silurian, and the upper Enticho Sandstone and Edaga Arbi glacials of the Late Carboniferous to Early Permian glacial epochs (Bussert and Schrank, 2007). They are of glaciations and fluvial activities that interrupted the peneplanation of the metamorphic terrains in the country in Paleozoic. Although these formations are patchy outcrops distributed throughout the country (Jepson and Athearn 1964; Russo et al. 1994), a greater thickness is exposed uncomformably overlaying the metamorphic formations in few places such as in Adigrat, an area near the border between Ethiopia and Eritrea.

2.3.3. The Mesozoic Sedimentary Rocks

The Mesozoic era holds most of the sedimentary formations in the country. The onset of the era is marked by the formation of the rifted basins (Blue Nile, Karoo, Ogaden), which is the beginning stage of Gondwana breakup (Bosellini 1989; Hunegnaw et al. 1998; Gani et al. 2009). The fluvial, fluviolacustrine, and deltaic environments in the basins were responsible for the formation of the Adigrat Sandstone in Triassic period (Beauchamp 1977; Bosellini et al. 1997, 2001; Wolela 2008). The Adigrat Sandstone formation has light grey to red color and is composed of quartz arenites with interbeds of conglomerates and intensely pedogenized red mudstones. Its thickness reaches up to 700 m at some places and varies at short distances. In most parts of the country, it is usually found unconformably resting on the Precambrian or Paleozoic formations, but in the Ogaden basin, a probable conformity with the Permo-Triassic Karoo deposites is reported by Hunegnaw et al. (1998).

The next major event in this era was the marine transgression from the northeastern (Paleotethys) and eastern (India/Madagascar nascent ocean) side of the country to the Horn of Africa following the breakup of Gondwana. The transgression covered large portion of the country, and after it regressed out from most part of the country by the end of Jurassic, it remained in cyclical transgression and regression in the Ogaden basin until Tertiary. The event, at the different stages of its occurrence, formed different types of rock formations that constitute larger portion of the sedimentary formations in the country. While the ocean was transgressing into the country, it activated transitional and shallow-water marine systems and formed formations of marls, evaporates and shales. In the Blue Nile basin, these formations are named as Gohatsion formation, and they conformably overlie the Adigrat Sandstones (Blanford 1870; Russo et al. 1994). While the transgressed water was resting as a big water body in the country, it formed the thick limestone formations in the country, Antalo Limestones or Hamanlai Limestones; its thickness reaches up to 1000 m. The regression stage was triggered by the faulting and tilting of the Nubian plate in Cretaceous, and it formed the Sandstone formation that unconformably rest on the limestone formations (Bosellini et al. 2001). This formation, named as Amba Aradam Sandstone, is associated with lenses of quartz conglomerates and red shales and, at its base, shows laterites. Its maximum thickness is found to be 200 m (Gortani 1973; Bosellini et al. 1999). These sedimentary

successions are a bit different and thicker in the Ogaden basin as the marine transgression stayed for a longer time in this area. This region exhibits deposits of shales and sandstones (Jesomma Sandstones), carbonates (Auradu Limestone), and evaporates (Taleh Evaporites) that were formed by the alternation of transitional, shallow-water marine, and open-sea environments which totally reach to a thickness of 1200 m (Barnes 1976; BEICIP 1985; Hunegnaw et al. 1998).

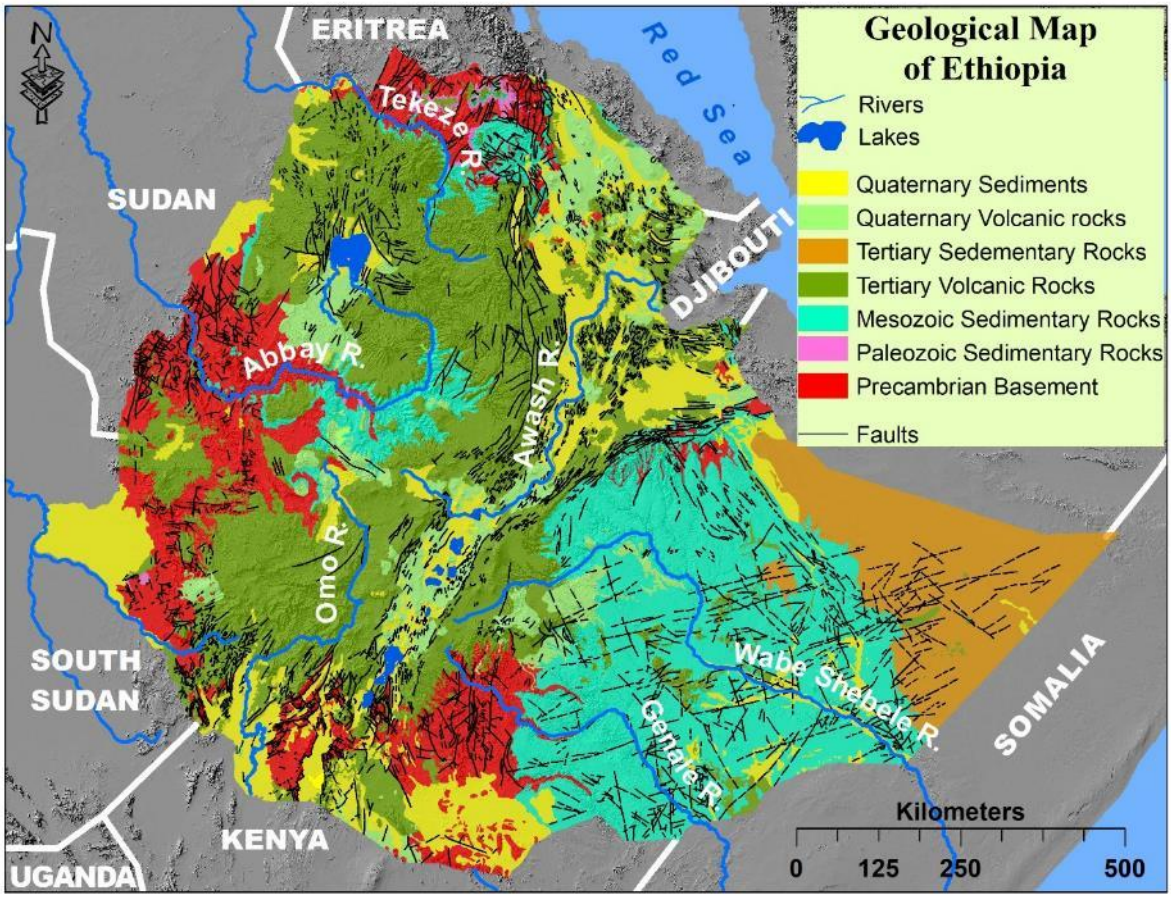

Figure 2.5: Geological Map of the study area. (Data Source: *GSE and BGS*)

2.3.4. Cenozoic Volcanic rocks

The next remarkable geological event in the study area was the huge volcanic activity and the rift valley formation in Cenozoic. The volcanic activity is subdivided into pre and post with respect to the rift valley formation. The pre rift volcanic activity, being supplied by large mantle plume, formed the huge pile of flood basalts of the central part of the country that are traditionally called

'Trap series' (following its stair like land form, *'trap'* means *'stair'* in Swedish (Blanford 1870; Kazmin 1973)) within short period of time, one million years, predominantly in Oligocene (Schilling 1973; White and McKenzie 1989). This formation, according to Mohr (1983), has 750, 000 m^2 surface areal coverage and is 350, 000 m^3 in volume.

The trap series, unconformably overling the basement, Paleozoic or Mesozoic formations, according to Abbate and Sagri (1980), is grouped into three major provinces based on their lithological development, type of activity, frequency of volcanic centers, and age of effusion: (1) volcanites of the northern plateau; this group is further subdivided into two (Ashangi and Magdala) by Blanford (1870), into four (Ashengi, Aiba, Alaji and Tarmaber) by Zanettin and Justin Visentin (1973) and Gregnanin and Piccirillo (1974), and into four (Basal sequence, Upper sequence, Shields and Quaternary basalt sequence) by Kieffer et al (2004). (2) volcanites of the southern plateau; this group constitutes the Amaro basalts, Gamo basalts, Omo basalts, and Jima basalts. (3) volcanites of the Somali plateau; this group constitutes the Arusi basalts and Bale basalts.

The formation of the rift valley in this region was commenced 25 Ma ago, and formed the rift system and the rocks that constitutes the valley. These rocks were collectively named as Aden Series (Blanford 1870; Mohr 1962). The Ethiopian Rift System comprises two distinct sections: the Afar and Main Ethiopian Rift (MER). The Afar is a quazi triangular area where the three rifts (Gulf of Aden, Red Sea and MER) join together forming a triple junction. In its 25 Ma geological history, the Afar triangle experienced two major events: continental rifting that began in the Gulf of Aden 24 Ma ago and incipient oceanization commenced 4 Ma ago (Barberi et al. 1975). The older volcanites in the Afar triangle are the Adolei Basalts, Mabla Rhyolites, and Dalha Basalts; associated with these volcanites are the alkaline and peralkaline granites aged 25–22 Ma that indicates first stage of continental rifting (Barberi al. 1975). However, it is the Stratoid Series, the transitional basalts, that has largest coverage in the area – two thirds of the Afar depression. The Stratoid Series lies unconformably on the Dalha Basalts and marks the second stage of the continental breakup. The prominent morphological features in the Afar are the NNW – SSE oriented axial volcanic ranges – Erta Ale, Tat Ale, Alayta, and Manda Hararo.

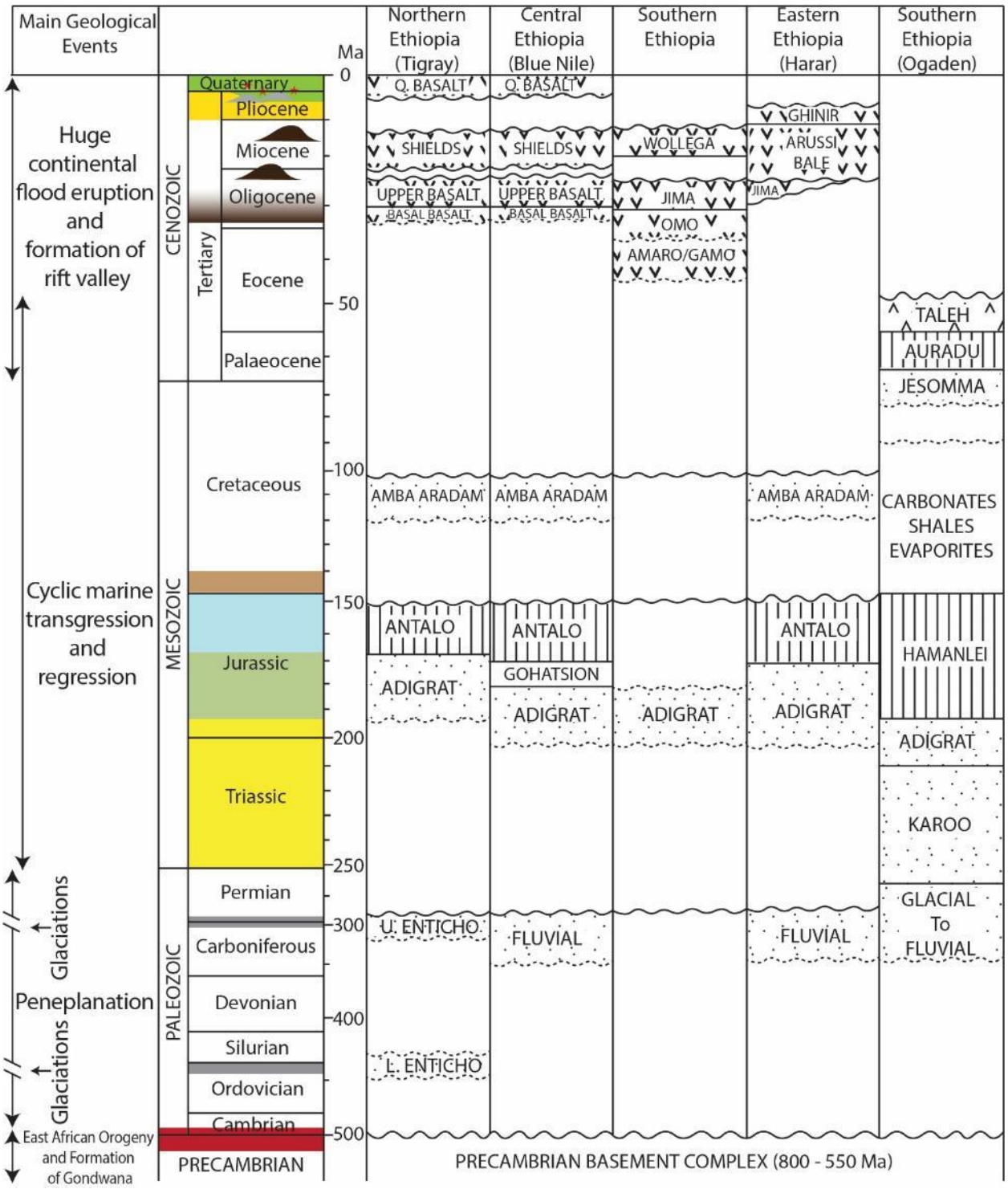

Figure 2.6: Geological stratigraphic chart with the main geological events. (Modified after Billi, 2015)

The MER is a NNE – SSW to N – S trending trough having 1000 Km length and 50 to 100 Km average width. It is in turn subdivided into three sectors: Northern, Central and Southern. The oldest volcanites in MER are shield volcanoes (Chillalo, Badda, Chike, Kecha) of the Mio-Pliocene age and mark the early stage of the rifting whereas the dominant rocks are Ignimbrites (Nazaret Group) and formed as a result of catastrophic eruptions at large calderas such as the Munesa caldera (3.5 Ma) (Corti, 2009). The most recent volcanic activity in MER is concentrated in the rift axis, and resulted basalt flows, scoria cones, large silicic central volcanoes known as Wonji Group and the associated oblique fault belt known as Wonji fault belt (Mohr 1962).

2.3.5. Quaternary Sediments

Loose sediment deposits are alluvial, lacustrine and colluvial products that are found filling up depressions, foothills and low energy stream portions. In the country's geomorphological context, the rift valley and lowlands at the foot of the highlands are ideal locations for sediment deposition. Consequently, sediment depositions have been forming dominantly in the eastern Ogaden, Danakil Depression, lower Omo valley, Southern Sidamo, Gambela, and western Gondar (around 25% of the surface area of the country) since Miocene (Kebede, 2013).

2.4. Hydrogeological setting

The aquifers in Ethiopia are of the geological formations of volcanic, sedimentary and metamorphic rocks, and loose sediments. The aquifers' stratigraphy and their spatial distribution is determined by the geological events that have formed the country's landmass since Precambrian. The metamorphic aquifers are formed by the process of East African Orogeny in Precambrian whereas the sedimentary aquifers are formed by the fluvial, glacial, lacustrine activities in Paleozoic as well as the sedimentation in Mesozoic. The volcanic aquifers are rock formations that are formed by the process of prolific magmatism in Cenozoic. The loose sediment aquifers represent the sediment depositions in different parts of the country by exogenic processes since Miocene.

In terms of areal coverage, the volcanic aquifers are the largest, but in terms of groundwater storage, the loose sediments occupy the largest proportion (Figure 2.7). Kebede (2013) provides an exhaustive description of the different aquifers in the country in terms of their formation history, hydrological characteristics, groundwater storage potentials, recharge mechanisms, quantity and quality of their waters, and the conceptual model that describes the groundwater system.

Although it differs from place to place, the general hydrostratigraphy in the country shows that Metamorphic aquifers and the associated regoliths and wadi bed deposits are the oldest. Next to the basement aquifers are the Mesozoic sedimentary rock aquifers, Cenozoic volcanic rock aquifers and Quaternary sediments sequentially (Kebede, 2013).

The metamorphic aquifers in Ethiopia are known for having limited groundwater storage due to their limited porosity and permeability (Chernet, 1993). Moreover, larger portion of the metamorphic aquifers constitute the country's peripheral lowlands where there is low rainfall. In this formation, groundwater is stored in fractures, shear zones and regolith layers (regolith layers are layers of weathering products formed above parent materials and known to enhance storage of groundwater in metamorphic terrains such as in Uganda and Central Africa (Kebede, 2013; Deyassa *et al*., 2014). According to Kebede (2013) and Deyassa et al (2014), compared to the northern part, metamorphic aquifers of the western and southern part of the country have higher potential due to much higher rainfall in the area and their thicker layer of regolith.

Kebede (2013) identified that the sedimentary aquifers in Ethiopia, unlike their counterparts in many other countries, are less significant groundwater storages due to their reduced porosity and permeability as a result of an overburden. He also noted that they are less karistified due to their high elevation and anticline arrangement, which makes them less suitable for the formation of caves.

As the volcanic rock formations in the country are highly deformed due to the rift valley process in Cenozoic, fractures are the most important means of porosity and permeability. Consequently, degree of fracture, aperture opening, spacing and length are significant characteristics in determining groundwater potentials of the Ethiopian volcanic formation. Systematic fractures in some big shield volcanoes form large springs of high yields such as Timket Bahir (1045 l/s), Jiga (400 l/s), and Lomi Wuha (120 l/s) (Kebede, 2013). Carrying larger proportion of the country's

human population, generally, the volcanic aquifers are characterized as having medium groundwater potential.

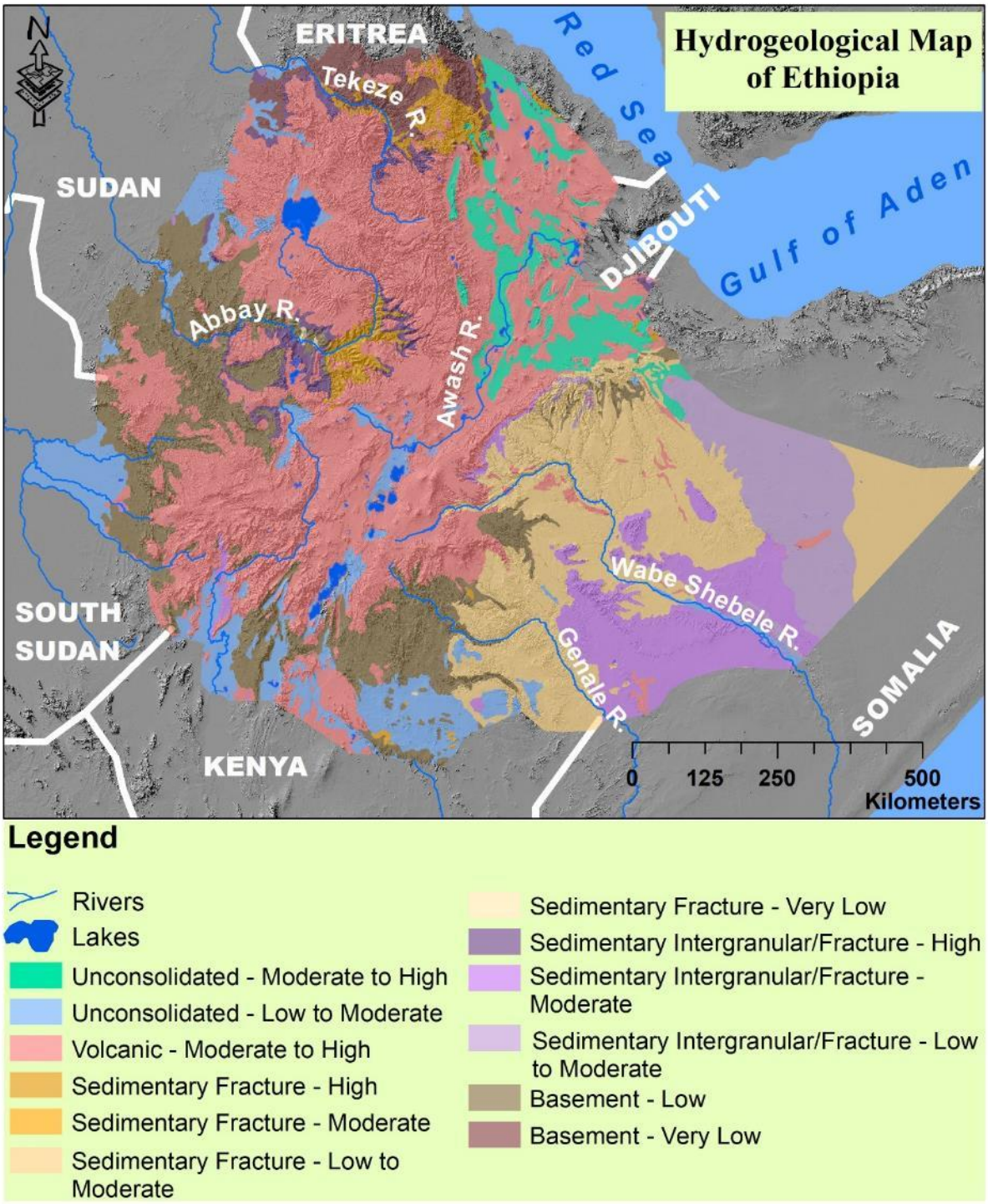

Figure 2.7: Hydrogeological Map of the study area. (Data source: *GSE and BGS*)

Loose sediments in Ethiopia are dominantly found in the Main Ethiopian Rift (MER), grabens of the rift escarpments, on river beds, and lake margins (Kebede, 2013). These deposits hold groundwater in primary porosity. Water table in this aquifers is very shallow and have the highest yield in the country (Kebede, 2013).

CHAPTER THREE

3. DEVELOPING A CONCEPTUAL MODEL OF GROUNDWATER RECHARGE

3.1. Introduction

Groundwater recharge is one of the hydrological components that are unsuitable for direct measurement. Thus, it is estimated by using different kinds of estimation methods that are developed on the basis of the conditions and realities at the different zones of the hydrologic cycle (Figure 3.1). However, uncertainties are inherently associated with estimations. Among the identified sources of uncertainties, the major contribution is found to be from the inconsistency between the conceptual model of groundwater recharge and the assumptions in the estimation methods applied in the area (Healy and Scanlon, 2010). To significantly reduce uncertainties in groundwater recharge estimations, Scanlon and Healy (2010) suggests that before implementing a recharge estimation method in an area, a conceptual model of groundwater recharge has to be developed, and it has to be evaluated that the assumptions in the recharge estimation method that is about to be implemented are consistent with the conceptual model of groundwater recharge developed for the area.

A conceptual model reveals the fact that where, when and how recharge occurs (Healy and Scanlon, 2010; Scanlon *et al*., 2002). Therefore, conceptual models can be used to evaluate not only the appropriateness of an estimation method to an area but also the consistency of its outputs with the model. In this study, the Multi Criteria Decision Analysis is used to develop a conceptual model of groundwater recharge to the study area by combining factors that significantly control groundwater recharge. The MCDA outputs will be monthly groundwater recharge potential maps that show groundwater recharge characteristics both in the spatial and temporal dimension.

3.2. Multi Criteria Decision Analysis (MCDA)

According to Malczewski (2006), multi criterial decision analysis (MCDA) is defined as "a rich collection of techniques and procedures for structuring decision problems, and designing, evaluating and prioritizing alternative decisions". There are three core elements both in MCDA in general and GIS based MCDA in particular: Decision maker (s), alternative decisions, and criteria (Zarghami and Szidarovszky, 2011). A decision maker can be an individual, a group of individuals or a government body that has a responsibility to make decisions (Malczewski, 2006).

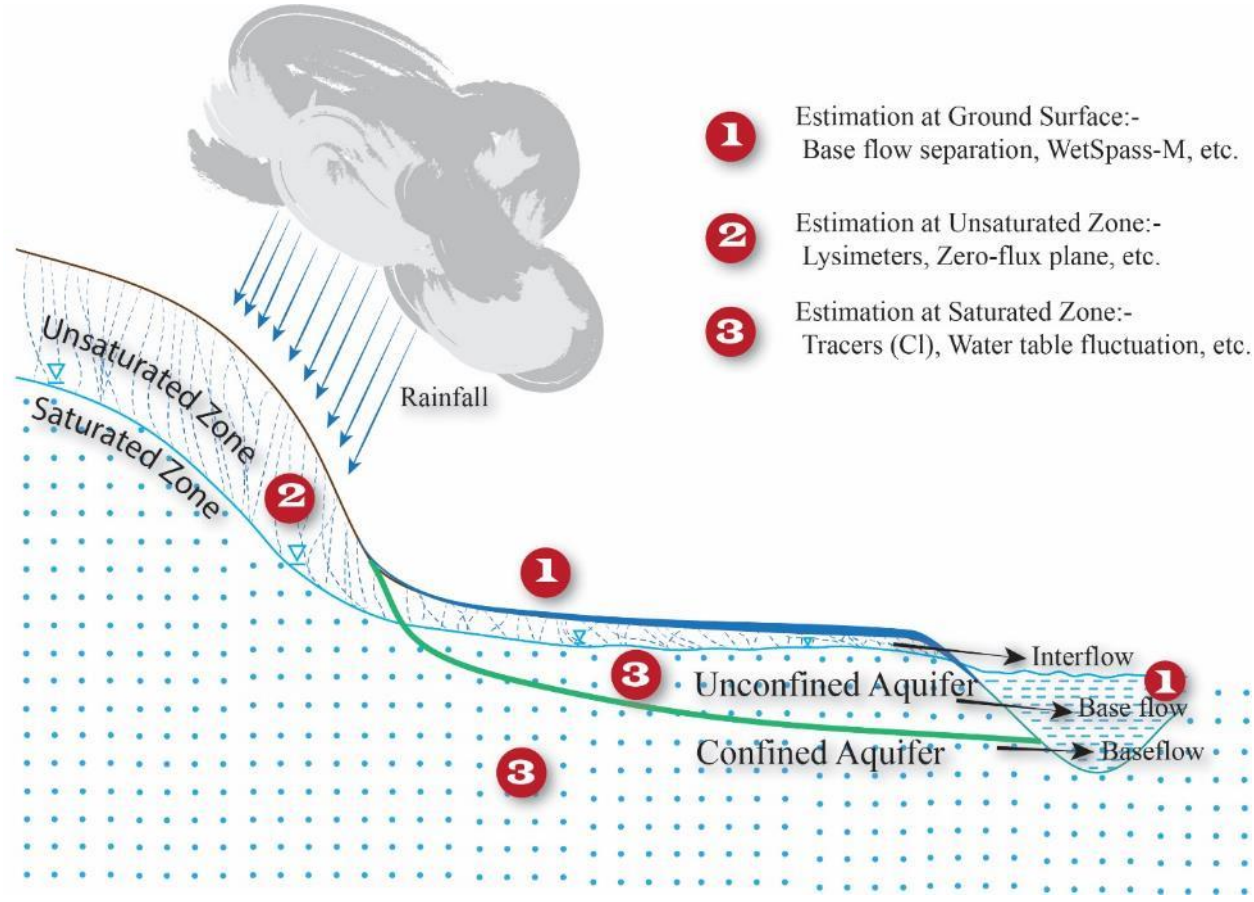

Figure 3.1: Schematization that show the different zones and layers in the hydrological cycle and the groundwater recharge methods that can be applied in the zones and layers.

An alternative decision represents variety of available decision alternatives that decision makers have to choose from based on criteria, and it has at least two elements: Action (what to do?) and location (where to do it?) (Malczewski 1999; Chakhar and Mousseau, 2008). Criteria in an MCDA carries attributes and objectives, and they are comprehensive, measurable, and the basis for the evaluation of the decision alternatives (Malczewski, 2006). Objectives and attributes of criteria have a hierarchical relationship in which the top most level occupies the most general objectives of the decision analysis and the lower levels occupy the attributes. Attributes are quantifiable indicators with which the associated objectives are realized (Saaty 1980).

An MCDA procedure involves three main steps (Figure 3.2): Value scaling or standardization, criteria weighting, and combination (decision) rule (Eastman *et al*., 1993; Thill 1999; Malczewski 1999, 2006; Greene et al. 2011). *Value scaling or standardization* is a transformation of raw attribute values into comparable units by using the different scaling procedures (Hwang and Yoon, 1981; Voogd, 1983; Massam, 1988). In this research, the value function method is used to standardize the raw criteria values. The value function is a mathematical representation by which decision makers' preferences can be transcribed into a standardized scale (Keeney, 1992; Beinat, 1997). It is given by Equations (*3.1*) and (*3.2*):

$$v(a_i) = \left(\frac{max\{a\} - a_i}{max\{a\} - min\{a\}}\right)^{\rho} \text{ for criteria to be maximized,} \quad (3.1)$$

$$v(a_i) = \left(\frac{a_i - min\{a\}}{max\{a\} - min\{a\}}\right)^{\rho} \text{ for criteria to be minimized,} \quad (3.2)$$

Where, a_i is a criteria value, $max\{a\}$ is the maximum criteria value, $min\{a\}$ is the minimum criteria value, ρ is a risk factor parameter and is greater than 0, and $v(a_i)$ is a standardized value or score.

This equation produces standardized values that range between 0 and 1, representing the least-desirable and the most-desirable scores respectively. The ρ parameter is used to include a risk factor in the analysis (Bodily 1985; Ligmann-Zielinska 2009), and a ρ value of 1 constructs a linear transformation between the raw and standardized values. In ArcGIS, this transformation is performed by the 'Fuzzy membership' tool.

The Criterion weighting refers to the value assignment to each criterion according to its importance to the objective under consideration. A higher value to a criterion indicate a greater importance to the objective under consideration. The pairwise comparison method, which was developed by Saaty (1980), was used in this research to assign weights to the criteria considered. The pairwise comparison employs a rating scale of 1 up to 9 to rate all the possible pairs that can be obtained from the criteria (Table 3.1). A pair wise comparison matrix is then formed. Then, the entries of the matrix are normalized (Equation 3.3) and averaged (Equation 3.4) over the normalized columns to get weight values for each criterion.

$$C_{kp}^{*} = \frac{C_{kp}}{\sum_{k=1}^{n} C_{kp}}, \text{ for all } k = 1,2,3, \ldots, n. \tag{3.3}$$

$$w_k = \frac{\sum_{p=1}^{n} C_{kp}^{*}}{n}, \text{ for all } k = 1,2,3, \ldots, n. \tag{3.4}$$

Where, C_{kp} is the pairwise comparison rating matrix for the k-th and p-th criteria and w_k is a weight value. The pairwise comparison test also measures its consistency by the Equation (3.5):

$$CR = \frac{\lambda_{max} - n}{RI\ (n-1)} \tag{3.5}$$

where RI is random index, which is the consistency index of a randomly generated pairwise comparison matrix, and CR is the consistency ratio. It can be shown that RI depends on the quantity of criteria being compared. For example, for n = 2, 3, 4, 5, 6, 7, and 8, RI = 0.00, 0.52, 0.89, 1.11, 1.25, 1.35, and 1.40, respectively (Saaty, 1980).

The Combination rule refers the integration of the standardized criteria according to their weight to get the possible alternative decisions. In ArcGIS, the overlay tool operates this function.

1/9	1/7	1/5	1/3	1	3	5	7	9
Extremely	Very Strongly	Strongly	Moderately	Equally Important	Moderately	Strongly	Very Strongly	Extremely
Less Important					More Important			

Table 3.1: Saaty's scale of relative importance (Saaty, 1980)

3.3. Criteria selection

This research implemented certain guiding principles to select important criteria (factors) that control groundwater recharge in the study area. The guiding principles are infiltration capacity, residence time, and the amount of available water. These guiding variables vary both spatially and temporally, and their importance in controlling groundwater recharge in the area was incorporated in the MCDA by using factors that can be quantified and qualified (Table 3.2).

The a*mount of available water* represents the amount of water availed in an area in several possible forms such as rainfall, snow, dew and so on. In this study, it was represented by the rainfall variable, and its amount was quantified and its spatial and temporal variability was determined from the rainfall time series data obtained from weather stations distributed over the study area. *Infiltration capacity* refers the characteristics of an area to infiltrate water into the subsurface. It determines how much of the available water could possibly be infiltrated. Although there are several variables that can be used to evaluate the infiltration characteristics of an area, in this study, only the significantly important and easily available variables are used: lithology, lineament density, drainage density and soil texture. *Overland-flow resistance*, on the other hand, represents resistance generated on surfaces due to their roughness characteristics such as topography and vegetation (Bergkamp, 1998).

Guiding variables	***Refers to***	***Quantifiable variables***
Water Availability	The amount of water available in the study area	Rainfall
Infiltration Capacity	The characteristics of the area to infiltrate water	Soil texture Lithology Lineament density Drainage density
Overland-flow resistance	The roughness characteristics of land surfaces	Land use/land cover (LULC) Slope

Table 3.2: Identified variables (factors) that control groundwater recharge in an area.

3.3.1. Groundwater recharge factors and their Standardization

The input datasets of MCDA were collected from different sources (Table 3.3), and besides characterizing the study area in different aspects, they have different spatial resolution. Therefore, for the purpose of optimization and consistency, an average spatial resolution was calculated, which is found to be 250 meters.

3.3.1.1. Rainfall

For the existence of groundwater recharge in an area, availability of water is the first requirement. Although it needs the consideration of the other factors, areas with greater amount of available water usually have higher groundwater recharge. In Ethiopia, rainfall is the major source of water in almost all areas, and it has variable distribution both spatially and temporally. The analysis of the spatio-temporal rainfall pattern in the country identifies three regimes (Figure 3.3) (Berhanu, Seleshi and Melesse, 2014). Regime A is the northern, central and eastern part of the country and is characterized by bimodal monthly rainfall pattern, receiving high rainfall from the month of June to September (named 'Kiremt' season locally) and a little rain from March to May (named 'Belg' season locally). Regime B represents the western part of the country and is characterized by unimodal monthly rainfall, receiving rainfall for longer period – from February to November. Regime C represents the south and southeastern part of the country, and it is characterized by a distinctive bimodal rainfall pattern receiving high rainfall from February to May (named 'Bega' season locally) and from October to November. The largest amount of rainfall in the country is obtained in kiremt season amounting up to 350 mm/month in the wettest regions. Following that is of belg (100 – 200 mm/ month). The least amount is obtained in bega season (100 mm/month), and in this season, most part of the country is dry.

The long-term average rainfall raster maps for each of the months of the year were prepared from weather station data obtained from the National Meteorological Agency (NMA) (Table 4.1) and the FAO LocClim database (Figure 4.6) by using the geostatistical kriging interpolation method in ArcGIS (Figure 3.4). The interpolated layers were standardized into the range of values between 0 and 1 for the multi-criteria analysis by using the Fuzzy member tool in ArcGIS (Figure 3.5). One represented all areas that receive highest rainfall during the month under consideration.

	Time Period	*Resolution (meters)*	*Source*
Rainfall	2000-2018	250	NMA and FAO/New_LocClim_1.10
Soil Texture	2015	250	AfSIS
Land use/Land cover	2016	30	WLRC
Lithology	1993 and 2002	250	GSE and BGS
Lineament Density	1996	250	GSE
Slope	2014	30	NASA SRTM
Drainage Density	2016	250	WLRC

Table 3.3: Time periods, resolutions, sources of input datasets of MCDA.

3.3.1.2. Lithology

Ethiopian landmass, composed of lithologies that are formed by different geological processes since 850 Ma, is highly variable both horizontally and vertically, and is compartmented and dissected in relatively shorter distances. The infiltration properties of lithologies is directly related to their permeability. Chernet (1993), based on field measurements and pump test analysis conducted on more than 300 wells across the country, categorizes lithology of the county into three permeability rating groups – high, medium and low. The British Geological Survey (BGS), on the other hand, suggests six rating classes according to its analysis by using satellite remote sensing techniques, reviewing national and sub-national hydrogeological maps, papers, reports, and analyzing borehole yields: Very high (VH), high (H), moderate (M), low to moderate (LM), low (L) and very low (VL).

This study adopted the permeability classification scheme of the BGS due to its elaborated characterization (Figure 3.6). The highest permeable class in the study area was found to be the unconsolidated sediments; however, when evaluated in terms of surface area coverage, it was the volcanic rocks that had the largest coverage (55%). The volcanic rock formations, since they constitute the highlands of the country, host around 90% of the total population of the country (Taddese, 2001). On the other hand, the 'very low' rating class in both of the classification schemes was given to the metamorphic formations in the northern part of the country. Kebede (2013) and

Deyassa et al (2014) have identified that these formations are low groundwater storages due to their thin regolith layer compared to the similar formations in the other parts of the country.

The dataset was transformed to the common scale of 0 to 1 by using the 'fuzzy membership tool' in ArcGIS, 1 representing the highest permeable class and 0 the lowest (Figure 3.7).

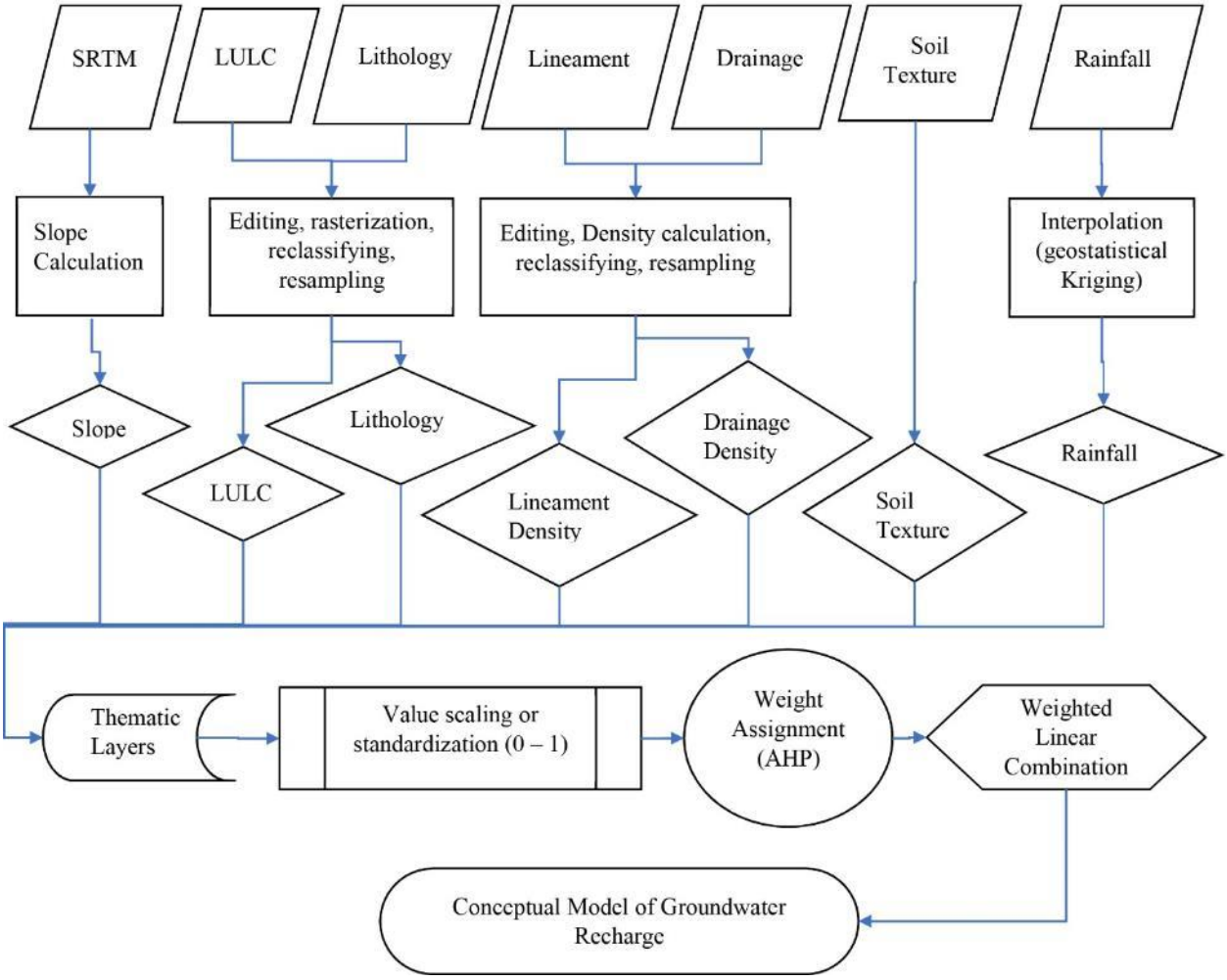

Figure 3.2: Flow chart of the methods implemented in the MCDA.

3.3.1.3. Soil

Since soil forms the top most part of the terrestrial earth in most areas, it significantly controls the quantity and distribution of groundwater recharge in an area. Among the different characteristics of soils, it is with the soil texture that groundwater recharge has the most obvious relationship. Soil texture is a physical property of soils and refers to the sizes of the grains that compose a soil type (Brady and Well, 2002). Normally, a soil class is made up of several textural classes. When big grains come together to form a soil class, larger void spaces are formed among their contacts so that the infiltration property of the soil becomes higher. With small grains, conversely, infiltration property of soils decreases.

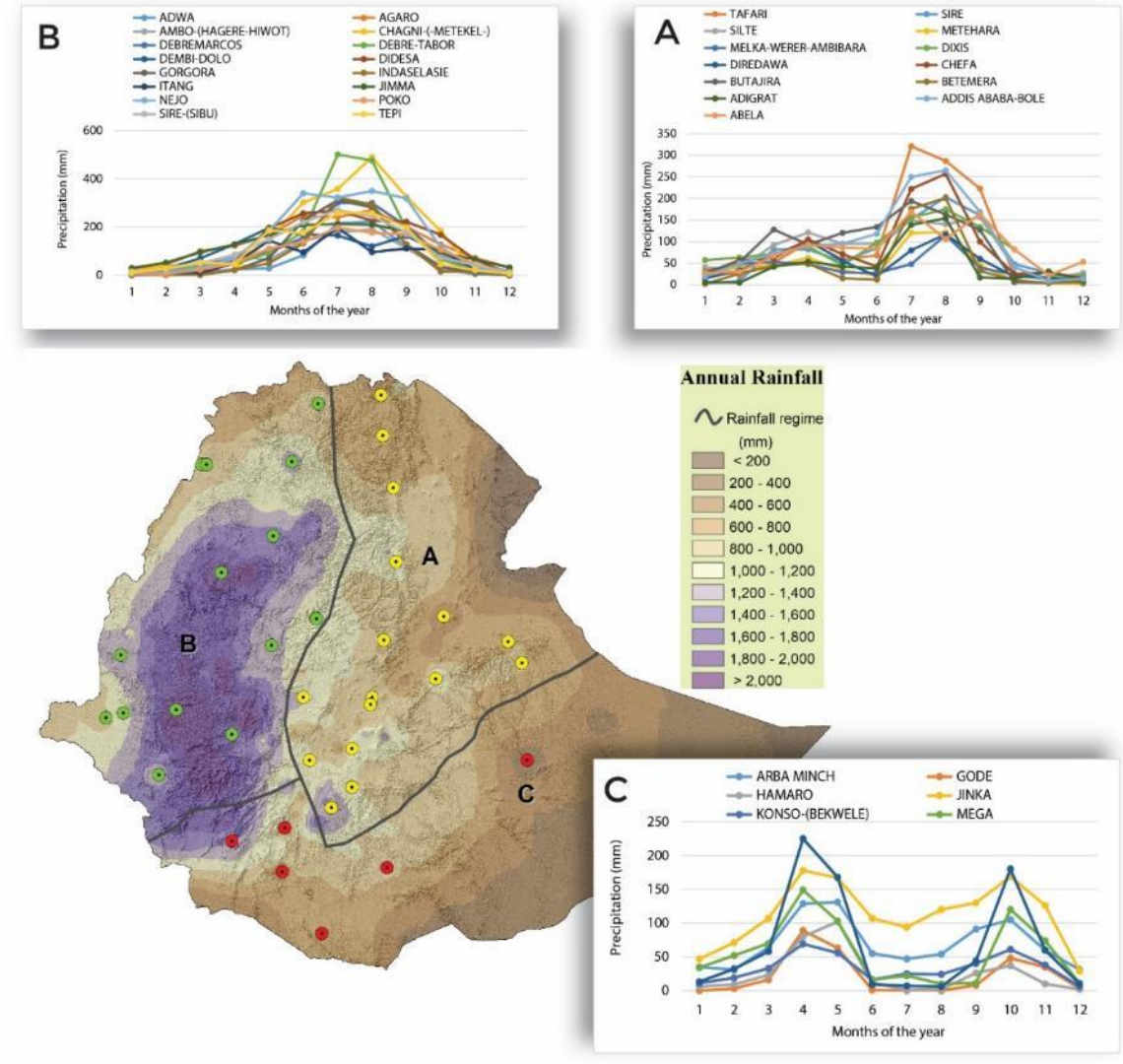

Figure 3.3: Annual rainfall distribution and spatio – temporal rainfall regimes in the study area.

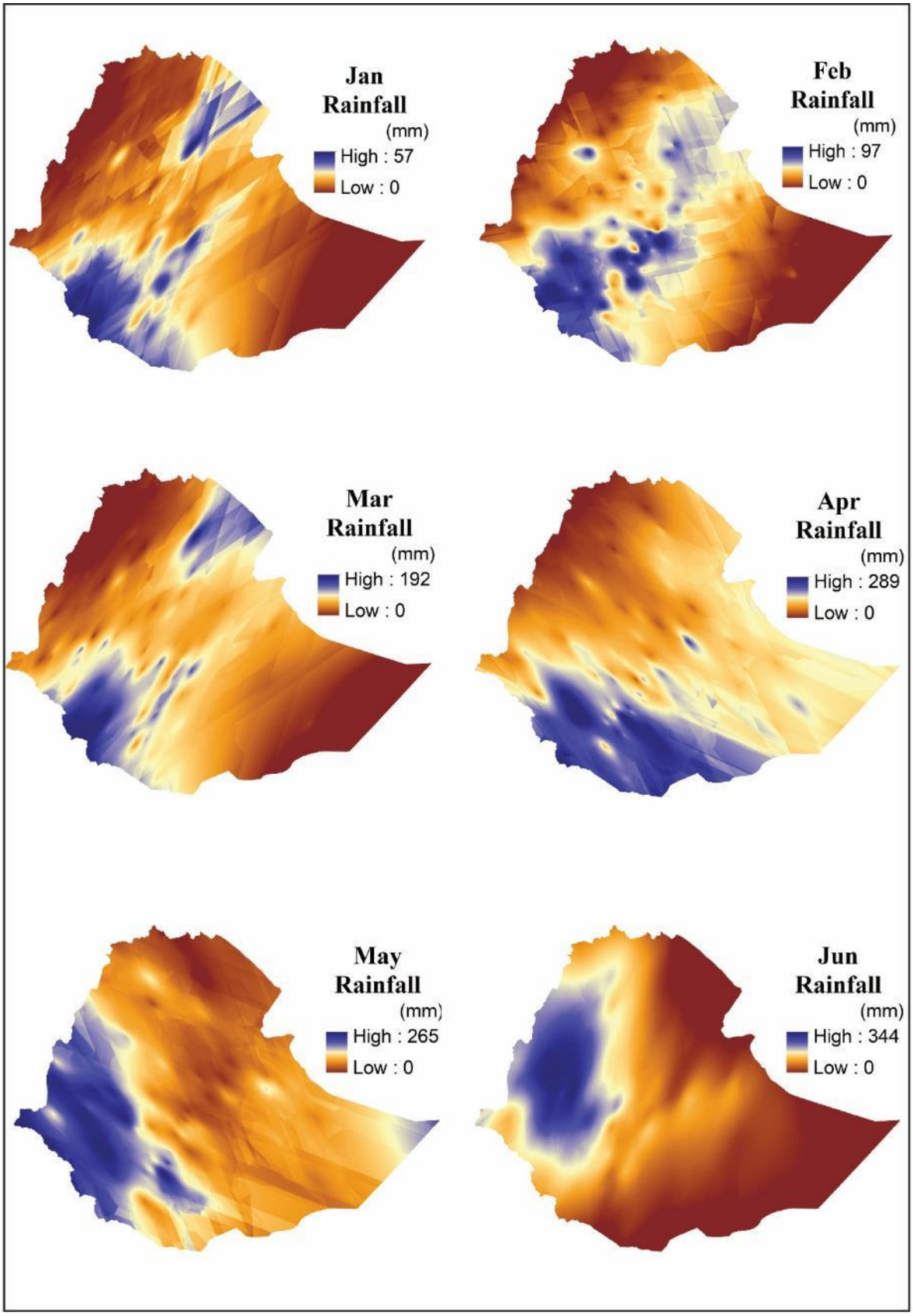
Jan
Rainfall
(mm)
High : 57
Low : 0
Feb
Rainfall
(mm)
High : 97
Low : 0
Mar
Rainfall
(mm)
High : 192
Low : 0
Apr
Rainfall
(mm)
High : 289
Low : 0
May
Rainfall
(mm)
High : 265
Low : 0
Jun
Rainfall
(mm)
High : 344
Low : 0

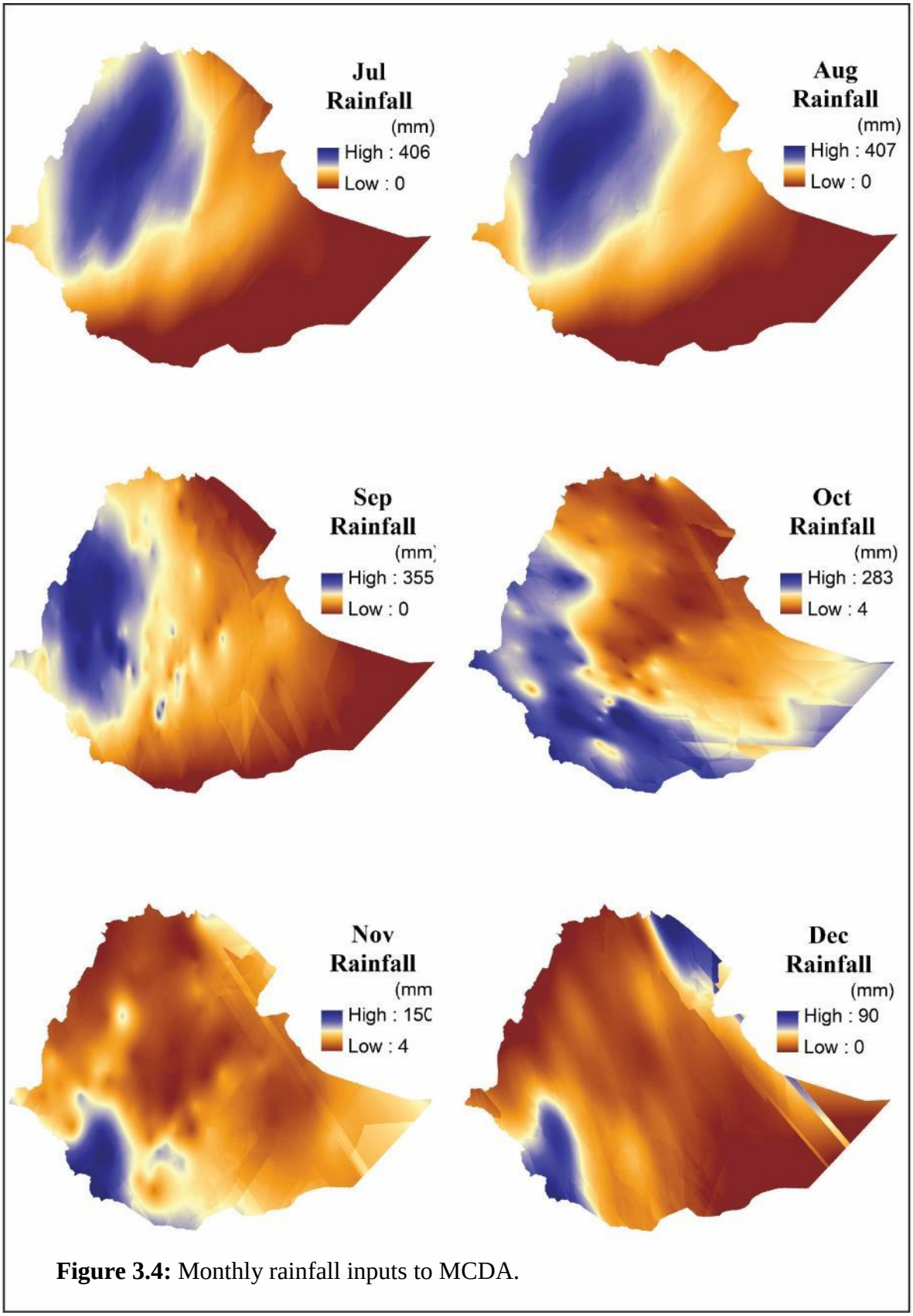

Figure 3.4: Monthly rainfall inputs to MCDA.

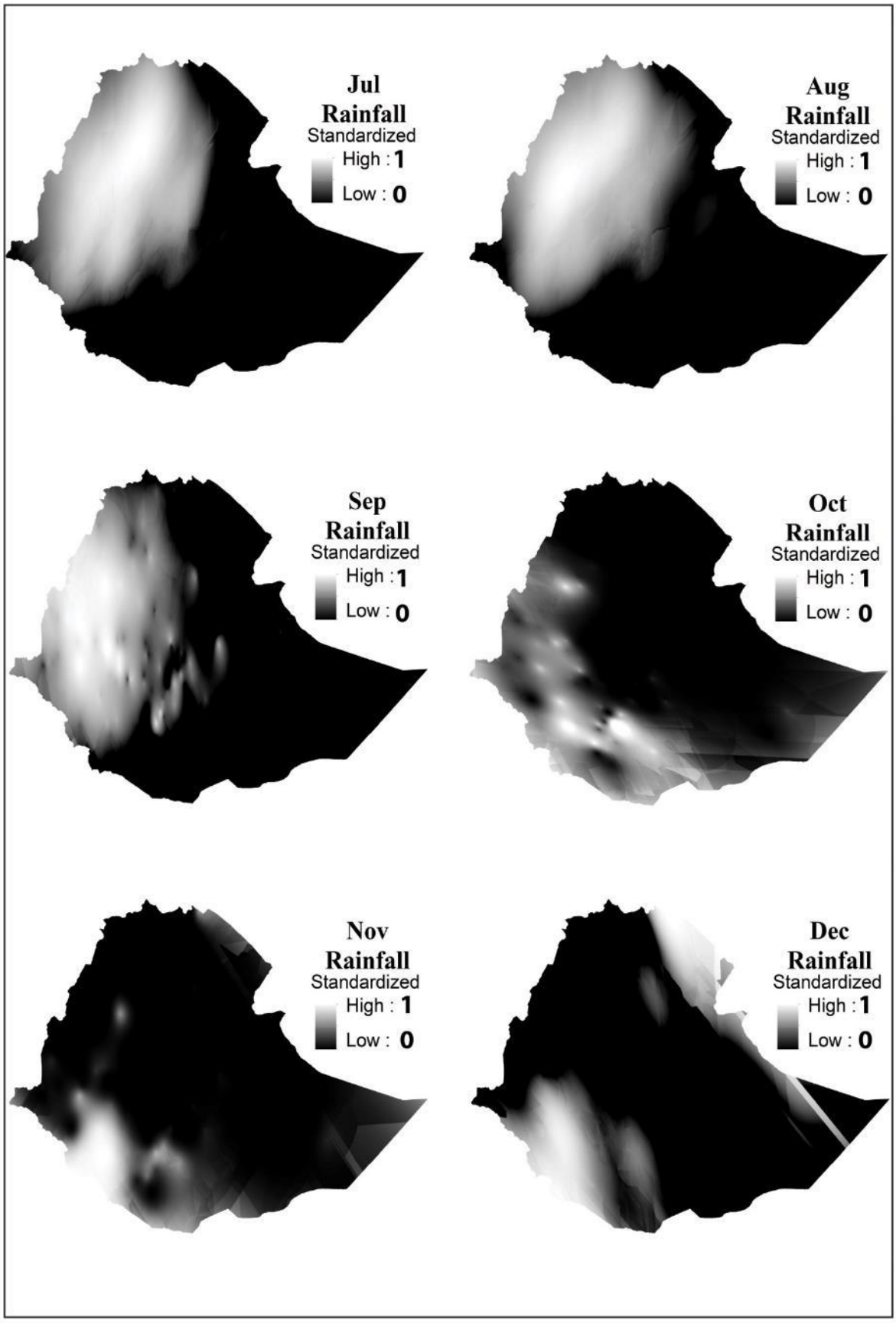
Jul
Rainfall
Standardized
High : 1
Low : 0
Aug
Rainfall
Standardized
High : 1
Low : 0
Sep
Rainfall
Standardized
High : 1
Low : 0
Oct
Rainfall
Standardized
High : 1
Low : 0
Nov
Rainfall
Standardized
High : 1
Low : 0
Dec
Rainfall
Standardized
High : 1
Low : 0

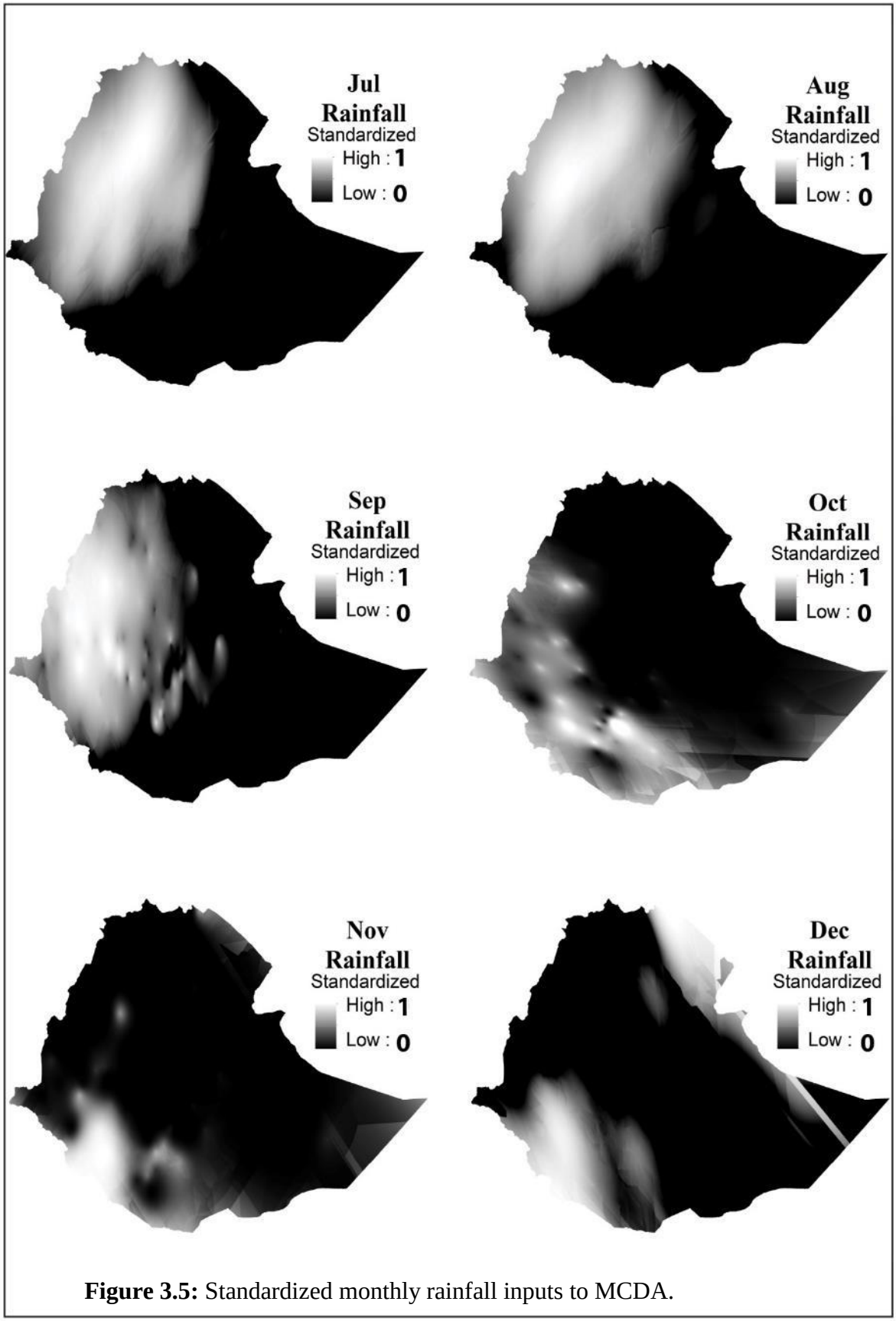

Figure 3.5: Standardized monthly rainfall inputs to MCDA.

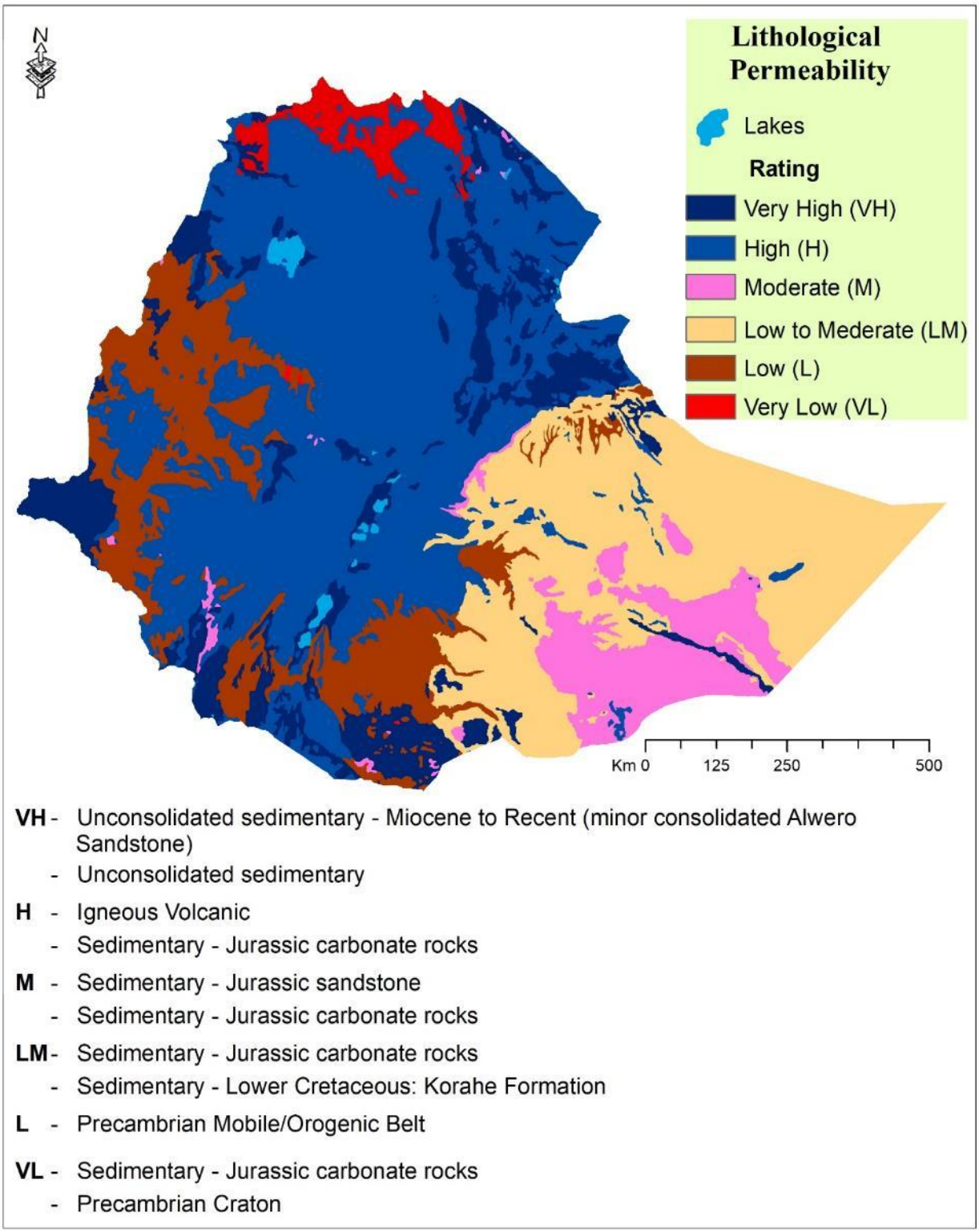

Figure 3.6: Lithological input to MCDA.

This study used the 'SoilGrids250m' dataset (Hengl et al., 2017). This dataset is preferred to the other available datasets not only because it has soil texture attribute but also due to its finer resolution (250m) and easily manageable preparation. The dataset, implementing the United States Department of Agriculture (USDA) system of soil classification, shows four dominant textural classes in the study area: Clay, Clay Loam, Sandy Clay Loam and Loam (Figure 3.8). The Clay and Clay Loam textural classes dominantly occupy the highlands whereas the Sandy Clay Loam textural class occupy the northern and south eastern part of the country. The rift valley and northern part of the country is dominantly occupied by the Loam texture.

The dataset is transformed to the standardized range of the model, which is between 0 and 1, by using the ArcGIS software. The standardized value of 1 represents the coarsest soil texture in the study area, and 0 the finest (Figure 3.9).

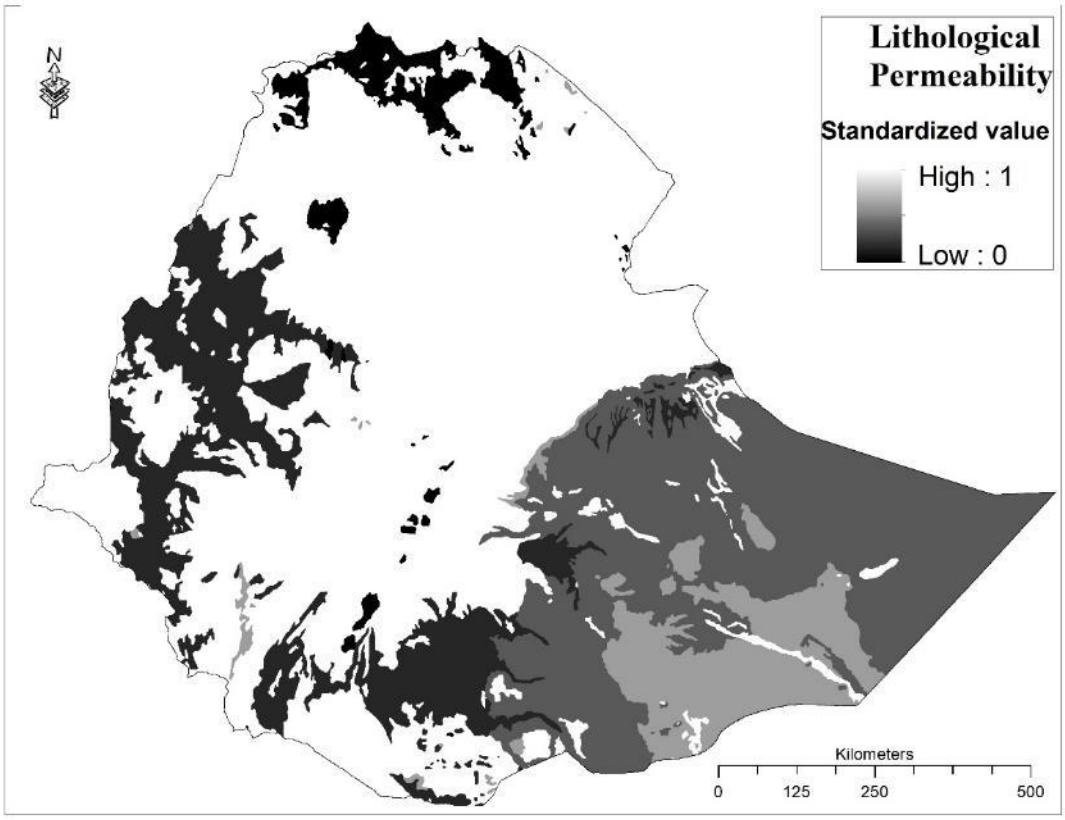

Figure 3.7: Standardized lithological input to MCDA.

3.3.1.4. Lineament Density

Lineament density is the total length of linear geological structures within a square unit area. As linear geological structures are among the types of void spaces in which groundwater is stored and flows, high density of lineament in an area can indicate high groundwater recharge potential. The study area possesses a lot of geological structures that are formed by different geological processes since Precambrian. Among them, the NNW – SSE trending structures that were formed by the East African Orogeny in Precambrian, multiply oriented structures that were formed by the rifting process along with the rifted basins (Ogaden, Blue Nile and Karoo) in Paleozoic, and the N-S to NE-SW oriented structures that were formed by the East African Rift system in Cenozoic are the dominant and densely populated geological structures in the study area (GSE, 1996).

Figure 3.10 depicts the geological structures that are identified through extensive field investigation and the application of GIS and remote sensing techniques (GSE, 1996). As the figure shows, the Afar depression, broadly rifted zone, and Main Ethiopian Rift (MER) are areas where the highest lineament density is observed.

The dataset was transformed to the standardized values, which is between 0 and 1, by using the fuzzification process in ArcGIS. 1 represents areas with highest density lineament whereas 0 with lowest density (Figure 3.11).

3.3.1.5. Land use/Land cover (LULC)

Overland flow in different LULC classes encounters different overland-flow resistance since each LULC class has unique textural and compositional setting (Bergkamp, 1998). Higher overland-flow resistance favors higher quantity of groundwater infiltration in an area. Usually, overland flow in forest LULC types is slower than that in bare lands since forest LULC types generate higher flow resistance due to greater vegetation coverage (Prosser et al., 1995; Dunkerly, 2003). Taking groundwater infiltration into consideration, a general categorization of LULC classes into four groups is possible: Vegetation, bare lands, impervious surfaces and water bodies (Batelaan and Smedt, 2001). Obviously, water bodies are groundwater discharge points where groundwater infiltration barely occur. Similarly, at impervious surfaces, due to low porosity, groundwater infiltration is minimum. Bare lands include rocky surfaces and soil surfaces without vegetation.

The LULC dataset used in this analysis was obtained from Water and Land Resource Center (WLRC), and according to the dataset, ten major LULC classes were identified (Figure 3.12). The dataset was standardized to the MCDA by the fuzzy membership tool in ArcGIS (Figure 3.13) (Table 3.4). The forest LULC was standardized to the value of 1 implying an excellent condition for groundwater infiltration. On the other hand, the standardization rate of 0 was given to water bodies implying a minimum occurrence of infiltration.

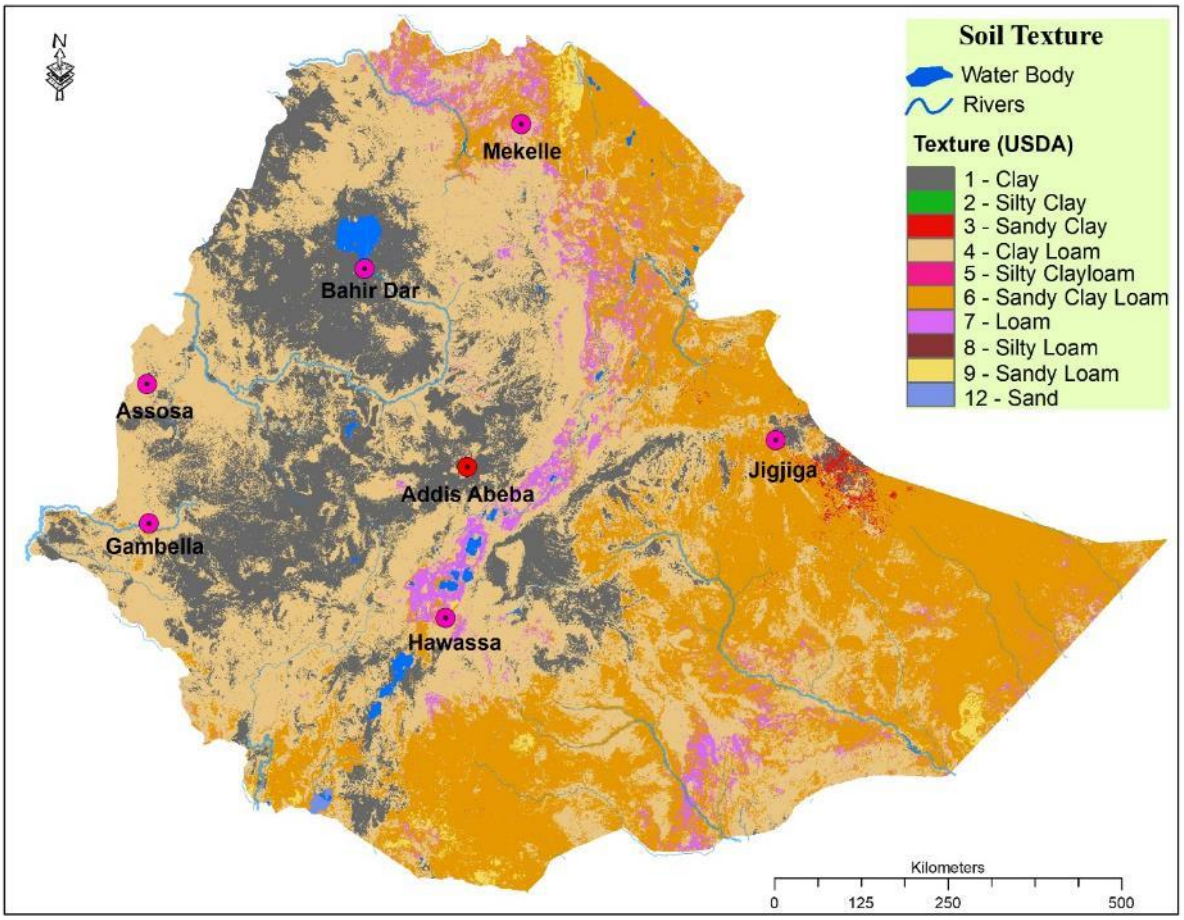

Figure 3.8: Soil texture input to MCDA.

3.3.1.6. Slope

Slope is a physical variable that can characterize ground surfaces in terms of resistance to overland-flow provided that the other factors remaining constant. Overland-flow on surfaces having higher slopes encounters lower resistance from surface roughness features so that it usually has shorter infiltration time than on lower slopes, indicating less favorable condition for the occurrence

groundwater infiltration. Rodier and Ribstein (1988) showed an increase of runoff coefficient from 0.25 to 0.30 for a growth of slope by 5%.

The slope data of the country is calculated from the 30 m spatial resolution DEM of SRTM by the slope tool in ArcGIS (Figure 3.14). The quality of the data was assessed by making a comparison with the 250,000 topographic map of the Ethiopian Mapping Agency (EMA), and showed no significant discrepancy. The data shows a slope range between 0 and 77 degrees. Lower degree slopes are flat tops of the highlands, floor of the rift, and the low lands of the peripheral part of the country radially adjoined with the highland. High slopes on the other hand are dominantly the highland margins, the rift margin, and the lineament scarps.

The dataset is standardized to the common scale of the model (0 to 1) by the fuzzy membership tool in ArcGIS. One represents areas with the lowest slope, zero with the highest slope (Figure 3.15).

Land use classes		*Area (%)*	*Characteristics*	*Fuzzy membership*
Vegetated	Forest	10	Higher overland-flow resistance so that groundwater infiltration is more facilitated.	0
	Woodland	24.5		
	Shrub land	24.5		
	Cropland	20		
	Grassland	10		
Bare land	Bare land	10.4	Lower overland-flow resistance due to absence of vegetation.	
Impervious	Settlement	0.2	Absence of groundwater recharge due to absence of porosity.	
Waterbody	Wetland	0.4	It is rather a discharge area.	
	Waterbody			1

Table 3.4: Infiltration ratings to the different LULC classes in the study area.

3.3.1.7. Drainage Density

Drainage density is defined as the total length of drainage channels per square unit area (Horton, 1945). Areas with high drainage density tend to have high surface runoff. Conversely, areas with lower drainage densities can be characterized as recharge areas.

The dataset of the drainage network of the study area is obtained from the WLRC EthioGIS II dataset collections, and its drainage density was calculated by using the Line Density tool in ArcGIS (Figure 3.16). The dataset was transformed to the common standardization range of values (0 to 1) by ArcGIS. One represents recharge areas (lower drainage density areas), zero discharge areas (higher drainage density areas) (Figure 3.17).

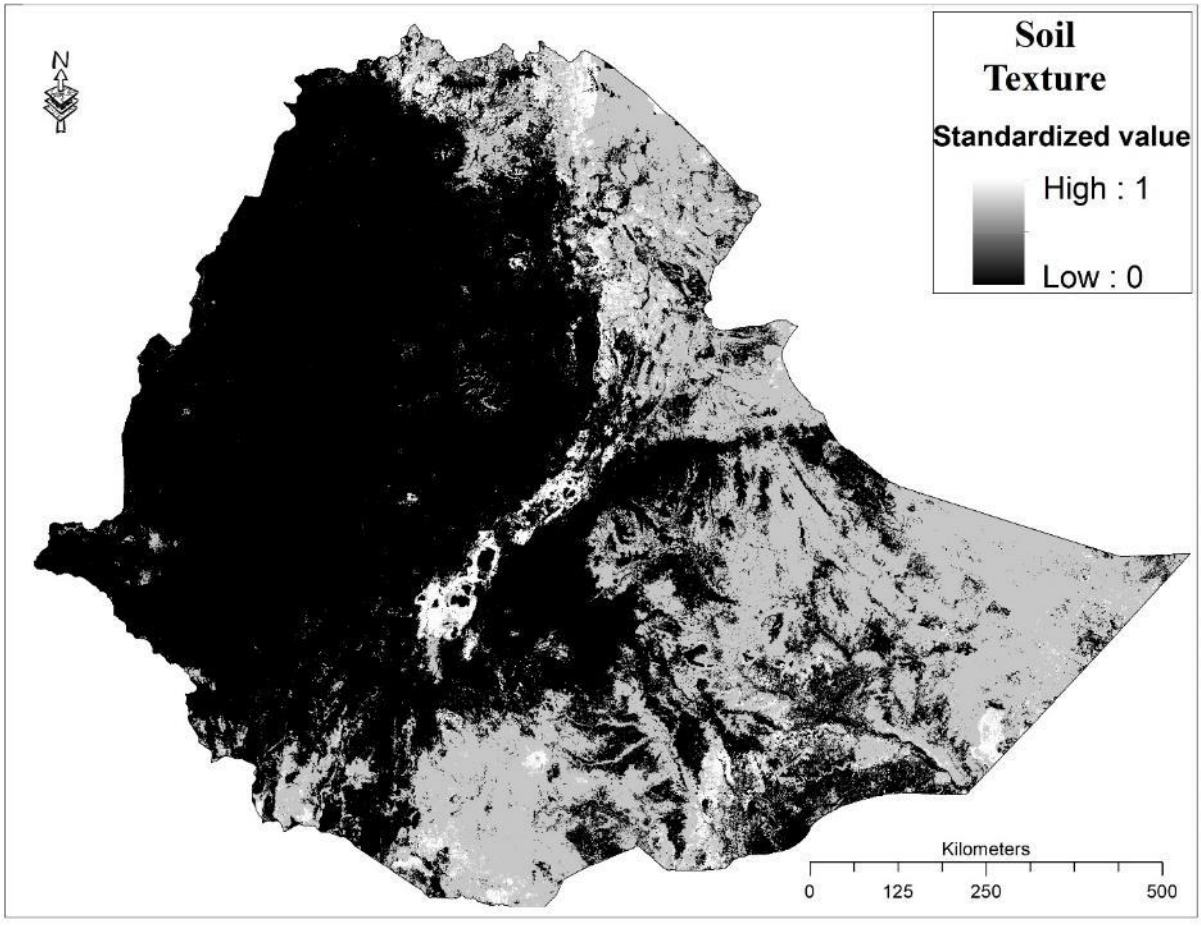

Figure 3.9: Standardized soil texture input to MCDA.

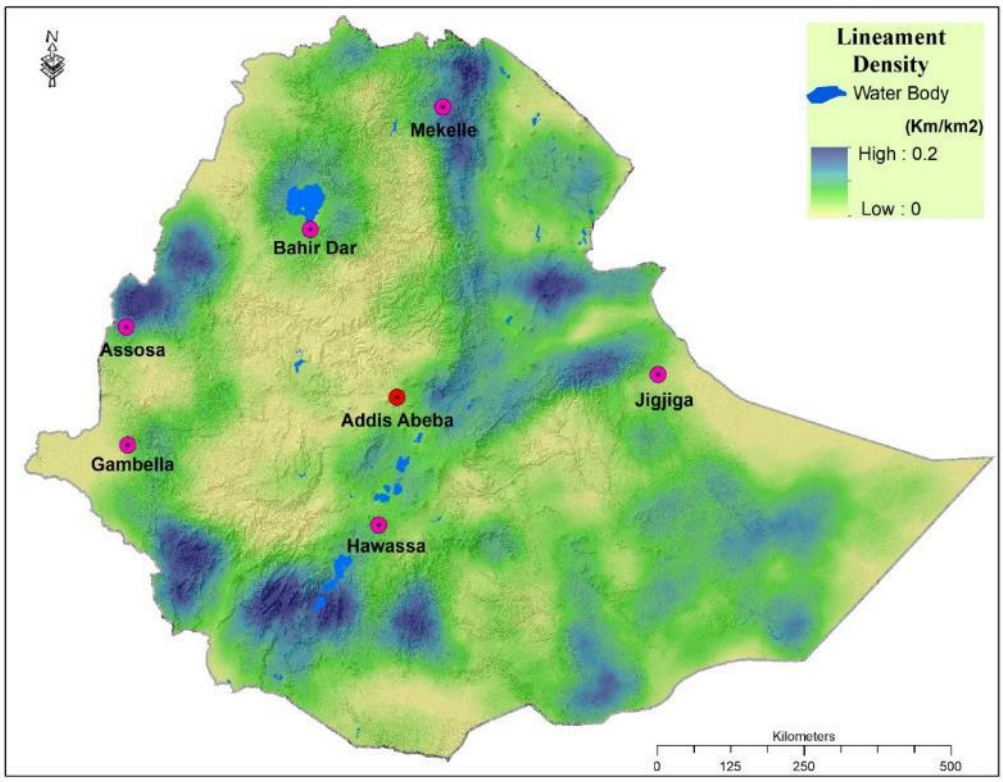

Figure 3.10: Lineament density input to MCDA.

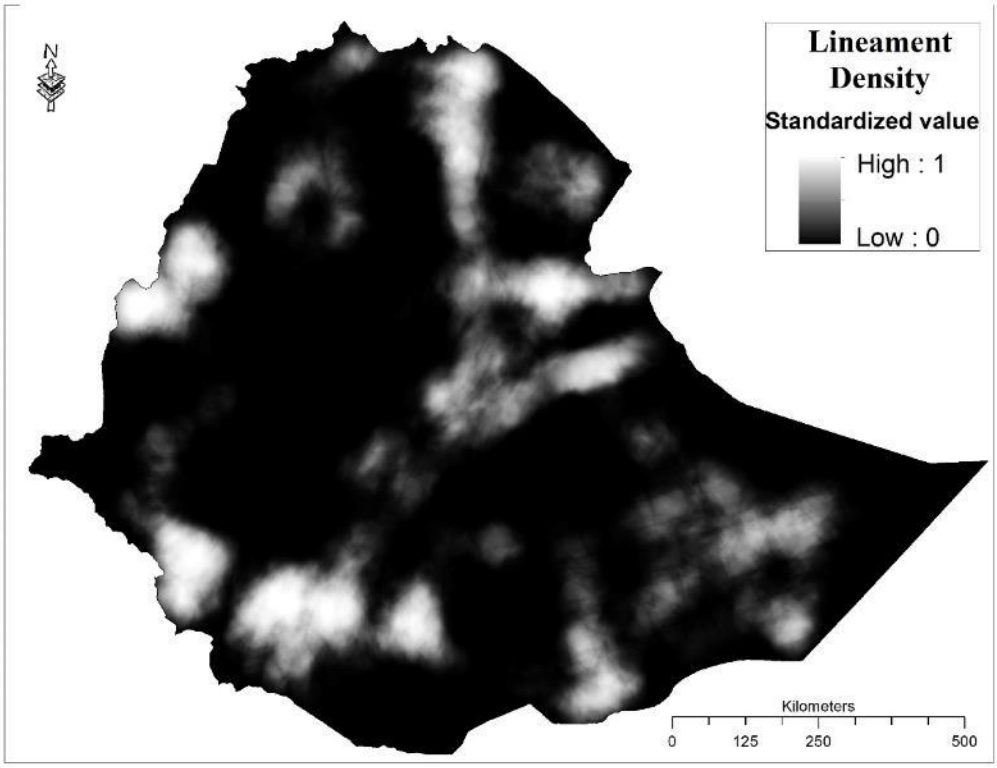

Figure 3.11: Standardized lineament density input to MCDA.

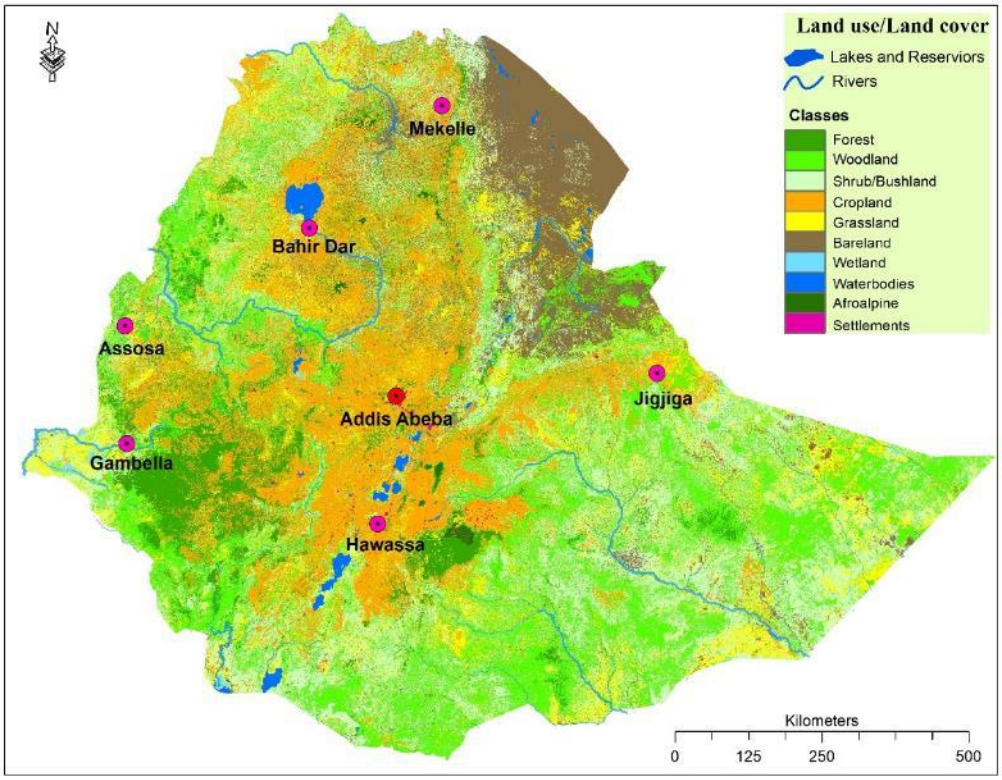

Figure 3.12: LULC input to MCDA.

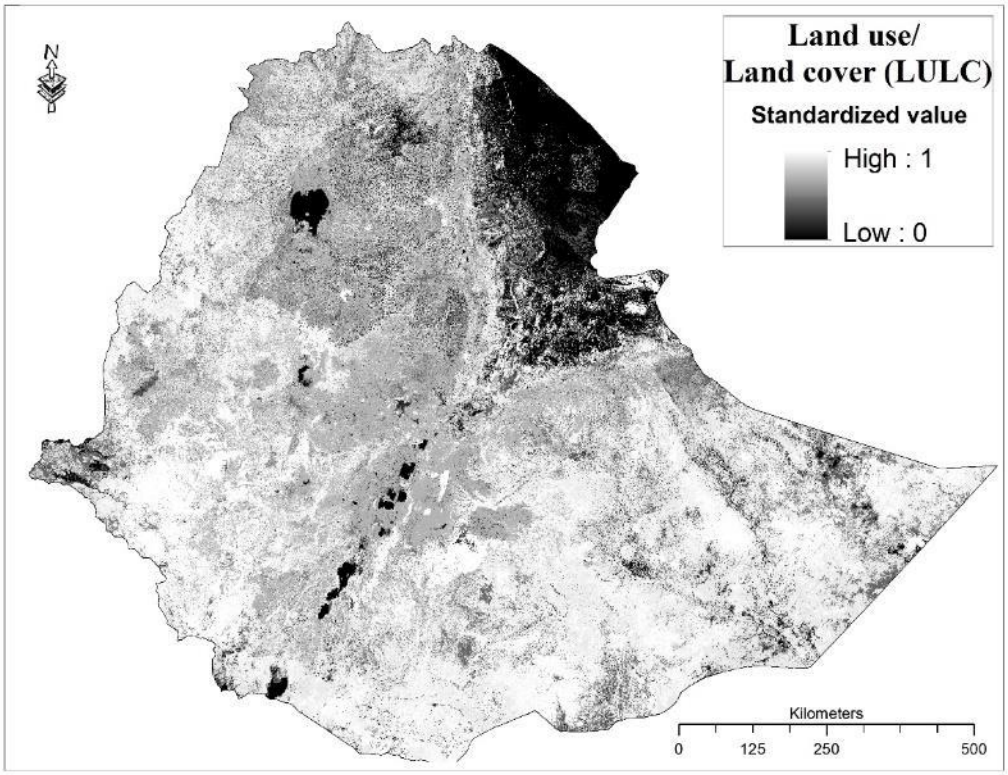

Figure 3.13: Standardized LULC input to MCDA.

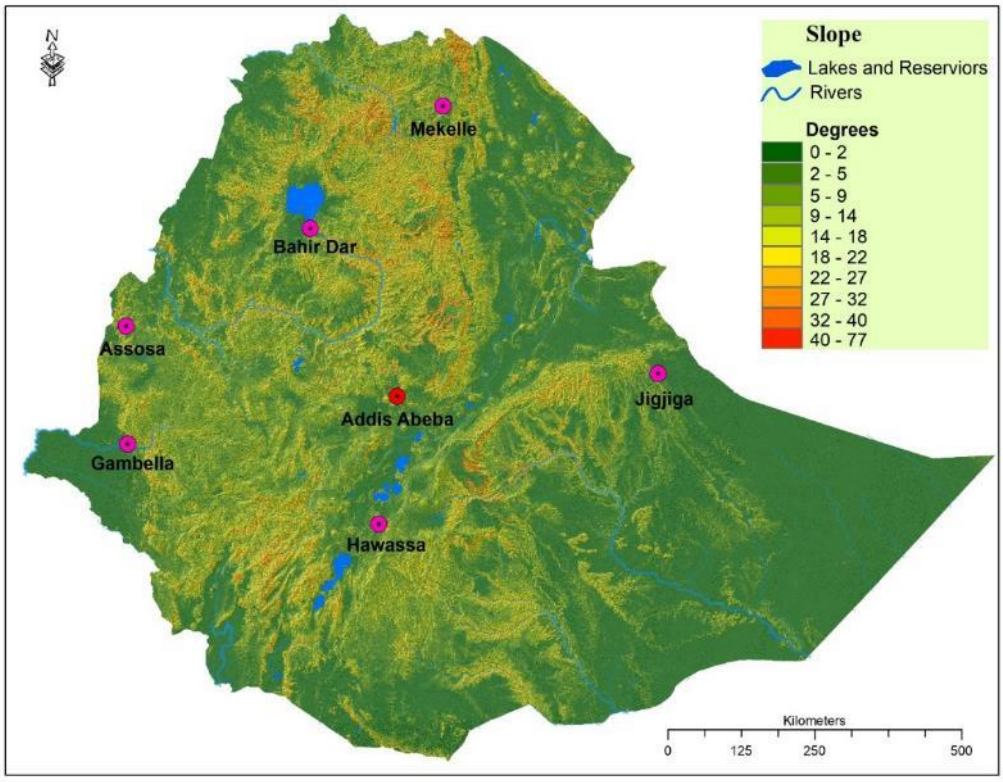

Figure 3.14: Slope input to MCDA.

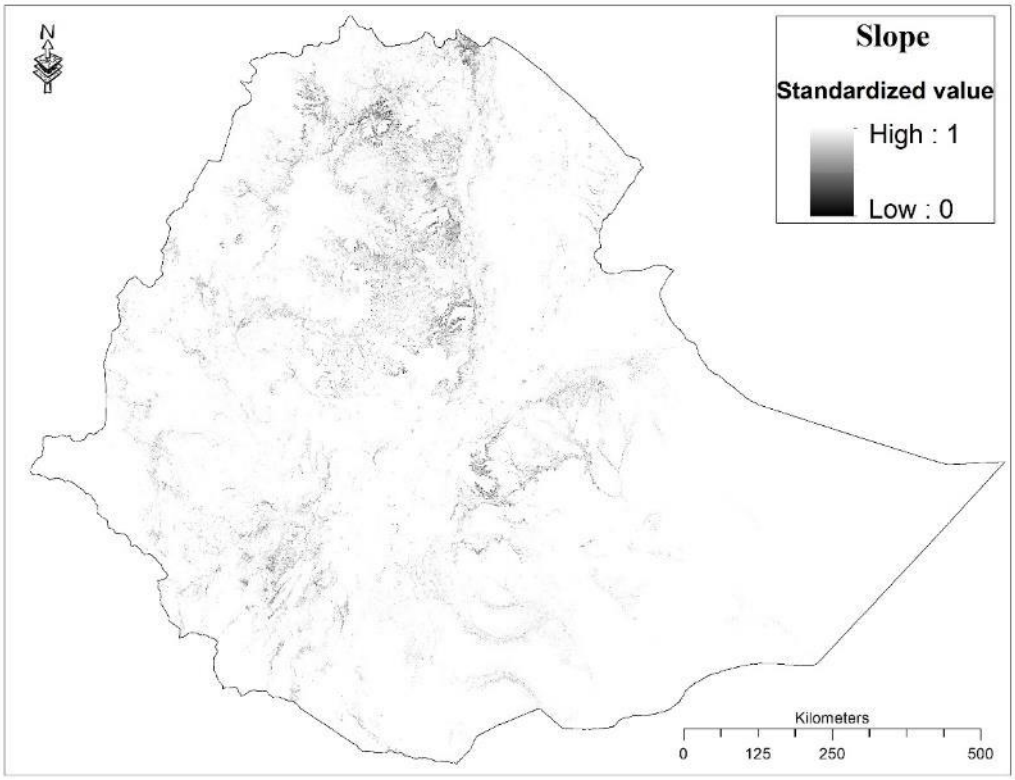

Figure 3.15: Standardized slope input to MCDA.

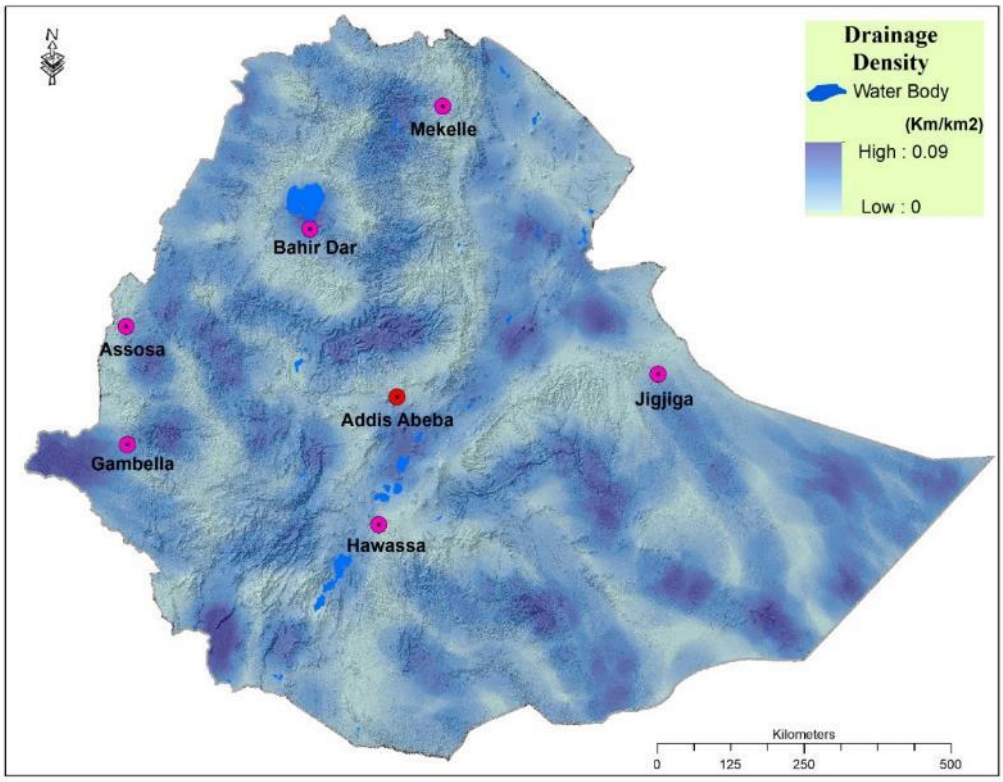

Figure 3.16: Drainage density input to MCDA.

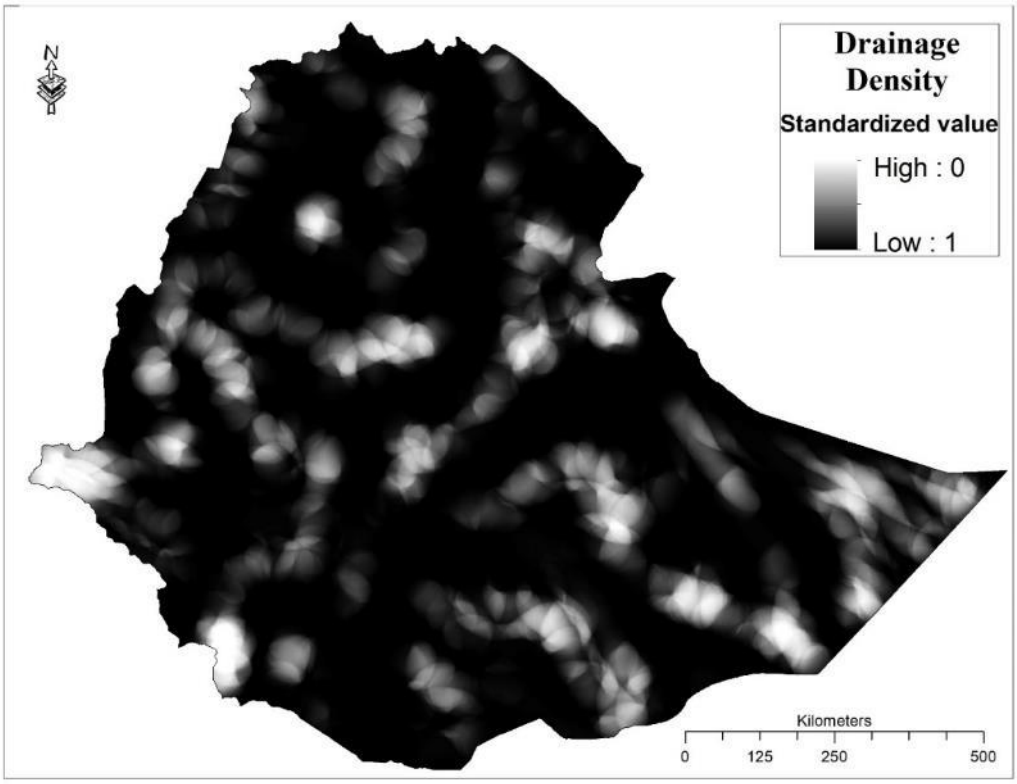

Figure 3.17: Standardized drainage density input to MCDA.

3.3.2. The Pairwise Comparison and weight assignment

Although the pairwise comparison method is a subjective decision process, findings from other professionals were included in the decision process from literatures to minimize personal biases (Yeh et al., 2009; Senanayake et al., 2016; Selvam et al., 2015; Saraf et al., 2004). According to the pairwise comparison and weight assignment that was carried out on the factors, it is the rainfall factor (41.16%) that has the highest weight of controlling groundwater recharge in the study area (Table 3.6). Following that are LULC (22.34%) and soil texture (14.71%) respectively. The lowest influential factor was found to be drainage density (2.49%).

3.3.3. Combining the factors

The factors that control groundwater recharge in the study area were combined according to the assigned weight by the overlay tool in ArcGIS. The combination operation was performed for each of the months; the only dynamic variable across the months was the rainfall. The combination operation resulted a conceptual model of groundwater recharge that shows both temporal and spatial recharge characteristics in the study area (Figure 3.18).

	Rainfall	*Lulc*	*Soil*	*Lithology*	*Lineament Density*	*Slope*	*Drainage Density*	*Weight*
Rainfall	1	3	4	5	7	8	9	0.4116
Lulc	1/3	1	2	3	5	6	7	0.2234
Soil	¼	1/2	1	2	3	5	6	0.1472
Lithology	1/5	1/3	1/2	1	3	4	5	0.1042
Lineament Density	1/7	1/5	1/3	1/3	1	2	3	0.0535
Slope	1/8	1/6	1/5	1/4	1/2	1	2	0.0353
Drainage Density	1/9	1/7	1/6	1/5	1/3	1/2	1	0.0248
							Consistency Ratio (CR) = 0.03	

Table 3.5: The pairwise comparison among the input variables and relative weight of each input variables.

3.4. Result and Discussion

This study implemented MCDA to develop a conceptual model of groundwater recharge to the study area. The MCDA resulted a groundwater recharge conceptual model that showed recharge characteristics both in the spatial and temporal domain (Figure 3.18). The temporal characteristics of the model was represented by the long term monthly outputs of MCDA. The spatial characteristics, on the other hand, was represented by the relative recharge potential in each pixel in each monthly output.

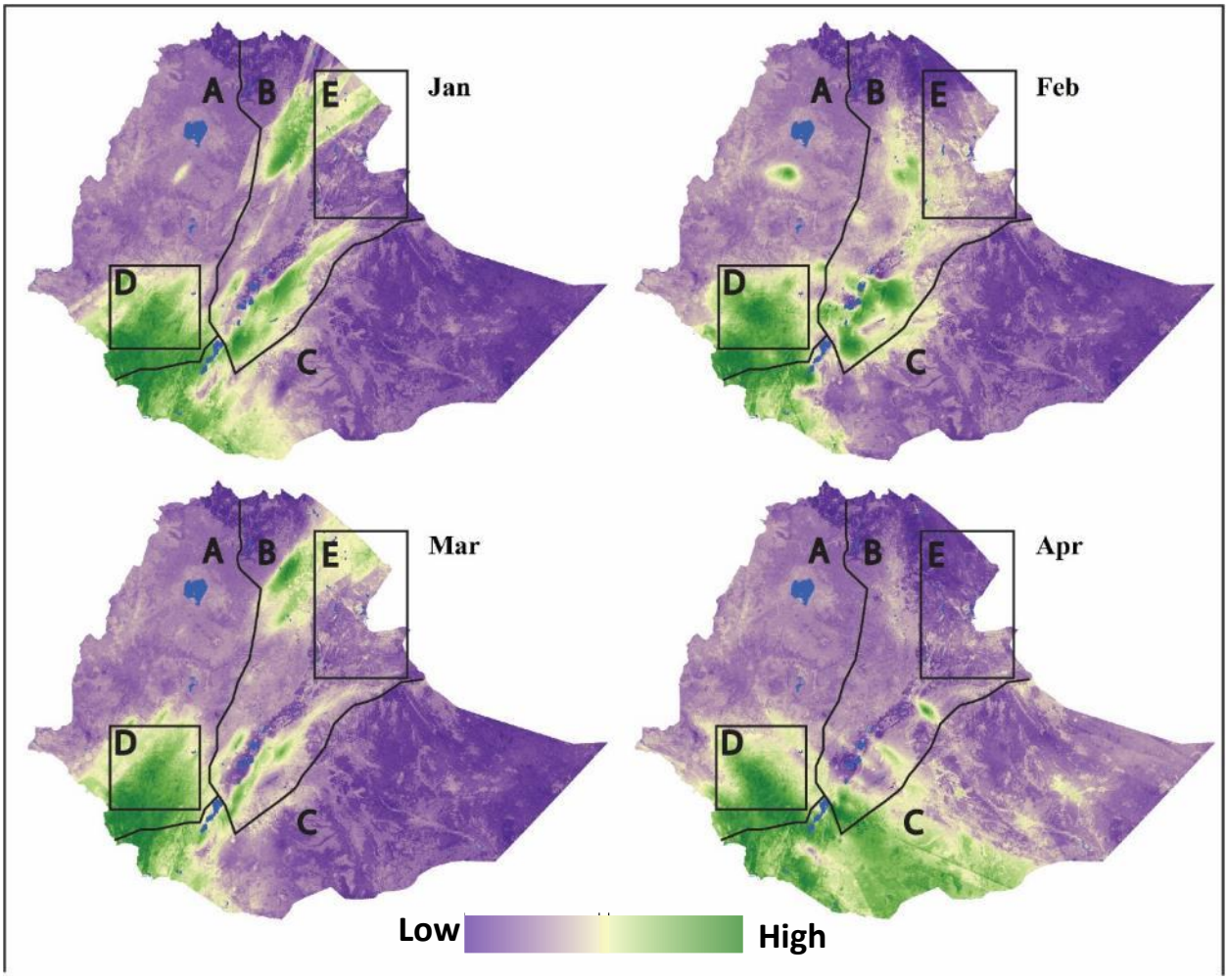

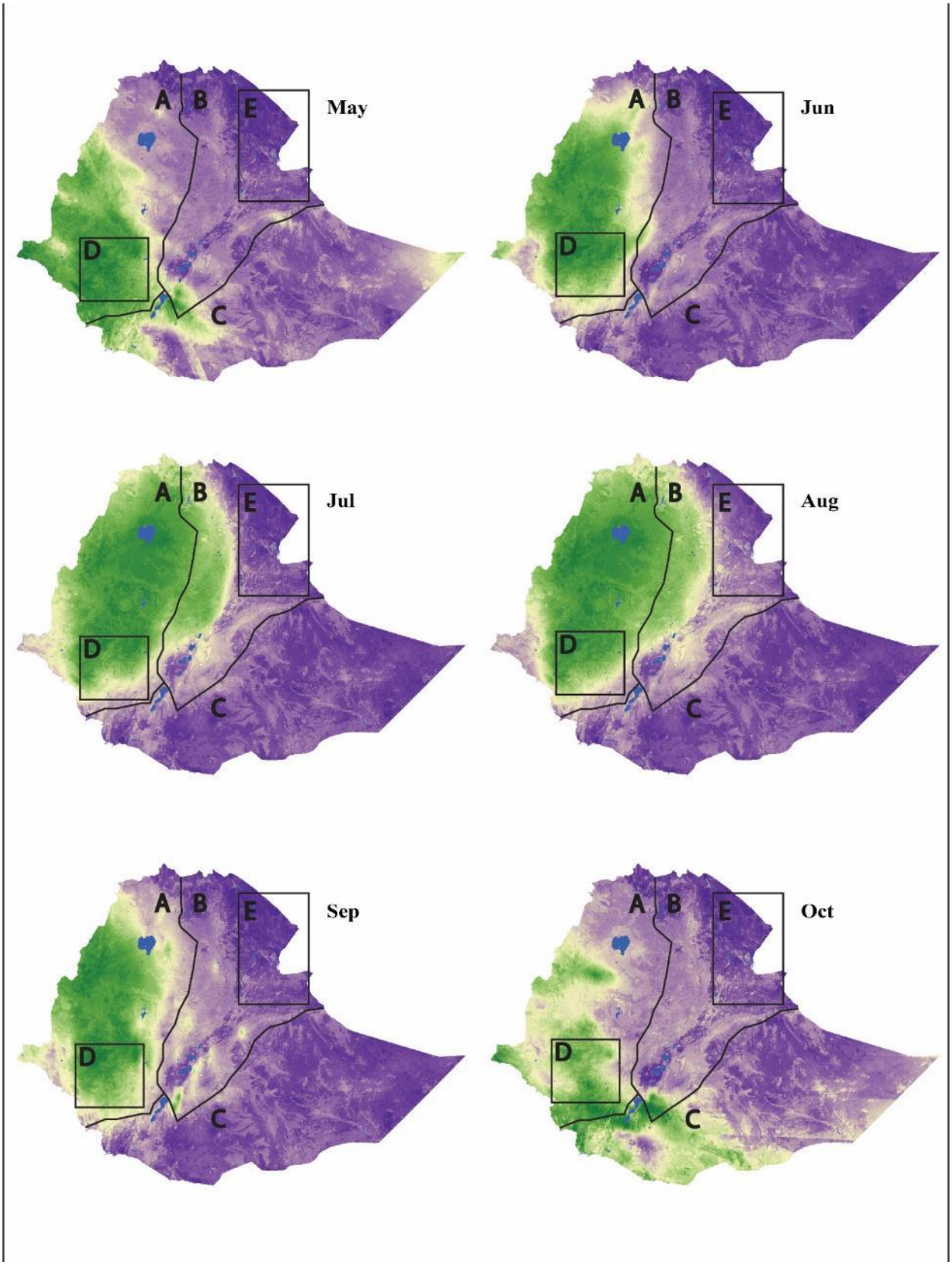
A
B
E
May
D
C
A
B
E
Jun
D
C
A
B
E
Jul
D
C
A
B
E
Aug
D
C
A
B
E
Sep
D
C
A
B
E
Oct
D
C

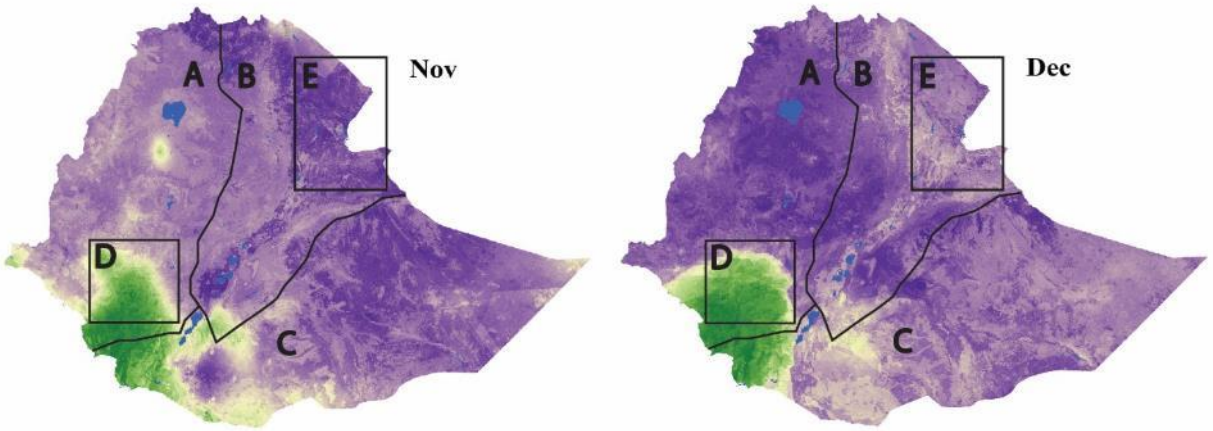

Figure 3.18: Spatial and temporal characteristics of the conceptual model of groundwater recharge of the study area.

3.4.1. Temporal groundwater recharge characteristics in the study area.

The model showed a temporal variability of groundwater recharge in each cell (Figure 3.18). Among the input variables of the MCDA, because it was the rainfall factor that was varying across the months of the year, the temporal variability of groundwater recharge in the study area could be attributed to the control of the rainfall factor. Thus, the temporal pattern of groundwater recharge potential in the country followed that of the rainfall. Hence, the western part of the country (labelled "A" in Figure 3.18) showed unimodal monthly pattern, having peak recharge potentials from February up to November whereas the northern, central and eastern part of the country (labelled "B" in Figure 3.18) showed two high recharge potential periods, from June to September and from March to May, of which the former was higher. On the other hand, the southern and the southeastern part of the country (labelled "C" in Figure 3.18) showed a strictly bimodal pattern, higher recharge potential from February to May and from October to November. Apart from that, some areas such as Goro (labelled "D" in Figure 3.18), and the Afar depression (labelled "E" in Figure 3.18), due to their specific rainfall characteristics, showed specific groundwater recharge patterns. The former areas, because they receive large amount of rainfall for longer period, showed higher groundwater recharge potential almost throughout the year. Conversely, the latter areas, because they receive a little rainfall in their rainy period, showed lower groundwater recharge potential for longer period.

3.4.2. Spatial groundwater recharge characteristics in the study area

The conceptual model, like the temporal pattern, showed high spatial variation of groundwater recharge in the study area. To understand the degree of influence that the input factors have on the spatial characteristics of groundwater recharge, the Cramer's correlation (Eastman, 1999) test was carried out between the input factors and the annual recharge potential dataset (the annual recharge potential dataset is the sum of all the monthly recharge potential datasets). The Cramer's correlation can be applied on images that have nominal values, and its coefficient ranges between 0 and 1 in which 0 represents absence of overlap between two images and 1 perfect overlap. The input factors and the annual recharge potential datasets were reclassified into equal number of classes by the reclassify tool in ArcGIS. Then, the Cramer's V correlation coefficients were determined by the CROSSTAB tool in IDRISI32 (Eastman, 1999).

According to the correlation test (Table 3.6), the most important factor in determining the spatial variation of groundwater recharge in the study area was found to be the rainfall. Thus, it was due to their high rainfall that some specific areas such as Goro in southwestern part of the country showed high groundwater recharge potential. The mean annual rainfall in Goro is more than 2000 mm (Fazzini, Bisci and Billi, 2015). Conversely, it was due to their low annual rainfall that the Afar depression and Ogaden areas showed low groundwater recharge potential.

	Conceptual Model
Drainage Density	0.3244
Lineament Density	0.322
Slope	0.3202
Soil texture	0.4315
Land use/Land cover	0.3234
Rainfall	0.4435
Lithology	0.3908

Table 3.6: Cramer's V correlation coefficient between the annual MCDA result (annual conceptual model map) and annual input variables to MCDA.

Next to the rainfall factor, the soil texture was found to be the most important factor in determining the spatial variation of groundwater recharge in the study area (Table 3.6). However, unlike what is expected theoretically, groundwater recharge potential decreased as soil texture increased in the study area. Thus, areas with the finest soil texture class exhibited the highest potential recharge. As Figure 3.19 shows, the reason to that could be attributed the influence of rainfall since the finest soil texture class constitutes the high rainfall receiving areas.

According to the correlation, slope has the least influence on groundwater recharge in the study area.

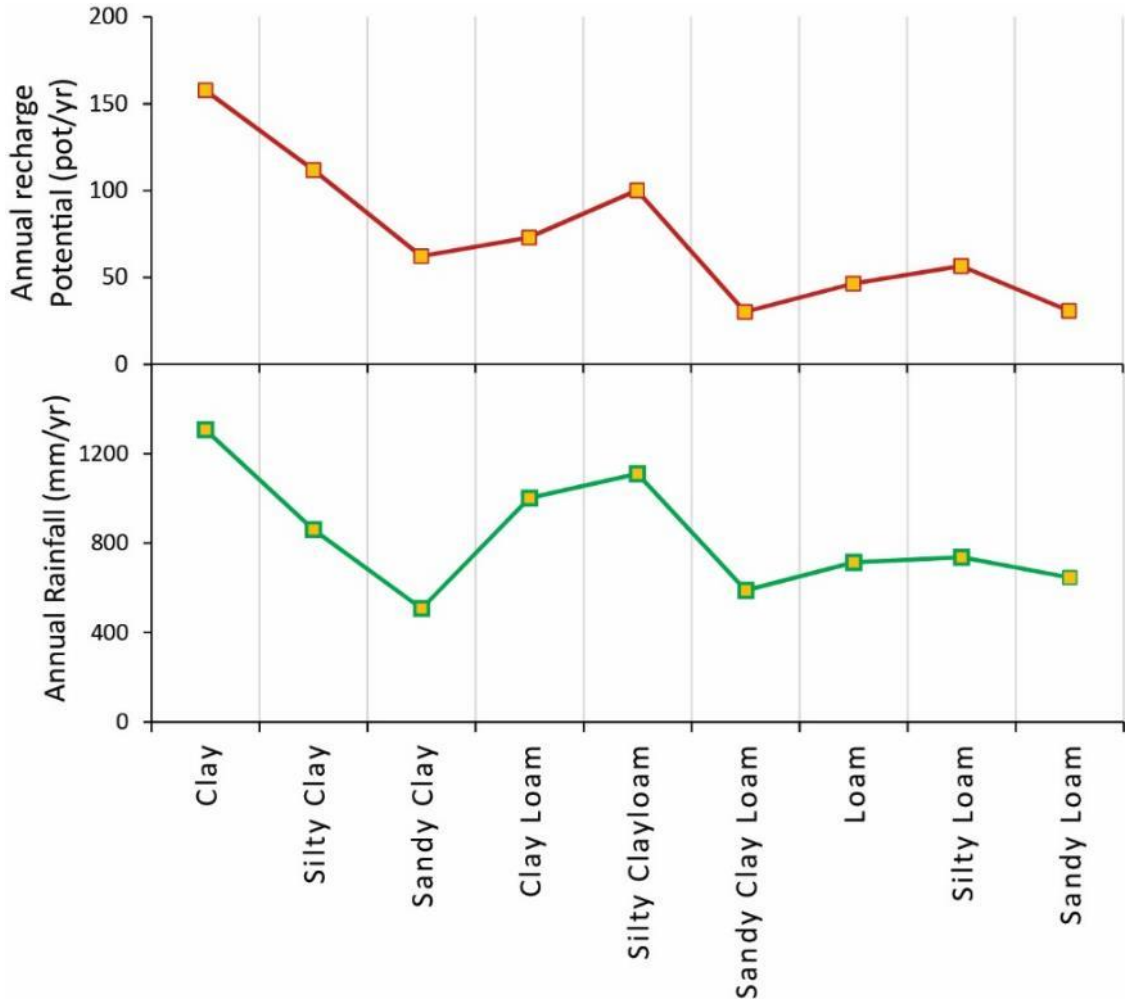

Figure 3.19: Annual rainfall and groundwater recharge potential in each of the soil texture classes.

3.4.3. Selecting appropriate estimation methods

The conceptual model of groundwater recharge developed for the study area showed high spatial and temporal variation. This variation was resulted from the spatial and temporal variation of the input variables (Figure 3.3 up to Figure 3.17). Thus, the methods that would be selected to estimate groundwater recharge in the study area should have the capability to consider the spatial and temporal variation of groundwater recharge in the study area. As Healy and Scanlon (2010) recommends, selection and application of recharge estimation methods in an area has to be preceded and guided by development of a conceptual model of groundwater recharge.

Since modelling methods are based on the water balance equation, they are generally universal and adaptable so that they are unbounded by attributes such as area limitation and recharge mechanism. Similarly, the chloride mass balance and base flow separation methods have universal and adaptable characteristics since they can be applied in areas where their input data are available. Thus, the WetSpass-M model, recursive digital filter base flow separation, chloride mass balance methods were found to be appropriate for capturing the characteristics of rate of groundwater recharge in the study area.

CHAPTER FOUR

4. GROUNDWATER RECHARGE ESTIMATION BY USING WETSPASS-M MODEL

4.1. Introduction

Advancements in remote sensing, geographical information system (GIS), and computing systems have enormously supplemented data production and distribution as well as model development in many disciplines (Li *et al*., 2009; Geza and McCray, 2008; Chen *et al*., 2005). Although models oversimplify reality so that they might result wrong outputs, if used with appropriate procedures, they can produce better estimations than conventional methods alone do, and be applied over larger spatial extents and temporal domains to analyze trends and make forecasts.

WetSpass is the acronym for the model name "Water and Energy Transfer between Soil, Plants and Atmosphere under quasi Steady State". It is a distributed water balance model that estimates groundwater recharge, actual evapotranspiration and surface runoff for an area. Batelaan and Smedt (2001) first developed WetSpass for estimating long term average groundwater recharge in an area having humid temporal condition. It was also applied for estimating actual evapotranspiration and surface runoff in an area (Batelaan and Smedt, 2007). Asefa et al (2000) and Batelaan et al (2000) applied it in scenario modelling to simulate the impact of land use/land cover (LULC) change on groundwater recharge and discharge in Grote-Nete river basin, Belgium. Rossum et al., (2001) applied the WetSpass model to assess the hydrological characteristics of Kikbeek sub-basin, Belgium. Moreover, several studies have been conducted by using the WetSpass model for different kinds of purposes in different climatic zones (Gebreyohannes *et al*., 2013; Armanuos *et al*., 2016; Tilahun and Merkel, 2009; Meresa and Taye, 2018; Wang *et al*., 2012; Gebremeskel and Kebede, 2017; Kahsay *et al*., 2019; Zhang *et al*., 2017).

Originally, WetSpass was designed to estimate groundwater recharge at seasonal time step, but as more refined input datasets become available due to the advancements in remote sensing and GIS capabilities, WetSpass has been upgraded to WetSpass-M to accommodate estimation at monthly step by Abdollahi et al (2017). Unlike the previous version which was scripted in Avenue and implemented as an extension in ArcView-GIS, this version of the model is scripted in IronPython v2.7 (open-source implementation of Python for Microsoft.NET Framework v4.0, www.ironpython.net) and is made to be a standalone model. It uses the Hydrology and Hydraulic Programming Library (H2PL) developed by Abdollahi (2015). Apart from the refined temporal capability, this version of the model runs faster and has the capacity of handling larger area (Abdollahi et al., 2017).

4.2. Working principle of WetSpass-M model

WetSpass-M is a distributed model and calculates the water balance of an area by accounting the water and energy transfer among soil, plants and atmosphere. Thus, it first requires an optimal spatial resolution to be set to the model based on the characteristics of each of the input datasets, and the preparation of parameter lookup tables for certain input variables. In the model, each raster cell is subdivided into fractions of four major land use/cover (LULC) types for the purpose of water balance computation: Vegetated area, bare-soil, open-water, and impervious area. The Vegetation LULC class represents all the vegetation types in the study area such as forests, shrubs, woodlands, croplands and so on. The Bare-soil LULC class represents land covers of un-vegetated and bare soil types. The Open water LULC represents all surface water bodies including lakes, rivers, reservoirs and so on. Impervious land cover types dominantly refer human made constructions in urban areas and land cover types that have the lowest infiltration.

The input datasets of the model are land use/land cover (LULC), soil texture, elevation, slope, groundwater depth and climate data (rainfall, potential evapotranspiration and temperature). Among the input datasets, some of them such as LULC, soil texture, elevation, and slope are essentially single frequency input variables whereas the climatic variables are monthly input variables. Lookup tables are prepared for LULC and soil texture.

The water balance of the study area is calculated by summing the water balance calculations for each cell in the order of calculating interception, runoff, evapotranspiration, and recharge

respectively. Additionally, each input datasets of the model, has to be prepared with the same spatial coordinate system and spatial resolution, and each cell of the input datasets has to perfectly overlap each other. The water balance equation is given as follows (Equation 3.1):

$$ET_{raster} = a_v ET_v + a_a ET_s + a_o ET_o + a_i ET_i$$

$$S_{raster} = a_v S_v + a_a S_s + a_o S_o + a_i S_i$$

$$R_{raster} = a_v R_v + a_a R_s + a_o R_o + a_i R_i \quad (3.1)$$

Where ET_{raster}, S_{raster}, and R_{raster} are the total evapotranspiration, surface runoff, and groundwater recharge of a raster cell respectively, and a_v, a_a, a_o, and a_i are ratios of vegetated, bare-soil, open-water and impervious area components respectively.

4.2.1. Interception

Interception is defined as the part of rainfall retained on vegetation surfaces and evaporated back to the atmosphere without falling to the ground surface (Hamilton and Rowe, 1949). Thus, interception varies with land use/land cover (LULC) types since each LULC types have different leaf area indices (LAI). Interception is determined in the model by the following Equation (3.2):

$$I_m = P_m I_R \quad (3.2)$$

Where I_m is interception (mm/month), P_m is monthly precipitation (mm/month), and I_R is interception ratio which in turn is given by Equation (3.3) (De Groen and Savenije, 2006) :

$$I_R = \frac{I_m}{P_m} = 1 - \exp\left(\frac{-I_D dp}{P_m}\right) \quad (3.3)$$

Where dp is the number of rainy days per month (day/month) and I_D is the daily interception threshold that depends on LULC (Sutanto et al. 2012) (Equation 3.4):

$$I_D = aLAI\left(1 - \frac{1}{1 + \frac{P_m[1-exp(-0.463LAI)]}{aLAI}}\right) \quad (3.4)$$

Where a is the interception parameter, determined by calibrating with observed surface runoff. Sutanto et al (2012) determined for a clipped grass to be 4.5. According to De Groen and Savenije (2006), the amount of interception in an area can be determined by calculating the daily

interception threshold. If the amount of rainfall in the area is below the threshold, then the specified threshold is considered as an interception, otherwise, the interception is determined by using the Equation (3.4). Because each LULC type has different leaf area index, the determination of the daily interception threshold to an area is controlled by LULC types (Simunek et al., 2008).

4.2.2. Surface runoff

Runoff is estimated by using rational method that includes two coefficients (Equation 3.5): C_{sr} and C_h. C_h is the coefficient of soil moisture condition and C_{sr} is the actual runoff coefficient.

$$SR_m = C_{sr} C_h (P_m - I_m) \tag{3.5}$$

The coefficient of soil moisture designates the amount of runoff generated over an area due to soil moisture condition (Behremand et al., 2007) and is given by the following Equation (3.6).

$$C_h = \left(\frac{\theta_s}{\theta_{sat}}\right)^b \tag{3.6}$$

Where θ_s is soil moisture content (m^3/m^3), θ_{sat} is soil porosity (m^3/m^3), and b defines the relationship between C_h and soil moisture content. When $b = 1$, the relationship is linear. Although Equation (3.6) can be used to capture the effect of soil moisture on surface runoff, it is difficult to find monthly soil moisture data. Therefore, C_h is determined by the equation of evaporative efficiency ratio that incorporates the effect of precipitation and potential evapotranspiration (Equation 3.7 and 3.8) (Zhang and Lindstrom, 1997; Guntner et al., 1999; Creutzfeldt et al., 2010) into the adapted method of Turc (1955) at monthly scale (Pistocchi et al., 2008).

$$C_h = \frac{P_m}{LP(P_m^{\alpha} + ET_m^{\alpha})^{\frac{1}{\alpha}}} \text{ if } ET_m > P_m \tag{3.7}$$

$$C_h = 1 \quad \text{if } ET_m \leq P_m \tag{3.8}$$

Where LP and α are calibration parameters that regulate an overestimation of surface runoff in arid and semi-arid areas by controlling the potential evapotranspiration depending on the soil moisture condition. The default values of LP and α are 0.65 and 1.5 respectively (Abodollahi et al, 2017).

The actual runoff coefficient is determined by combining the coefficients estimated for permeable (C_{per}) and impermeable (C_{Imp}) parts. The potential runoff coefficient for the permeable part is calculated from the weighted sum of land use, soil, and slope factors as given by the Equation (3.9):

$$C_{per} = w1\left(\frac{0.02}{n}\right) + w2\left(\frac{\theta_w}{1-\theta_w}\right) + w3\left(\frac{S}{10+S}\right) \quad (3.9)$$

where n is the Manning's roughness coefficient, and its value varies according to LULC type (Kalyanapu et al., 2010; Dhakal et al., 2011), θ_w is the volumetric soil water content at wilting point (Saxton and Rawls, 2006; USDA-NRCS, 1993), and S is the land surface slope in percentage. $w1$, $w2$ and $w3$ are the weights for the three components contributing to C_{per}. In the original WetSpass model, the weight combination of $w1 = 0.4$, $w2 = 0.3$, and $w1 = 0.3$ has been found acceptable; therefore, it is adopted in this model too. The manning coefficient, soil moisture at wilting point, and slope parameter values are supplied to the model as parameter look up tables.

The weighted potential runoff coefficient (C_{wp}) for a specific grid cell is, therefore, calculated by dividing a grid cell into permeable and impermeable surfaces as given in the Equation (3.10):

$$C_{wp} = \left(1 - \frac{A_{Imp}}{100}\right) C_{per} + \frac{A_{Imp}}{100} C_{Imp} \quad (3.10)$$

where C_{Imp} is the potential runoff coefficient of the impervious area; it is obtained from Nationwide Urban Runoff Program (NURP US EPA 1983) according to the relationship between impervious areas and runoff coefficient. A_{Imp} is the percentage of impervious surface per grid cell.

The actual runoff coefficient is determined by incorporating the effect of rainfall depth into the potential runoff coefficient, and adjusting C_{wp} by the average daily rainfall in rainy days [$\bar{P}_{24}$ (mm/day per month)] (Critchley and Siegert 1991; Merz et al. 2006). It is given by Equation (3.11).

$$C_{sr} = \frac{C_{wp}\bar{P}_{24}}{C_{wp}\bar{P}_{24} - RCD \times C_{wp} + RCD} \quad (3.11)$$

Where RCD [regional consecutive dryness level (mm)] represents the intensity of rain and the number of consecutive rainy days. RCD ranges between 1 and 10. One represents very heavy or torrential rainfall and more than 10 consecutive rainy days per month, and ten represents a low

regional intensity rainfall and less than 2 consecutive rainy days per month. No adjustment is needed if the rainfall is less than the RCD range; in this case $C_{sr} = C_{wp}$.

Monthly volumetric runoff is calculated by incorporating the effect of surface storage in Equation (3.12):

$$Q_{(t)} = xQ_{(t-1)} + 0.001(1-x)ASR_m \quad (3.12)$$

where x is delay factor (values range between 0–1), $Q_{(t)}$ volumetric runoff of the current month, $Q_{(t-1)}$ volumetric runoff of the previous month (m3/month) contributing to the current month and A is area (m2). The constant 0.001 is applied for unit conversion.

4.2.3. Evapotranspiration

WetSpass-M estimates actual evapotranspiration from potential evaporation and reference transpiration. Reference transpiration (T_{rv}) is calculated from potential evapotranspiration (ET_p) and vegetation coefficient (c) by using Equation (3.13):

$$T_{rv} = cET_p \quad (3.13)$$

A vegetation coefficient is given by (Equation 3.14):

$$c = \frac{1+\frac{\gamma}{\Delta}}{1+\frac{\gamma}{\Delta}\left(1+\frac{r_c}{r_a}\right)} \quad (3.14)$$

Where γ is the psychrometric constant (KPa/^{o}C), which is the gradient of the first derivative of saturated vapor pressure curve (slope of saturation vapor pressure at the temperature of atmosphere), r_c (bulk) surface resistance (s m^{-1}), and r_a aerodynamic resistance (s m^{-1}) (Equation 3.15).

$$r_a = \frac{1}{K^2 U_a Z_a}\left(ln\left(\frac{Z_a - Z_d}{Z_0}\right)\right)^2 \quad (3.15)$$

where K is the von Karman constant (0.41), U_a (m/s) is the wind speed at elevation Z_a (m), Z_d is zero displacement elevation (m), and Z_0 is the aerodynamic roughness height of surface (m).

In vegetated groundwater discharge areas, due to the insignificant effect of soil surfaces and an abundance of water, the reference transpiration is equal to the potential evapotranspiration – meaning that the vegetation coefficient is equal to 1. However, in vegetated areas where groundwater is below groundwater level, actual transpiration (T_v) is given by Equation (3.16):

$$T_v = \left(1 - a_1^{w/T_{rv}}\right) T_{rv} \tag{3.16}$$

where a_1 is a calibrated parameter (adopted from WetSpass) that is related to the sand content of the soil type, and w is the available water for transpiration that is defined by Equation (3.17):

$$w = P_m + \left(\theta_{fc} - \theta_{pwp}\right) R_d \tag{3.17}$$

where R_d is the rooting depth, $\theta_{fc} - \theta_{pwp}$ is the plant available water content per time step, stated as the difference in water content at field capacity and at permanent wilting point.

4.2.4. Recharge

The groundwater recharge (R_m) calculation takes place at the last step of the modelling process, and it is determined as a residual term in the water balance equation given by the Equation (3.18).

$$R_m = P_m - SR_m - ET_m \tag{3.18}$$

The estimated monthly groundwater recharge is incorporated in the calculation of the volumetric base flow ($Q_{b(t)}$) which is given by Equation (3.19):

$$Q_{b(t)} = \beta Q_{b(t-1)} + 0.001 N_m (1 - \beta) \emptyset R_m \tag{3.19}$$

where β is a storage parameter (between 0 and 1), $Q_{b(t-1)}$ is the base-flow from the previous month (m^3/month), N_m is number of days per month, and $\emptyset$ (m2/day) is the recharge contribution parameter to the current base flow. For a grid cell area A (m^2) and the recession index k (day), the recharge contribution parameter is given as Equation (3.20) (after Arnold and Allen 1999):

$$\emptyset = \frac{1.15A}{k} \tag{3.20}$$

The model provides the monthly volumetric runoff and base flow estimates as a text file for calibration purpose.

4.3. The input Data of the WetSpass-M model

The input data of the WetSpass-M model are land use/land cover (LULC), soil texture, slope, groundwater depth, and climate variables (precipitation, temperature, potential evapotranspiration and wind speed). To integrate the input datasets for the estimation of water balance of the study area, the model first requires each of the datasets to perfectly overlap each other, by having the same coordinate system and spatial resolution. The spatial resolution of the model was calculated from the average of all the spatial resolutions of the input datasets, and accordingly, it was found to be 250 meters (Table 4.1). The input datasets are obtained from different organizations (Table 4.1) and largely span in the time range between 2000 and 2018.

Dataset	*Time period*	*Resolution (m)*	*Source*
Rainfall	2000-2018	250	NMA + FAO/New_LocClim_1.10
LAI	2000-2018	500	NASA LP DAAC at the USGS EROS Center
GW depth	2002-2018	5500	BGS & NASA-USDA SMAP Global Soil Moisture Data
Temperature	2000-2018	110	NMA + FAO/New_LocClim_1.10
PET	2000-2018	110	NMA + FAO/New_LocClim_1.10
Wind speed	2000-2018	110	NMA + FAO/New_LocClim_1.10
Land use /Land cover	2016	30	WLRC
Elevation	2014	30	NASA SRTM
Slope	2014	30	NASA SRTM
Soil	2008	250	AfSIS

Table 4.1: WetSpass-M input datasets with their time span, resolution, and source**.**

4.3.1. Slope

The slope of the study area is calculated from the DEM of the NASA SRTM (3 arc-second [90 m by 90 m]) by the slope tool of ArcGIS. The quality of the data was assessed by making a comparison with the 250,000 topographic map of the Ethiopian Mapping Agency (EMA). The assessment showed that there is no significant discrepancy between the datasets. The slope map (Figure 4.1) shows that the study area has a slope range between 0 and 77 degrees, 77% of which is below 9 degrees and largely constitutes the low lands in the rift and peripheral parts of the country. On the other hand, the higher slopes constitute the edges that formed the rift escarpments, the highlands, and deeply incised gorges in the highlands (Figure 4.1).

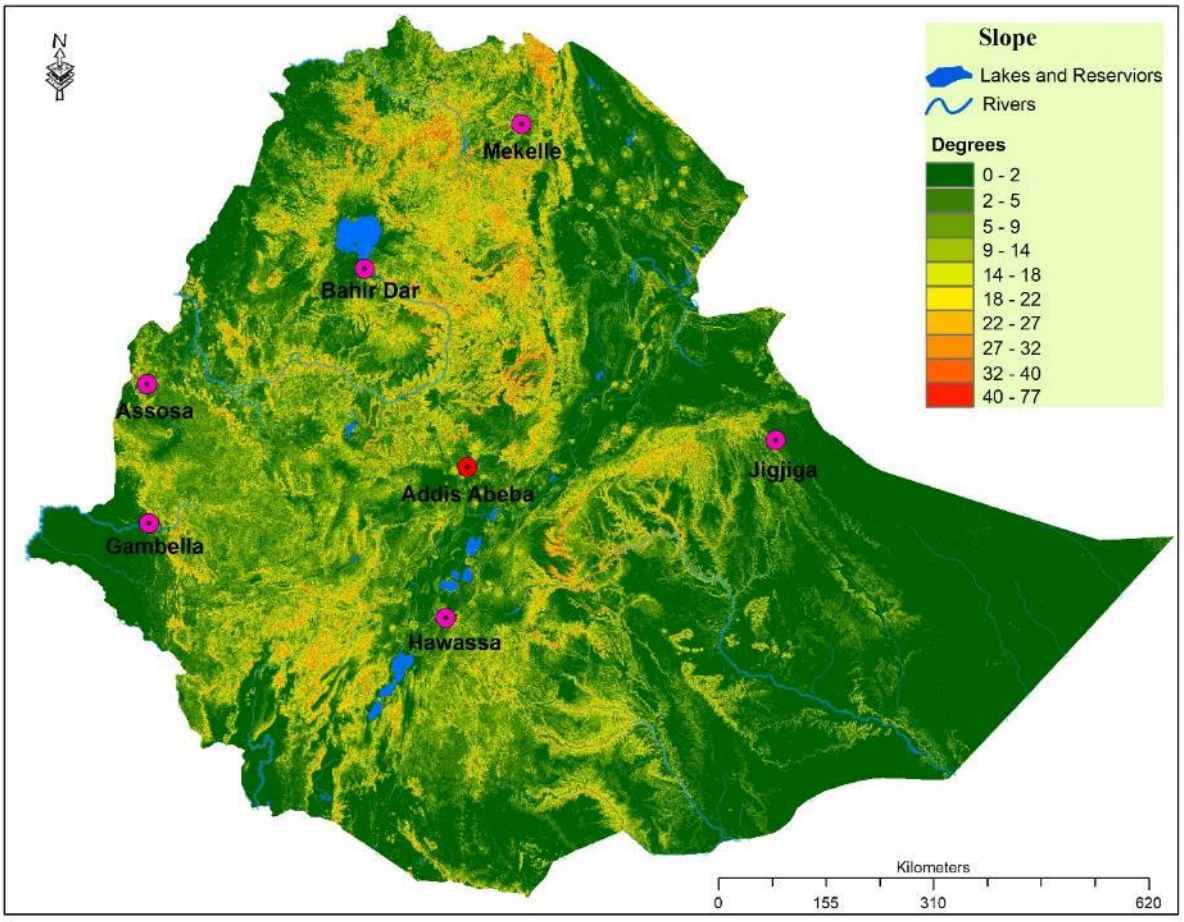

Figure 4.1: Slope of the study area.

4.3.2. Soil texture

There are several soil datasets of the study area: The Woody Biomass Study Projects in Amhara, Oromia, SNNPR and Tigray Regional States (WBSP, 2000, 2002), the Integrated River Basin Master Plan Studies carried out during 1989–2007 (MoWR, 1996, 1997, 1998a, b; PDRE, 1989), and the different project based feasibility studies. However, they lack the soil texture attribute. Thus, in this study, due to its soil texture attribute and finer spatial resolution (250m), the 'SoilGrids250m' soil dataset was selected to supply the soil texture input data to the model (Hengel et al., 2015). 'SoilGrids250m' is a soil dataset produced by the Africa Soil Information Service (AfSIS) project for the African continent by using the Africa Soil Profiles (legacy) database and the AfSIS Sentinel Site database. These datasets contain over 28 thousand sampling locations and represent the most comprehensive soil sample datasets of the African continent to date.

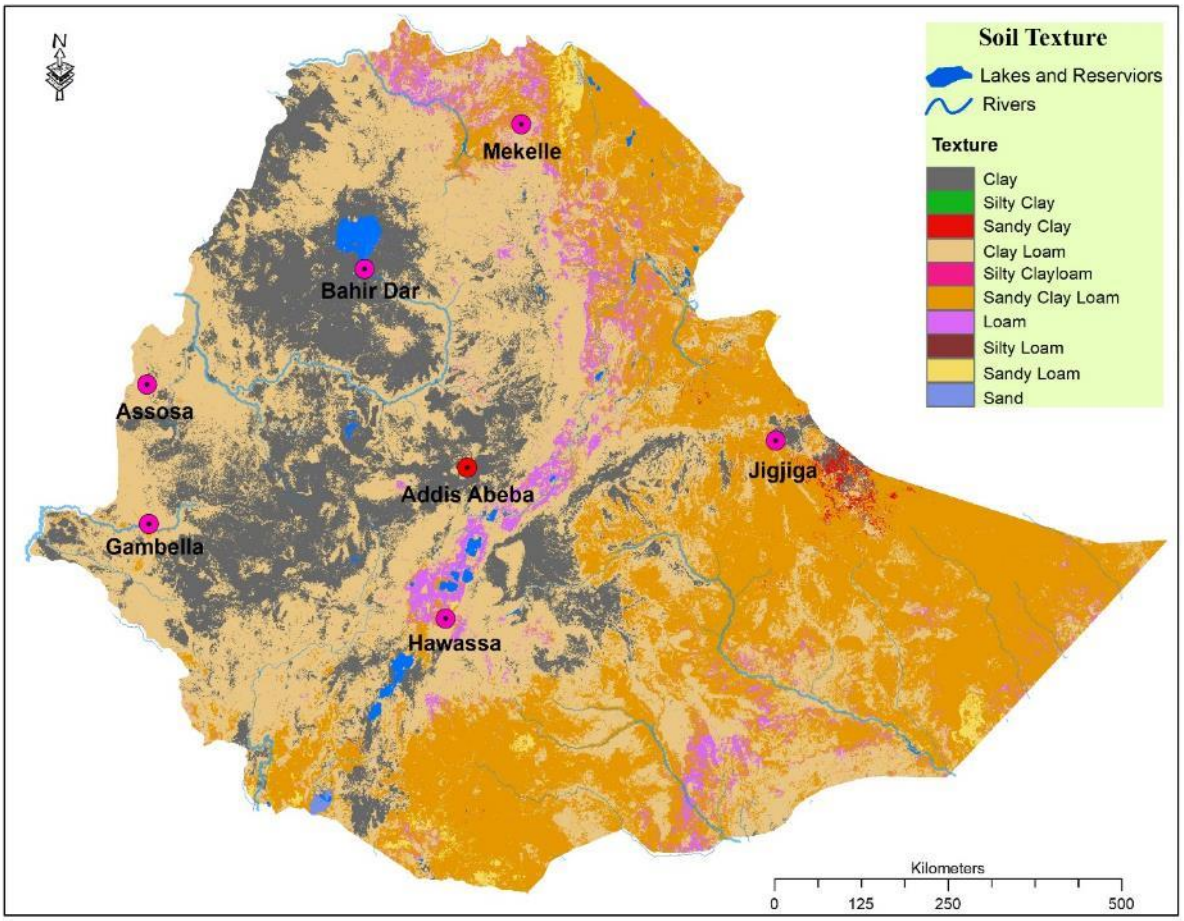

Figure 4.2: Soil texture map of the study area to WetSpass-M model.

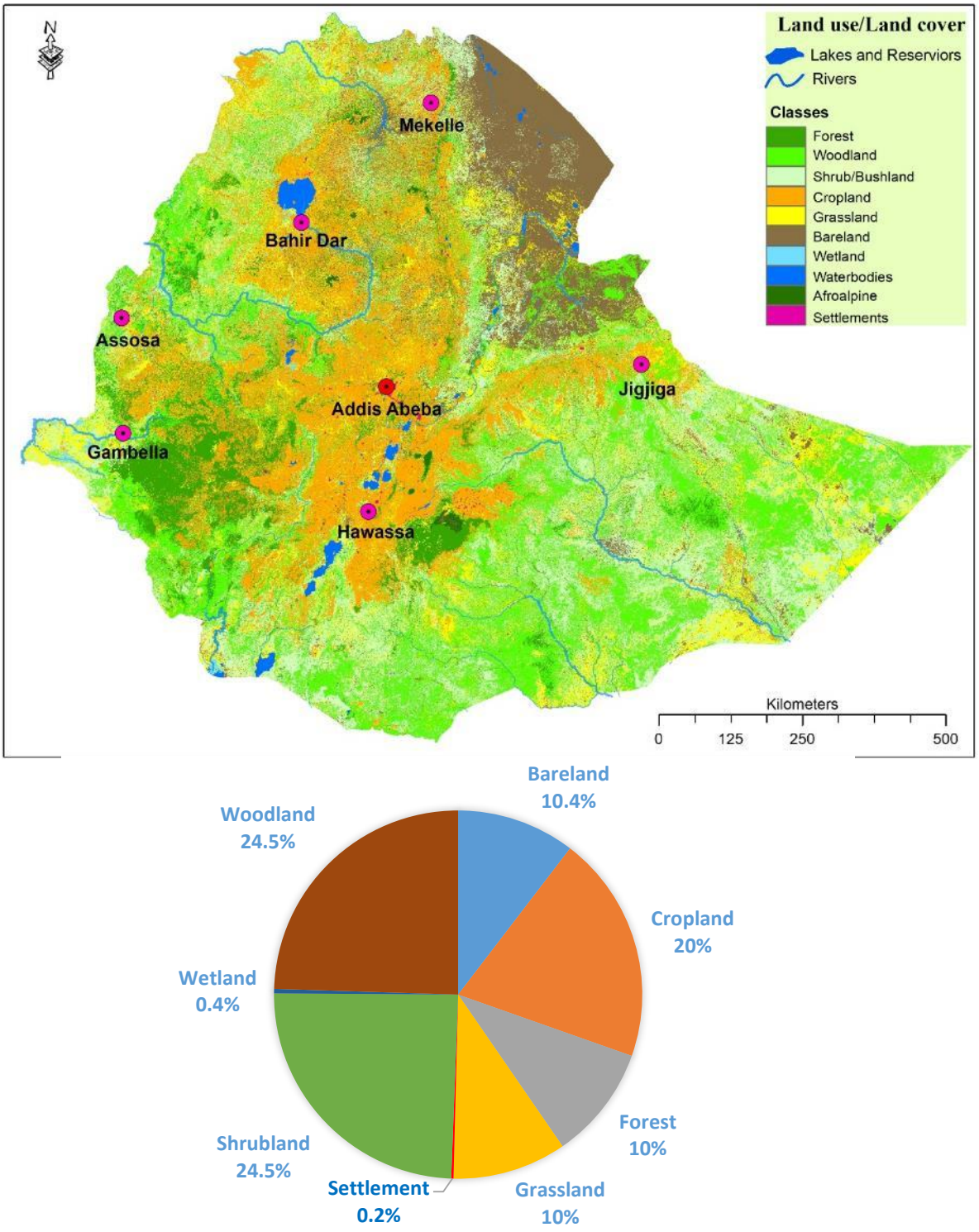

Figure 4.3: LULC map of the study area and the areal coverage of the major LULC classes.

Extracting the SoilGrids250m dataset by the boundary of the study area shows that there are nine different USDA soil texture classes in the study area (Figure 4.2), of which the clay and clay loam textural classes dominantly occupy the central part of the study area which forms the highlands of the study area.

4.3.3. Land use/land cover (LULC)

LULC map of the study area was obtained from the Water and Land Resource Center (WLRC). The dataset is produced from the Landsat images by integrating multiple techniques: Subdividing heterogeneous landscapes into homogeneous segments, unsupervised clustering, and supervised classification (Kassawmar et al., 2016). The Landsat images' spatial resolution (30 meter) is sufficient enough to capture the hydrologic dynamics at greater detail since the water balance calculation in this model is primarily based on the LULC data of the study area. The first level (LULC level-I) of the dataset has ten major classes (Figure 4.3) – forests, woodland, shrub/bushland, cropland, grassland, bare land, wetland, waterbodies, afroalpine, and settlements – of which the cropland alone accounts for 20 % of the study area and constitutes the largest portion of the highlands of the country that is home for 90% of the country's human population.

4.3.4. Groundwater depth

Monthly groundwater depth is one of the challenging datasets to obtain since monitoring groundwater wells and a comprehensive database are almost absent in the study area. Thus, this study calculated it from other available datasets: The GRACE satellite data, the Africa groundwater depth atlas (MacDonald et al., 2012), and the NASA-USDA SMAP Global Soil Moisture Data (Entekhabi et al., 2010; Bolten and Crow, 2012; Sazib et al., 2018). The GRACE data is a lump sum of monthly water storage anomalies in surface, unsaturated zone, and groundwater (Swenson and Wahr, 2016; Landerer and Swenson, 2012). The Africa groundwater depth atlas is a raster dataset of long term average static groundwater depth prepared by integrating all the information in published and unpublished literature including reports, journal articles, conference papers. On the other hand, the NASA-USDA SMAP global soil moisture dataset is generated by integrating satellite-derived Soil Moisture Active Passive (SMAP) Level 3 soil

moisture observations into the modified two-layer Palmer model using a 1-D Ensemble Kalman Filter (EnKF) data assimilation approach.

To obtain the monthly groundwater storage anomaly from GRACE data, the surface and the unsaturated zone components had to be subtracted. Assuming the surface water storage anomaly is negligible, the monthly groundwater storage anomaly could be obtained by subtracting the monthly average values of the NASA-USDA SMAP Global Soil Moisture from the original GRACE data (Figure 4.5). Then, the monthly groundwater storage anomaly, the subtraction result, could be added to the long term average static groundwater depth (the BGS dataset) to obtain the long term average monthly groundwater depth (Figure 4.4).

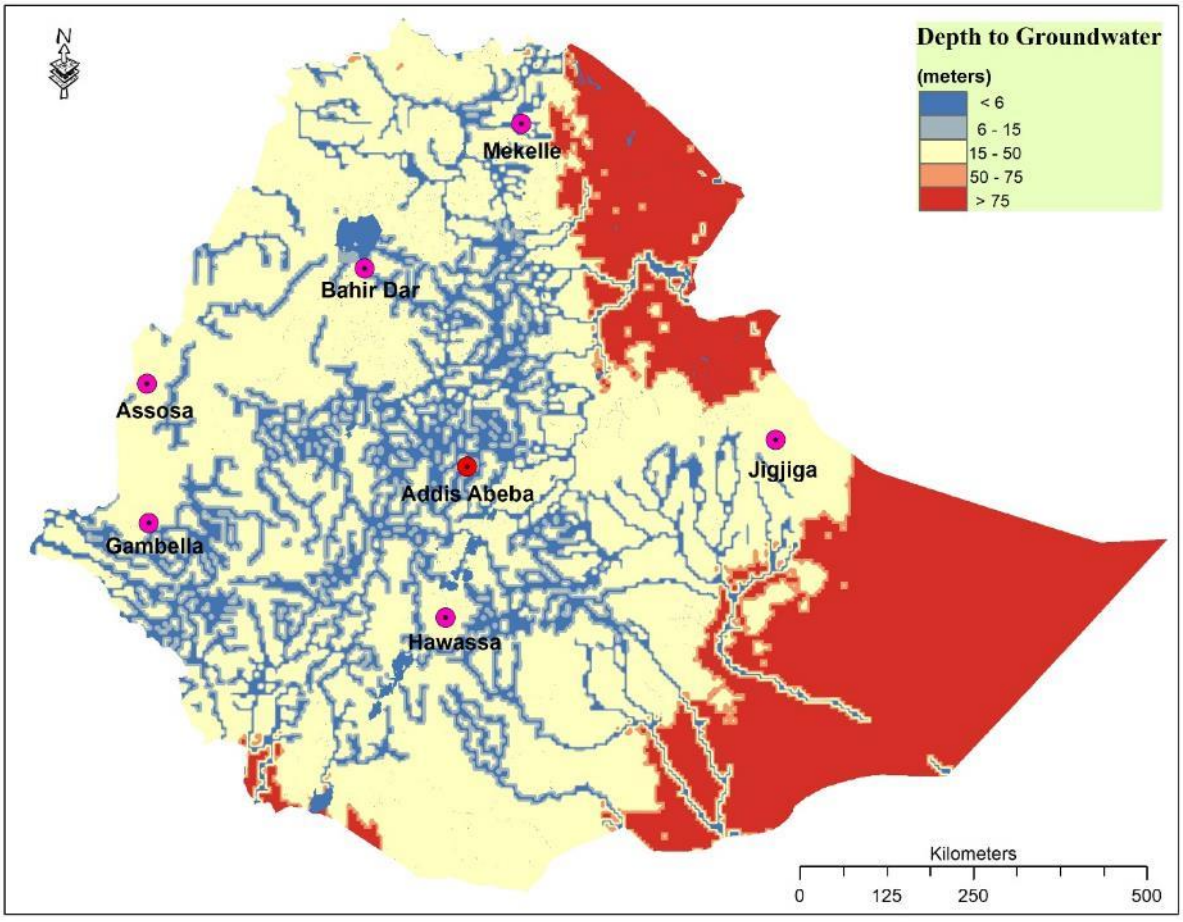

Figure 4.4: Depth to groundwater in the study area.

4.3.5. Climatological variables: Rainfall, temperature, potential evapotranspiration, wind speed

4.3.5.1. Rainfall

The monthly rainfall inputs were generated from weather station data obtained from the National Meteorological Agency (NMA) (Table 4.1) and the FAO LocClim database (Figure 4.6). After removing duplicate records, the data obtained from the two sources were merged and interpolated by using the geostatistical kringing method in ArcGIS (Figure 4.7). A detailed description of the rainfall characteristics in the study area is presented in section 3.1.1.1.

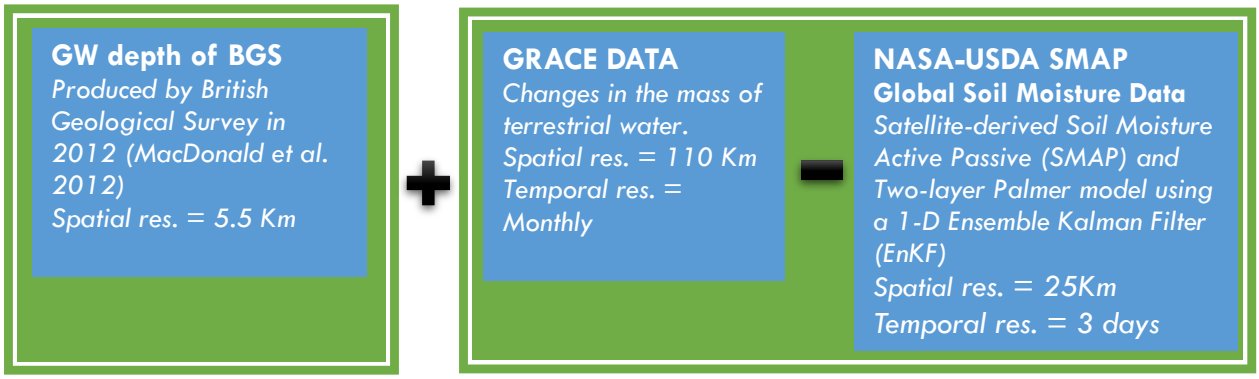

Figure 4.5: Schematization that shows the procedure used to calculate the monthly groundwater depth from the GRACE, Africa groundwater depth atlas, and NASA-USDA SMAP Global Soil Moisture Data.

4.3.5.2. Temperature

The monthly temperature datasets were generated from weather station data obtained from the National Meteorological Agency (NMA) (Table 4.1) and the FAO LocClim database (Figure 4.6) by the kringing geostatistical interpolation. A set of 463 stations located within and surrounding the study area were used to obtain the long term monthly mean temperature in the study area (figure). The kringing geostatistical interpolation method was applied and performed very good in each month (Figure 4.8).

Generally, the temperature of the study area shows significant spatial variability owing to the remarkable elevation variation and latitudinal effects in the country; however, it is rather uniform throughout the year (Billi, 2015). The lowest mean temperature in the study area (14 – 18 ^{o}C) is recorded in the highlands where elevations are over 2300 m.a.s.l. during the rainy months (June, July, August) (Figure 4.8). On the other hand, the highest mean temperature is observed in the northern section of the rift valley (Afar depression), and the lowlands occupying the peripheral part of the country during dry months (December, January, February).

4.3.5.3. Potential Evapotranspiration (PET)

The PET input datasets were generated from 225 station data obtained from the National Meteorological Agency (NMA) (Table 4.1) and the FAO LocClim database (Figure 4.6) by the kriging geostatistical interpolation technique (Figure 4.9). Generally, it can be observed that the highlands of the study area, more specifically areas over 2000 m a.s.l., are characterized by lower PET values. On the other hand, due to the fact that PET increases as elevation decreases, large portion of the study area –the whole Ogaden, the Afar triangle, the Danakil depression, the northern portion of the Rift Valley, and the belt along the border with Sudan – is characterized by higher PET.

4.3.5.4. Wind speed

The wind speed input datasets were generated from records of 213 stations obtained from the National Meteorological Agency (NMA) (Table 4.1) and the FAO LocClim database (Figure 4.6) by the kriging geostatistical interpolation (figure).

Wind speed in the study area generally has low velocity, and like the other climatic variables, it is controlled by the physiographic variation (Fazzini, Bisci and Billi, 2015). The temporal pattern of wind speed, however, except during deep convictive processes that happens rarely, is characterized by having a uniform pattern throughout the year (Figure 4.10). Mean wind speed is typically low in the highlands (12 Km h^{-1}) whereas in the Rift valley lakes region, in the sub-desert and bush lands of Ogaden, and along the border with Sudan, it is a bit higher – especially during the 'kiremt' season (Fazzini, Bisci and Billi, 2015).

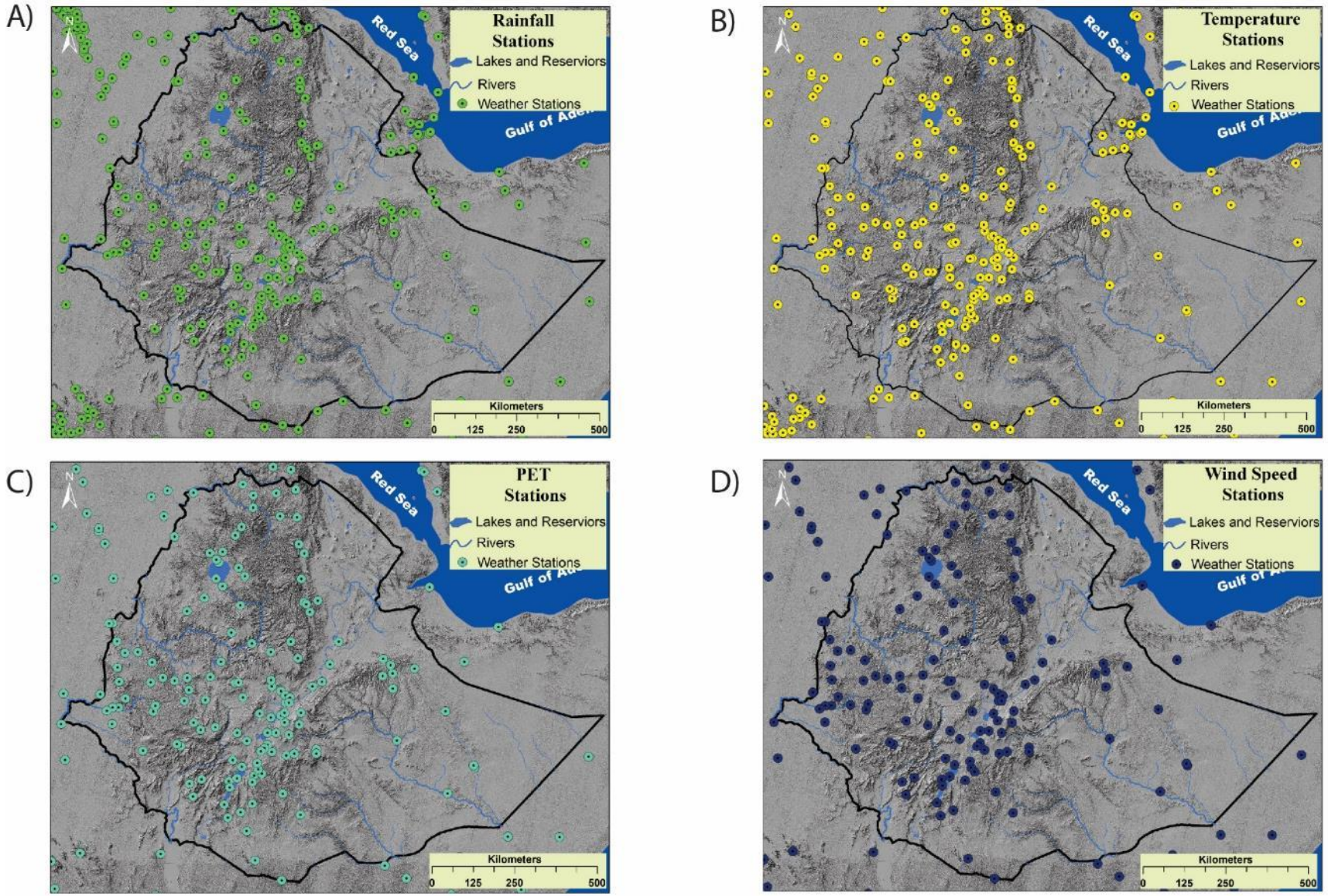

Figure 4.6: Stations: A) Rainfall B) Temperature C) PET D). Wind Speed

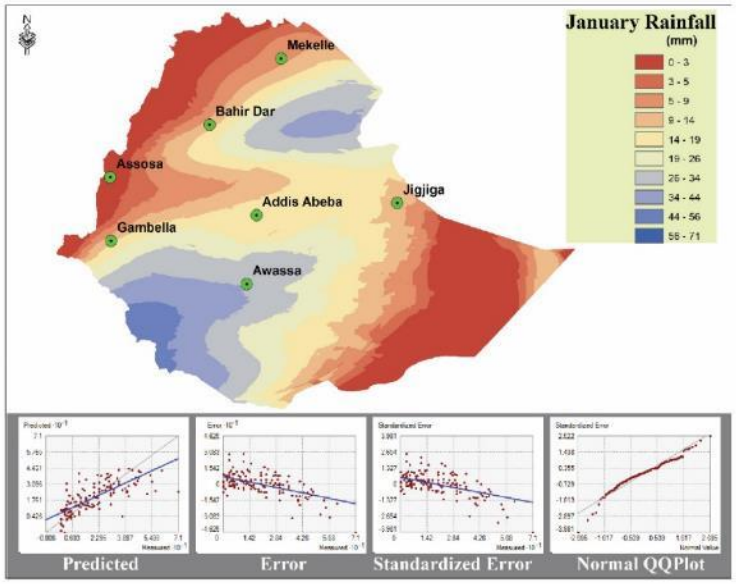
January Rainfall
(mm)
0 - 3
3 - 5
5 - 9
9 - 14
14 - 19
19 - 26
26 - 34
34 - 44
44 - 56
56 - 71
Mekelle
Bahir Dar
Assosa
Addis Abeba
Jigjiga
Gambella
Awassa
Predicted
Error
Standardized Error
Normal QQPlot

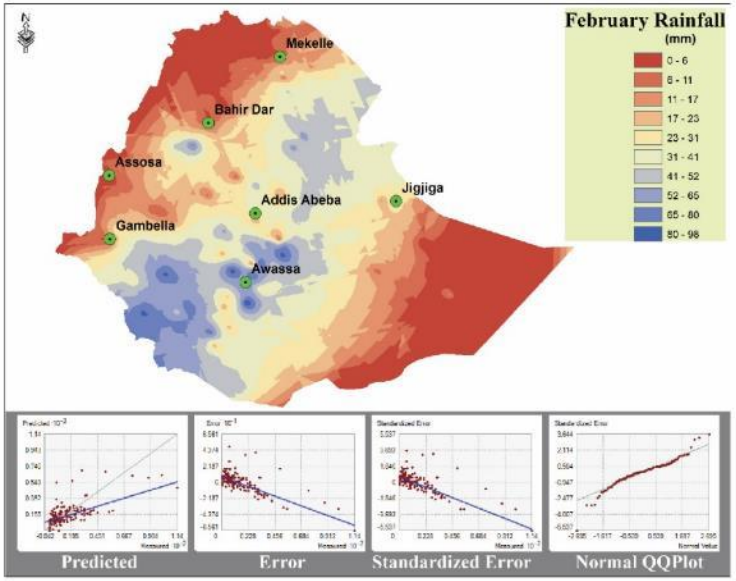
February Rainfall
(mm)
0 - 6
6 - 11
11 - 17
17 - 23
23 - 31
31 - 41
41 - 52
52 - 65
65 - 80
80 - 98
Mekelle
Bahir Dar
Assosa
Addis Abeba
Jigjiga
Gambella
Awassa
Predicted
Error
Standardized Error
Normal QQPlot

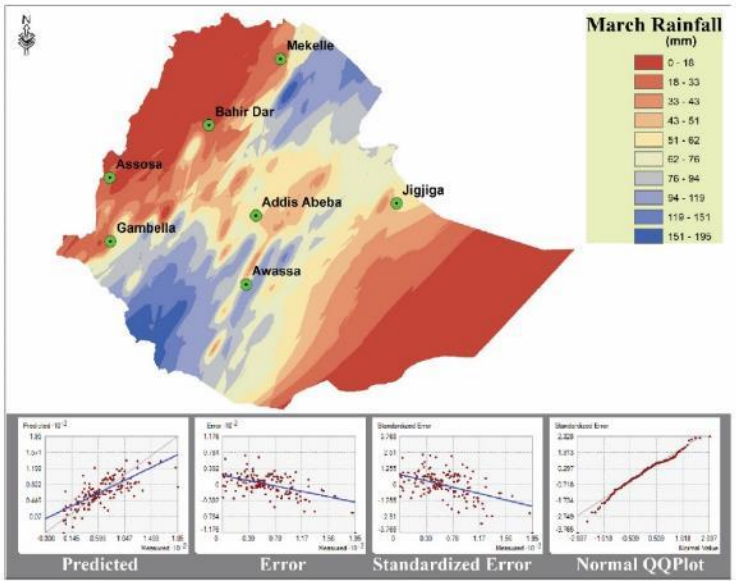
March Rainfall
(mm)
0 - 18
18 - 33
33 - 43
43 - 51
51 - 62
62 - 76
76 - 94
94 - 119
119 - 151
151 - 195
Mekelle
Bahir Dar
Assosa
Addis Abeba
Jigjiga
Gambella
Awassa
Predicted
Error
Standardized Error
Normal QQPlot

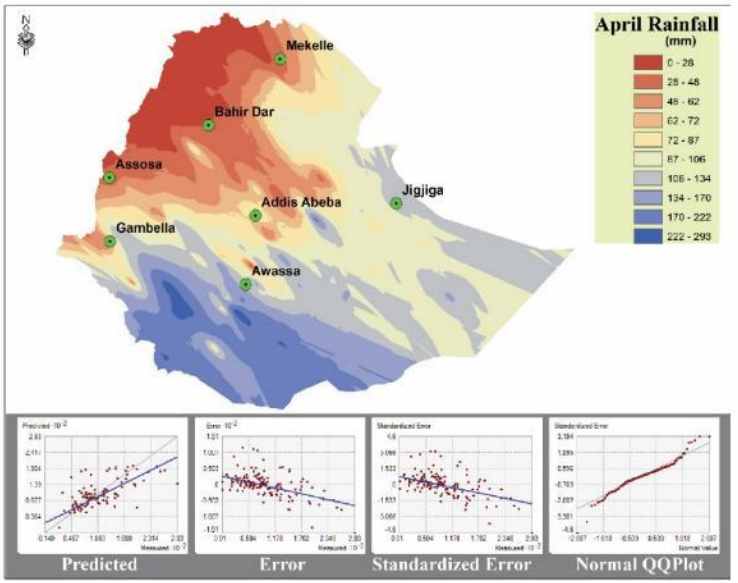
April Rainfall
(mm)
0 - 28
28 - 48
48 - 62
62 - 72
72 - 87
87 - 106
106 - 134
134 - 170
170 - 222
222 - 293
Mekelle
Bahir Dar
Assosa
Addis Abeba
Jigjiga
Gambella
Awassa
Predicted
Error
Standardized Error
Normal QQPlot

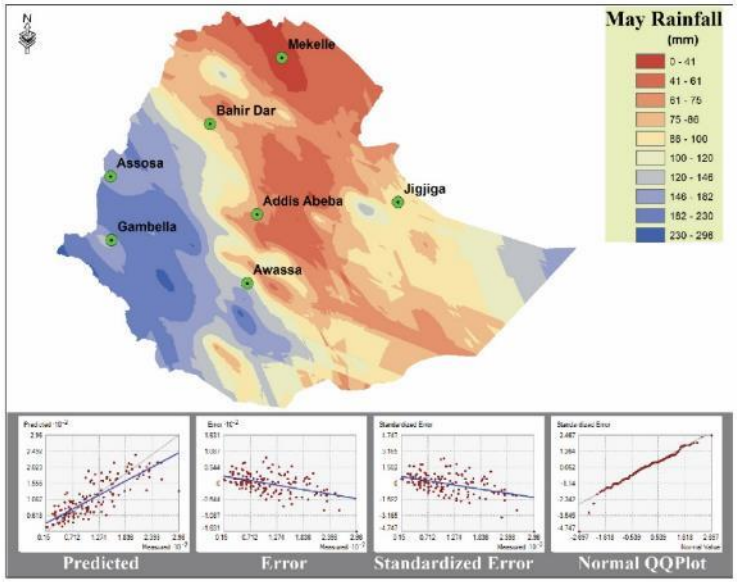
May Rainfall
(mm)
0 - 41
41 - 61
61 - 75
75 - 88
88 - 100
100 - 120
120 - 146
146 - 182
182 - 230
230 - 296
Mekelle
Bahir Dar
Assosa
Addis Abeba
Jigjiga
Gambella
Awassa
Predicted
Error
Standardized Error
Normal QQPlot

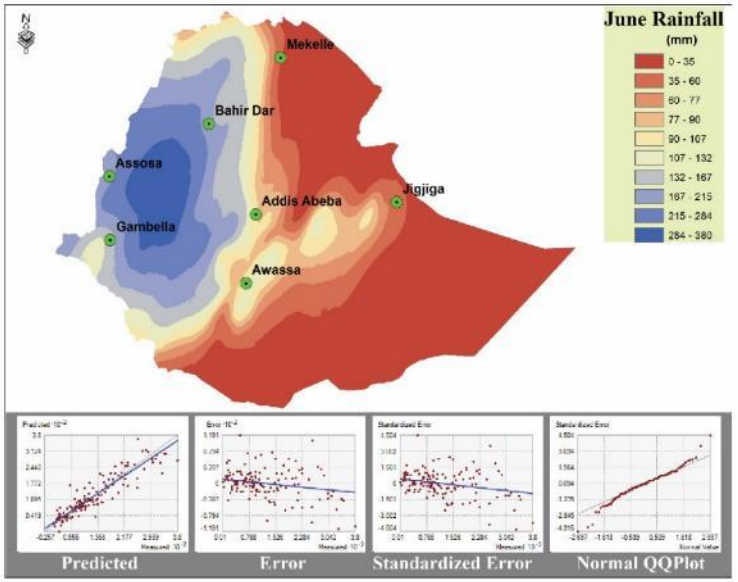
June Rainfall
(mm)
0 - 35
35 - 60
60 - 77
77 - 90
90 - 107
107 - 132
132 - 167
167 - 215
215 - 284
284 - 380
Mekelle
Bahir Dar
Assosa
Addis Abeba
Jigjiga
Gambella
Awassa
Predicted
Error
Standardized Error
Normal QQPlot

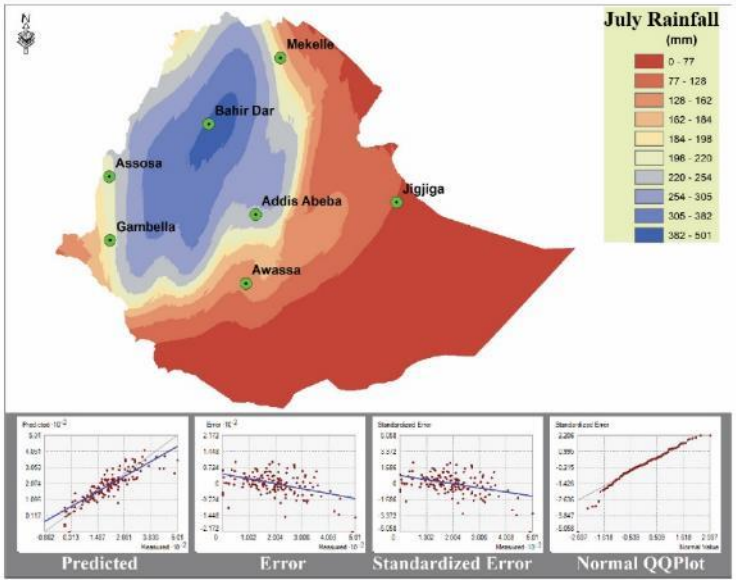
July Rainfall
(mm)
0 - 77
77 - 128
128 - 162
162 - 184
184 - 198
198 - 220
220 - 254
254 - 305
305 - 382
382 - 501
Mekelle
Bahir Dar
Assosa
Addis Abeba
Jigjiga
Gambella
Awassa
Predicted
Error
Standardized Error
Normal QQPlot

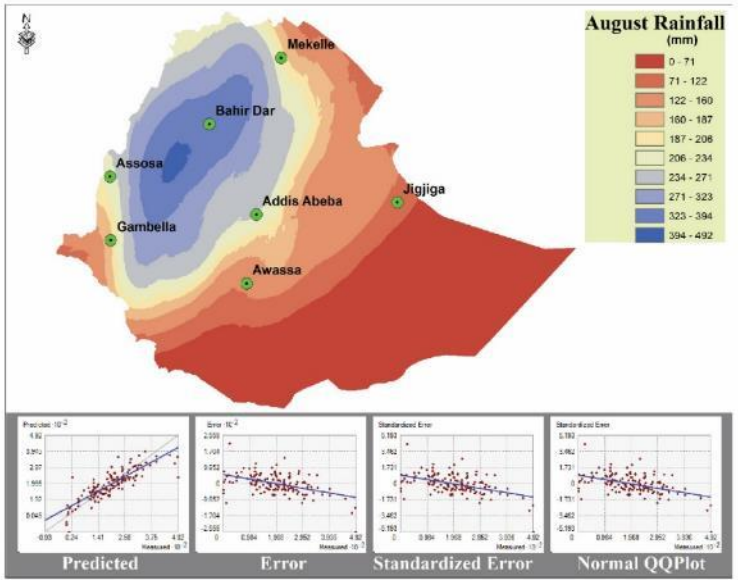
August Rainfall
(mm)
0 - 71
71 - 122
122 - 160
160 - 187
187 - 206
206 - 234
234 - 271
271 - 323
323 - 394
394 - 492
Mekelle
Bahir Dar
Assosa
Addis Abeba
Jigjiga
Gambella
Awassa
Predicted
Error
Standardized Error
Normal QQPlot

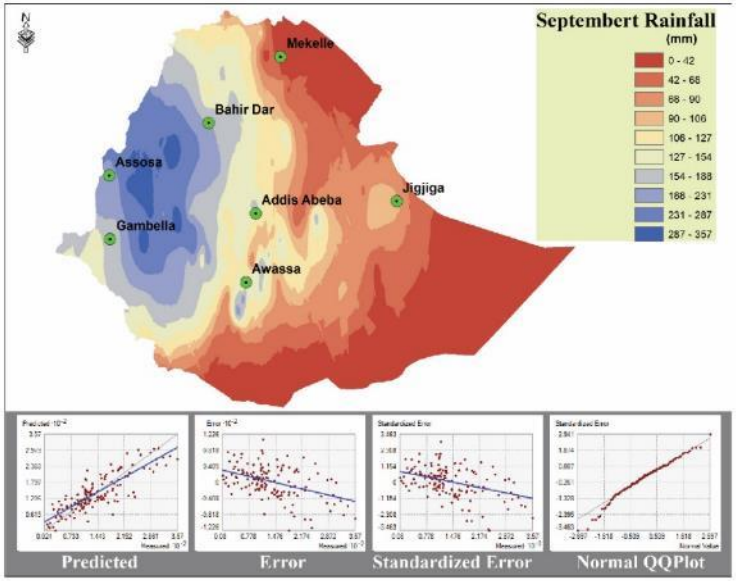

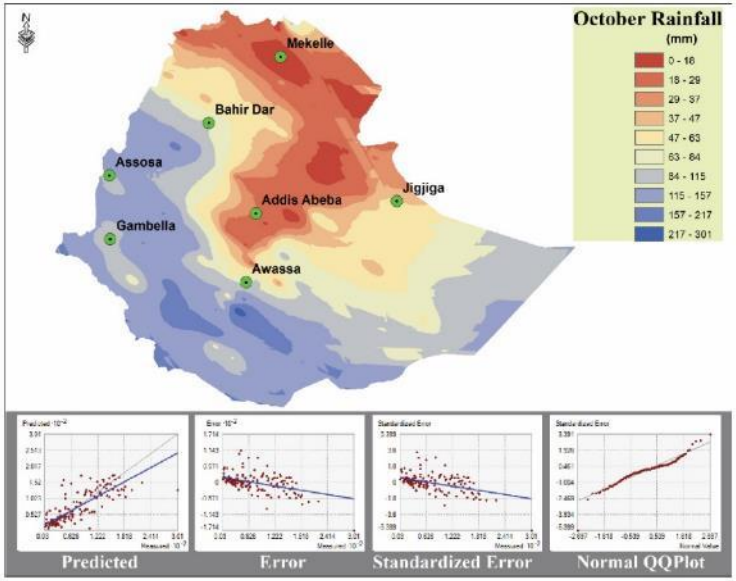

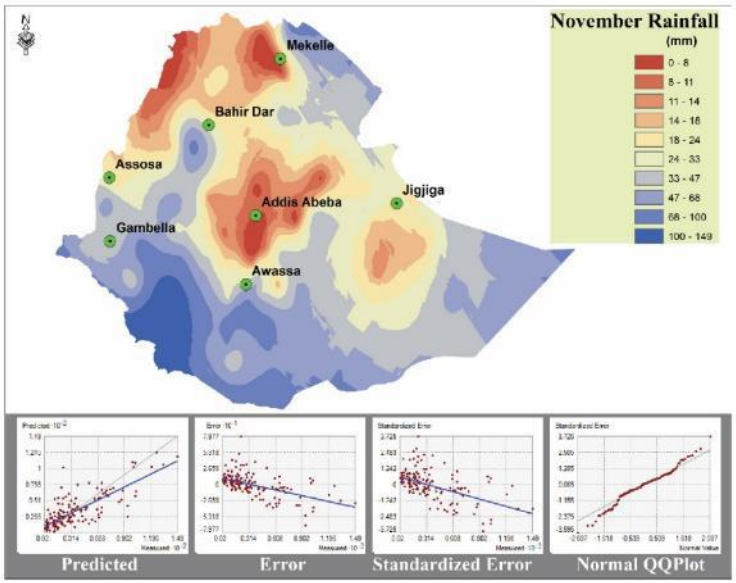

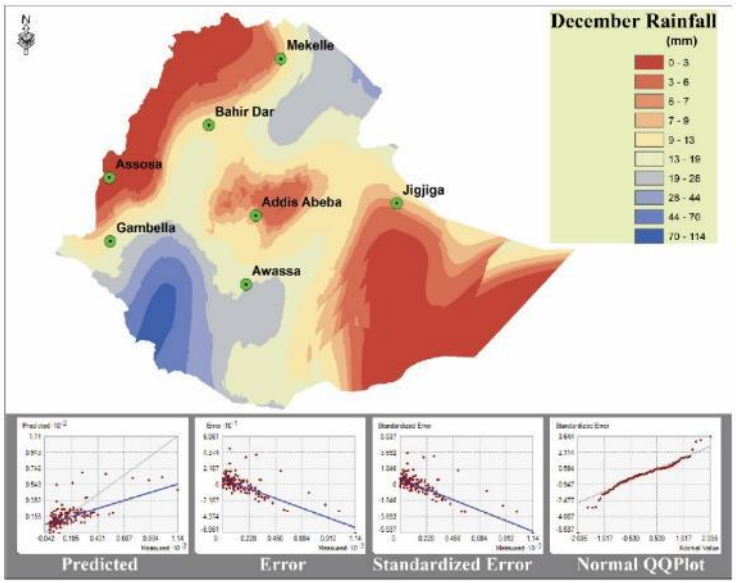

Figure 4.7: Monthly rainfall maps to WetSpass-M model.

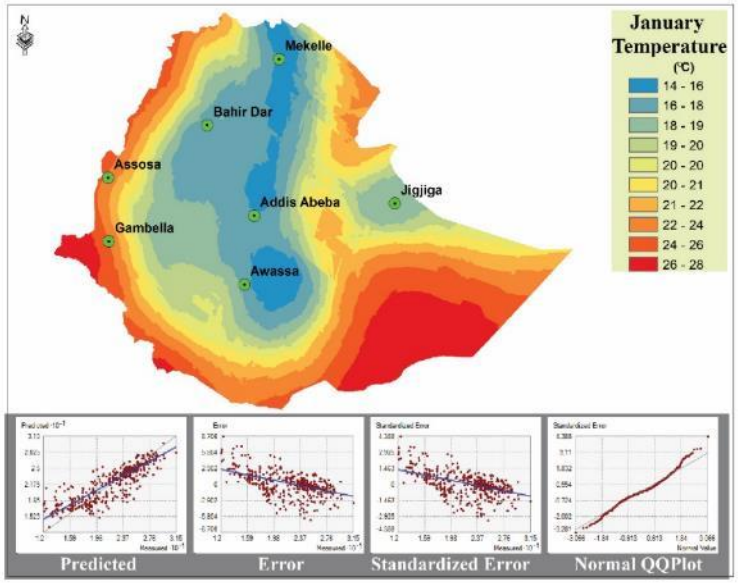
January Temperature
(°C)
14 - 16
16 - 18
18 - 19
19 - 20
20 - 20
20 - 21
21 - 22
22 - 24
24 - 26
26 - 28
Mekelle
Bahir Dar
Assosa
Addis Abeba
Jigjiga
Gambella
Awassa
Predicted
Error
Standardized Error
Normal QQPlot

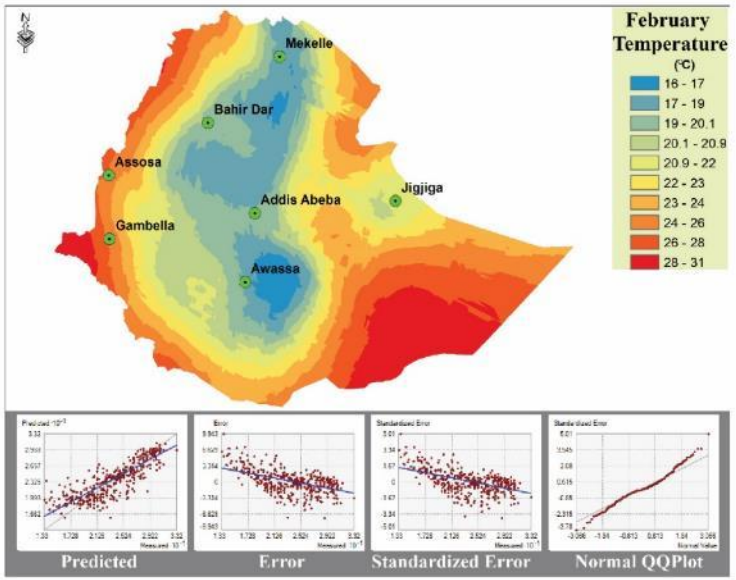
February Temperature
(°C)
16 - 17
17 - 19
19 - 20.1
20.1 - 20.9
20.9 - 22
22 - 23
23 - 24
24 - 26
26 - 28
28 - 31
Mekelle
Bahir Dar
Assosa
Addis Abeba
Jigjiga
Gambella
Awassa
Predicted
Error
Standardized Error
Normal QQPlot

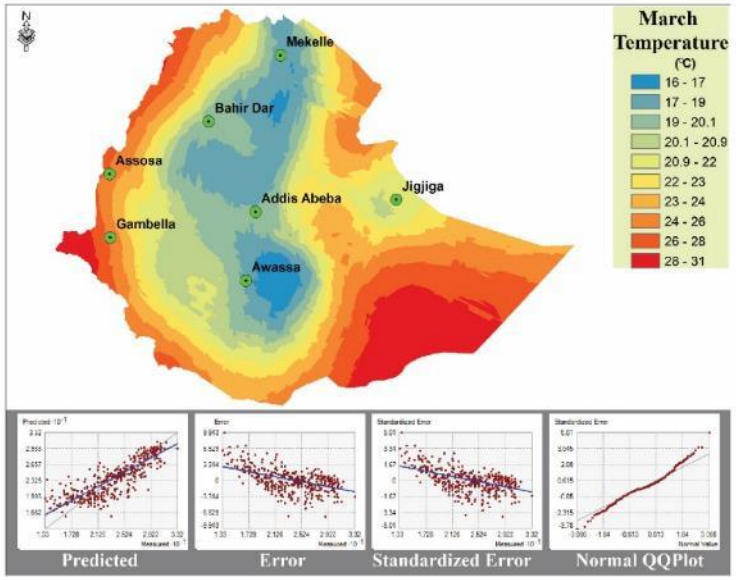
March Temperature
(°C)
16 - 17
17 - 19
19 - 20.1
20.1 - 20.9
20.9 - 22
22 - 23
23 - 24
24 - 26
26 - 28
28 - 31
Mekelle
Bahir Dar
Assosa
Addis Abeba
Jigjiga
Gambella
Awassa
Predicted
Error
Standardized Error
Normal QQPlot

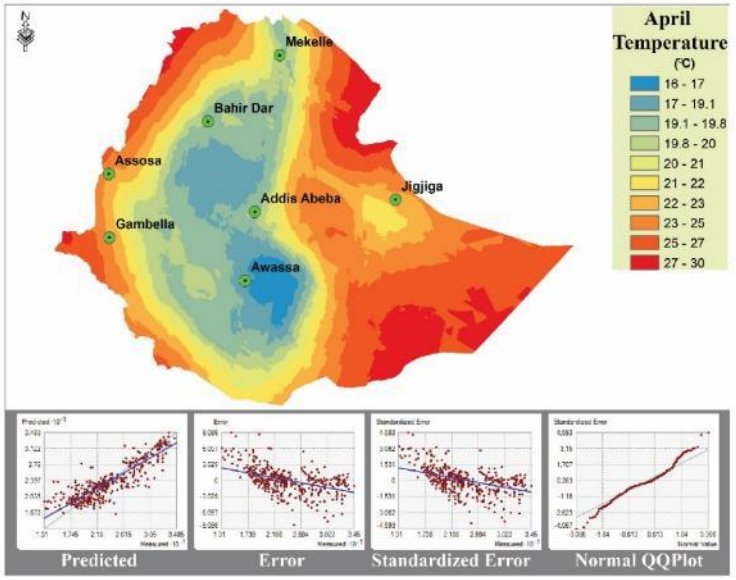
April Temperature
(°C)
16 - 17
17 - 19.1
19.1 - 19.8
19.8 - 20
20 - 21
21 - 22
22 - 23
23 - 25
25 - 27
27 - 30
Mekelle
Bahir Dar
Assosa
Addis Abeba
Jigjiga
Gambella
Awassa
Predicted
Error
Standardized Error
Normal QQPlot

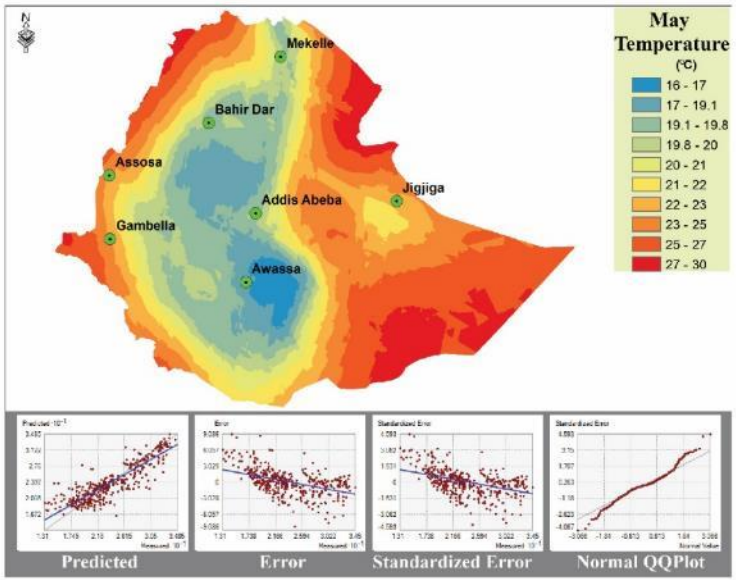
May
Temperature
(°C)
16 - 17
17 - 19.1
19.1 - 19.8
19.8 - 20
20 - 21
21 - 22
22 - 23
23 - 25
25 - 27
27 - 30
Mekelle
Bahir Dar
Assosa
Addis Abeba
Jigjiga
Gambella
Awassa
Predicted
Error
Standardized Error
Normal QQPlot

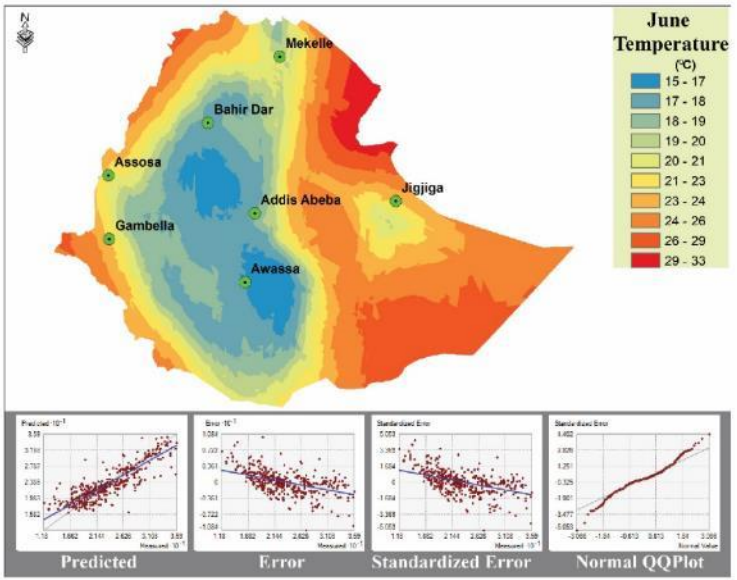
June
Temperature
(°C)
15 - 17
17 - 18
18 - 19
19 - 20
20 - 21
21 - 23
23 - 24
24 - 26
26 - 29
29 - 33
Mekelle
Bahir Dar
Assosa
Addis Abeba
Jigjiga
Gambella
Awassa
Predicted
Error
Standardized Error
Normal QQPlot

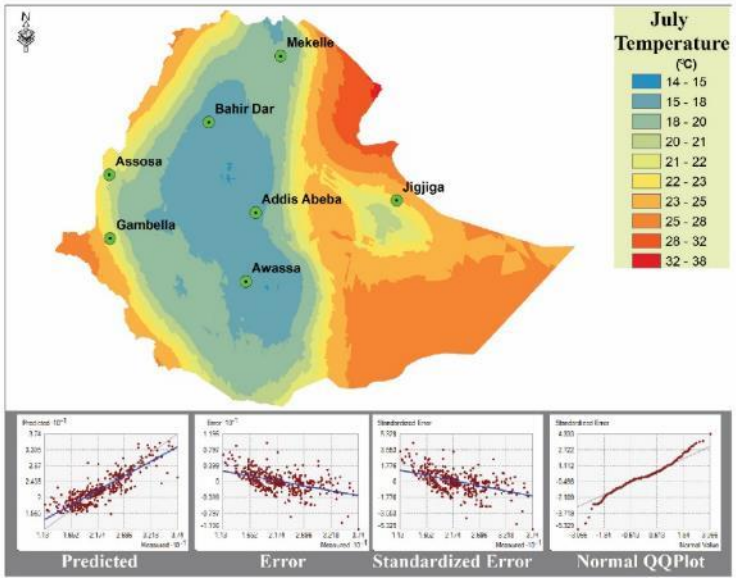
July
Temperature
(°C)
14 - 15
15 - 18
18 - 20
20 - 21
21 - 22
22 - 23
23 - 25
25 - 28
28 - 32
32 - 38
Mekelle
Bahir Dar
Assosa
Addis Abeba
Jigjiga
Gambella
Awassa
Predicted
Error
Standardized Error
Normal QQPlot

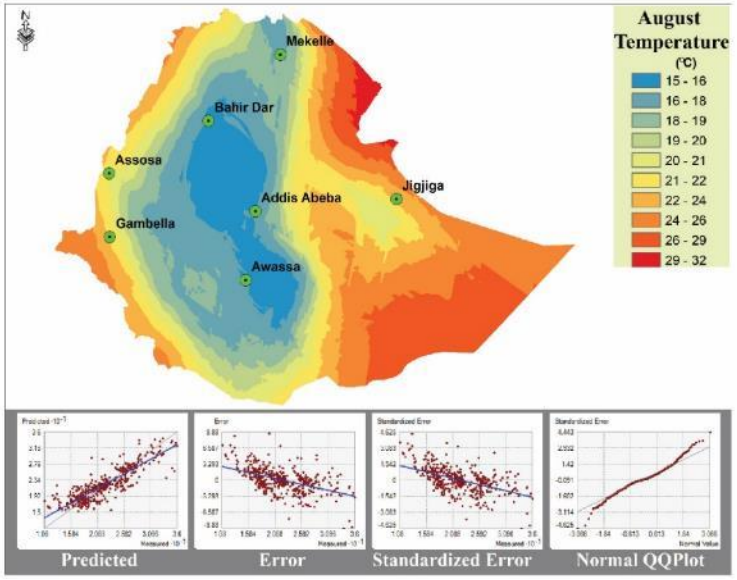
August
Temperature
(°C)
15 - 16
16 - 18
18 - 19
19 - 20
20 - 21
21 - 22
22 - 24
24 - 26
26 - 29
29 - 32
Mekelle
Bahir Dar
Assosa
Addis Abeba
Jigjiga
Gambella
Awassa
Predicted
Error
Standardized Error
Normal QQPlot

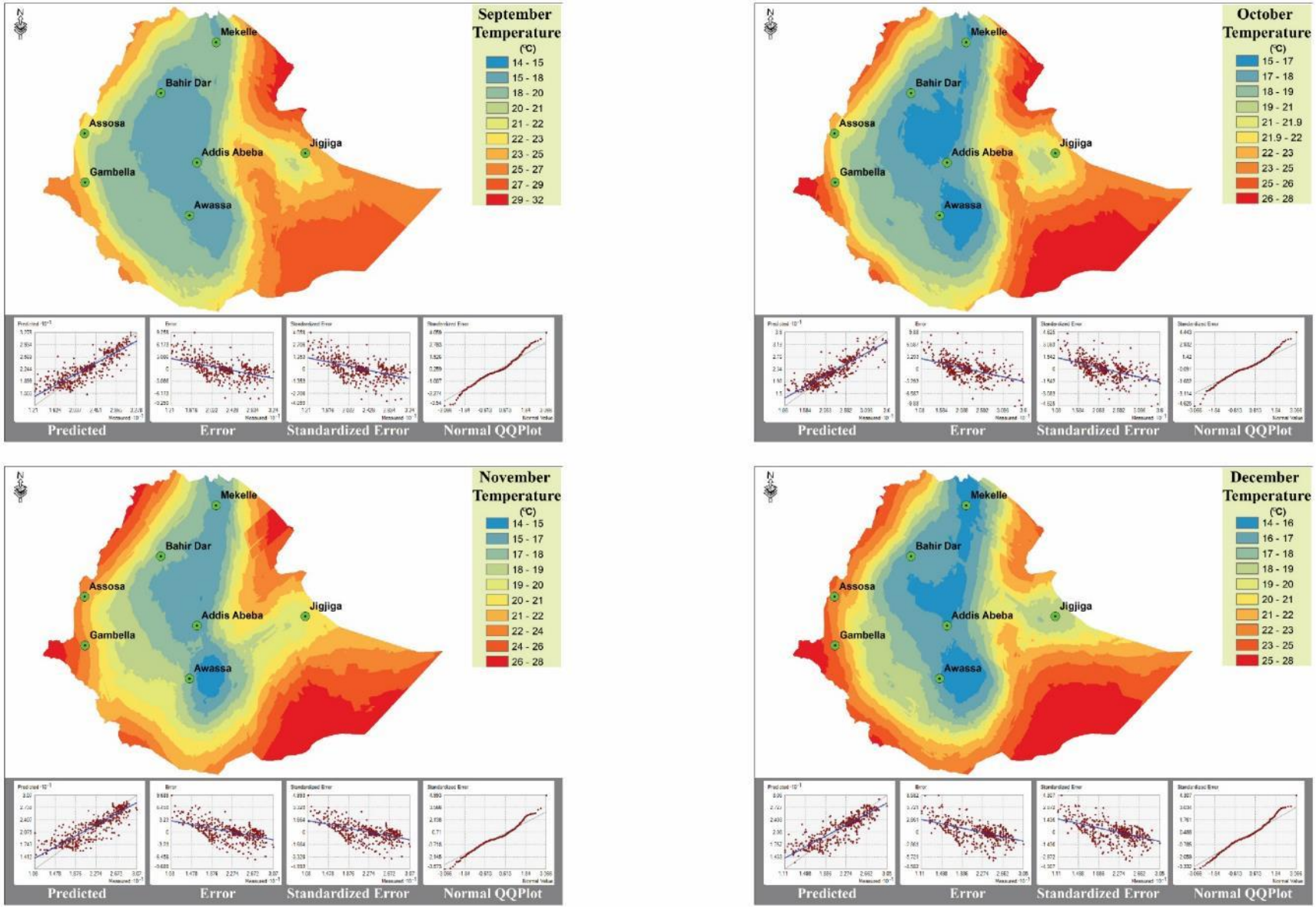

Figure 4.8: Monthly temperature maps to WetSpass-M model.

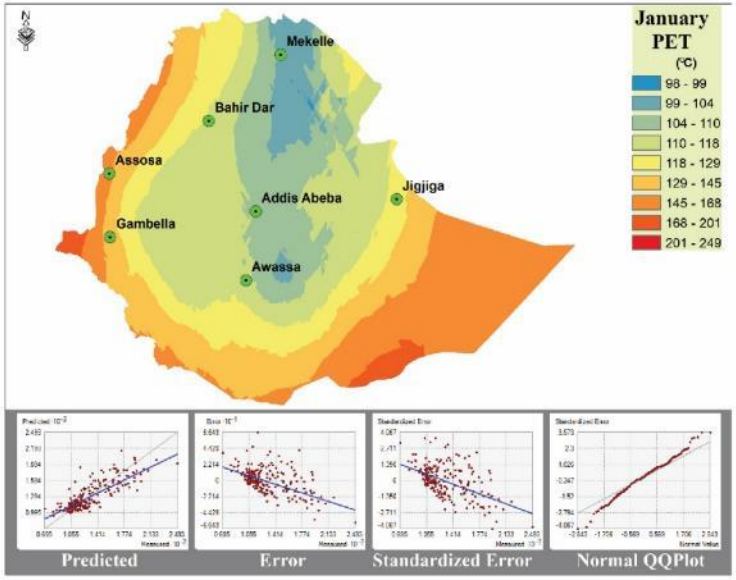
January
PET
(°C)
98 - 99
99 - 104
104 - 110
110 - 118
118 - 129
129 - 145
145 - 168
168 - 201
201 - 249
Mekelle
Bahir Dar
Assosa
Addis Abeba
Jigjiga
Gambella
Awassa
Predicted
Error
Standardized Error
Normal QQPlot

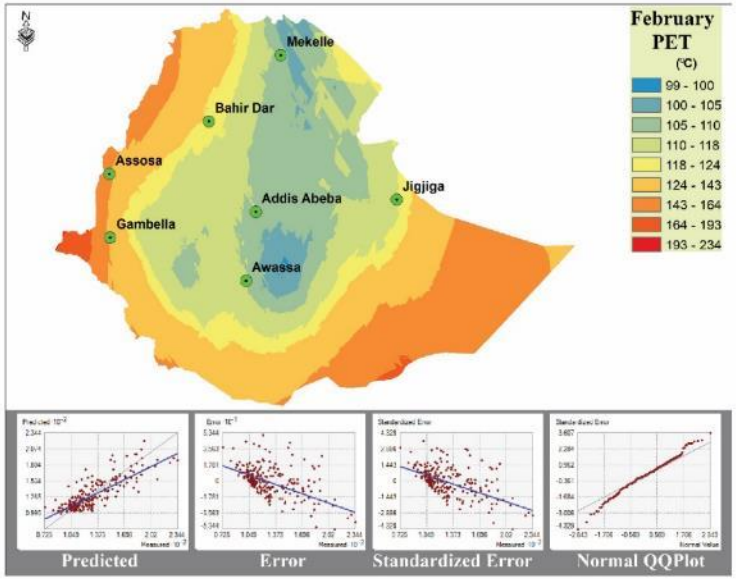
February
PET
(°C)
99 - 100
100 - 105
105 - 110
110 - 118
118 - 124
124 - 143
143 - 164
164 - 193
193 - 234
Mekelle
Bahir Dar
Assosa
Addis Abeba
Jigjiga
Gambella
Awassa
Predicted
Error
Standardized Error
Normal QQPlot

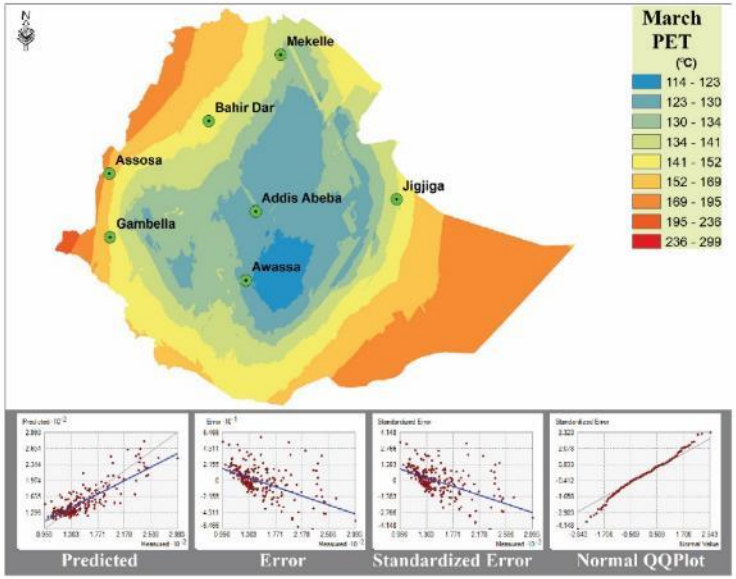
March
PET
(°C)
114 - 123
123 - 130
130 - 134
134 - 141
141 - 152
152 - 169
169 - 195
195 - 236
236 - 299
Mekelle
Bahir Dar
Assosa
Addis Abeba
Jigjiga
Gambella
Awassa
Predicted
Error
Standardized Error
Normal QQPlot

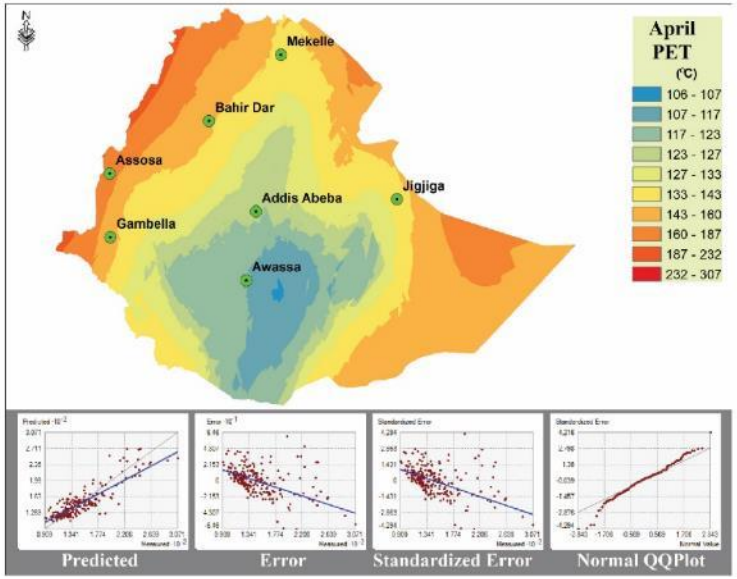
April
PET
(°C)
106 - 107
107 - 117
117 - 123
123 - 127
127 - 133
133 - 143
143 - 160
160 - 187
187 - 232
232 - 307
Mekelle
Bahir Dar
Assosa
Addis Abeba
Jigjiga
Gambella
Awassa
Predicted
Error
Standardized Error
Normal QQPlot

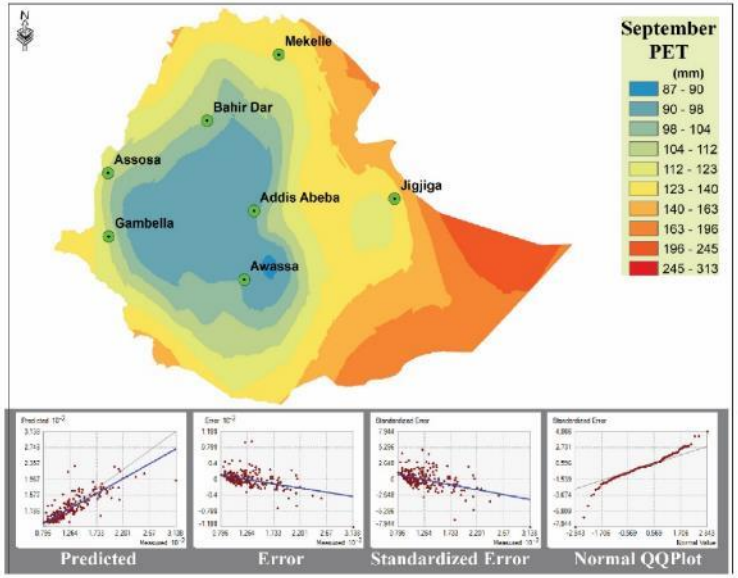
September
PET
(mm)
87 - 90
90 - 98
98 - 104
104 - 112
112 - 123
123 - 140
140 - 163
163 - 196
196 - 245
245 - 313
Mekelle
Bahir Dar
Assosa
Addis Abeba
Jigjiga
Gambella
Awassa
Predicted
Error
Standardized Error
Normal QQPlot

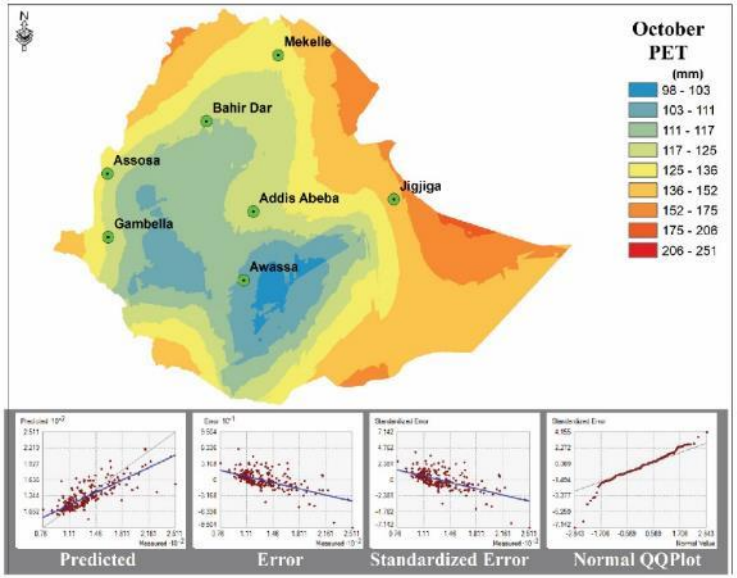
October
PET
(mm)
98 - 103
103 - 111
111 - 117
117 - 125
125 - 136
136 - 152
152 - 175
175 - 208
206 - 251
Mekelle
Bahir Dar
Assosa
Addis Abeba
Jigjiga
Gambella
Awassa
Predicted
Error
Standardized Error
Normal QQPlot

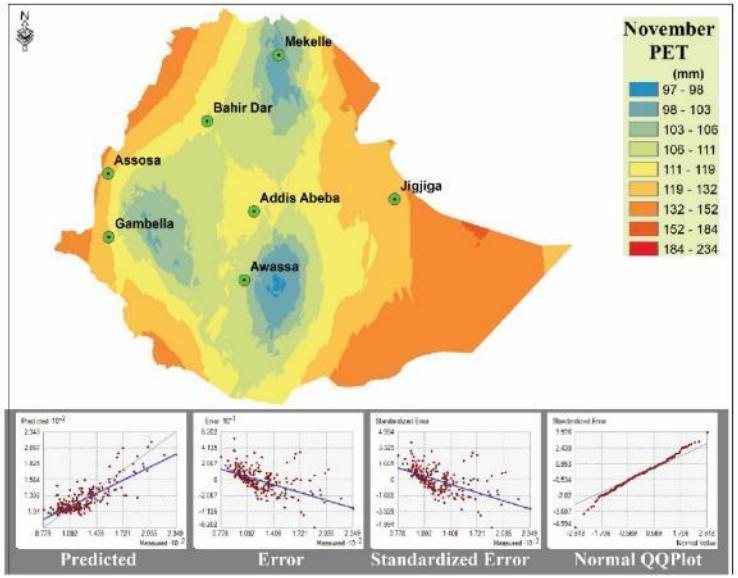
November
PET
(mm)
97 - 98
98 - 103
103 - 106
106 - 111
111 - 119
119 - 132
132 - 152
152 - 184
184 - 234
Mekelle
Bahir Dar
Assosa
Addis Abeba
Jigjiga
Gambella
Awassa
Predicted
Error
Standardized Error
Normal QQPlot

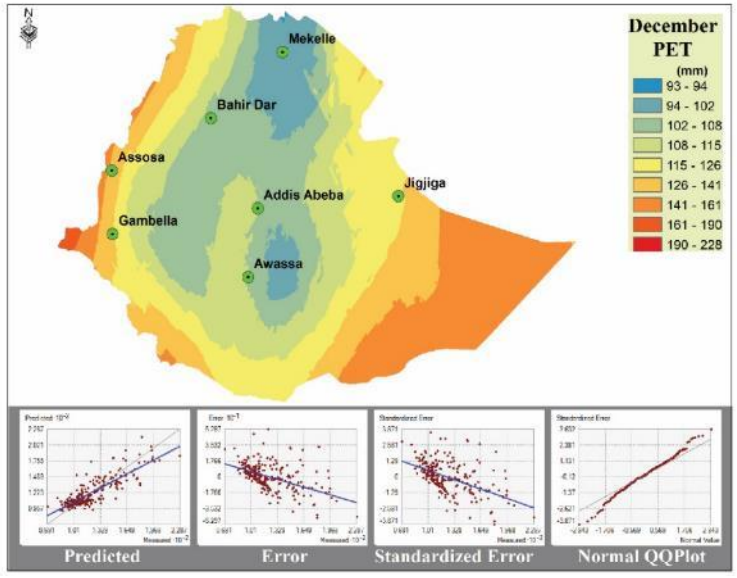
December
PET
(mm)
93 - 94
94 - 102
102 - 108
108 - 115
115 - 126
126 - 141
141 - 161
161 - 190
190 - 228
Mekelle
Bahir Dar
Assosa
Addis Abeba
Jigjiga
Gambella
Awassa
Predicted
Error
Standardized Error
Normal QQPlot

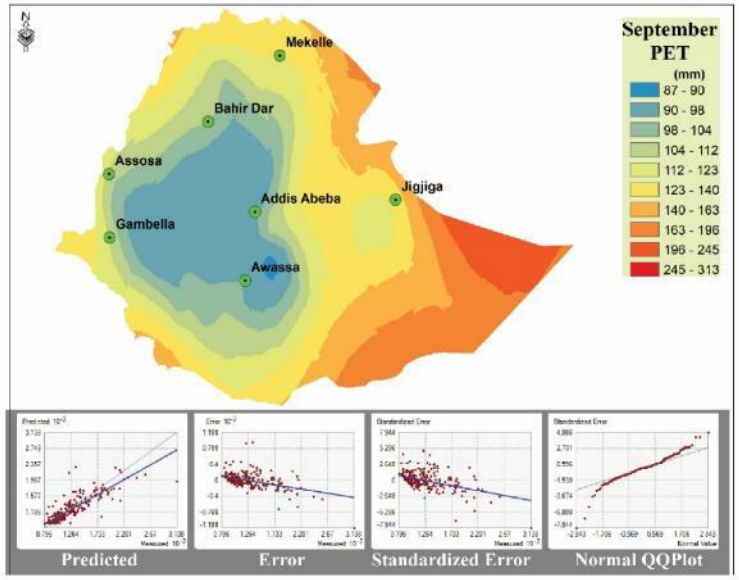

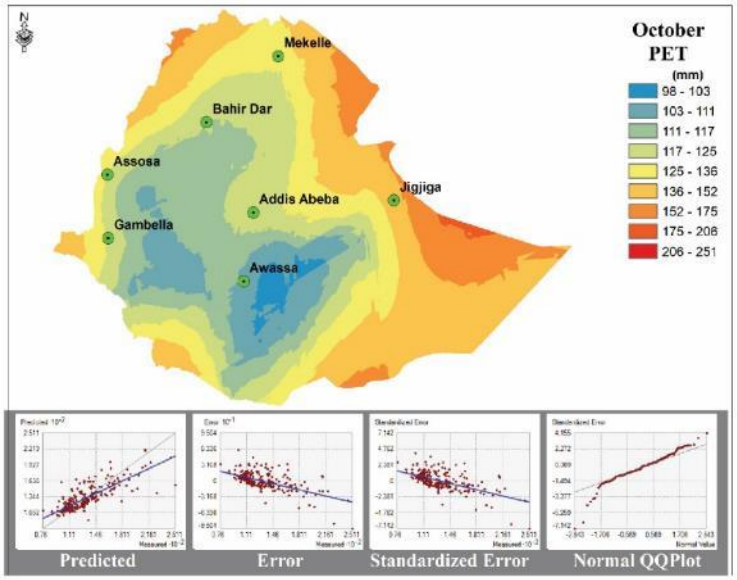

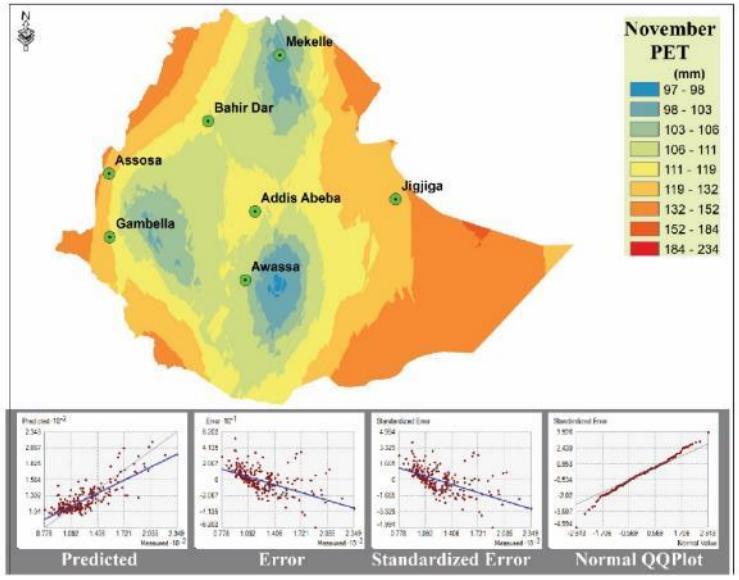

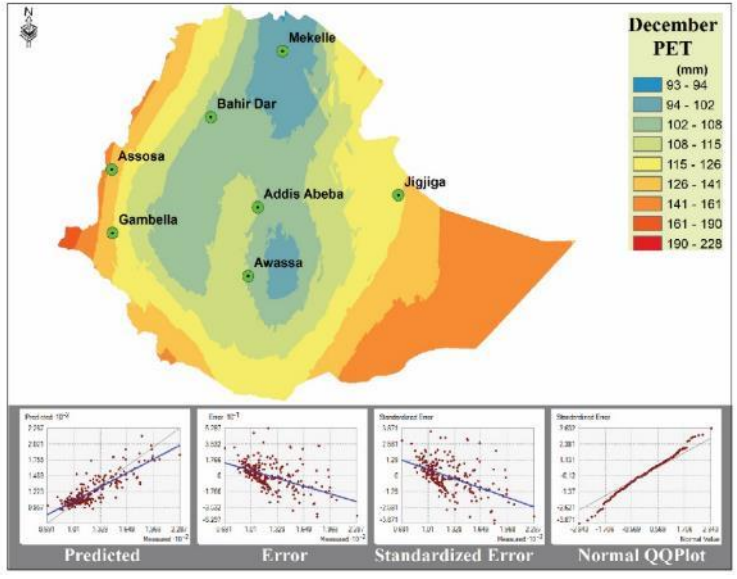

Figure 4.9: Monthly PET maps to WetSpass-M model.

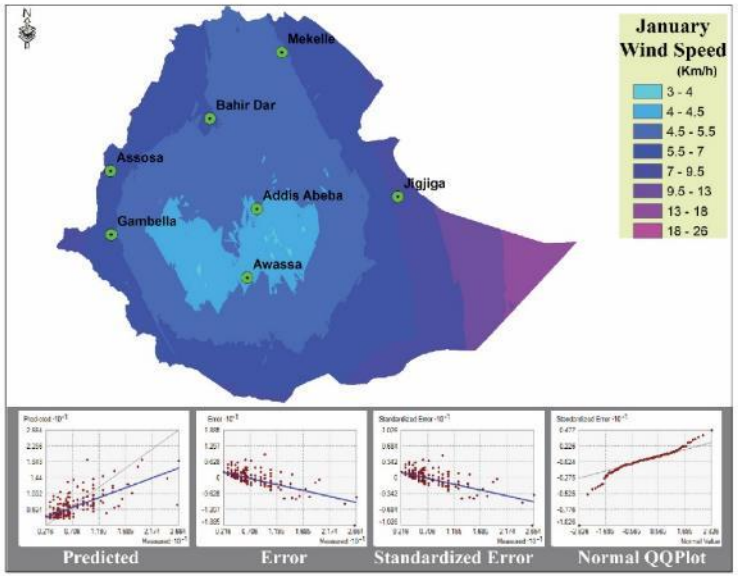
January
Wind Speed
(Km/h)
3 - 4
4 - 4.5
4.5 - 5.5
5.5 - 7
7 - 9.5
9.5 - 13
13 - 18
18 - 26
Mekelle
Bahir Dar
Assosa
Addis Abeba
Jigjiga
Gambella
Awassa
Predicted
Error
Standardized Error
Normal QQPlot

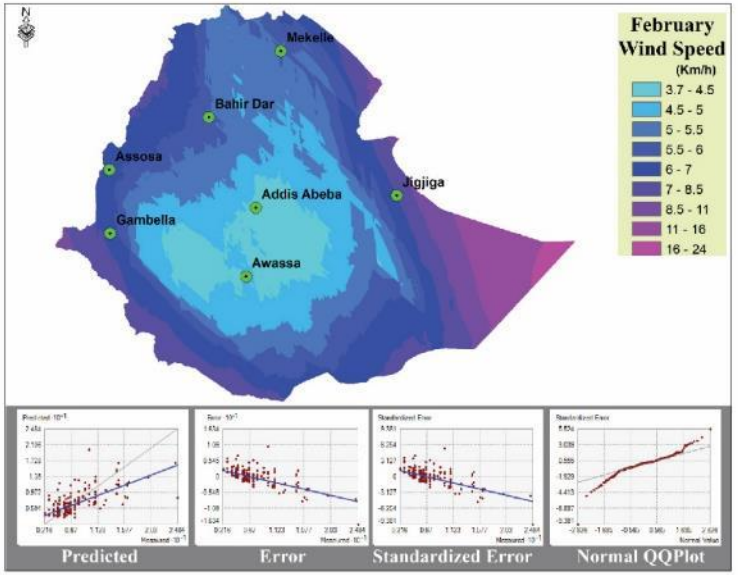
February
Wind Speed
(Km/h)
3.7 - 4.5
4.5 - 5
5 - 5.5
5.5 - 6
6 - 7
7 - 8.5
8.5 - 11
11 - 16
16 - 24
Mekelle
Bahir Dar
Assosa
Addis Abeba
Jigjiga
Gambella
Awassa
Predicted
Error
Standardized Error
Normal QQPlot

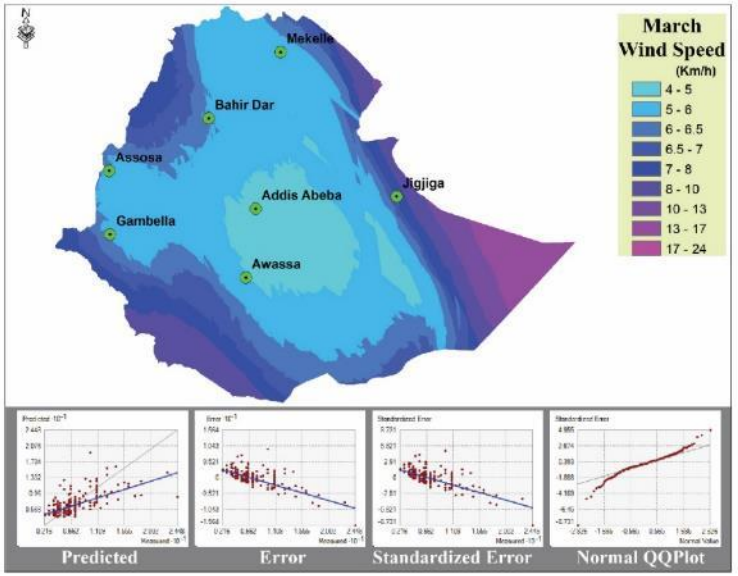
March
Wind Speed
(Km/h)
4 - 5
5 - 6
6 - 6.5
6.5 - 7
7 - 8
8 - 10
10 - 13
13 - 17
17 - 24
Mekelle
Bahir Dar
Assosa
Addis Abeba
Jigjiga
Gambella
Awassa
Predicted
Error
Standardized Error
Normal QQPlot

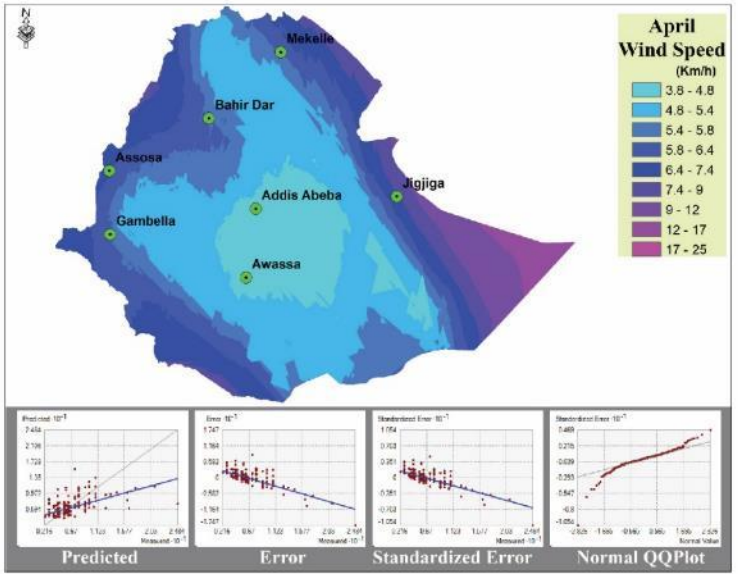
April
Wind Speed
(Km/h)
3.8 - 4.8
4.8 - 5.4
5.4 - 5.8
5.8 - 6.4
6.4 - 7.4
7.4 - 9
9 - 12
12 - 17
17 - 25
Mekelle
Bahir Dar
Assosa
Addis Abeba
Jigjiga
Gambella
Awassa
Predicted
Error
Standardized Error
Normal QQPlot

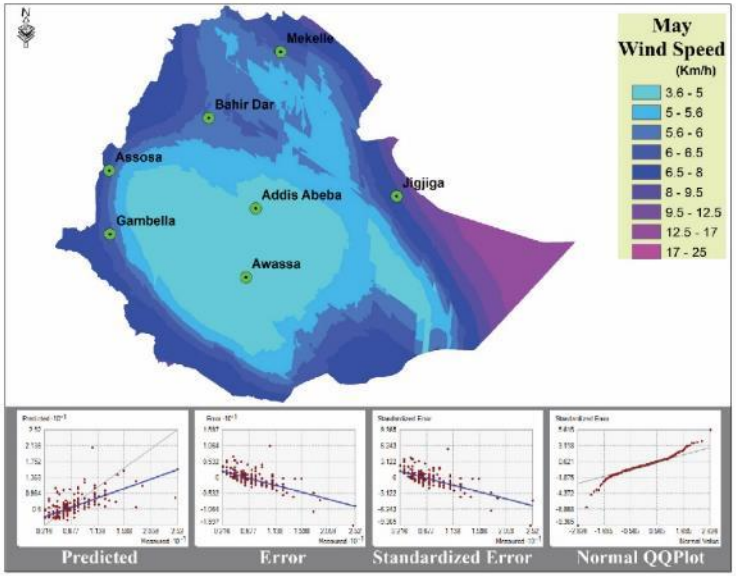
May
Wind Speed
(Km/h)
3.6 - 5
5 - 5.6
5.6 - 6
6 - 6.5
6.5 - 8
8 - 9.5
9.5 - 12.5
12.5 - 17
17 - 25
Mekelle
Bahir Dar
Assosa
Addis Abeba
Jigjiga
Gambella
Awassa
Predicted
Error
Standardized Error
Normal QQPlot

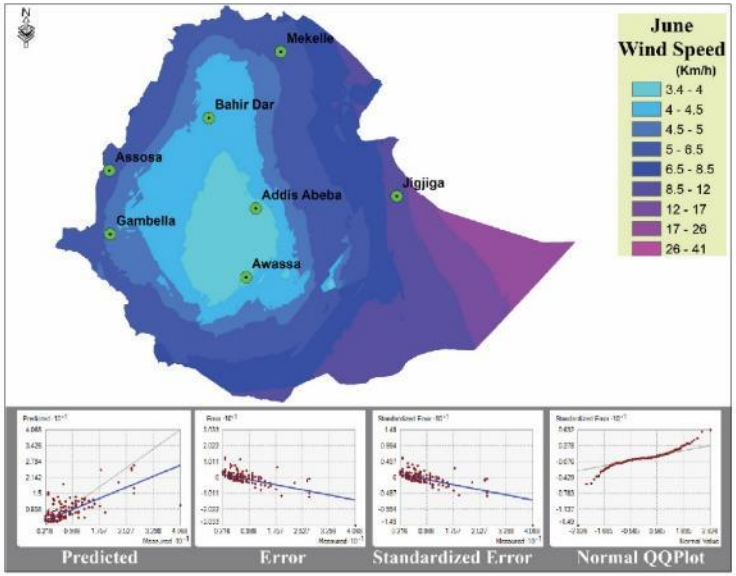
June
Wind Speed
(Km/h)
3.4 - 4
4 - 4.5
4.5 - 5
5 - 6.5
6.5 - 8.5
8.5 - 12
12 - 17
17 - 26
26 - 41
Mekelle
Bahir Dar
Assosa
Addis Abeba
Jigjiga
Gambella
Awassa
Predicted
Error
Standardized Error
Normal QQPlot

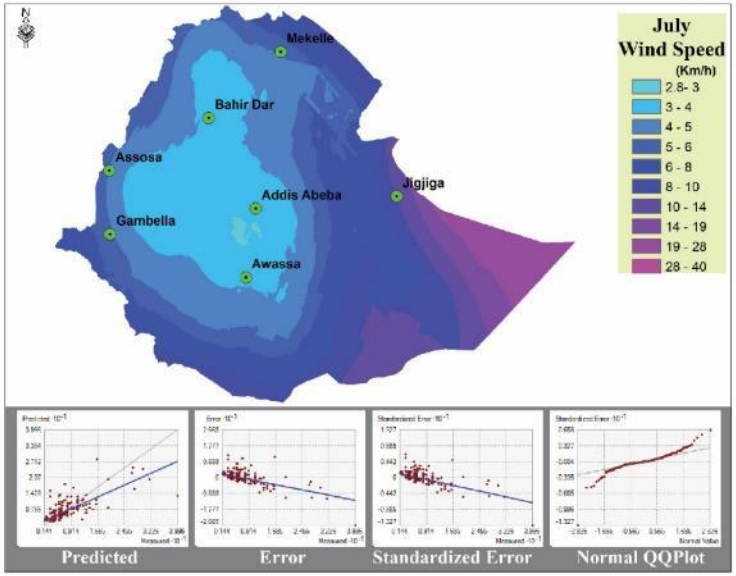
July
Wind Speed
(Km/h)
2.8- 3
3 - 4
4 - 5
5 - 6
6 - 8
8 - 10
10 - 14
14 - 19
19 - 28
28 - 40
Mekelle
Bahir Dar
Assosa
Addis Abeba
Jigjiga
Gambella
Awassa
Predicted
Error
Standardized Error
Normal QQPlot

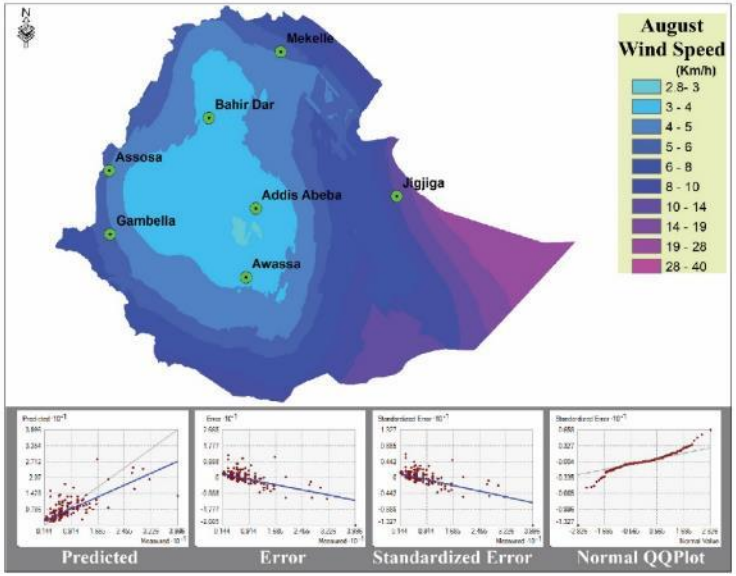
August
Wind Speed
(Km/h)
2.8- 3
3 - 4
4 - 5
5 - 6
6 - 8
8 - 10
10 - 14
14 - 19
19 - 28
28 - 40
Mekelle
Bahir Dar
Assosa
Addis Abeba
Jigjiga
Gambella
Awassa
Predicted
Error
Standardized Error
Normal QQPlot

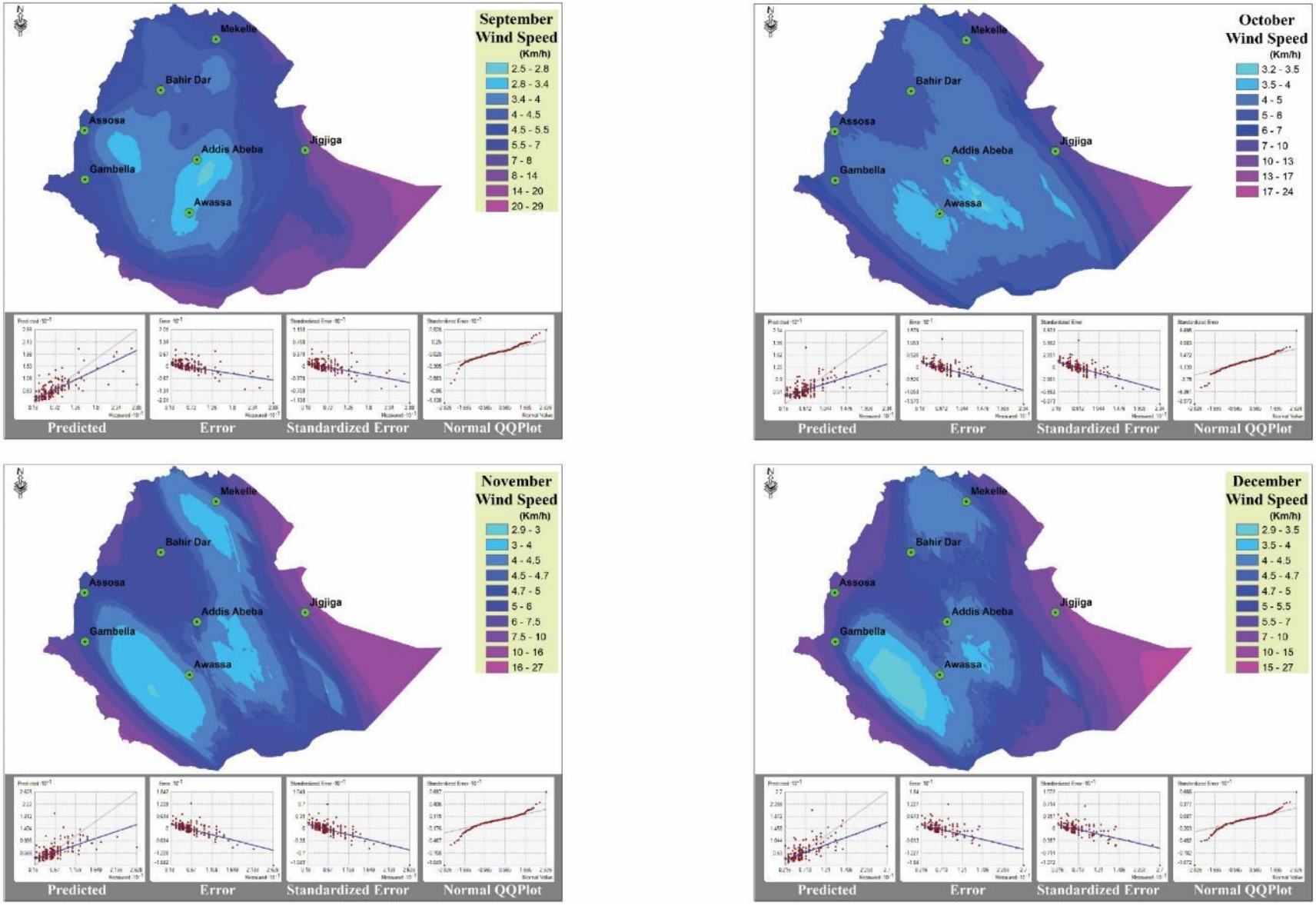

Figure 4.10: Monthly wind speed maps to WetSpass-M model.

4.4. Sensitivity Analysis

For the sensitivity analysis, the monthly input datasets (rainfall, temperature, PET and wind speed) were represented by datasets obtained from the average of the monthly values. Then, each parameter was allowed to be increased by a reasonable amount while the other parameter values kept constant.

The sensitivity analysis result showed that the model was highly sensitive to the alfa coefficient ($\propto$) and the interception parameter (a) (Figure 4.12). A similar result is found by Abdollahi et al (2017). On the other hand, the model was only slightly sensitive to the LP, rainfall intensity, Mannining's coefficient, volume of soil water content, and slope parameters, and it was non-responsive to the delay factor, beta, and contribution parameters.

4.5. Calibration and validation

Among the model inputs, the monthly input datasets (rainfall, temperature, potential evapotranspiration, wind speed, and groundwater depth) were subdivided into two time periods for the purpose of the calibration and validation: From 2000 – 2010 for the purpose of calibration, and from 2010 – 2018 for validation. The calibration process was achieved by changing parameter values one at a time until an acceptable fit is attained between the measured and predicted flows (Figure 4.11) whereas the validation process was performed by running the model by using the parameter values obtained from the calibration process.

One of the outputs of the WetSpass-M model is a text file that holds volumetric surface runoff and base flow values for each of the stress periods (12 months) for the purpose of calibration. The estimated river flow for each of the months was found by adding the surface and base flow component values in the text file. Observed volumetric river discharge of the study area was calculated from river flow data collected from 19 stations located on the outlet of the major rivers in the study area (Figure 5.1).

In order to evaluate the model performance, in addition to the graphical techniques (Figure 4.11), three quantitative statistics were implemented: Nash-Sutcliffe efficiency (NSE), percent bias (PBIAS), and ratio of the root mean square error to the standard deviation of measured data (RSR). The model scored acceptable ratings in all of the model performance indicators (Table 4.3).

The Nash-Sutcliffe efficiency (NSE) is a normalized statistic that determines the relative magnitude of the residual variance ("noise") compared to the measured data variance ("information") (Nash and Sutcliffe, 1970). NSE indicates how well the plot of observed versus simulated data fits the 1:1 line. NSE is computed as shown in Equation (4.1):

$$NSE = 1 - \left[\frac{\sum_{i=1}^{n}(Y_i^{obs} - Y_i^{sim})^2}{\sum_{i=1}^{n}(Y_i^{obs} - Y_i^{mean})^2}\right] \quad (4.1)$$

where Y_i^{obs} is the ith observation for the constituent being evaluated, Y_i^{sim} is the ith simulated value for the constituent being evaluated, Y_i^{mean} is the mean of observed data for the constituent being evaluated, and n is the total number of observations.

NSE ranges between $-\infty$ and 1.0 (1 inclusive), with NSE = 1 being the optimal value. Values between 0.0 and 1.0 are generally viewed as acceptable levels of performance, whereas values <0.0 indicates that the mean observed value is a better predictor than the simulated value, which indicates unacceptable performance.

Percent bias (PBIAS) measures the average tendency of the simulated data to be larger or smaller than their observed counterparts (Gupta et al., 1999).

The optimal value of PBIAS is 0.0, with low-magnitude values indicating accurate model simulation. Positive values indicate model underestimation bias, and negative values indicate model overestimation bias (Gupta et al., 1999). PBIAS is calculated with Equation (4.2):

$$PBIAS = \left[\frac{\sum_{i=1}^{n}\left(Y_i^{obs} - Y_i^{sim}\right)*100}{\sum_{i=1}^{n}\left(Y_i^{obs}\right)}\right] \quad (4.2)$$

RSR is calculated as the ratio of the RMSE and standard deviation of measured data, as shown in Equation (4.3):

$$RSR = \frac{RMSE}{STDEV_{obs}} = \frac{\left[\sqrt{\sum_{i=1}^{n}(Y_i^{obs} - Y_i^{sim})^2}\right]}{\left[\sqrt{\sum_{i=1}^{n}(Y_i^{obs} - Y_i^{mean})^2}\right]} \quad (4.3)$$

RSR varies from the optimal value of 0, which indicates zero RMSE or residual variation and therefore perfect model simulation, to a large positive value. The lower RSR, the lower the RMSE, and the better the model simulation performance.

Process	*Input data*	*Model parameters*
Interception	Precipitation, LAI	a
Surface Runoff	Precipitation, Land use, Soil moisture content, Soil texture, Elevation and Slope	LP, $\propto$, W1, W2, W3, intensity, x, Q_{surf}
Evapotranspiration	Precipitation, Temperature, PET, Wind speed, Rooting Depth, GW depth	
Recharge	Precipitation, Surface runoff, Interception, Evapotranspiration	Contribution, $Q_{sub\text{-}surf}$, β

Table 4.2: The hydrological processes involved in WetSpass-M model together with the required input data and parameters in each of the processes.

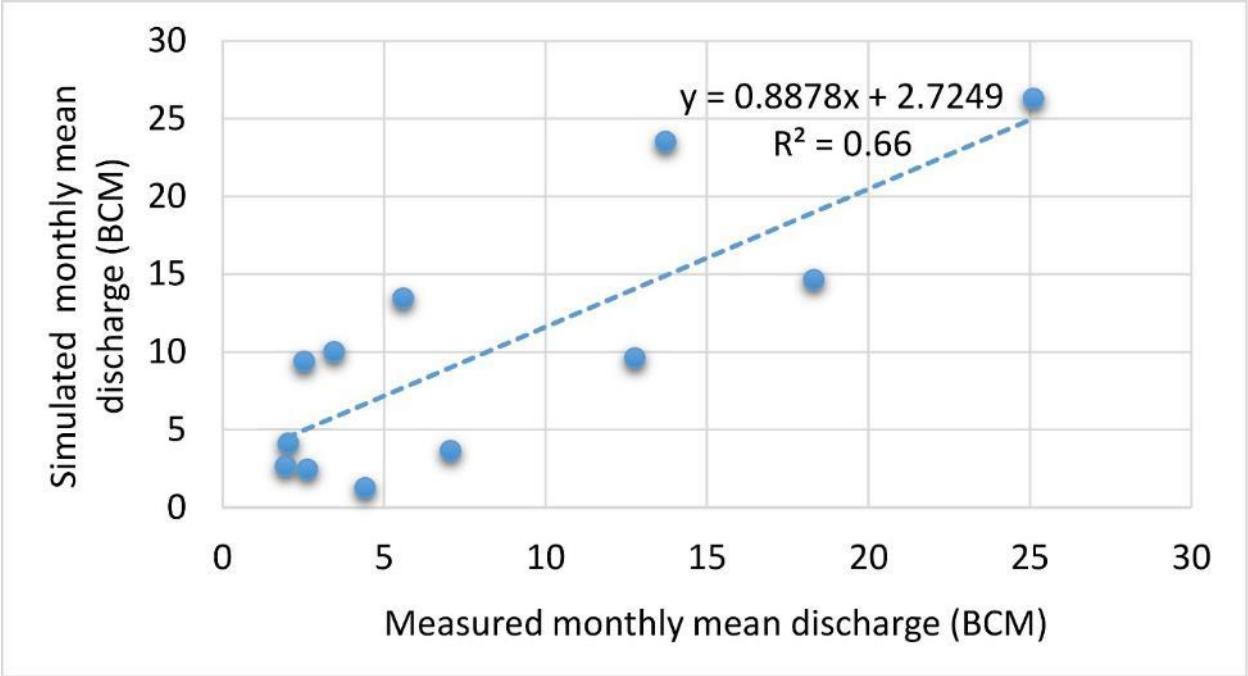

Figure 4.11: Regression of simulated monthly mean discharge and measured monthly mean discharge.

Type	***Evaluation***	***Values***	***Rating***
Calibration	r	0.88	Good
	RSR	0.66	Satisfactory
	NSE	0.52	Satisfactory
	PBIAS	21.6	Satisfactory
Validation	r	0.79	Good
	RSR	0.66	Satisfactory
	NSE	0.58	Satisfactory
	PBIAS	11.4	Good

r = Pearson's correlation coefficient.
RSR = RMSE standard deviation ratio.
NSE = Coefficient of efficiency [Nash and Sutcliffe].
PBIAS = Percent bias.

Table 4.3: WetSpass-M model performance evaluation results

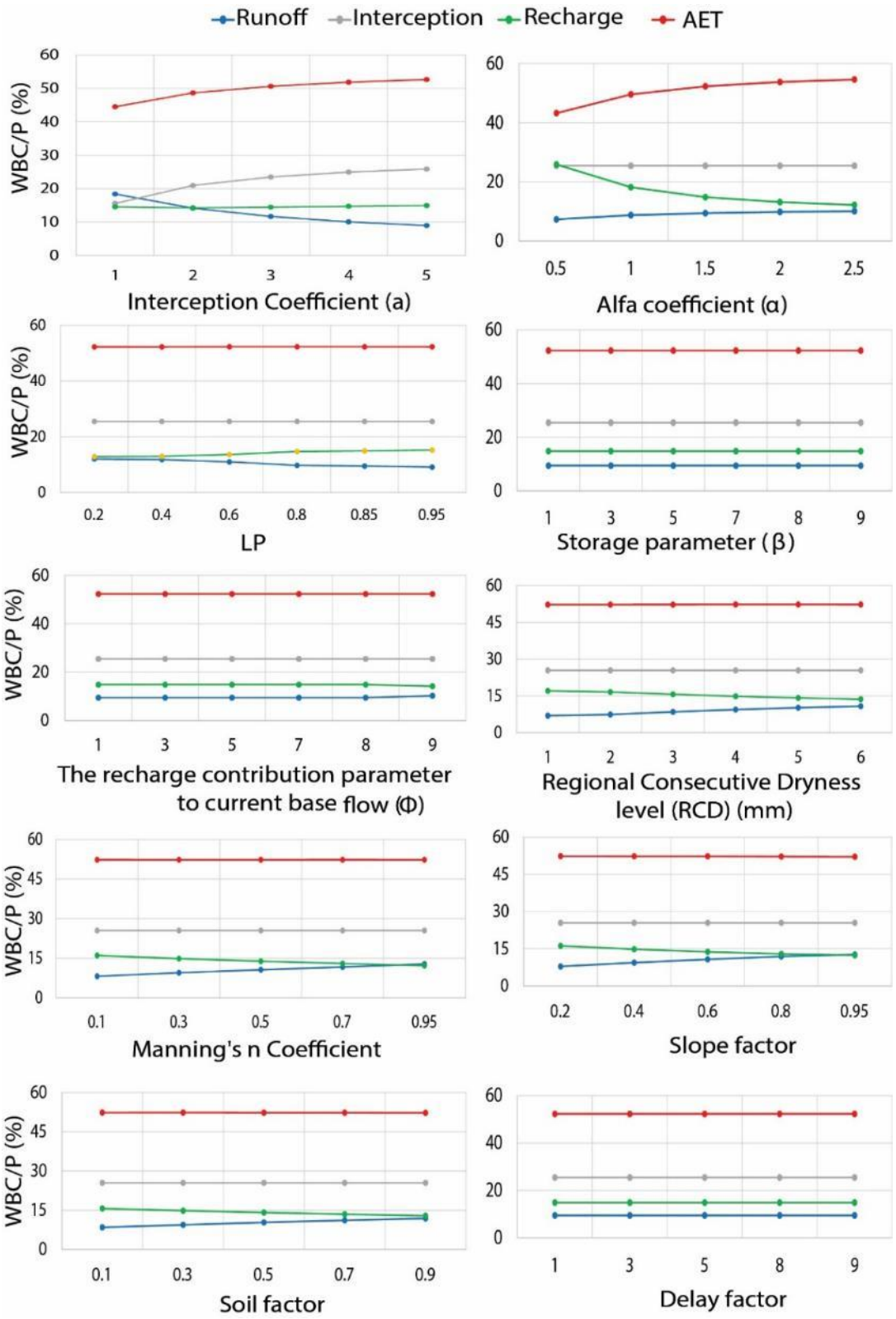

Figure 4.12: Graphs that show sensitivity analysis on each of the parameters. The y axes represent the percentages of the water balance components with respect of precipitation (WBC/P).

4.6. Results

A few national scale researches have been carried out to estimate the groundwater recharge rate in the study area: WAPCOS (1990), by implementing multiple estimation methods, estimated that the exploitable annual groundwater recharge in the study area is 2.6 BCM; Chernet (1993), by using a base flow separation method, estimated that groundwater recharge in the study area ranges between 0 and 400 mm; and Kebede (2013), by compiling basin master plan studies and literatures, estimated that the average annual groundwater recharge in the study area is 39 mm. There are also several researches that estimated recharge by using different methods for small catchments in the study area (Kahsay et al., 2019; Tilahun and Merkel, 2009; Yenehun et al., 2017; Gebru and Tesfahunegn, 2019; Dereje and Nedaw, 2019; Gebreyohannes et al., 2013; Gebremeskel and Kebede, 2017; Meresa and Taye, 2018; Demlie et al., 2005; Demlie, 2015; Abiy et al., 2016; Yimam, 2019; Berehanu et al., 2017).

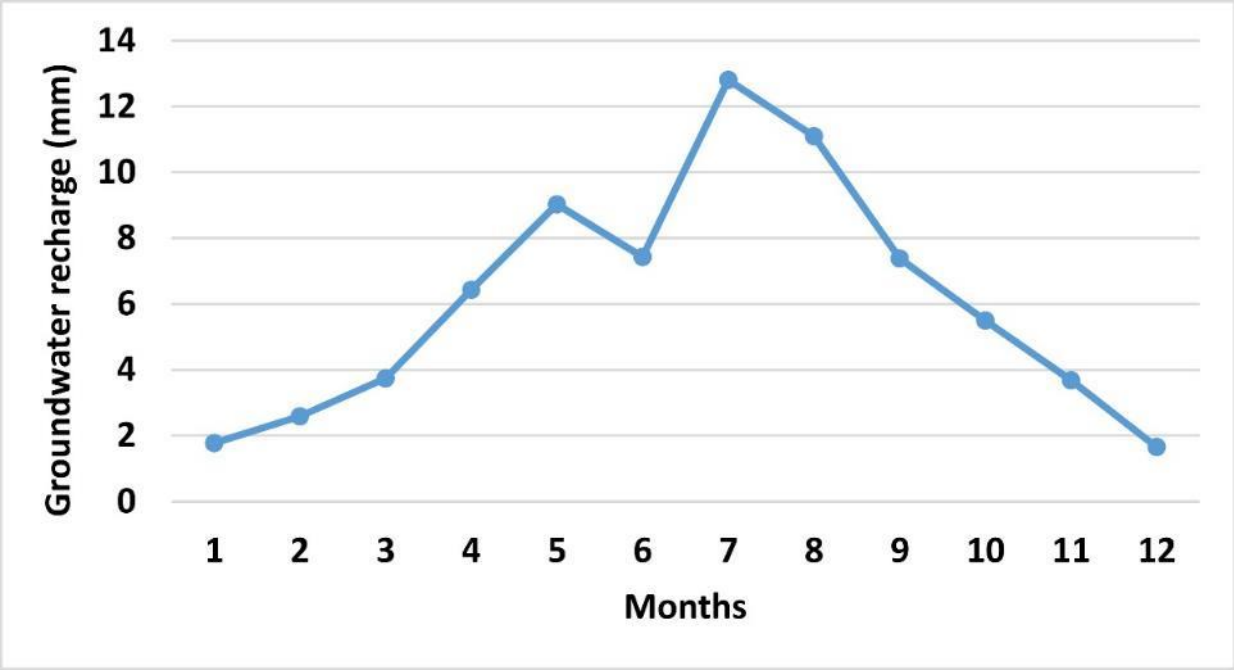

Figure 4.13: Monthly groundwater recharge estimation by WetSpass-M model.

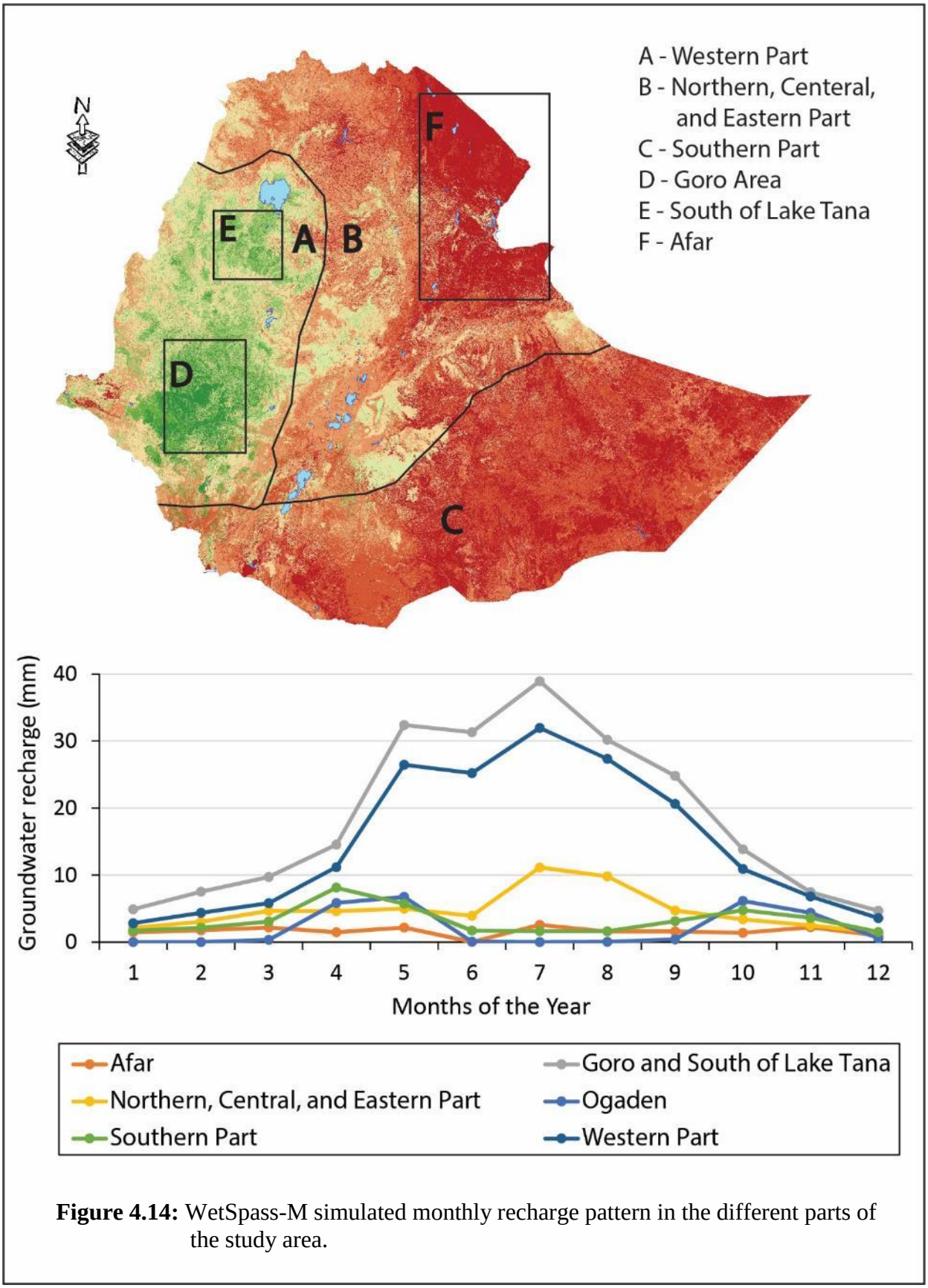

Figure 4.14: WetSpass-M simulated monthly recharge pattern in the different parts of the study area.

In this study, the WetSpass-M model was used to estimate groundwater recharge that is distributed and show variation across the months of the year. Accordingly, the annual average groundwater recharge in the study area, which was found by adding all the monthly average outputs of the model, was estimated to be 73 mm. This figure was much lower than the estimations for the actual evapotranspiration and surface runoff in the study area, 608 mm and 121 mm respectively (Figure 4.16). A similar relationship was obtained in the monthly estimations; actual evapotranspiration attained the highest in all months of the year (Figure 4.15). However, in the dry months (November, December, January and February), even though the actual evapotranspiration was the highest, the groundwater recharge rate was a bit higher than that of the surface runoff (Figure 4.15). In fact, the recharge estimation in the study area showed a unimodal pattern, the highest (18 mm/month) being in August and the lowest in December (2.1 mm) (Figure 4.13).

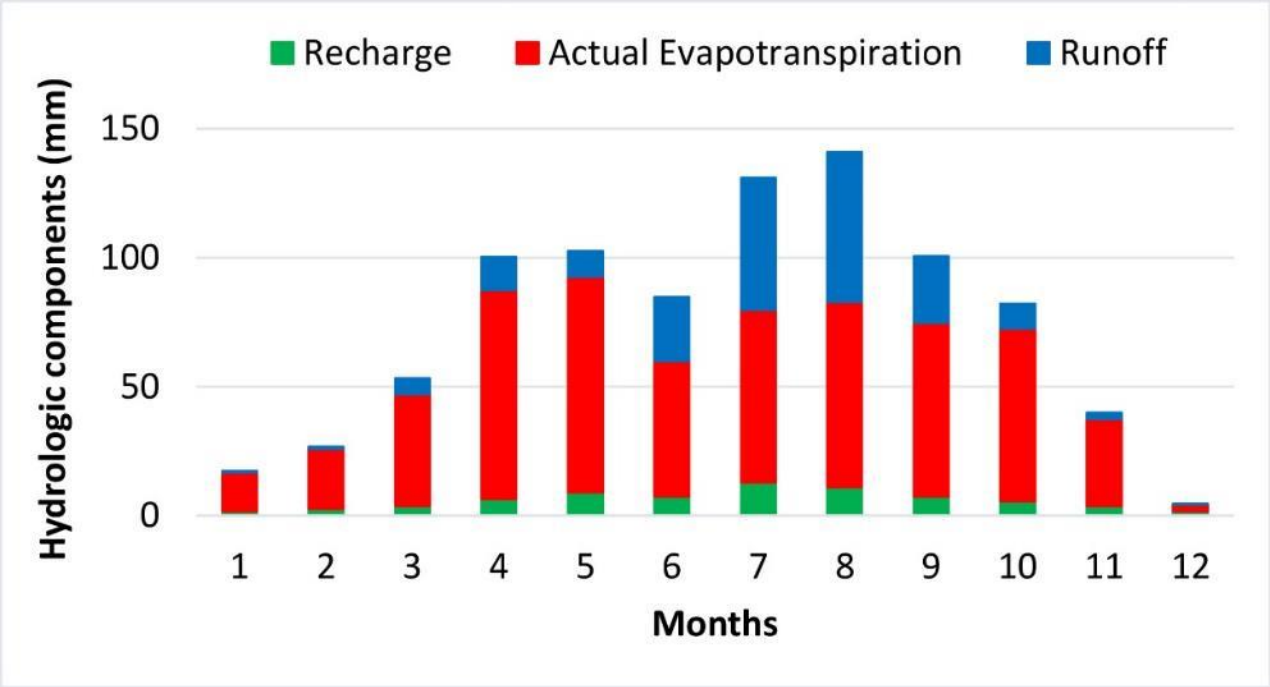

Figure 4.15: Graph that shows monthly estimations of recharge, evapotranspiration, and surface runoff by WetSpass-Model.

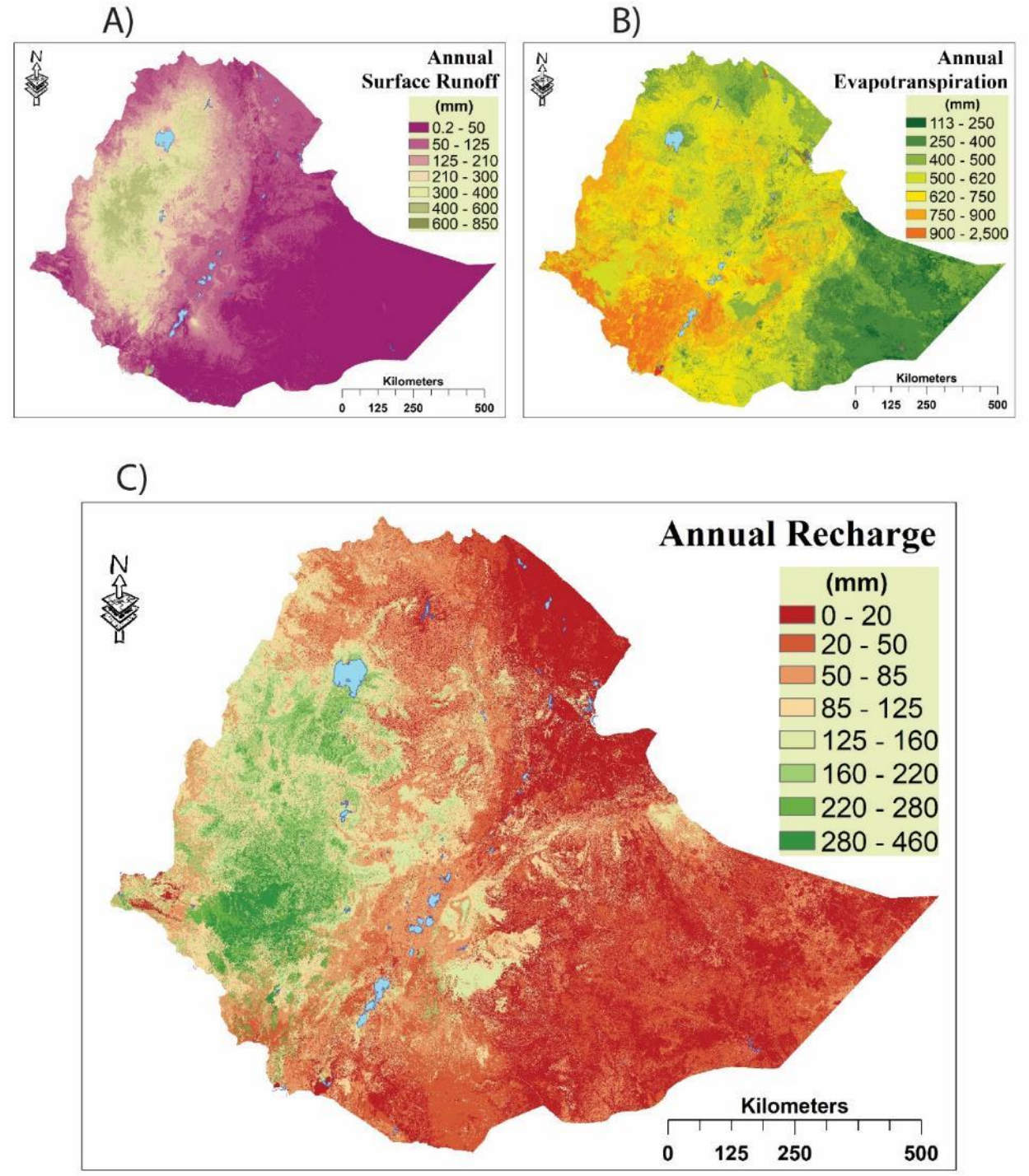

Figure 4.16: WetSpass-M simulated annual A) Surface Runoff B) Actual Evapotranspiration C) Recharge

Figure 4.17 shows maps and graphs of monthly distributed groundwater recharge rates estimated by the Wetspass-M model. As it can be observed from the figure, the groundwater recharge amount and distribution in each month was different, and it was significantly higher in rainy months (June to September). On the other hand, the figure also shows that during October to April, although the amount was small compared to the other months, there was broad occurrence of groundwater recharge in the study area. In fact, in these months, the dominant occurrence was in the southern part of the study area, and as moving further in the range to April, the occurrence extended more to the southern part of the study area. April appears to be the end of the extension. Then, on May, the dominant occurrence of groundwater recharge changed its position to the western part of the study area. In the following months, from May to August, the dominant occurrence of groundwater recharge progressed its extension upward from southwestern to northwestern of the study area, attaining its maximum average in July. In September, it started rebounding along its journey.

Besides the general spatio-temporal pattern, the figure also shows that some particular areas such as the southwestern part of the country specifically Goro area (labeled “D” in figure 4.14), south of Lake Tana (labelled “E” in figure 4.14), Denakil depression (labelled “F” in figure 4.14), and south eastern periphery of the study area (labelled “C” in figure 4.14) had particular groundwater recharge patterns. The Goro area specifically had a large amount of groundwater recharge almost throughout the year (400 mm/yr). Similarly, the area at the south of Lake Tana, except in December and April, showed higher rate of groundwater recharge (240 mm/yr). On the contrary, the Denakil depression (11 mm/yr) and south eastern peripheral part of the study area showed the lowest groundwater recharge almost throughout the year.

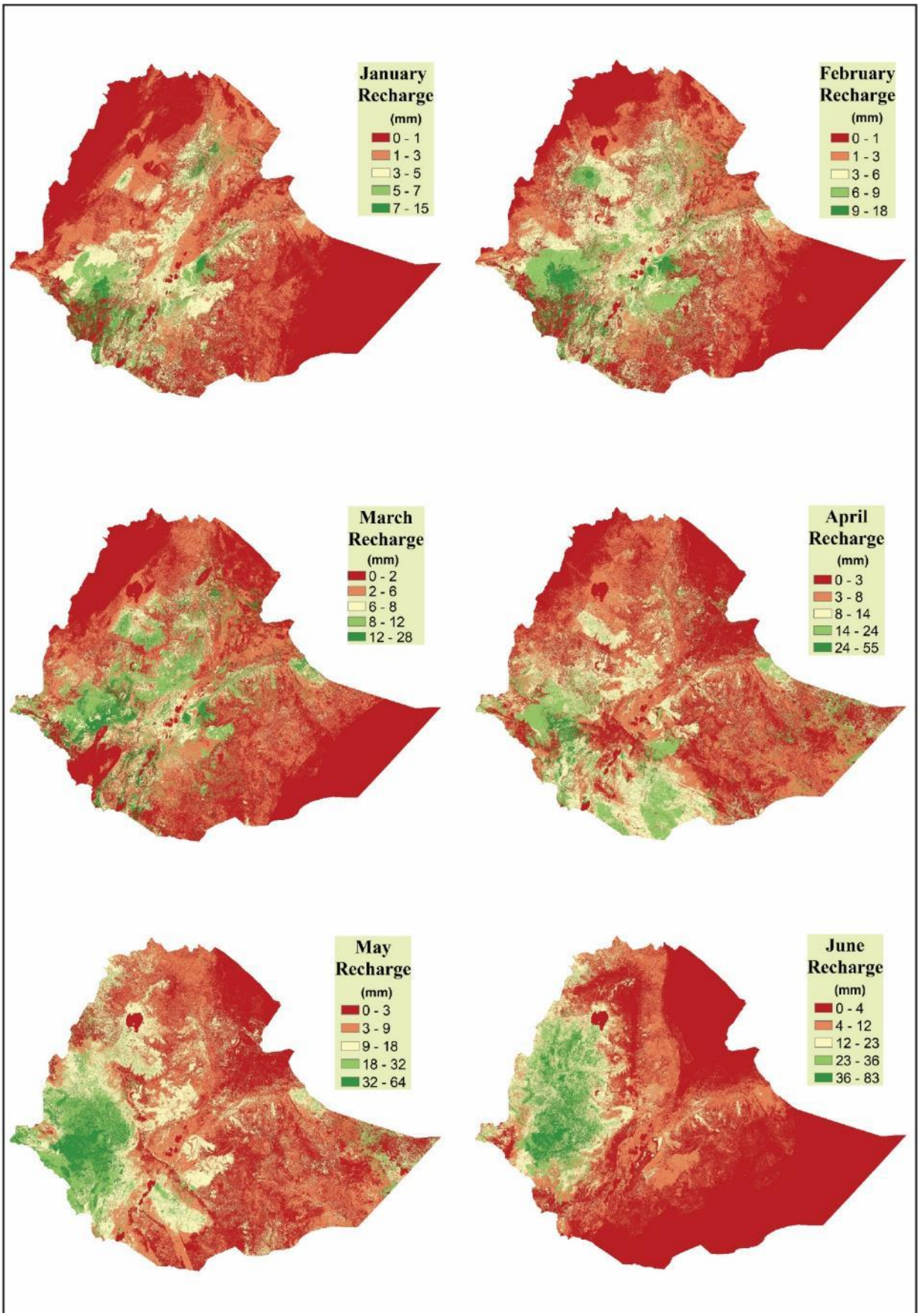
January Recharge
(mm)
0 - 1
1 - 3
3 - 5
5 - 7
7 - 15
February Recharge
(mm)
0 - 1
1 - 3
3 - 6
6 - 9
9 - 18
March Recharge
(mm)
0 - 2
2 - 6
6 - 8
8 - 12
12 - 28
April Recharge
(mm)
0 - 3
3 - 8
8 - 14
14 - 24
24 - 55
May Recharge
(mm)
0 - 3
3 - 9
9 - 18
18 - 32
32 - 64
June Recharge
(mm)
0 - 4
4 - 12
12 - 23
23 - 36
36 - 83

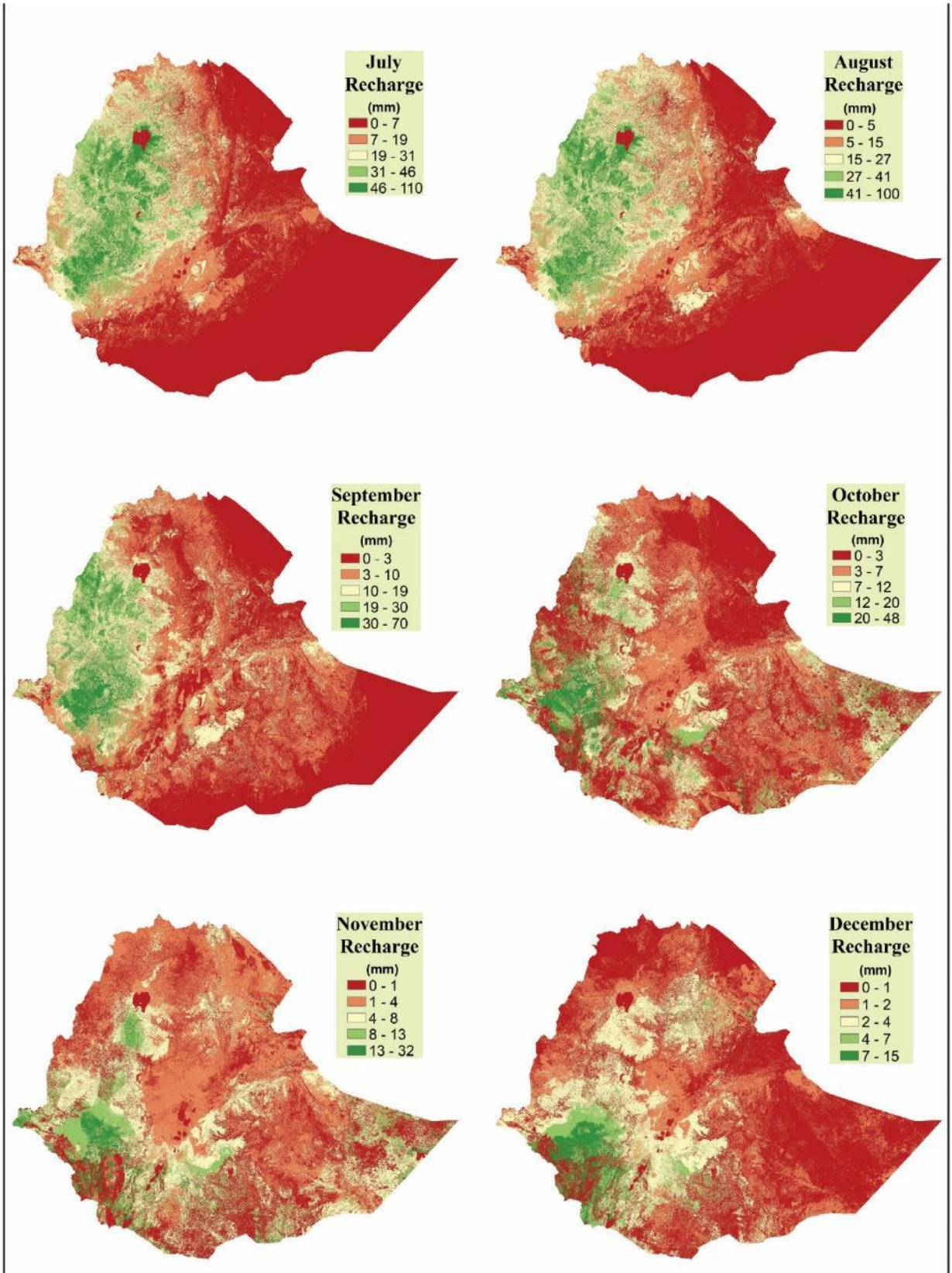

Figure 4.17: Monthly groundwater recharge maps estimated by WetSpass-M model.

4.7. Discussion

To understand the results of WetSpass-M model, it is useful to consider how the model works. WetSpass-M performs its estimation by quantifying the amount of water that goes to each of the hydrological processes involved in the simulation. Additionally, it is a distributed model so that it takes and results datasets that can be viewed both in the spatial and temporal dimensions. The temporal dimension of the recharge estimation is represented by the variations of values among the monthly outputs and that of the spatial dimension is represented by the variation of pixel values in each month according to the resolution set to the model.

4.7.1. Temporal groundwater recharge variability

Temporal analysis on the outputs of WetSpass-M showed that there was groundwater recharge in the study area almost throughout the year, and it is directly related to the co-occurrence of multiple weather system in the study. Thus, in most of the months, there were areas that comparatively had plenty amount of recharge and areas that had low (Figure 4.17). To identify which of the input variables determined the temporal pattern of groundwater recharge in the study area, the Pearson's

	Groundwater recharge											
	Jan	*Feb*	*Mar*	*Apr*	*May*	*Jun*	*Jul*	*Aug*	*Sep*	*Oct*	*Nov*	*Dec*
Rainfall	0.61	0.59	0.35	0.40	0.70	0.80	0.80	0.76	0.76	0.33	0.37	0.37
Slope	0.13	0.15	0.14	-0.11	0.02	0.23	0.35	0.33	0.25	-0.06	-0.05	0.04
PET	-0.42	-0.59	-0.62	-0.49	-0.46	-0.63	-0.68	-0.71	-0.71	-0.11	0.08	-0.19
Temperature	-0.27	-0.50	-0.62	-0.01	-0.21	-0.54	-0.64	-0.62	-0.59	0.07	0.20	-0.13
Wind	-0.46	-0.47	-0.19	0.04	0.01	-0.56	-0.66	-0.66	-0.62	0.06	0.17	0.01
GW depth	-0.21	-0.34	-0.20	0.11	-0.28	-0.57	-0.57	-0.52	-0.63	-0.13	0.09	0.12

Table 4.4: Pearson correlation coefficient between monthly WetSpass-M groundwater recharge result maps and the monthly WetSpass-M input maps. It shows that recharge has the strongest correlation with the rainfall variable, and the rainy months even have the highest coefficients of all the months.

correlation test was carried out between the input variables and the groundwater recharge estimation at each month (Table 4.4). The correlation showed that the rainfall variable had the strongest correlation with the recharge estimations (r = 0.33 to 0.8), and the correlation even became stronger on rainy months (June to September) (table). Additionally, the visual analysis of the spatio-temporal pattern of the recharge estimation showed a close resemblance with that of the rainfall.

4.7.2. Spatial groundwater recharge variability

To understand the spatial variability of groundwater recharge in the study area, the Cramer's V correlation test was carried out between the annual groundwater recharge estimation and the model input datasets. The Cramer's V correlation test (Bonham-Carter, 1994) was implemented because it can be applied on ordinal datasets such as land use/land cover (LULC) and soil texture. The Cramer's V test is one of the linear statistical tools that measures degree of association (correlation) between two images by taking degree of overlap between the images. The resulting coefficient values range between 0 and 1, 0 representing an absence of correlation between the images and 1 a perfect match between the images. Before calculating the Cramer's V correlation by using the CROSSTAB tool in IDRISI32 (terrset version), each of the datasets were reclassified into equal number of classes by using the Reclassify tool in ArcGIS.

	Recharge	*AET*	*Runoff*
Soil texture	0.35	0.41	0.41
LULC	0.33	0.38	0.33
Slope	0.24	0.18	0.26
Rainfall	0.36	0.28	0.37
PET	0.27	0.26	0.28
Temperature	0.27	0.25	0.30
Wind speed	0.24	0.23	0.26
GW depth	0.31	0.25	0.31

Table 4.5: Cramer's V correlation coefficient between WetSpass-M output maps and the WetSpass-M input maps.

The statistical test showed that ground water recharge had the strongest correlation with the rainfall variable (Table 4.5), indicating that in the study area, the spatial variability of groundwater recharge was largely controlled by the spatial pattern of rainfall. To further clarify the spatial

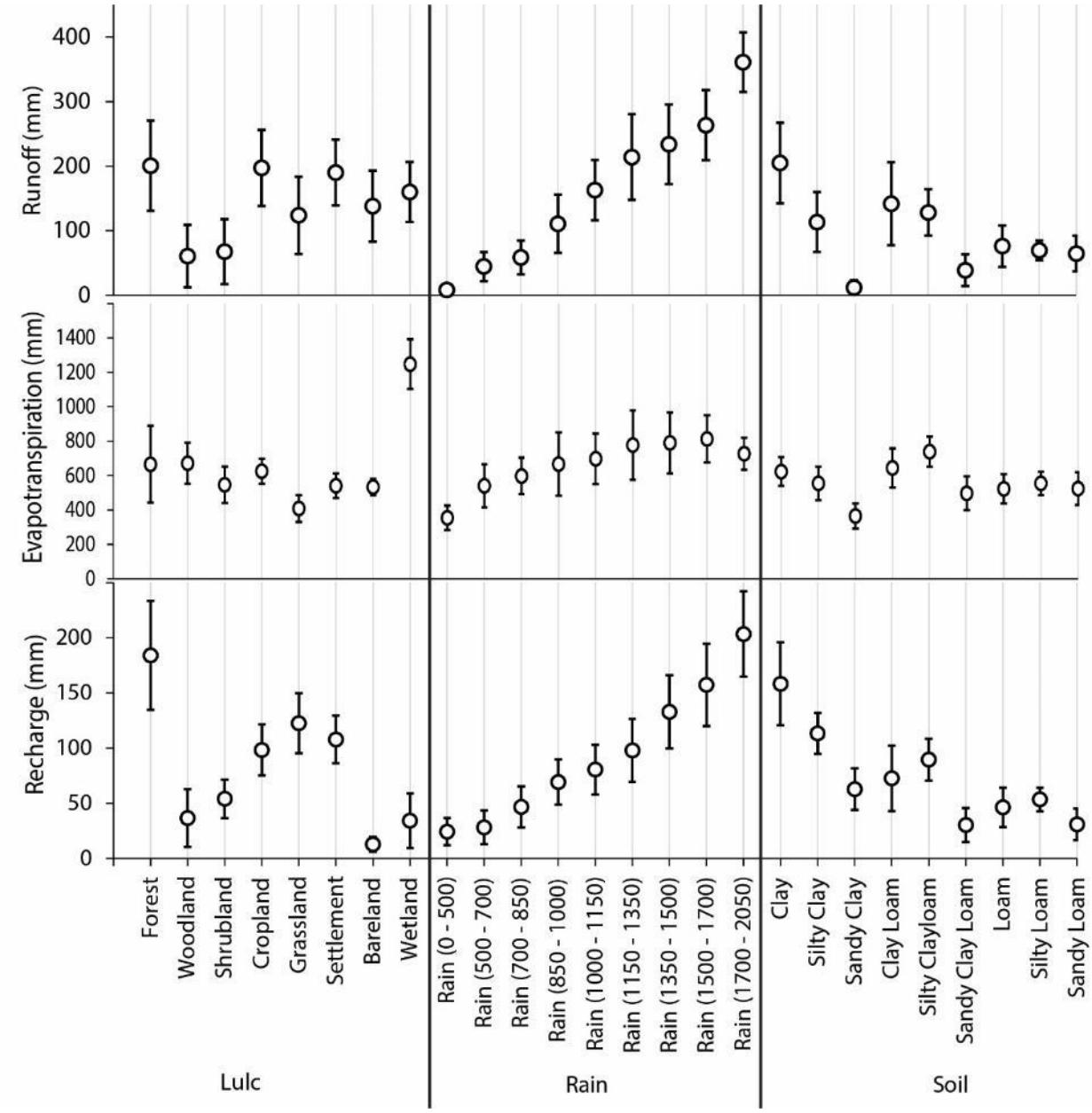

Figure 4.18: Mean and standard deviation of WetSpass-M simulated runoff, evapotranspiration, and recharge per land cover, rainfall, and soil texture classes for the total study area.

relationship between the amount of groundwater recharge and rainfall in the study area, a comparison was carried out among the means and standard deviations of the recharge estimations in the different rainfall classes (Figure 4.18). The comparison showed a proportional increment of recharge with the amount of rainfall, and this relationship explained the highest recharge in Goro area (400 mm/yr) and south of Tana (300 mm/yr) and the low recharge in Denakil (11 mm/yr) depression and Ogaden (17 mm/yr) (Figure 4.14).

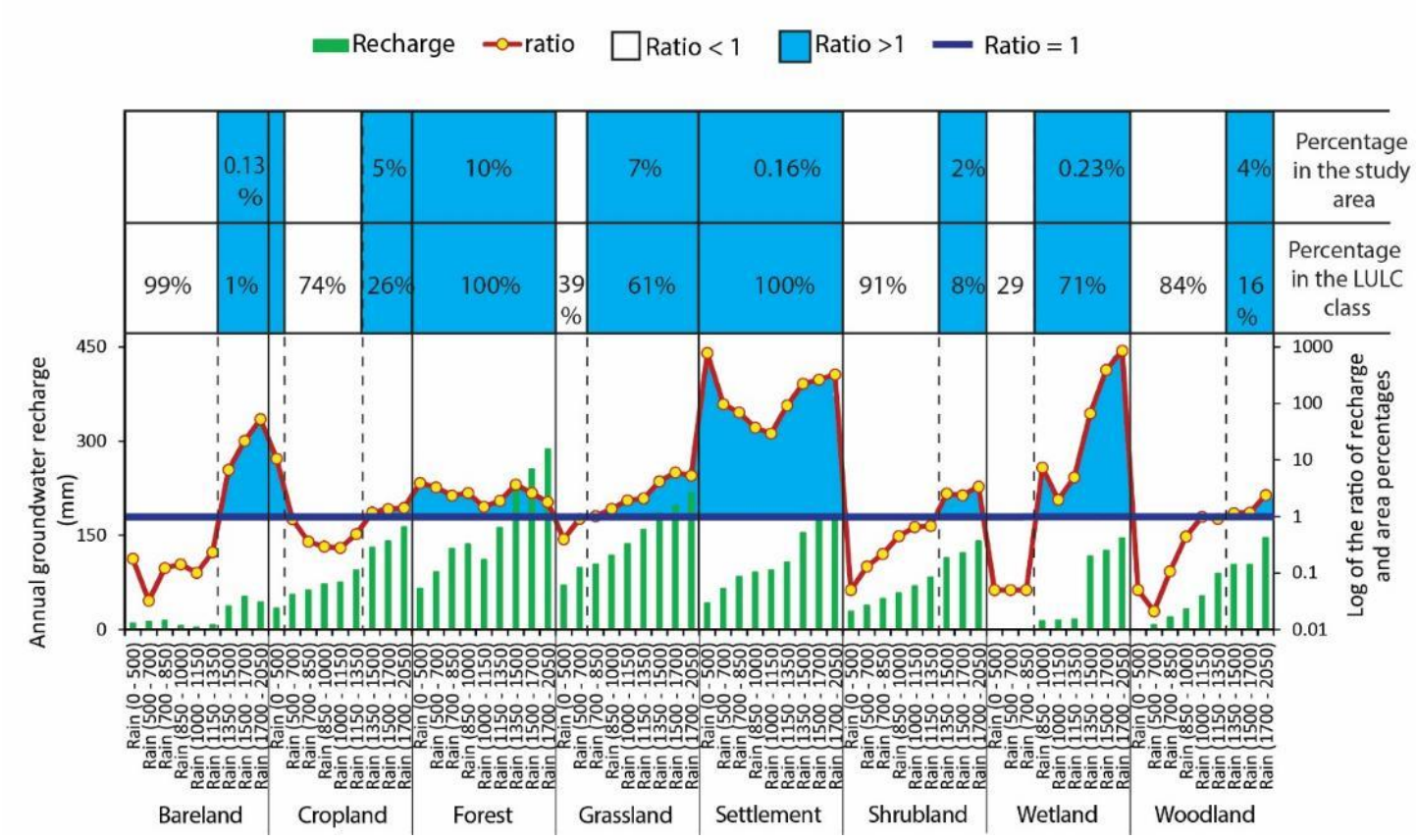

Figure 4.19: The ratio of recharge and area percentages in the different rainfall subclass of the LULC classes.

Next to rainfall, it was the LULC and soil texture that are the most important variables in controlling the spatial variability of groundwater recharge in the study area (Table 4.5). The comparison of the means and standard deviations of the recharge estimations in the different soil texture classes, in contrast to what is known theoretically, showed an inverse relationship between soil texture and groundwater recharge in the study area (Figure 4.18) – a decrease in the amount of groundwater recharge as soil texture coarsened. In order to understand the reason behind the relationship, the annual rainfall in the soil texture classes were compared each other (Figure 4.21). According to the comparison, rainfall and soil texture were found to have inverse relationship in the study area, and the soil texture class that received the highest amount of rainfall was found to be the finest soil texture class. Additionally, finer soil texture classes in the study area, due to their higher rainfall, were found to have not only higher groundwater recharge but also higher evapotranspiration and surface runoff (Figure 4.21).

Similarly, among the LULC classes, the forest, cropland, grassland and settlement, because they constitute areas with higher rainfall, showed higher groundwater recharge and surface runoff (Figure 4.20). On the other hand, shrub lands, wood lands, and bare lands, because they belong to areas with low rainfall, showed lower groundwater recharge estimations. In fact, Figure 4.20 also shows that the lowest groundwater recharge estimation in the study area was obtained in the bare lands. Moreover, possibly due to the influence of their high leaf area index, the estimated surface runoff in the shrub lands and wood lands was the lowest whereas their estimated evapotranspiration was among the highest values.

Groundwater recharge was found to be the least correlated with slope and wind speed variables (Table 4.5).

As the output of this study has the finest spatial and temporal resolutions, it could have enormous advantage for different kinds of applications. For example, as it is shown in Figure 4.19, by taking the ratio of the amount of the annual groundwater recharge in the different rainfall classes of each LULC class and their areal coverage, it was possible to identify which part of the study area was important for the sustenance of groundwater resource in the study area. This analysis could supplement groundwater management works in the study area. The analysis showed that all the rainfall subunit classes of the forest LULC class had a ratio greater than one, i.e., the forest LULC played a very crucial role in sustaining groundwater resource of the study area. Indeed, the largest proportion of the forest LULC class exists in the southwestern part of the country where there is

high rainfall almost throughout the year. Similarly, the settlement class had a ratio greater that one indicating that the major and minor cities of the study area are founded on areas that are crucial for the sustenance

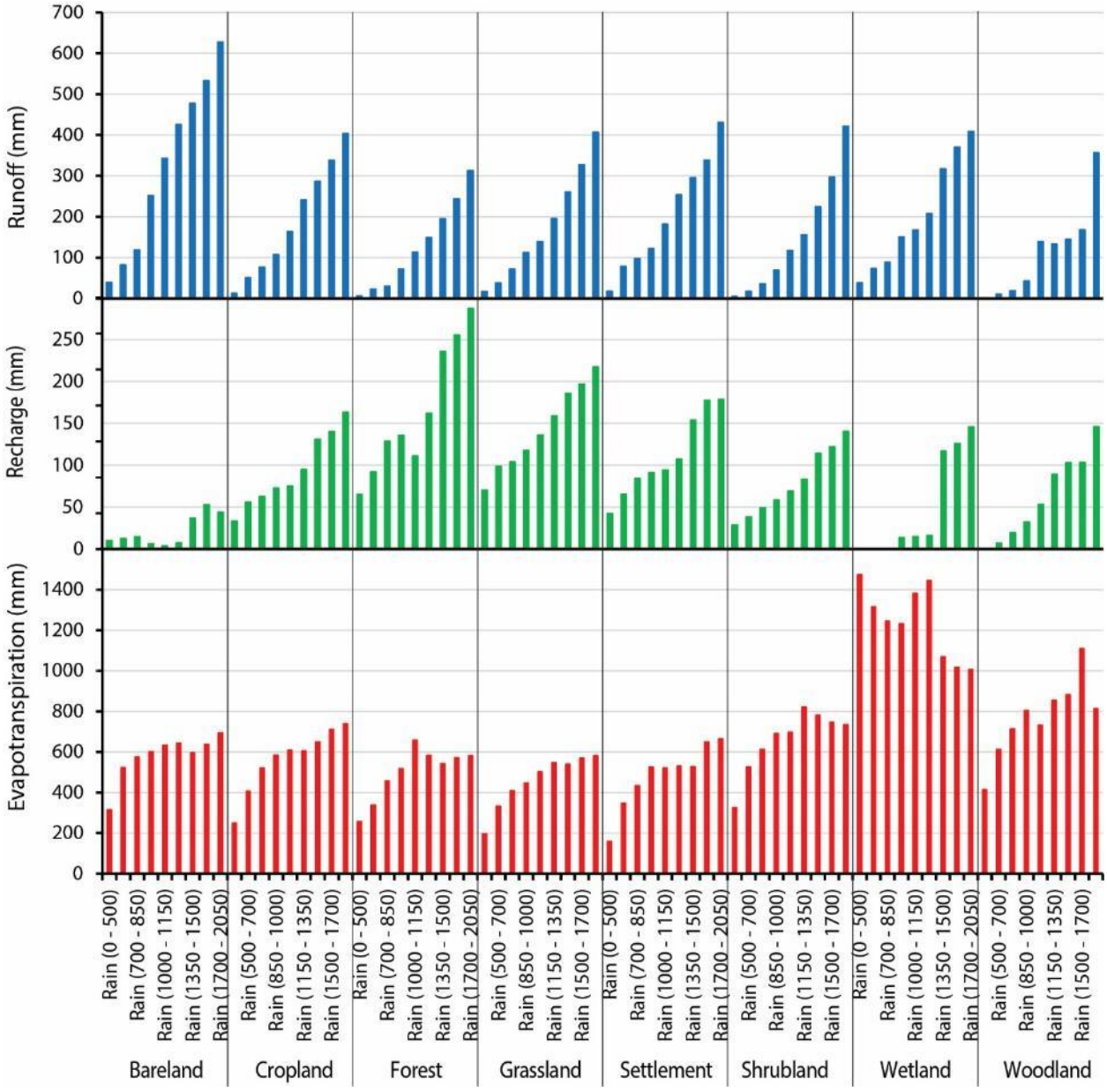

Figure 4.20: Graph of the WetSpass-M model mean annual evapotranspiration, recharge, and runoff estimations in each LULC classes.

groundwater resource in the study area. In contrast to that, 26% of the cropland class had a ratio above one. In Bareland and wetland classes also, there were subunit classes with high groundwater recharge potential although they account only 0.4% of the total area of the study area. On the other

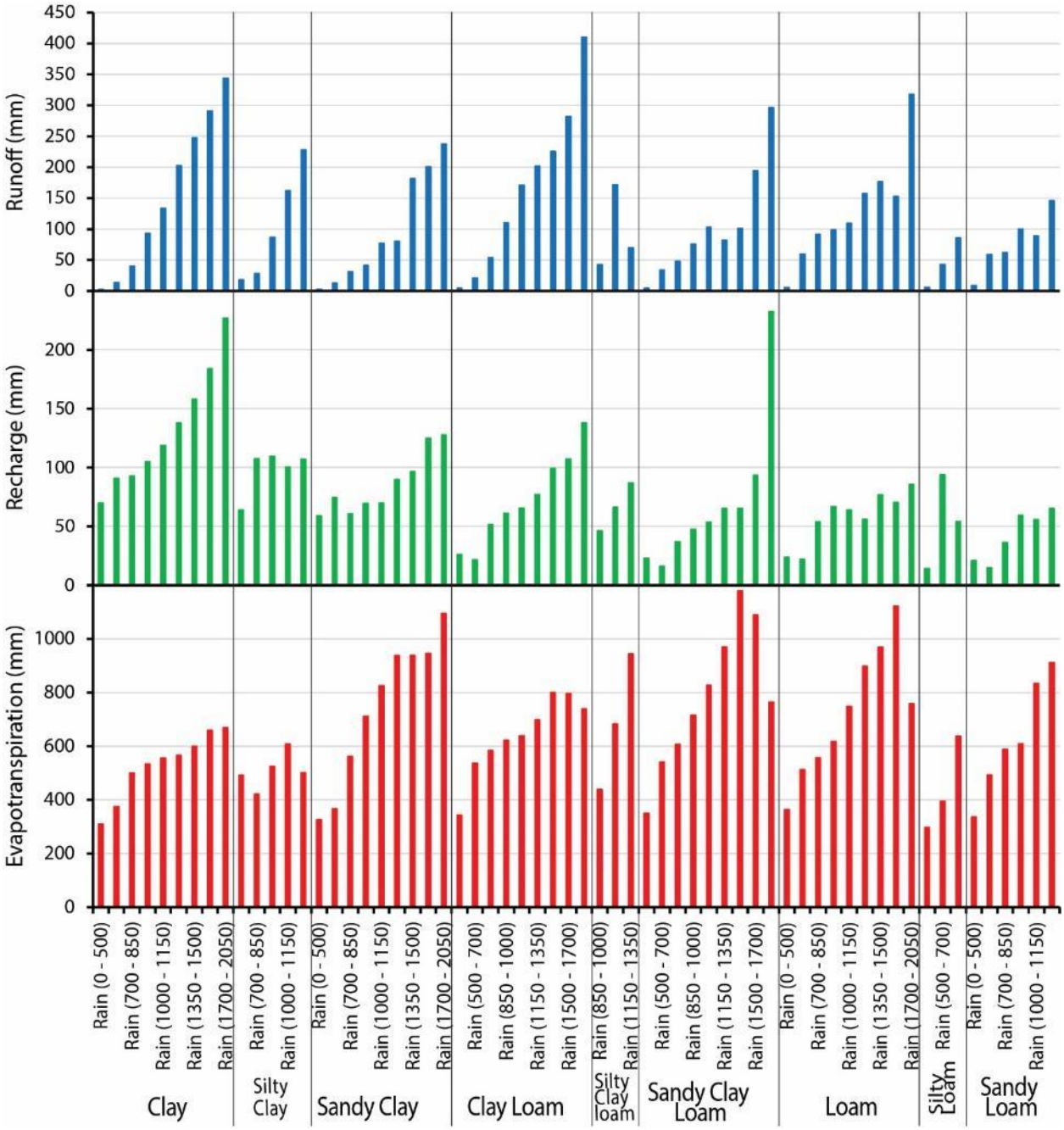

Figure 4.21: Graph of the WetSpass-M model mean annual evapotranspiration, recharge, and runoff estimations in each soil texture classes.

hand, although a few subclasses of Woodland and Shrubland scored a ratio value greater than one, their areal coverage was not the smallest; they covered 6% of the study area.

Additionally, due to its finer spatial resolution, the outputs of the model could be used in large scale groundwater recharge potential studies such as catchment levels. Furthermore, it could also be very important to identify and manage aquifers that are susceptible to contamination.

CHAPTER FIVE

5. GROUNDWATER RECHARGE ESTIMATION BY USING THE RECURSIVE DIGITAL FILTER BASE FLOW SEPARATION METHOD

5.1. Introduction

This chapter deals about the application of the recursive digital filter base flow separation method to estimate the monthly groundwater recharge in the study area. Several base flow separation methods have been developed to estimate groundwater recharge from stream flow records, and have been applied at various parts of the world having different physical, hydrological and climatological settings (Pettyjohn and Henning, 1979; Institute of Hydrology, 1980; Wahl and Wahl, 1988; Nathan and McMahon, 1990; Rutledge, 1998; Arnold et al., 1995; Arnold and Allen, 1999; Sloto and Crouse, 1996; Lim et al., 2005). The methods quantify the base flow component of a stream flow and assigns it as a groundwater recharge estimation to the catchment drained by the stream. In the methods, the base flow component of a stream flow is equated to the groundwater recharge of a catchment by taking two assumptions. The first assumption is that base flow is considered to be all the water that joined an aquifer and discharged out to a stream without any loss. The second is that the groundwater and surface water catchments are assumed to be the same (Healy and Scanlon, 2010).

In the literature, base flow is used interchangeably with 'low flow'. However, there are situations where each of them are specific. According to Ward and Robinson (1990), base flow represents portion of a stream flow fed from deep subsurface and delayed shallow subsurface storage between precipitation or snowmelt events. On the other hand, low flow specifically represents minimum flows in dry season (Smakhtin, 2001).

In this research, the digital recursive filter base flow separation technique was applied (Nathan and Mchamon, 1990). This method is adopted from techniques originally applied in signal analysis and processing (Lyne and Hollic, 1979). Although the method has no true physical basis, it is objective and reproducible. In the digital recursive filter technique, a stream flow dataset is taken as a main input signal data in the processing. Then, it is separated into high and low frequency components: The high frequency component represents the surface runoff, the quickest response of a rainfall event, and the low frequency component represents the base flow, the slowest response a rainfall event. The equation of the filter is given as:

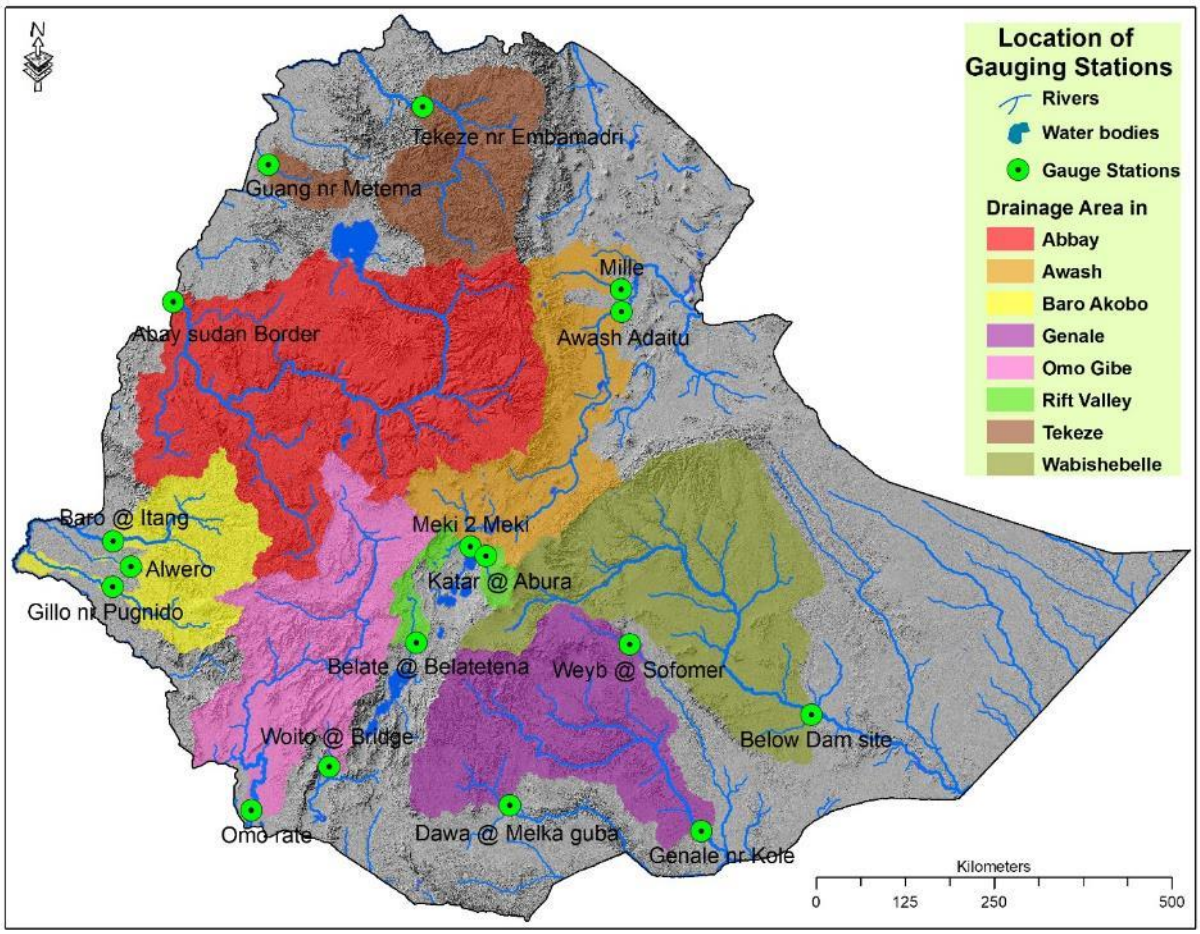

Figure 5.1: Map river gauge stations used in the study.

$$q_t = \beta q_{t-1} + \frac{(1 + \beta)}{2} * (Q_t - Q_{t-1})$$

Where q_t is the filtered surface runoff (quick response) at the t time step (one day), Q is the original streamflow, β is the filter parameter. According to many studies in different parts of the world, the filter parameter is set to be 0.975 (Grayson *et al*., 1996).

Base flow (b_t) is calculated with the equation:

$$b_t = Q_t - q_t$$

The technique was executed under the River Analysis Package (RAP) software. To run the estimation process, the RAP requires a full year daily flow data without any gap. Thus, the stream flow data was organized into a long term daily average for each day of the year.

5.2. River discharge data

For the estimation of groundwater recharge in the study area by using the digital recursive base flow separation method, 18 river stations were selected (Table 5.2). The stations are located at the outlets of the main rivers of the study area (Figure 5.1). However, there are still some areas that were not included in the estimation due to the absence of gauge station. As these areas constitute the dry parts of the country and are known to have low flows almost throughout the year, the groundwater recharge estimation from these locations could not add much on the amount estimated for the rest of the study area.

The missing values in the data were handled according to size. In the case of a few missing values in the record, it was the average of the neighboring values in the record that were used. In the case of a big gap in the record, since the estimation is a long term average, the best solution to minimize a bias was found to be disregarding the whole year from the estimation.

5.3. Result and Discussion

Previous base flow separation estimations in the study area showed different results: Chernet (1993) estimated that the annual groundwater recharge in the study area ranges between 0 and 400 mm, and WAPCOS (1990) estimated an annual base flow of 22 BCM. In this study, the recursive digital base flow separation method was implemented, and a long term average groundwater recharge was estimated for each month of the year. Additionally, the annual recharge estimation in the study area was calculated from the monthly estimations.

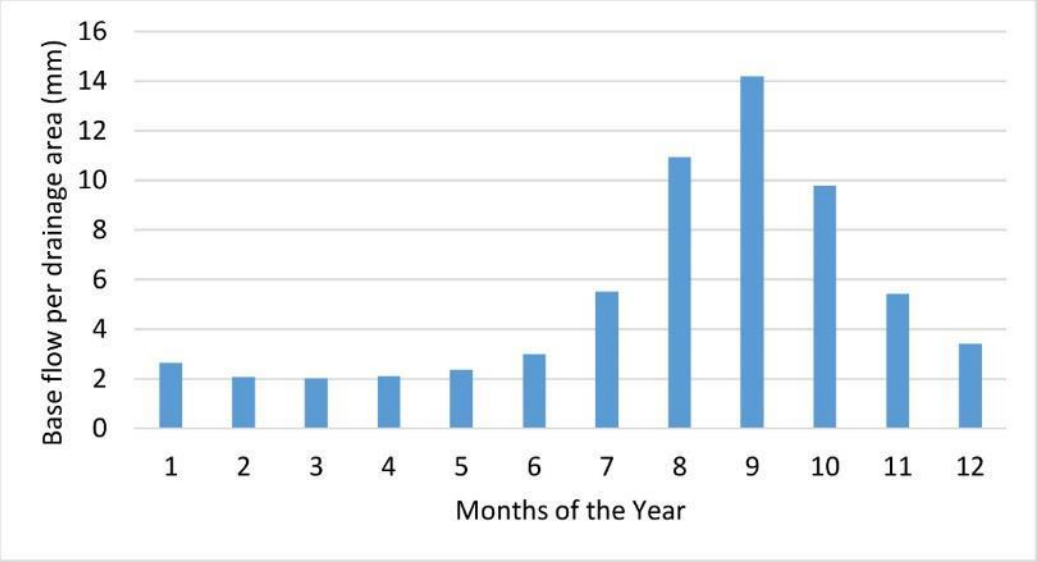

Figure 5.2: Graph of the monthly base flow of the study area (mm) from the estimation of the recursive digital filter base flow separation method.

Figure 5.2 and 5.3 show the monthly estimates of groundwater recharge in the study area. According to the estimation, the annual groundwater recharge in the study area was found to be 63 mm (40 BCM), and the highest recharge estimation was found in the rainy season which is from June up to September. Generally, the rainy months had huge base flow volumes, and hold the lowest BFI in July and the largest base flow in September (10 BCM) (Figure 5.3). The huge base flow volumes could be taken as a justification to the characterization given to the aquifers in the country, i.e. the aquifers in the study area are characterized as having low groundwater storages (Kebede, 2013). In fact, it is due to the high elevation of the central part of the study area that most of the rivers in the country are large and flow out to the neighboring countries. Furthermore, Figure

5.3 shows that there is a month gap between the highest base flow and the highest river flow in the study area. This situation could be related to the capacity of the aquifers of the study area to buffer external changes.

Month	*Abbay*	*Tekeze*	*Baro*	*Awash*	*Rift*	*Omo*	*Genale*	*Wabi*
1	5.4	1.2	7.8	0.9	1.2	1.7	1.5	0.3
2	4.3	1	5.5	1	1.1	1.3	1	0.3
3	4.2	1.1	5	1	1.5	1.2	0.9	0.2
4	4	1	4.9	1.1	1.8	1.8	1.4	0.3
5	4	0.9	5.9	1.1	2.4	2.4	2.2	0.5
6	5.5	1.3	8.3	0.9	2.8	2.4	2.7	0.5
7	12.4	4.3	14.2	1	4.2	2.6	2.9	0.5
8	26.5	12.8	25.9	1.8	6.6	2.8	3.3	0.7
9	35.5	12	36.9	2.9	7.7	2.7	3.7	1
10	20	6.1	38.6	2.8	3.7	2.9	4.1	1
11	11	3	18.3	2.1	1.9	2.5	3.3	0.3
12	6.6	1.9	11.2	1.4	1.6	2.1	2.5	0

Table 5.1: Monthly groundwater recharge estimation in the major river basins of the study area by the recursive digital filter base flow separation method.

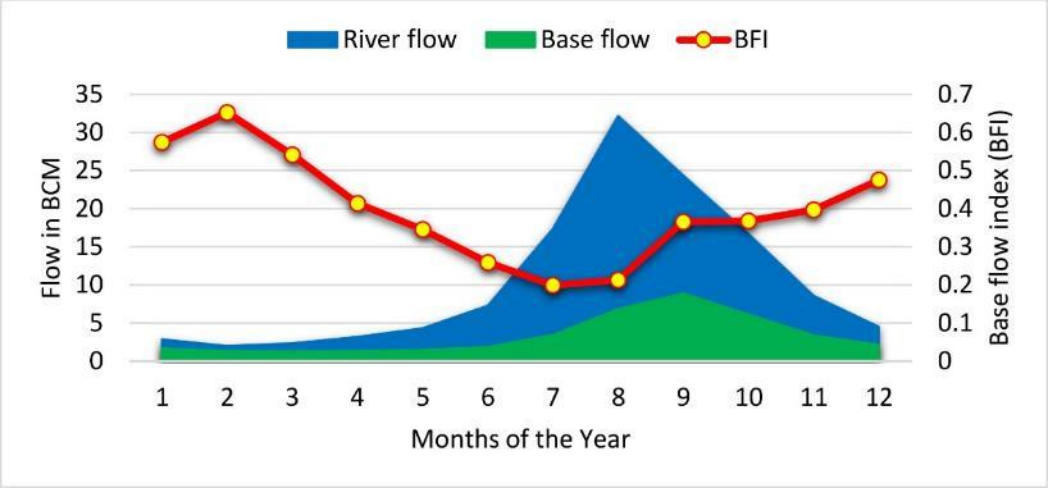

Figure 5.3: Graph of the monthly river flow, base flow, and base flow index (BFI) of the study area (mm) from the estimation of the recursive digital filter base flow separation method.

On the other hand, Figure 5.1 and 5.5 shows the monthly groundwater recharge in the major river basins of the study area. From this summary, it was possible to observe both the spatial and temporal groundwater recharge variation in the study area. Analysis on the timings of flow picks among the basins could suggest a classification of the basins into three groups (Figure 5.4). Group A consists of the river basins in the western part of the study area: Abbay, Tekeze and Baro. Group B represents river basins in the southern and south eastern part of the study area: Omo, Genale and Wabishebelle. Group C are basins in the Ethiopian rift valley: Awash and Rift valley.

Name	*Basin*	*Area (Km^2)*	*Time period*
Tekeze nr Embamadri	Tekeze	45977	1990 – 2015
Guang nr Metema	Tekeze	6590	1990 – 2015
Abay sudan Bodrder	Abay	164150	1990 – 2015
Baro @ Itang	Baro-Akobo	25102	1974 – 1980
Alwero	Baro-Akobo	3440	2008 – 2015
Gillo nr pugnido	Baro-Akobo	11754	1977 – 1990
Omo rate	Omo-Gibe	23854	2006 – 2014
Omo @ Woito Bridge	Omo-Gibe	4892	1990 – 2007
Rift @Belate	Rift valley	4161	1990 – 2007
Rift @Abura	Rift valley	716	1990 – 2010
Rift @Meki	Rift valley	2562	1969 – 2010
Awash @ Adaitu	Awash	50470	1990 – 2015
Awash @ Mille	Awash	4866	1990 – 2015
Genale @ Sofomar	Genale Dawa	5105	1990 – 2015
Genale @ Melka guba	Genale Dawa		1990 – 2015
Genale @ kole	Genale Dawa	55152	1990 – 2015
Wabi @ Burkur	Wabishebelle	55598	1976 – 2011
Wabi @ jigjiga	Wabihsebelle	633	1976 – 2011

Table 5.2: Selected gauge stations with their drainage area and record range.

Group A basins had unimodal river and base flow patterns. The highest river and base flow values were observed in the rainy months of the country, which is from June to September, and the average monthly river flow values in the rainy months for the Abbay, Tekeze, and baro basins was found to be 200, 000 m3, 105,000 m3, and 40,000 m3, and that of the base flow, 15,000 m3, and 37,000 m3 and 27,000 m3 respectively. The total amount of base flow in this group was the highest and accounted 84% of the total base flow in the study area. This result could show that the aquifers in this part of the study area has low storage due to their tendency to discharge water rather than store.

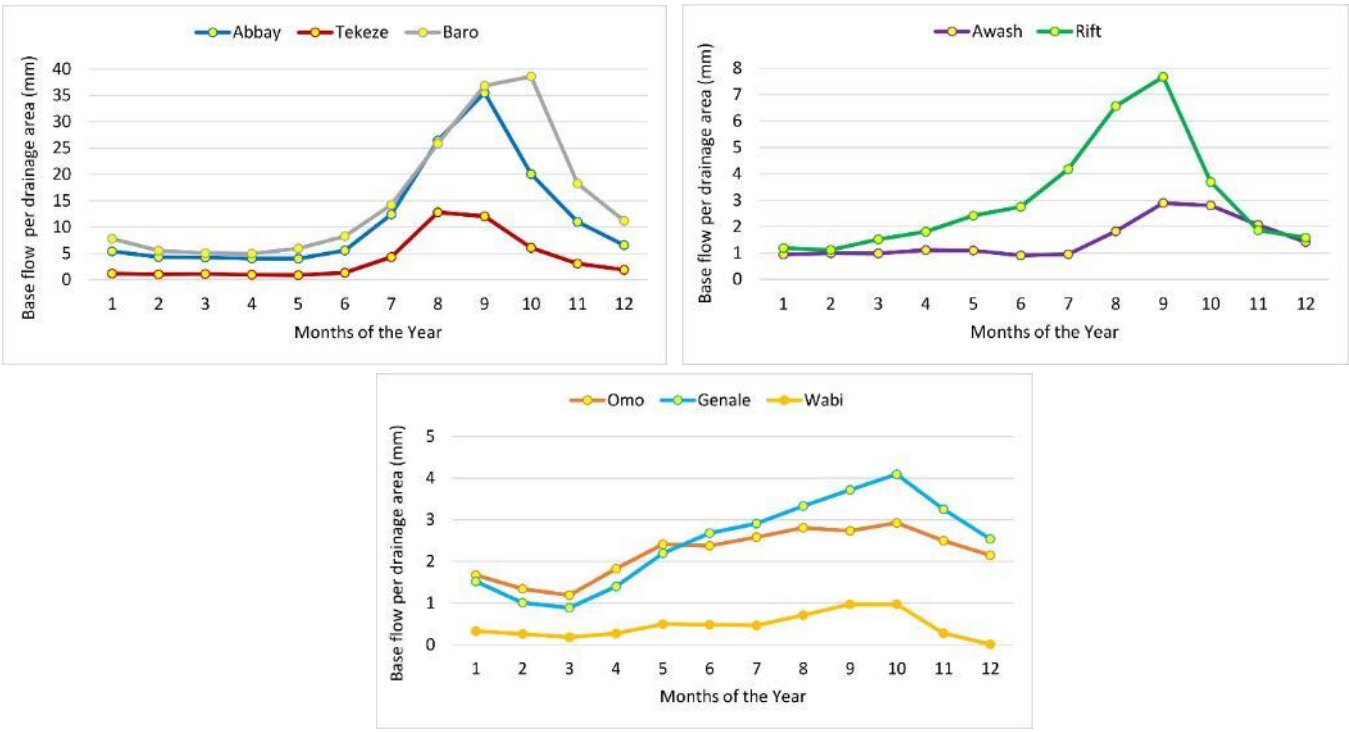

Figure 5.4: Graphs that show A) Monthly recharge (base flow (mm)) pattern in Abbay, Tekeze, Baro basins (group A basins). B) Monthly recharge pattern in Awash and Rift valley basins. C) Monthly recharge pattern in Omo, Genale, and Wabishebele basins (group C bains).

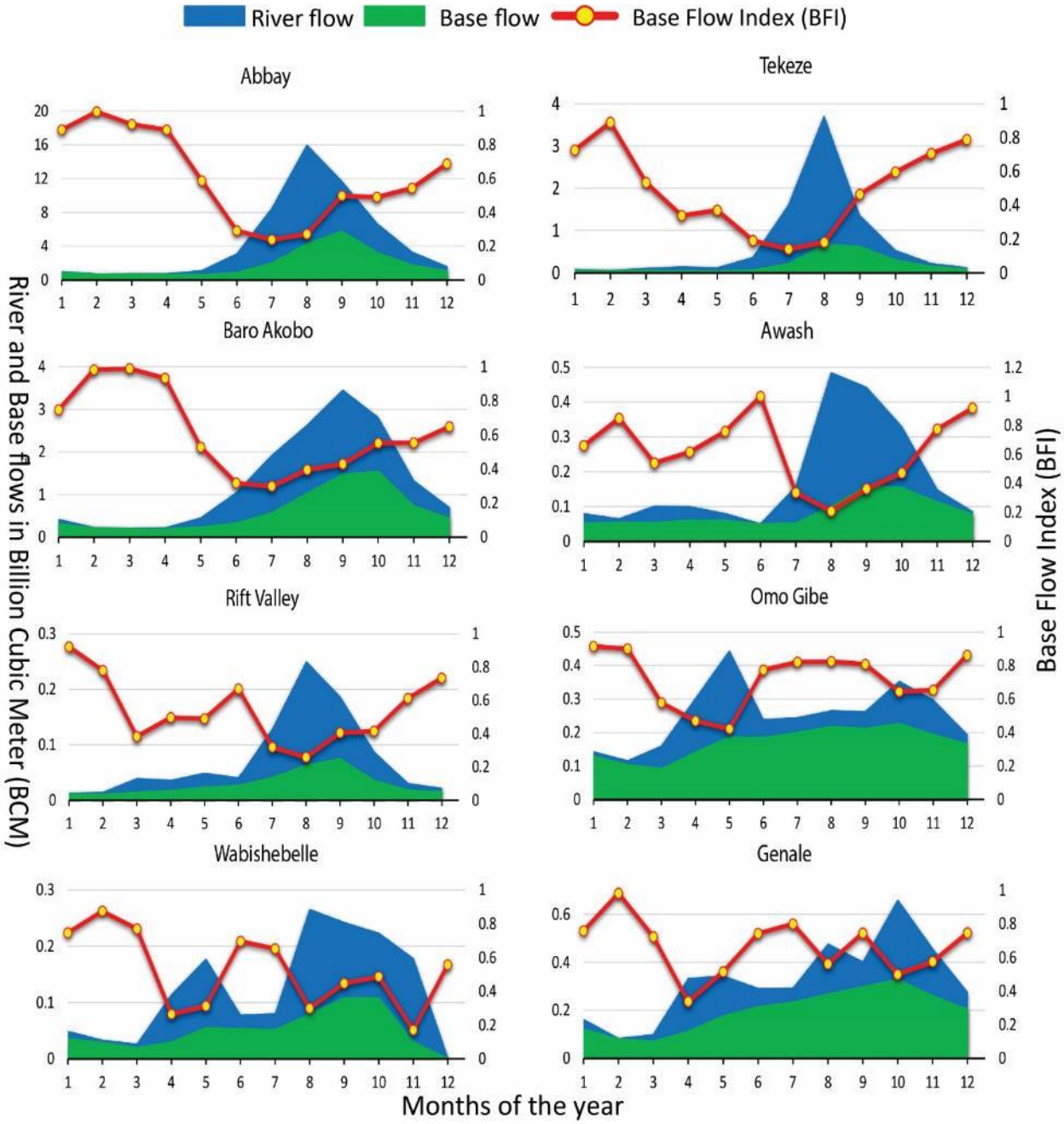

Figure 5.5: The monthly river flow, base flow, and base flow index (BFI) estimations in the major rivers basins by the recursive digital base flow separation method.

32.8Evaluation of the basins in terms of their annual base flow revealed that the group A (Abbay, Tekeze and Baro Akobo) had the higher flow, and its annual base flow sum (32.8 BCM) was larger than five times the flow in the rest of the groups (6.4 BCM) (Table 5.3). In fact, it is the Abbay basin (22.9 BCM) that accounted the greatest proportion of the flow; it is by far greater than the rest of the flow in the other basins combined (16.3 BCM). Additionally, when the groups were compared in terms of agricultural land they have and the population size they carry, the group A basins seemed to have greater groundwater potential – they had 37% of the agricultural land and 40% of the population in the study area. However, their real potential should be determined by considering the amount of water they lose as base flow to neighboring countries.

Basin	*Area (Km^2)*	*Population (in Million)*	*Base flow (BCM)*	*Recharge (mm)*	*Cropland (%) (Total = 20.4 MHa)*
Abbay	200718	24.9	22.9	139	36.2
Tekeze	86672	8.3	2.5	46	12.2
Baro Akobo	75604	6.7	7.4	182	4.6
Genale Dawa	177402	7.3	2.4	30	4.2
Omo Gibe	98092	14.3	2	26	12.6
Wabi Shebele	189661	11	0.6	5	10.8
Awash	114123	15.1	1	18	11.8
Rift valley	32150	12.3	0.4	36	7.6

Table 5.3: The population size, mean annual base flow, mean annual recharge, and cropland percentage in the major basins of the study area.

CHAPTER SIX

6. GROUNDWATER RECHARGE ESTIMATION BY USING CHLORIDE MASS BALANCE METHED

6.1. Introduction

This section describes the estimation of groundwater recharge by using chloride mass balance method. The method requires precipitation amount, chloride concentration in precipitation, chloride concentration in groundwater as input datasets. In the study area, except in few highly elevated areas such as the Bale Mountains where few days of frost is common in its small portions in specific rainy months (Fazzini, Bisci and Billi, 2015), most part of the country receive rainfall as a major source of water.

In the study area, rainfall infiltrates to the groundwater dominantly in five different recharge mechanisms: (a) direct diffuse recharge, (b) indirect recharge from flood waters during high flood stage, (c) mountain block and mountain front recharge, (d) fast selective recharge from heavy rains, and (e) recharge from losing streams and flash floods (Kebede, 2013). Since the CMB method is not specific to a recharge mechanism, it is one of the recommended methods to estimate groundwater recharge in the study area.

6.2. The chloride Mass Balance Method (CMB)

The chloride mass balance method uses the concentration of chloride ion in precipitation and groundwater for the estimation groundwater recharge in an area. Chloride ion is one of the tracers that can dissolve in water and record the movement history of water. Ideal tracers are ions, isotopes, or gases that are highly soluble in water, move with water, unaffected by adsorption or other geochemical or biochemical processes, and measurable accurately and inexpensively.

Therefore, tracers can be used to identify water sources and estimate the amount of water associated with the accumulation of a certain tracer in a medium.

The chloride ion is specifically used to estimate groundwater recharge in unsaturated and saturated zones. The dominant source of meteoric chloride is the ocean, and it reaches to the ground surface with precipitation. A chloride ion that reach to the ground surface might leave the surface with surface runoff or infiltrate to groundwater. In fact, precipitation is not the only source of chloride on the surface of the earth; wind is also the other agent. In that case it is called dry deposition. Gardner (1967) has shown that, in the subsurface, chloride concentration is a bit elevated up to the zero flux plain (ZFP) due to evapotranspiration. A uniform condition of chloride concentration is maintained below the ZFP. Generally, chloride concentration in precipitation decreases as distance from oceans increases.

The Chloride Mass Balance (CMB) method estimates groundwater recharge by relating the mass of chloride in groundwater with the rate of arrival at land surface. The method implements the fact that groundwater recharge is indirectly proportional with the chloride concentration in the subsurface; high groundwater recharge rates favor low concentration of chloride in the subsurface due to lack of sufficient accumulation time whereas low groundwater recharge rates favor high concentration of chloride in the subsurface due to accumulation time sufficiency. The method yields estimations that are integrated spatially over watersheds and temporally over long periods. Many researches have implemented the chloride mass balance method in different parts of the world and found results comparable with physically based methods.

The basic equation of the chloride balance method (Wood and Sanford, 1995) is:

$$q = P\ (\frac{Cl_p}{Cl_{gw}}) \tag{6.1}$$

where q is the recharge flux, P is average annual precipitation, Cl_p is the weight-average chloride concentration in precipitation, and Cl_{gw} is the average chloride concentration in ground water.

The CMB equation inherently assumes that: -

- Precipitation is the sole source of the chloride in the groundwater.
- The chloride is conservative in the system.
- A steady state chloride-mass flux condition exists in the system.

- The chloride is not produced through recycling in the system.
- Precipitation in the aquifer area is converted to only evaporation and groundwater recharge, indicating absence of chloride leaving the area with surface runoff.

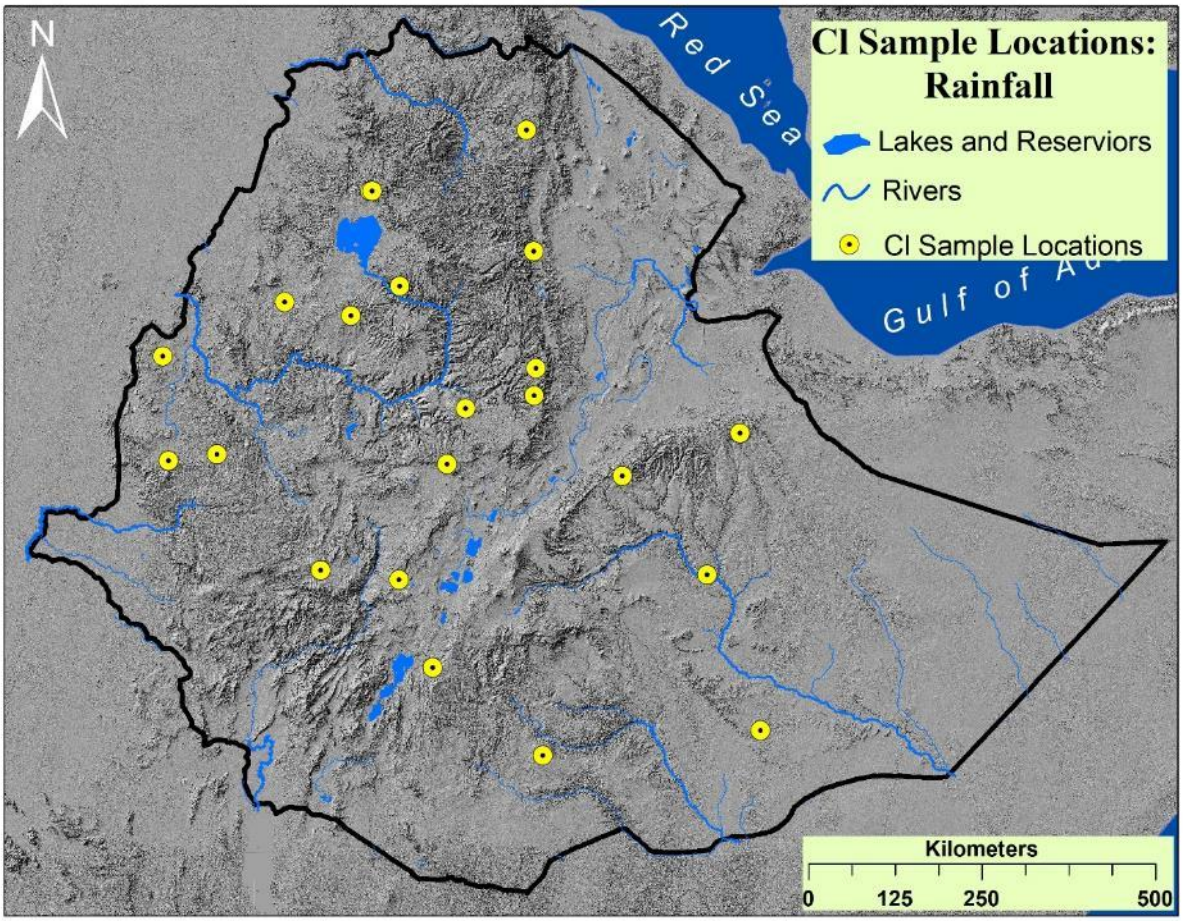

Figure 6.1: Map showing chloride sample locations in rainfall.

6.3. Chloride Concentration in Precipitation

Rainfall chemistry is one of the scarce datasets in the study area. However, a few points having representative spatial distribution (Figure 6.1) were found from the hydrogeological reports produced by Geological Survey of Ethiopia (GSE). According to the data, the minimum concentration of chloride in rainfall in the study area was found to be 0.1 mg/l whereas the maximum 8.9 mg/l. Additionally, to understand the spatial distribution of chloride concentration in rainfall in the study area, the data was interpolated for the whole study area by using the ordinary kriging geostatistical method in ArcGIS (Figure 6.2). The interpolation showed that rainfall

chloride concentration in the study area showed a pattern that increases radially outward from the western part of the study area to the eastern, southeastern, and northern part of the country. The reason for this spatial pattern, as it is evidenced from other studies (Wood, 1995), could be linked to the proximity of the Indian ocean, Red Sea, and Mediterranean Sea to the northern, eastern, and southeastern periphery of the country.

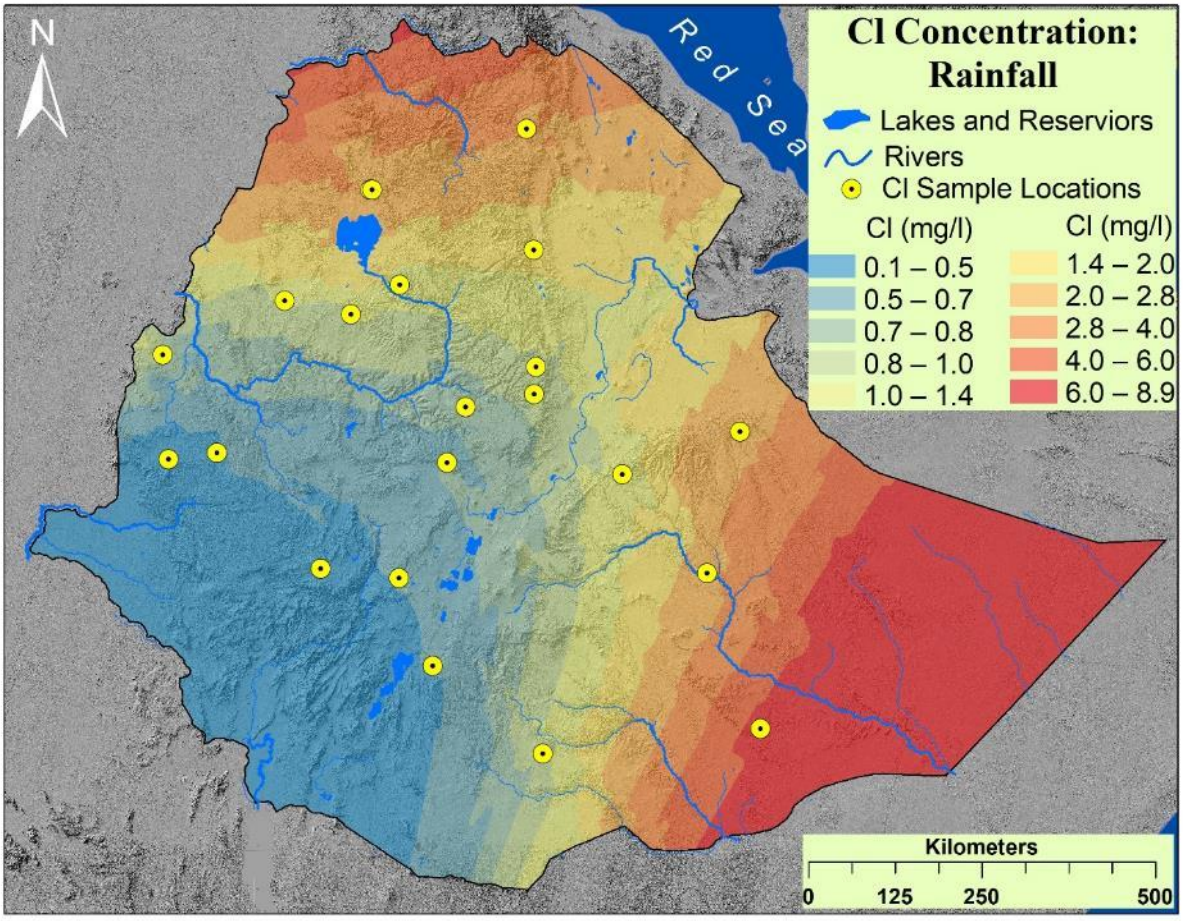

Figure 6.2: Map showing spatial distribution of chloride in rainfall.

6.4. Chloride concentration in groundwater

The groundwater chloride concentration data in the study area were found from several hydrogeological reports that GSE has conducted in the different sections of the country. In addition to that, some data points were found from the National Groundwater Information System (NGIS) developed by the Ministry of Water, Irrigation, and Electricity (MoWIE). Totally, more than 5000 data points were collected, and they were found to be well distributed in the study area (Figure

6.3). According the data, groundwater chloride concentration in the study area has wide range, the minimum being 0.07 mg/l and the maximum more than 11,000 mg/l. The highly exaggerated chloride concentration in the north eastern and eastern parts of the country could be linked to a supply of chloride from country rocks. In the Dallol area, samples taken from hot spring sites show chloride concentration greater than 210,000 mg/l (Cavalazzi et al., 2018). To understand the spatial distribution of groundwater chloride concentration in the study area, the data was interpolated for the whole study area by using the ordinary kriging geostatistical method in ArcGIS (Figure 6.4). The interpolation showed a general pattern of chloride increment from the western to the eastern part of the country, most likely following the spatial distribution of rainfall amount in the study area.

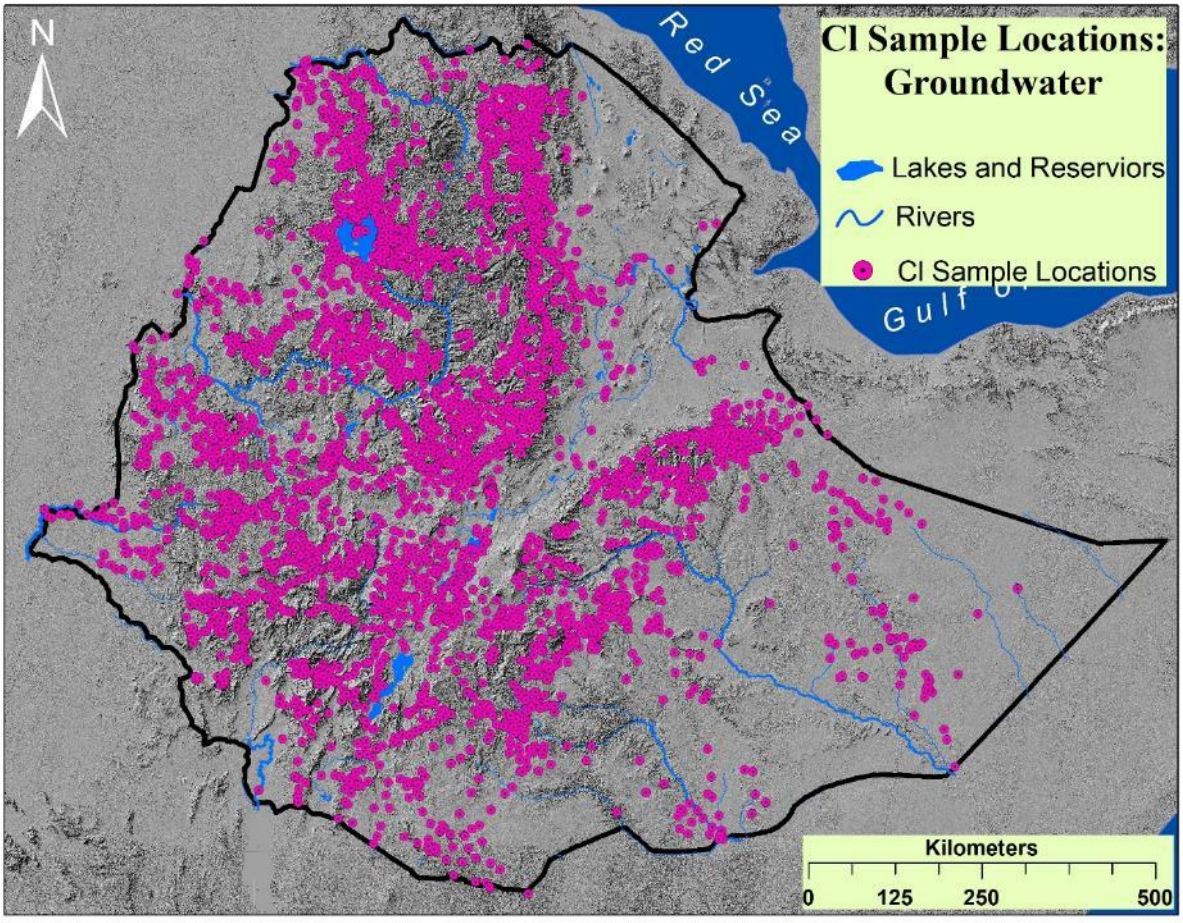

Figure 6.3: Map showing chloride sample location in groundwater.

6.5. Result and Discussion

The estimation of groundwater recharge by the chloride mass balance method to the study area showed wide spatial variability (Figure 6.5), having an annual average of 65 mm which is 8 % of the average annual rainfall in the study area. Generally, the CMB recharge estimation showed a decreasing spatial pattern from the eastern to the western part of the country. The highest groundwater recharge (400 mm) estimation was observed in the western part of the country between Goro and Lake Tana. On the other hand, the lowest recharge estimation was observed in the north eastern, southern, and south eastern part of the country. The recharge estimation in these parts of the country could have greater amount of uncertainty as there is additional source of chloride to the groundwater from the country rock formations (Cavalazzi et al., 2018).

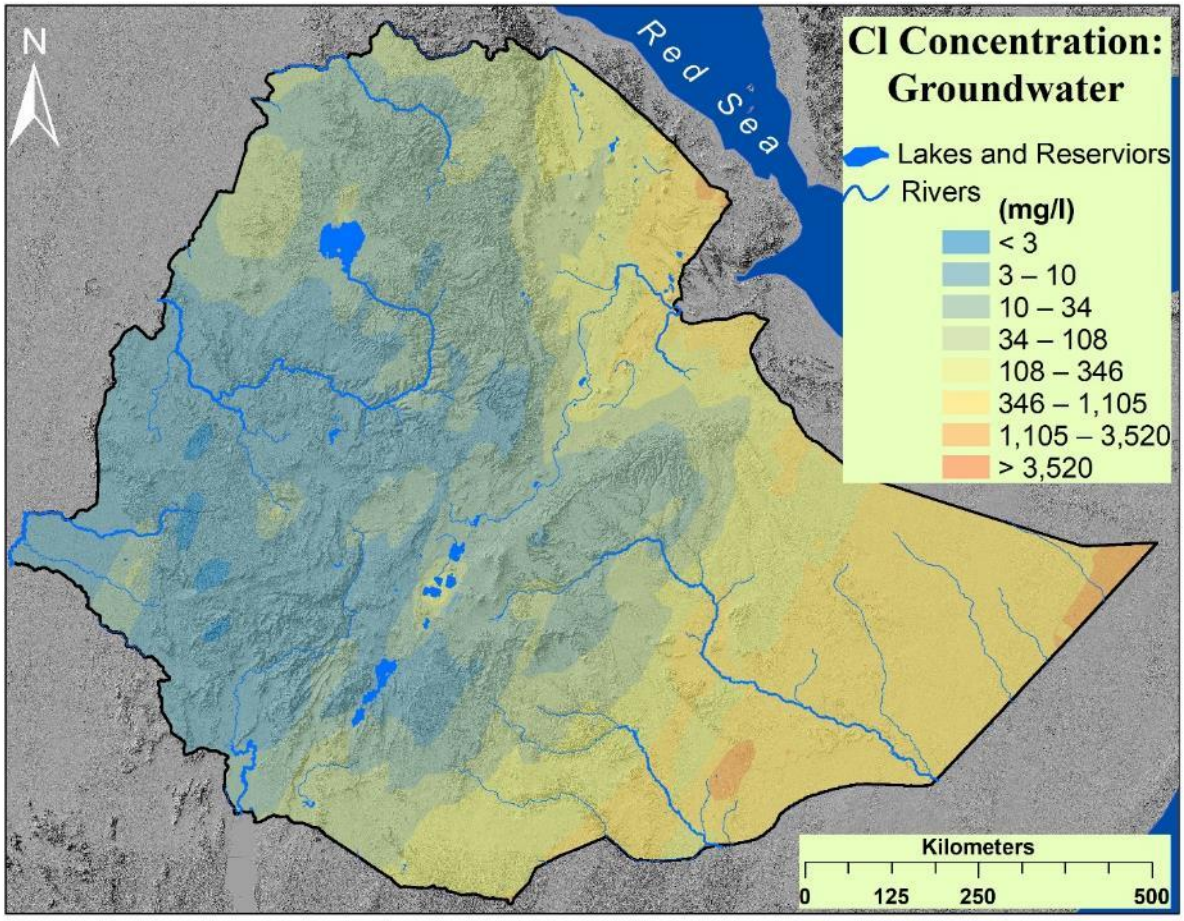

Figure 6.4: Map showing spatial distribution of chloride in groundwater.

As the groundwater recharge estimation by the chloride mass balance is not specific to a recharge mechanism, its estimation represents the total groundwater recharge rate in an area that infiltrated to groundwater through the different recharge mechanisms. However, to characterize the spatial distribution, the estimated recharge was correlated with the important groundwater recharge controlling factors that are identified in the conceptual model development section and the WetSpass-M model: Rainfall, slope, PET, temperature, wind speed, groundwater depth. The correlation result, like that in the other estimation methods in this research, showed a strong correlation with rainfall (Cramer's V = 0.38), strengthening the finding that rainfall is the most important groundwater recharge controlling factor in the study area (Table 6.1). The next important factor, according to the correlation, was the soil factor.

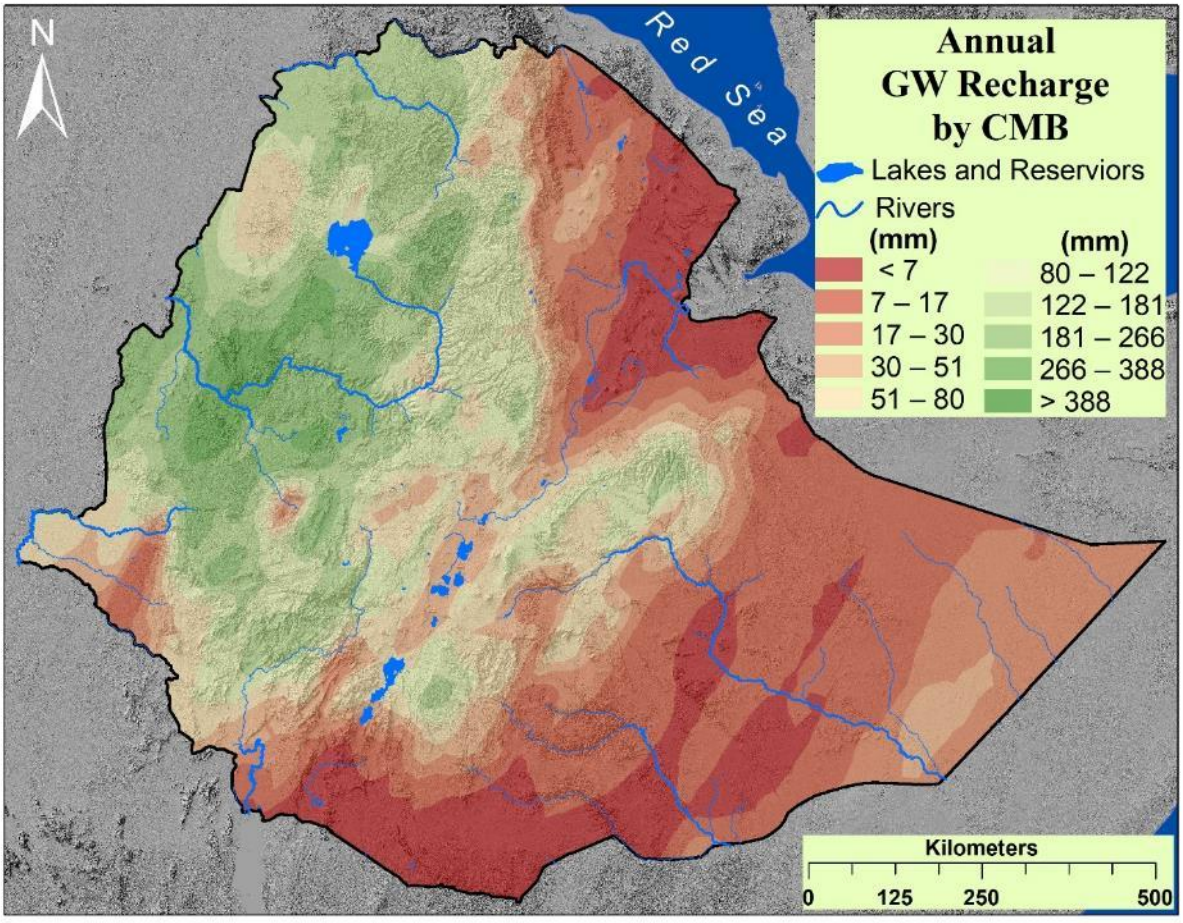

Figure 6.5: Map showing estimation of the annual groundwater recharge by the CMB method.

Factors	Recharge (CMB)
Rainfall	0.3874
PET	0.2939
Temperature	0.3001
Wind	0.2815
LULC	0.2530
Soil	0.3438
GW depth	0.3394
Slope	0.2647

Table 6.1: Cramer's V correlation between groundwater recharge by estimated by CMB and the important factors that control groundwater recharge in an area.

CHAPTER SEVEN

7. COMPARING THE RESULTS OF THE ESTIMATION METHODS

7.1. Introduction

Studies have found that implementing multiple estimation methods increase the accuracy of groundwater recharge estimation in an area (Healy and Scanlon, 2010). There are several groundwater recharge estimation methods developed for different hydrological zones. The methods have been grouped into several schemes based on their conceptual framework, the hydrologic zones they are developed for, their applicable spatial and temporal scale, etc. (Healy and Scanlon, 2010; Scanlon et al., 2002). Applying multiple estimation methods in an area, because of their different conceptual framework, enables to understand the characteristics of rate of groundwater recharge in multiple ways.

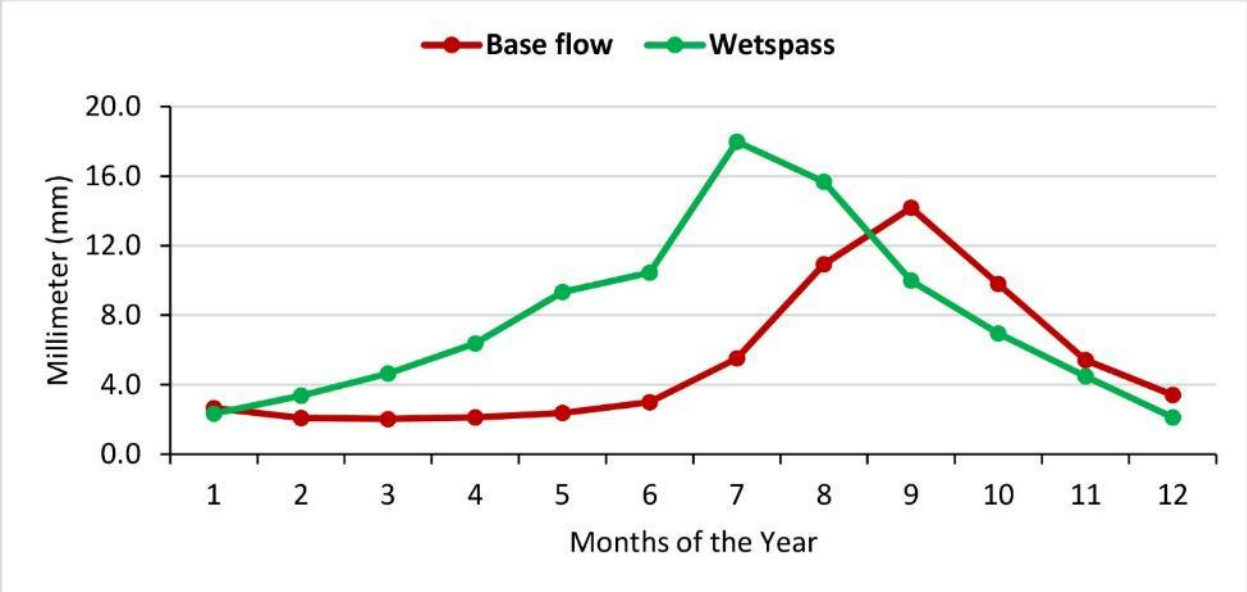

Figure 7.1: The patterns of the monthly groundwater recharge estimations by WetSpass-M and recursive digital base flow separation method.

Months	*1*	*2*	*3*	*4*	*5*	*6*	*7*	*8*	*9*	*10*	*11*	*12*
Base flow (mm)	2.6	2.1	2.0	2.1	2.4	3.0	5.5	10.9	14.2	9.8	5.4	3.4
WetSpass-M (mm)	2.3	3.4	4.7	6.4	9.3	10.5	18.0	15.7	10.0	6.9	4.5	2.1

Table 7.1: The monthly groundwater recharge estimations by the WetSpass-M and recursive digital base flow separation methods.

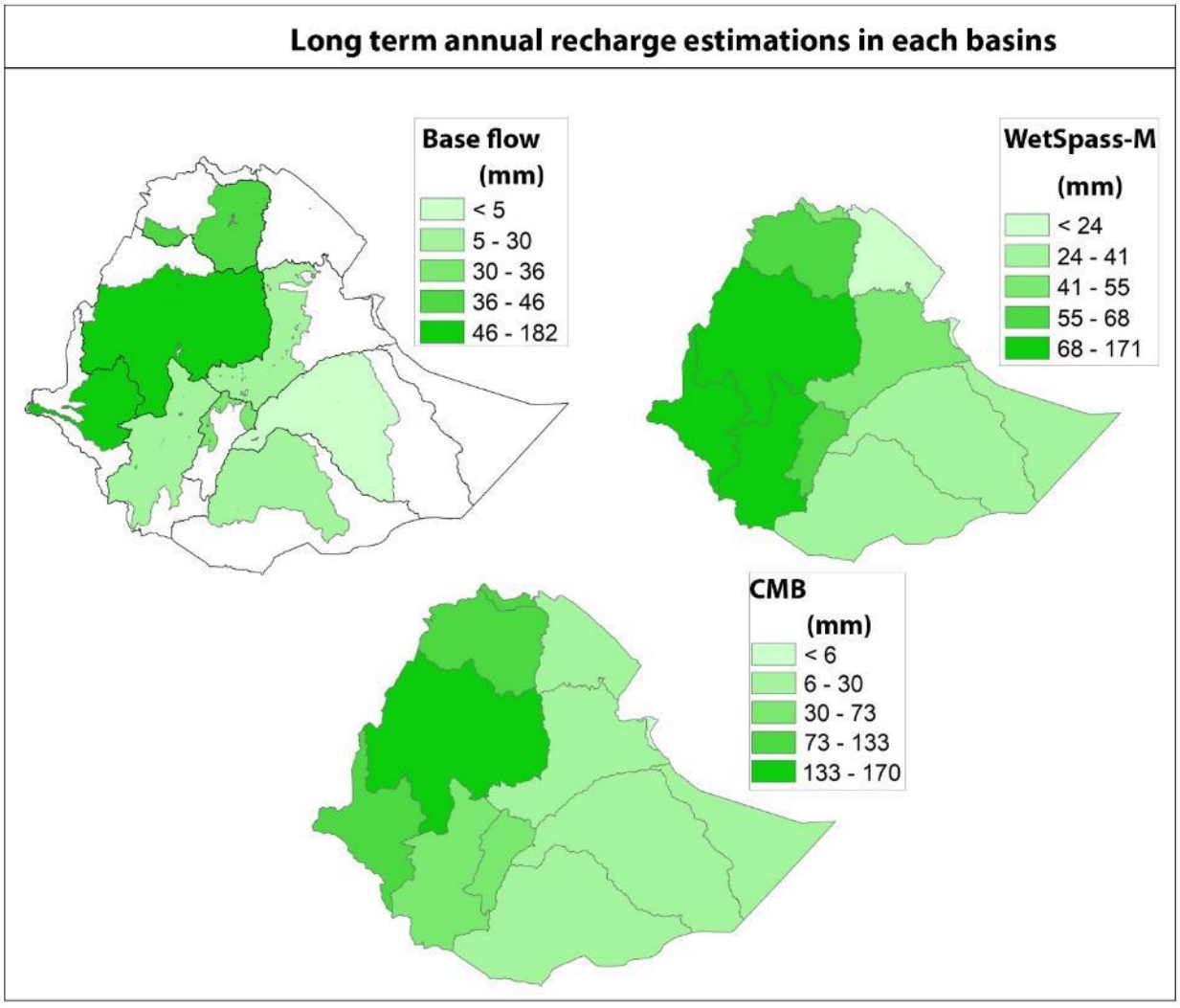

Figure 7.2: The spatial extents that are covered in the base flow separation method and WetSpass-M model, and the mean annual recharge estimations in the river basins by the estimation methods.

	1998-2002		2003-2007		2013-2017	
Agricultural water withdrawal (10^9 m3/year)	2002	5.204 I	2005	7 I	2016	9.687 K[1]
Industrial water withdrawal (10^9 m3/year)	2002	0.021 I	2005	0.0511 L		
Municipal water withdrawal (10^9 m3/year)	2002	0.333 I	2005	0.81 L		
Total water withdrawal (10^9 m3/year)	2002	5.558 I	2005	7.861 I	2016	10.55 K
Irrigation water withdrawal (10^9 m3/year)					2016	9 I
Irrigation water requirement (10^9 m3/year)	2001	1.475 I				
Agricultural water withdrawal as % of total water withdrawal (%)	2002	93.63 I	2005	89.05 I	2016	91.82 K
Industrial water withdrawal as % of total water withdrawal (%)	2002	0.3778 I	2005	0.65 I		
Municipal water withdrawal as % of total withdrawal (%)	2002	5.991 I	2005	10.3 I		
Total water withdrawal per capita (m3/inhab/year)	2002	78.84 I	2005	97.05 K	2016	100.5 K
Total freshwater withdrawal (10^9 m3/year)	2002	5.558 I	2005	7.861 I	2016	10.55 K

Metadata:
[1] - [Components] | Including 0.687 for livestock
E - External data
I - AQUASTAT estimate
K - Aggregate data
L - Modelled data

Table 7.2: Groundwater withdrawal from wells from AQUASTAT main database (FAO, 2016)

7.2. Comparing the results of the WetSpass-M, base flow feparation, chloride mass balance methods

The annual groundwater recharge estimations obtained from the methods showed certain difference; the WetSpass-M estimation was 73 mm/year (81 BCM), the base flow separation was 64 mm/year (40 BCM), and that of the chloride mass balance method was 65 mm (72 BCM). The difference in their estimation could largely be attributed to the difference in their conceptual framework, and the assumptions inherent to the methods. As base flow separation methods use river flow data and assume that the amount of water recharging aquifers ultimately discharges to a river, they ignore the amount of water that diverts to groundwater evapotranspiration, deep groundwater circulations, or pumping wells so that base flow separation estimations are usually underestimated. There are few studies on quantifying the amount of water that is lost as

groundwater evapotranspiration or deep groundwater circulations from aquifers in the study area. However, Alemayehu et al (2018) has indicated a loss of bulk amount of groundwater from the Baro Akobo basin through regional geological structures. Furthermore, the FAO's global information system on water and agriculture, AQUASTAT, indicates withdrawal of 10.55 BCM of groundwater for industrial, agricultural, and municipal uses in the study area in 2016 (FAO, 2016) (Table 7.2).

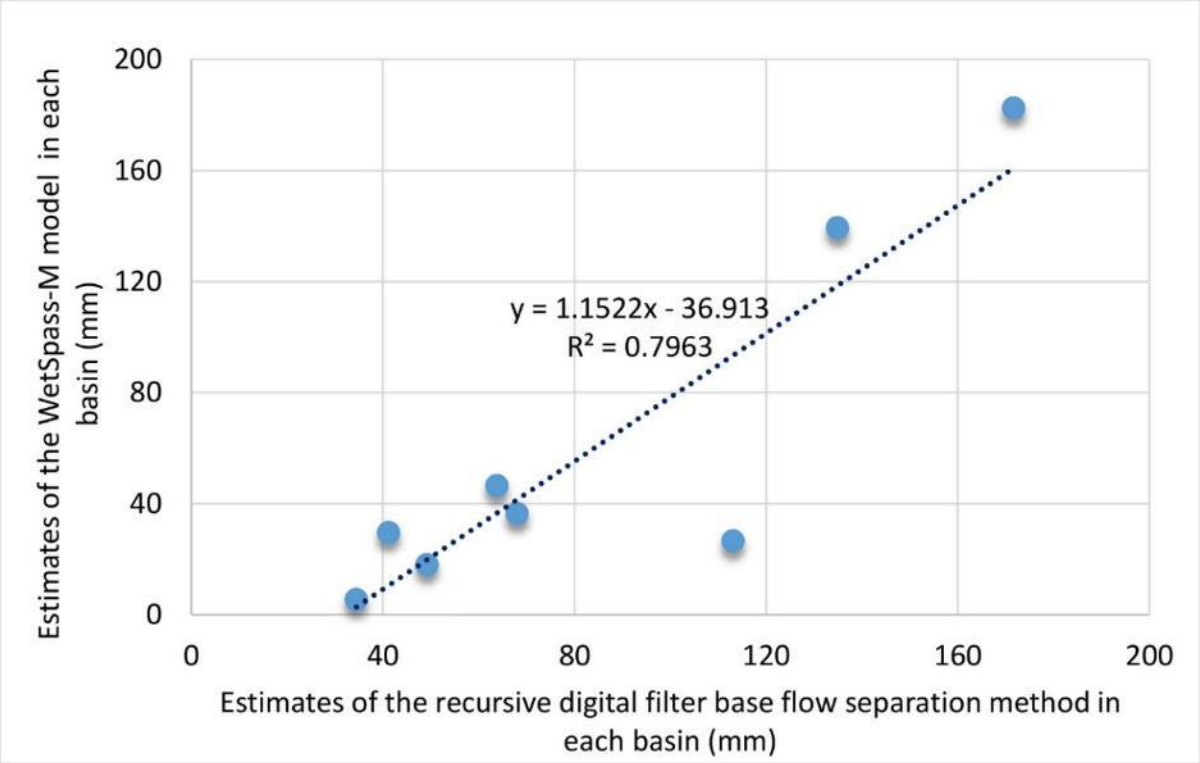

Figure 7.3: Regression of the annual groundwater recharge estimations of WetSpass-M and recursive digital base flow separation methods in the basins.

Additionally, the difference in the annual estimation between the methods could also be attributed to the difference in the areal extent represented in their estimations. In the base flow separation method, due to the scarcity of river gauge stations, the dry basins (Denakil, Ayisha, Mereb, and Ogaden) were disregarded from the study, and the Rift valley and Wabishebelle basins were partially represented (Figure 7.2). To compare the monthly groundwater estimations of WetSpass-M model and the base flow separation, the estimation of the WetSpass-M model was summarized

into the major basins of the study area (Figure 7.2). Then, the basins were used to carry out both spatial and temporal comparisons between the estimations of the base flow separation and WetSpass-M methods.

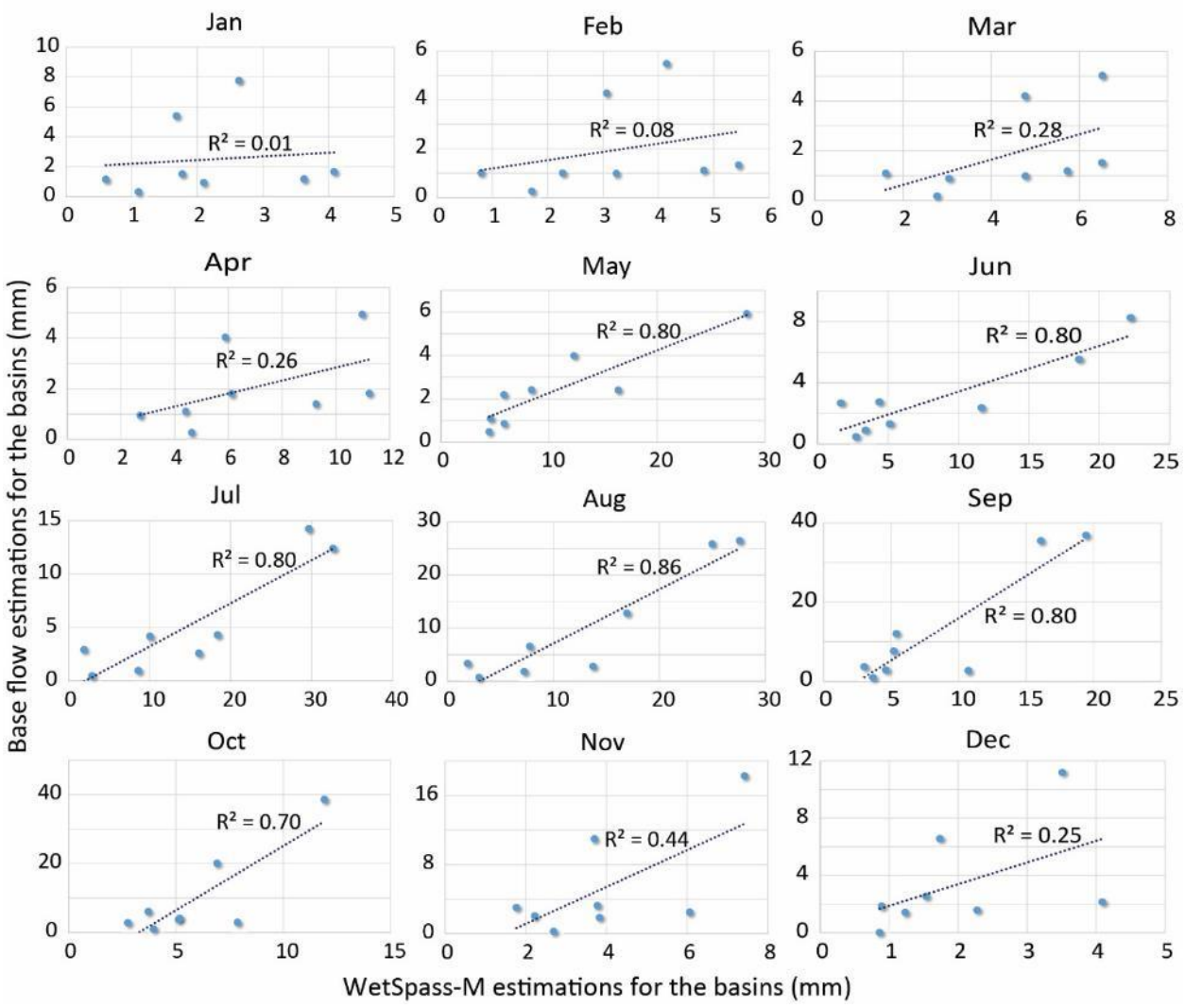

Figure 7.4: Regression of groundwater recharge estimations of WetSpass-M and recursive digital base flow separation methods in the basins in each month.

Figure 7.4 shows that the correlation between the monthly estimations in each of the basins by the base flow separation and WetSpass-M methods was the strongest in the rainy season. This result showed that rainfall was the most important factor in controlling groundwater recharge in the study area, as discussed in sections 4.7 and 5.3. Thus, the strongest correlation between the results was obtained in July (r^2 = 0.86), and in this month, the top three recharge estimation values were obtained in Abbay, Baro, and Tekeze river basins, which are 28 mm, 25 mm, and 17 mm by the WetSpass-M, and 26 mm, 26 mm, and 13 mm by the base flow separation. A similar result was also obtained in the annual estimations (Figure 7.3 and Table 7.3).

Figure 7.5, on the other hand, shows that although the monthly estimations in each of the basins by the base flow and WetSpas-M methods show general similarity, their pick and low values occur at different months. The WetSpass-M's pattern is almost similar with that of the rainfall whereas the base flow's pattern lagged behind the rainfall pattern in one up to two months. The same relation is obtained for the whole basins (Figure 7.1 and Table 7.1). During the major rainy season in the study area (from June to September), the base flow pattern lagged behind the WetSpass-M pattern in two months. Similarly, during the transition from the dry to rainy season (April to June), the base flow pattern showed slower rise (Figure 7.1). A similar result was also found in each basin (Figure 7.5).

Basin	*WetSpass-M (mm)*	*Base flow (mm)*	*CMB (mm)*
Genale Dawa	41	30	18
Wabishebele	34	5	29
Baro Akobo	172	182	105
Awash	49	18	29
Tekeze	64	46	134
Rift Valley	68	36	60
Omo Gibe	113	26	73
Abbay	135	139	170

Table 7.3: Annual groundwater recharge estimations in each basin by the recursive digital filter base flow separation method

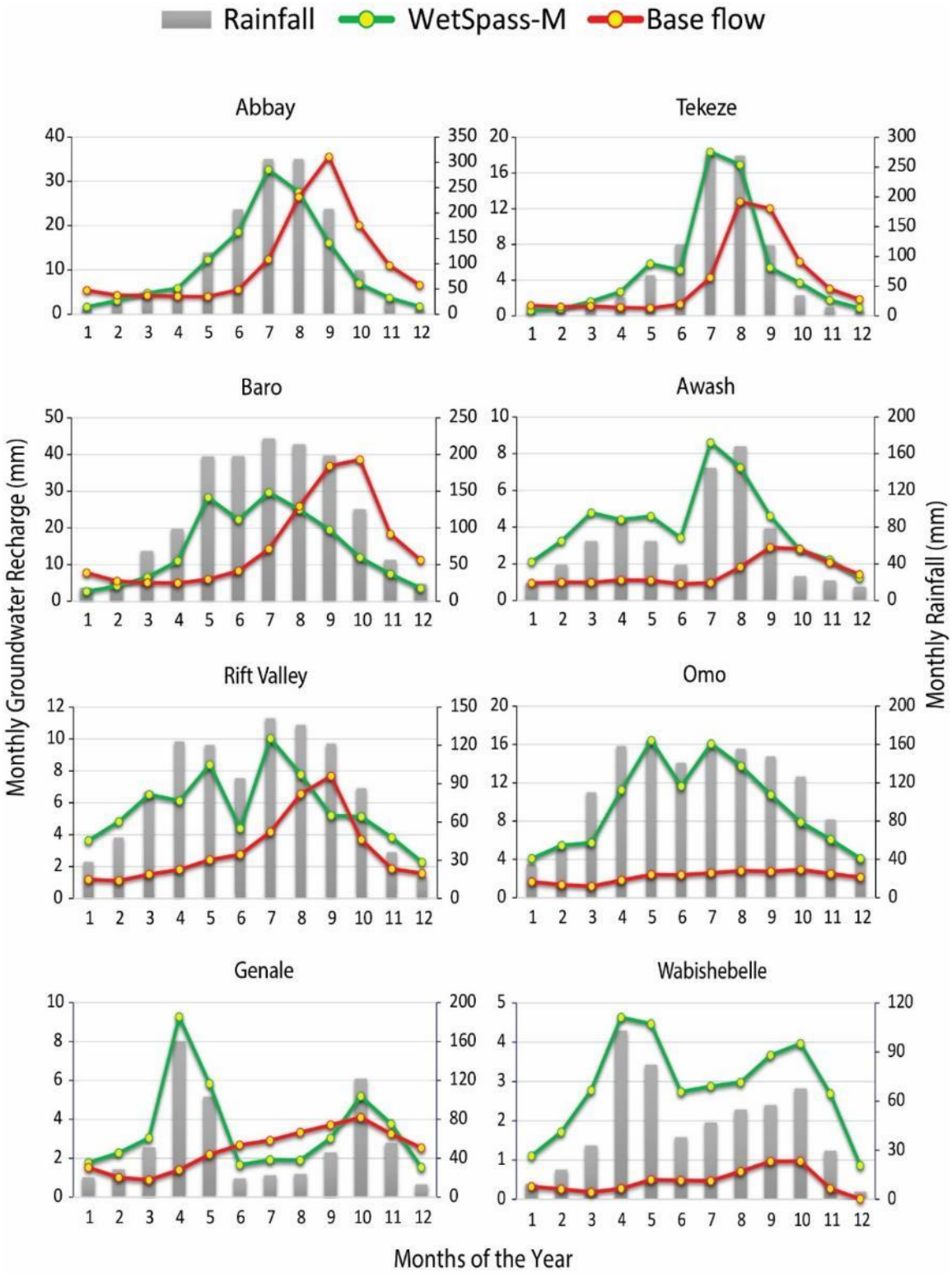

Figure 7.5: Graphs that show monthly groundwater recharge patterns of the WetSpass-M and recursive digital filter base flow separation estimations in the major basins.

The difference in the patterns can be attributed to the difference in the conceptual frameworks of the estimation methods. i.e. base flow estimations use base flow, one of the slow responses of a rainfall event, as a singular input variable for its estimation whereas WetSpass-M model uses the rainfall and other quick response variables as an input variable. Thus, the monthly estimation patterns from these methods essentially cannot be similar. However, the comparison of their patterns can be used to understand the capacity of the aquifers in the study area to buffer external changes.

CHAPTER EIGHT

8. CONCLUSION AND RECOMMENDATION

8.1. Conclusion

Understanding the rate of groundwater recharge is crucial to studies of water availability, wellhead protection, contaminant transport, ground-water and surface-water interactions, effects of urbanization, and aquifer vulnerability to contamination (Scanlon and others, 2002). Groundwater provides more than 90% of the water supply for domestic and industrial uses in the country (Kebede, Hailu, Crane, Ó Dochartaigh and Bellwood-Howard, 2018). However, there are only limited researches regarding groundwater recharge estimation in the study area especially at the national scale.

Although it needs a lot of investigation to determine the actual rate of groundwater recharge in the study area, this research aimed at getting a better estimation by applying multiple estimation methods (the WetSpass-M model, digital recursive base flow separation, chloride mass balance) and implementing finer spatial (250m) and temporal (long term monthly) resolutions. Additionally, the estimation methods were guided and evaluated by a groundwater recharge conceptual model developed for the area by considering several factors.

The conceptual model of groundwater recharge was developed by considering several important factors that control groundwater recharge in an area: rainfall, LULC, soil texture, lithology, lineament density, slope, and drainage density. The model conceptualized how, when and where groundwater recharge occurs in the study area. It showed that both the spatial and temporal characteristics of the groundwater recharge was significantly controlled by the rainfall factor. Accordingly, the dominant rainy months (June to September) were found to be the most important potential months for the occurrence of groundwater recharge in the study area. Particularly, some areas such as Goro in the western part of the country and the area in south of Lake Tana, due to their rainfall pattern, were found to be the most potential areas for the occurrence of groundwater

recharge almost throughout the year. Additionally, the conceptual model showed that groundwater recharge estimation methods that would be applied in the study area should have the characteristics of adaptability and universality. Accordingly, the WetSpass-M, digital recursive base flow separation method, and chloride mass balance methods were found suitable to be applied in the study area.

The WetSpass-M model requires land use/land cover (LULC), soil texture, slope, groundwater depth and meteorological data (rainfall, temperature, potential evapotranspirtion (PET) and wind speed) as input data for its estimation. Base flow separation needs the river flow time series data. The chloride mass balance method, on the other hand, requires precipitation amount, chloride concentration in precipitation, chloride concentration in groundwater as input datasets. The river flow time series data used in the base flow separation method was also used for calibrating the WetSpass-M model.

It was possible to determine the long term monthly groundwater recharge of the study area by using the three estimation methods, and it was found that although majority of the study area received groundwater recharge at different rate at each month, it was higher for higher rainfall regimes and months (from June to September). According to WetSpass-M, the long term monthly average estimation of groundwater recharge to the study area from June to September was found to be 10.5 mm, 18 mm, 15.7 mm and 10 mm, but with that of base flow separation method, it was 3 mm, 5.5 mm, 10.9 mm, and 14.2 mm. Some particular areas such as Goro in western part of the study area and some areas in south of Lake Tana, due to their higher and extended rainfall characteristics, receive higher amount of groundwater recharge almost throughout the year. In Goro, groundwater recharge reached up to 400 mm which is 20% of the average rainfall in that particular location. The long term annual average groundwater recharge of the study area from WetSpass-M, base flow separation, and chloride mass balance methods were found to be 73 mm (81 BCM), 63 mm (40 BCM), and 65 mm (72 BCM) respectively.

The Cramer's V correlation between the input and output variables of the WetSpass-M model showed that LULC and soil texture were the most important variables next to rainfall in controlling groundwater recharge in the study area. Among the LULC classes, it was the forest class that was found to have highest groundwater recharge. In the case of soil texture classes, unlike what is presumed theoretically, groundwater recharge increased as soil texture decreased so that clay soil

texture class had the highest groundwater recharge in the study area. The reason for that was found to be that rainfall is extremely higher in finer soil texture classes.

The comparison between the monthly outputs of WetSpass-M and base flow separation showed that although the estimations of WetSpass-M were generally higher, they were strongly correlated ($r = 0.86$) in rainy months and wet areas. The reason for the difference in the estimations between WetSpass-m and base flow separation methods was found to be largely due to the difference between the areas considered in each methods. In the case of the base flow separation method, due to scarcity of river gauge stations, a considerable area was ignored from the estimation process. Apart from that, the comparison also showed that the pattern of the monthly estimations of the base flow separation method lagged behind that of the WetSpass-M in one month. The reason for the difference between the patterns was attributed to the difference in their conceptual frameworks. Due to the assumptions inherent in base flow separation methods, processes that can be important in some areas are ignored in the estimation such as groundwater evaporation, migration to deeper groundwater circulation systems, and extraction of groundwater by pumping wells.

8.2. Recommendation

In base flow separation methods, due to the inherent assumption, water diverted from groundwater storages to routes such as groundwater evaporation, deep groundwater circulations, and pumping wells are disregarded. Thus, the amount of diverted water is needed to be estimated to compensate for the loss of water in the estimation. However, there are few studies in this regard in the study area.

Researches show that one of the most important sources of uncertainties in groundwater recharge estimations is insufficient representation of a study area that can be evaluated by the density of meteorological and hydrological stations in the study area. In the study area, even though the density of stations is increasing, but significant locations are not sufficiently covered. Thus, researches have to be conducted to increase quality of input data, especially in ungauged areas.

In this study, three distinctive groundwater recharge estimation methods that differ in many characteristics were applied to observe the groundwater recharge characteristics of the study area in different aspects. With the same analogy, if other estimation methods are implemented in the

area, it will increase the knowledge on the rate and characteristics of groundwater recharge in the study area.

As groundwater recharge is a hydrologic process that is determined by estimation, its estimated values involve uncertainty. Thus, implementing methods that are not applied in this study can be very important such as estimating amount of uncertainty in estimated values.

REFERENCES

Abbate E, Sagri M (1980). Volcanites of Ethiopian and Somali Plateaus and major tectonic lines. Atti Convegni Acc Lincei Roma 47:219 – 227

Abdollahi K, Bashir I, Verbeiren B, Harouna MR, Van Griensven A, Huysmans M, Batelaan O (2017). A distributed monthly water balance model: formulation and application on Black Volta Basin. Environ Earth Sci 76(5):198

Abdollahi K (2015). Basin scale water balance modeling for variable hydrological regimes and temporal scales. PhD Dissertation, Department of Hydrology and Hydraulic Engineering, Vrije Universiteit Brussel, Brussels, p 173

Abiye, TA. (2006). Groundwater occurrence in Ethiopia. Addis Ababa University Press, Addis Ababa, 105 pp.

Abiy, A. Z. et al. (2016). Groundwater Recharge and Contribution to the Tana Sub-basin, Upper Blue Nile Basin, Ethiopia, in Melesse, A. M. and Abtew, W. (eds) Landscape Dynamics, Soils and Hydrological Processes in Varied Climates. Cham: Springer International Publishing (Springer Geography), pp. 463–481. doi: 10.1007/978-3-319-18787-7_22.

Alemayehu, T., Kebede, T. and Liu, L. (2018). Basin characterization and determination of hydraulic connectivity of mega basins using integrated methods: (The case of Baro-Akobo and mega watershed beyond), Journal of African Earth Sciences, 137, pp. 32–45. doi: 10.1016/j.jafrearsci.2017.09.011.

Armanuos, A. M. et al. (2016). Application of WetSpass model to estimate groundwater recharge variability in the Nile Delta aquifer, Arabian Journal of Geosciences, 9(10), p. 553. doi: 10.1007/s12517-016-2580-x.

Arnold JG, Allen PM (1999). Automated methods for estimating baseflow and groundwater recharge from stream-flow records. J Am Water Resour Assoc 35(2):411–424

Arnold, J. G., Allen, P. M., Muttiah, R. S. and Bernhardt, G. (1995). Automated baseflow separation and recession analysis techniques. Ground Water, 33, 1010–1018.

Arnold, J. G. and Allen, P. M. (1999). Automated methods for estimating baseflow and ground water recharge from streamflow records. J. Amer. Water Resour. Assoc., 35, 411–424.

Asefa, T.A., Batalann, O., Campenhout, A. and Smedt, D.F., (2000). Characterizing recharge/discharge areas of Grote-Nete (Belgium) using hydrological modeling, vegetation-mapping and GIS. In: Verhoest, N.E.C., Van Herpe, Y.J.P. and De Troch, F.P. (Eds.), Book of abstract of European Network of Experimental and Representative Basins (ERB) Conference: Monitoring and Modelling Catchment Water Quantity and Quality, Ghent, Belgium, 27–29 September, 2000, pp. 233–237

Bahremand A, De Smedt F, Corluy J, Liu YB, Poorova J, Velcicka L, Kunikova E (2007). WetSpa model application for assessing reforestation impacts on floods in Margecany–Hornad watershed, Slovakia. Water Resour Manag 21(8):1373–1391

Barberi F, Ferrara G, Santacroce R, Varet J (1975). Structural evolution of the Afar triple junction. In: Pilger A, Roesler EA (eds) Afar Depression of Ethiopia. Schweizerbart, Stuttgart, pp 38–54

Barnes SU (1976). Geology and oil prospects of Somalia, East Africa. Am Assoc Pet Geol Bull 60:389–413

Beauchamp J (1977). La série sédimentaire en Ethiopie central and oriental. Ph.D. thesis, University Claude Bernard Lyon, 419 pp

BEICIP (1985). Geological map of Ogaden and surrounding area, scale 1:1,000,000. Ministry of Mines and Energy Addis Ababa

Beinat, E. (1997). Value functions for environmental management. Dordrecht: Kluwer Academic Publishers.

Beltrando G, Camberlin P (1993). Interannual variability of rainfall in the eastern Horn of Africa and indicators of atmospheric circulations. Int J Climatol 13:533–546.

Berehanu, B. et al. (2017). ‘Inter-Basin Groundwater Transfer and Multiple Approach Recharge Estimation of the Upper Awash Aquifer System’, Journal of Geoscience and Environment Protection, 05(03), pp. 76–98. doi: 10.4236/gep.2017.53007.

Berhanu, B., Seleshi, Y. and Melesse, A. M. (2014). 'Surface Water and Groundwater Resources of Ethiopia: Potentials and Challenges of Water Resources Development', in Melesse, A. M., Abtew, W., and Setegn, S. G. (eds) Nile River Basin: Ecohydrological Challenges, Climate Change and Hydropolitics. Cham: Springer International Publishing, pp. 97–117. doi: 10.1007/978-3-319-02720-3_6.

Batelaan, O., Smedt, F.D., (2007). GIS-based recharge estimation by coupling surface - subsurface water balances. Journal of Hydrology 337 (3–4), 337–355.

Batelaan, O., Asefa, T., Campenhout, F.A. and Smedt, D.F., (2000). Studying the impact of land-use changes on discharge and recharge areas. In: Verhoest, N.E.C., Van Herpe, Y.J.P. and De Troch, F.P. (Eds.), Book of abstracts of European Network of Experimental and Representative Basins (ERB) Conference: Monitoring and Modelling Catchment Water Quantity and Quality, Ghent, Belgium, 27–29 September, 2000, pp. 215–218.

Batelaan O, De Smedt F (2001). WetSpass: a flexible, GIS based, distributed recharge methodology for regional groundwater modeling, vol 269. IAHS Publication, pp 11–18

Bergkamp, G., (1998). A hierarchical view of the interactions of runoff and infiltration with vegetation and microtopography in semiarid shrublands. Catena 33, 201–220.

Beyth M, Avigadb D, Wetzelc HU, Matthewsb A, Berhe SM (2003). Crustal exhumation and indications for Snowball Earth in the East African Orogen: north Ethiopia and east Eritrea. Precambr Res 123:187–201

Billi, P. (2015). 'Geomorphological Landscapes of Ethiopia', in Billi, P. (ed.) Landscapes and Landforms of Ethiopia. Dordrecht: Springer Netherlands, pp. 3–32. doi: 10.1007/978-94-017-8026-1_1.

Blanford WT (1870). Observations on the geology and zoology of Abyssinia, made during the progress of the British expedition to that country in 1867–68. Macmillan, London, 487 pp

Bodily, S. E. (1985). Modern decision making: A guide to modeling with decision support systems. New York: McGraw-Hill Book Company.

Bolten, J., W.T. Crow, X. Zhan, T.J. Jackson, and C.A. Reynolds (2010). Evaluating the Utility of Remotely Sensed Soil Moisture Retrievals for Operational Agricultural Drought

Monitoring, IEEE Transactions on Geoscience and Remote Sensing, 3(1): 57-66. DOI 10.1109/JSTARS.2009.2037163 Google Scholar

Bonham-Carter, G.F., (1994). Geographic Information Systems for Geoscientists: Modelling with GIS, first ed. Pergamon, Kidlington.

Bosellini A, Russo A, Assefa G (2001). The Mesozoic succession of Dire Dawa, Harar Province, Ethiopia. J Afr Earth Sci 32:403–417

Bosellini A (1989). The continental margins of Somalia: their structural evolution and sequence stratigraphy. Mem Sci Geol Padova 41:373–458

Bosellini A, Russo A, Fantozzi PL, Assefa G, Solomon T (1997). The Mesozoic succession in the Mekele outlier (Tigrai province, Ethiopia). Mem Sci Geol Padova 49:95–116

Bosellini A, Russo A, Schroeder R (1999). Stratigraphic evidence for an Early Aptian sea-level fluctuation: the Graua Limestone of southeastern Ethiopia. Creta Res 20:783–791

Brady, C.N., Well, R.R., (2002). The Nature and Properties of Soils, Pearson Education (Singapore)13th ed. Pte. Ltd., Delhi, India.

Bussert R, Schrank E (2007). Palynological evidence for a latest Carboniferous-Early Permian glaciations in Northern Ethiopia. J Afr Earth Sci 49:201–210

Cavalazzi B, Barbieri R, Gómez F, Capaccioni B, Olsson-Francis K, Pondrelli M, Rossi AP, Hickman-Lewis K, Agangi A, Gasparotto G, Glamoclija M, Ori GG, Rodriguez N, Hagos M (2019). The Dallol geothermal area, northern Afar (Ethiopia)-an exceptional planetary field analog on earth. Astrobiology 19(4):554–577. https://doi.org/10.1089/ast.2018.1926Chakhar, S., & Mousseau, V. (2008). GIS-based multicriteria spatial modeling generic framework. International Journal of Geographical Information Science, 22(11–12), 1159–1196.

Chen, J.M., Chen, X., Ju, W., Geng, X., (2005). Distributed hydrological model for mapping evapotranspiration using remote sensing inputs. Journal of Hydrology 305 (1–4), 15–39.

Chernet T (1993). Hydrogeology of Ethiopia and water resources development. Report, Ethiopian Institute of Geological Surveys, Addis Ababa.

Clarke, R., Lawrence, A. and Foster, S. (1996). Groundwater: A threatened resource. Nairobi, Kenya: United Nations Environment Programme Environment Library No. 15.

Coltorti M, Dramis F, Ollier CD (2007). Planation surfaces in northern Ethiopia. Geomorphology 89:287–296

Corti G (2009). Continental rift evolution: from rift initiation to incipient break-up in the main Ethiopian Rift, East Africa. Earth Sci Rev 96:1–53

Creutzfeldt B, Gu¨ntner A, Vorogushyn S, Merz B (2010). The benefits of gravimeter observations for modelling water storage changes at the field scale. Hydrol Earth Syst Sci 14(9):1715

Critchley W, Siegert K (1991). Water harvesting: a manual for the design and construction of water harvesting schemes for plant production. AGL Miscellaneous Paper no. 17, FAO, Rome, Italy

De Groen MM, Savenije HH (2006). A monthly interception equation based on the statistical characteristics of daily rainfall. Water Resour Res 42(12): W12417. doi:10.1029/2006WR005013

Demlie, M. et al. (2007). 'Groundwater recharge in the Akaki catchment, central Ethiopia: evidence from environmental isotopes (δ18O, δ2H and 3H) and chloride mass balance', Hydrological Processes, 21(6), pp. 807–818. doi: 10.1002/hyp.6273.

Demlie, M. (2015). 'Assessment and estimation of groundwater recharge for a catchment located in highland tropical climate in central Ethiopia using catchment soil–water balance (SWB) and chloride mass balance (CMB) techniques', Environmental Earth Sciences, 74(2), pp. 1137–1150. doi: 10.1007/s12665-015-4099-y.

Dereje, B. and Nedaw, D. (2019). 'Groundwater Recharge Estimation Using WetSpass Modeling in Upper Bilate Catchment, Southern Ethiopia', Momona Ethiopian Journal of Science, 11(1), p. 37. doi: 10.4314/mejs.v11i1.3.

Deyassa, G. et al. (2014). 'Crystalline basement aquifers of Ethiopia: Their genesis, classification and aquifer properties', Journal of African Earth Sciences, 100, pp. 191–202. doi: 10.1016/j.jafrearsci.2014.06.002.

Dhakal N, Fang X, Cleveland TG, Thompson DB, Asquith WH, Marzen LJ (2011). Estimation of volumetric runoff coefficients for Texas watersheds using land-use and rainfall-runoff data. J Irrig Drain Eng 138(1):43–54

Doll P, Fiedler K (2008). Global-scale modeling of groundwater recharge. Hydrol Earth Syst Sci 12:863–885.

Dunkerly, D., (2003). Organic litter: dominance over stones as a source of interrill flow roughness on low-gradient desert slopes at Fowlers Gap, arid western NSW, Australia. Earth Surface Processes and Landforms 28, 15–29.

Eastman, J. R., Kyem, P. A. K., Toledano, J., & Jin, W. (1993). GIS and decision making. Geneva: UNITAR.

Eastman, J.R., (1999). Manual Geographic Information System IDRISI32. Clark Labs, Clark University.

GSE (1996). Geological map of Ethiopia at 1:2,000,000 scale. Geological Survey of Ethiopia, Addis Ababa.

Entekhabi, D, Njoku, EG, O'Neill, PE, Kellogg, KH, Crow, WT, Edelstein, WN, Entin, JK, Goodman, SD, Jackson, TJ, Johnson, J, Kimball, J, Piepmeier, JR, Koster, RD, Martin, N, McDonald, KC, Moghaddam, M, Moran, S, Reichle, R, Shi, JC, Spencer, MW, Thurman, SW, Tsang, L & Van Zyl, J (2010). The soil moisture active passive (SMAP) mission, Proceedings of the IEEE, 98(5): 704-716. DOI 10.1109/JPROC.2010.2043918 Article

FAO. (2016). AQUASTAT Main Database - Food and Agriculture Organization of the United Nations (FAO). Website accessed on [30/07/2020 17:5]

Fazzini, M., Bisci, C. and Billi, P. (2015). 'The Climate of Ethiopia', in Billi, P. (ed.) Landscapes and Landforms of Ethiopia. Dordrecht: Springer Netherlands, pp. 65–87. doi: 10.1007/978-94-017-8026-1_3.

Gani NDS, Abdelsalam MG, Gera S, Gani MR (2009). Stratigraphy and structural evolution of the Blue Nile Basin, Northwestern Ethiopia Plateau. Geol J 44:30–56

Gardner, W. R. (1967). Water uptake and salt distribution patterns in saline soils. In Proceedings of the Symposium on Isotope and Radiation Techniques in Soil Physics and irrigation studies. June 12–16, 1967. Istanbul. Vienna: International Atomic Energy Agency, 335–340.

Gebreyohannes, T. et al. (2013). 'Application of a spatially distributed water balance model for assessing surface water and groundwater resources in the Geba basin, Tigray, Ethiopia', Journal of Hydrology, 499, pp. 110–123. doi: 10.1016/j.jhydrol.2013.06.026.

Gebremeskel, G. and Kebede, A. (2017). 'Spatial estimation of long-term seasonal and annual groundwater resources: application of WetSpass model in the Werii watershed of the Tekeze River Basin, Ethiopia', Physical Geography, 38(4), pp. 338–359. doi: 10.1080/02723646.2017.1302791.

Gebru, T. A. and Tesfahunegn, G. B. (2019). 'Chloride mass balance for estimation of groundwater recharge in a semi-arid catchment of northern Ethiopia', Hydrogeology Journal, 27(1), pp. 363–378. doi: 10.1007/s10040-018-1845-8.

Geza, M., McCray, J.E., (2008). Effects of soil data resolution on SWAT model stream flow and water quality predictions. Journal of Environmental Management 88 (3), 393–406.

Gortani M (1973). La fauna mesocretacea degli Stati di Graua. In Missione Geologica dell'AGIP nella Dancalia Meridionale e sugli Altopiani Hararini (1936–1938). Acc Naz Lincei Roma 4:3–98

Grayson, R., Argent, R., Nathan, R., McMahon, T. and Mein, R., (1996). Hydrological Recipes. Cooperative Research Centre for Catchment Hydrology, Melbourne Victoria

Greene, R., Devillers, R., Luther, J. E., & Eddy, B. G. (2011). GIS-based multiple-criteria decision analysis. Geography Compass, 5(6), 412–432.

Gregnanin A, Piccirillo AM (1974). Considerazioni sulle serie vulcaniche e sulla struttura dell'Altopiano Etiopico centrale. Mem Mus Tridentino Sci Nat 20:79–100

Gupta, H. V., S. Sorooshian, and P. O. Yapo. (1999). Status of automatic calibration for hydrologic models: Comparison with multilevel expert calibration. J. Hydrologic Eng. 4(2): 135-143.

Guntner A, Uhlenbrook S, Seibert J, Leibundgut C (1999). Multicriterial validation of TOPMODEL in a mountainous catchment. Hydrol Process 13(11):1603–1620

Hamilton, E. L., and P. B. Rowe, (1949). Rainfall interception by chaparral in California, Calif. Dept. Nat. Resources, Div. Forestry, and U.S. Forest Serv., Calif. Forest and Range Expt. Sta., 43 pp.

Hengl, T. et al. (2015). 'Mapping Soil Properties of Africa at 250 m Resolution: Random Forests Significantly Improve Current Predictions', PLOS ONE, 10(6), p. e0125814. doi: 10.1371/journal.pone.0125814.

Horton, R. E. (1945). Erosional development of streams and their drainage basins: Geol. Soc. America Bull., v. 56, pp. 275-370.

Hunegnaw A, Sage L, Gonnard R (1998). Hydrocarbon potential of the intracratonic Ogaden Basin, SE Ethiopia. J Petrol Geol 21:401–425

Hwang, C. L., & Yoon, K. (1981). Multiple attribute decision making: Methods and applications. Berlin: Springer.

Institute of Hydrology (1980). Low flow studies: Research Report 1. Institute of Hydrology. Wallingford, UK.

Jepson DH, Athearn MJ (1964). Land and water resources of the Blue Nile Basin. Appendix II Geology US Dept Interior, Addis Ababa, p 221

Kahsay, G.H., Gebreyohannes, T., Gebremedhin, M.A., Gebrekirstos, A., Birhane, E., Gebrewahid, H., Welegebriel, L., 2019. Spatial groundwater recharge estimation in Raya basin, Northern Ethiopia: an approach using GIS based water balance model. Sustain. Water Resour. Manag. 5, 961–975. https://doi.org/10.1007/s40899-018-0272-2

Kalyanapu AJ, Burian SJ, McPherson TN (2010). Effect of land usebased surface roughness on hydrologic model output. JOSH 9(2):51–71

Kazmin V (1973). Geological map of Ethiopia, scale 1:2,000,000. Geological Survey of Ethiopia, Addis Ababa

Kebede S. (2013). Groundwater in Ethiopia: Features, vital numbers and opportunities. Springer, Berlin. ISBN 978 3 642 30390 6.

Kebede, S., Hailu, A., Crane, E., Ó Dochartaigh, B.É and Bellwood-Howard, I. (2018). Africa Groundwater Atlas: Hydrogeology of Ethiopia. British Geological Survey. Accessed [September 1, 2020]. http://earthwise.bgs.ac.uk/index.php/Hydrogeology_of_Ethiopia

Keeney, R. L. (1992). Value-focused thinking: A path to creative decision making. Cambridge: Harvard University Press.

Kieffer B, Srndt N, Lapierre H, Bastien F, Bosh D, Pecher A, Yirgu G, Ayalew D, Weis D, Jerram DA, Keller F, Meugniot C (2004). Flood and shield basalts from Ethiopia: magmas from the African superswell. J Petrol 45:793–834

Landerer F.W. and S. C. Swenson (2012). Accuracy of scaled GRACE terrestrial water storage estimates. Water Resources Research, Vol 48, W04531, 11 PP, doi:10.1029/2011WR011453.

Lerner, D. N., Isaar, A. S. and Simmers, I. (eds.) (1990). Groundwater Recharge: A Guide to Understanding and Estimating Natural Recharge, International Contributions to Hydrogeology Vol. 8. Hanover: Verlag Heinz Heise.

Li, H., Zhang, Y., Chiew, F.H.S., Xu, S., (2009). Predicting runoff in ungauged catchments using Xinanjiang model with MODIS leaf area index. Journal of Hydrology 370 (1–4), 155–162.

Lim, K. J., Engel, B. A., Tang, A. et al. (2005). Automated WEB GIS based hydrograph analysis tool, WHAT. J. Amer. Water Resour. Assoc., 41, 10.

Ligmann-Zielinska, A. (2009). The impact of risk-taking attitudes on a land use pattern: an agent based model of residential development. Journal of Land Use Science, 4(4), 215–232.

Lyne, V., Hollick, M., (1979). Stochastic time variable rainfall runoff modeling. Hydrology and Water Resources Symposium Berth, 1979, Proceedings, National Committee on Hydrology and Water Resources of the Institution of Engineers, Australia, pp. 89–92.

MacDonald A M, Bonsor H C, Ó Dochartaigh B É and Taylor R G. (2012). Quantitative maps of groundwater resources in Africa. Environmental Research Letters, 7 (2), 024009. https://doi.org/10.1088/1748-9326/7/2/02400

Malczewski, J. (1999). GIS and multicriteria decision analysis. New York: Wiley.

Malczewski, J. (2006). GIS-based multicriteria decision analysis: A survey of the literature. International Journal of Geographical Information Science, 20(7), 703–726.

Massam, B. H. (1988). Multi-criteria decision making (MCDM) techniques in planning. Progress in Planning, 30(1), 1–84.

Meresa, E. and Taye, G. (2018). 'Estimation of groundwater recharge using GIS-based WetSpass model for Birki watershed, the eastern zone of Tigray, Northern Ethiopia', Sustainable Water Resources Management. doi: 10.1007/s40899-018-0282-0.

Merz R, Blo¨schl G, Parajka J (2006). Spatio-temporal variability of event runoff coefficients. J Hydrol 331(3):591–604

McSweeney C, New M, Lizcano G (2010). UNDP climate change profile: Ethiopia. http://countryprofiles.geog.ox.ac.uk

Mohr P (1983). Ethiopian flood basalt province. Nature 303:577–584

Mohr P (1962). The geology of Ethiopia. University College of Addis Ababa Press, Ethiopia, 268 pp

Morris, B L, Lawrence, A R L, Chilton, P J C, Adams, B, Calow R C and Klinck, B A. (2003). Groundwater and its Susceptibility to Degradation: A Global Assessment of the Problem and Options for Management. Early Warning and Assessment Report Series, RS. 03-3. United Nations Environment Programme, Nairobi, Kenya.

MoWR (Ministry of Water Resources) (1996). Integrated development of Omo-Ghibe river Basin master plan study, vol. XI (F1, F2, F3, Addis Ababa, Ethiopia)

MoWR (Ministry of Water Resources) (1997). Integrated development of Baro Akobo River Basin master plan study, vol. II (Annex 1B, Annex 1H, Annex 1J, Addis Ababa, Ethiopia)

MoWR (Ministry of Water Resources) (1998a). Integrated development ofAbbay River Basin master plan study, vol. III (part 2, Vol. VI: Part 1, Vol. VI: part 3, Addis Ababa, Ethiopia)

MoWR (Ministry of Water Resources) (1998b). Integrated development of Tekeze River Basin master plan study, vol. VIII (WR3, Vol. X: WR5, Vol. X: WR4, Addis Ababa, Ethiopia)

Nace, R. L. (1967). Are we running out of water? US Geological Survey Circular 536.

Nash, J. E., and J. V. Sutcliffe. (1970). River flow forecasting through conceptual models: Part 1. A discussion of principles. J. Hydrology 10(3): 282-290.

Nathan, R. J. and McMahon, T. A. (1990). Evaluation of automated techniques for base flow and recession analyses. Water Resour. Res., 26, 1465–1473.

NMA (1996). Climatic and agroclimatic resources of Ethiopia. National meteorological services agency of Ethiopia. Meteorol Res Rep Ser 1:1–137.

NURP US EPA (1983). Results of the Nationwide Urban Runoff Program. Vol 1-Final report. Water Planning Division, NTIS PB84-18552, Washington DC

Peoples Democratic Republic of Ethiopia (PDRE), (1989). Master plan for the development of surface water resources in the Awash Basin. Ethiopian Valleys Development Studies Authority. : Final Report, vol. 6. Halcrow.

Pedgley DE (1967). Air temperature at Dallol, Ethiopia. Meteorol Mag 96(1967):265–271

Pettyjohn, W. A. and Henning, R. (1979). Preliminary estimate of ground-water recharge rates, related streamflow, and water quality in Ohio. Ohio State University Water Resources Center Project Completion Report 552.

Pistocchi A, Bouraoui F, Bittelli M (2008). A simplified parameterization of the monthly topsoil water budget. Water Resour Res 44: W12440. doi:10.1029/2007WR006603

Prosser, I.P., Dietrich, W.E., Stevenson, J., (1995). Flow resistance and sediment transport by concentrated overland-flow in a grassland valley. Geomorphology 13(1–4), 71–86.

Rodier J, Ribstein P (1988). Estimation of floods in small Sahelian basins under 10 km2. In french: estimation des caracte´ristiques de la crue decennale pour les petits basins versants du Sahel couvrant de 1 a 10 km2. ORSTOM, Montpellier, p 108

Rossum, V.P., Batelaan, O., Ghebremeskel, S., and Smedt, D.F., (2001). Discharge Coefficients for the Kikbeek Sub-basin, a Brook Sub-basin at the Belgian Side of the River Border Meuse (Grensmaas), VUB Contribution to the Final Report of the IRMA-SPONGE Subproject 2: Development of Flood Management Strategies for Rhine and Meuse Basins in the Context of Integrated River Management. 58pp.

Russo A, Getaneh A, Atnafu B (1994). Sedimentary evolution of the Abbai River (Blue Nile) Basin, Ethiopia. N J B Geol Palaeo Mh 5:291–308

Rutledge, A. T. (1998). Computer programs for describing the recession of ground-water discharge and for estimating mean groundwater recharge and discharge from streamflow records: update. US Geological Survey WaterResources Investigations Report 98–4148.

Saaty, T. L. (1980). The analytic hierarchy process. New York: McGraw-Hill.

Saraf, A. K. et al. (2004). 'GIS based surface hydrological modelling in identification of groundwater recharge zones', International Journal of Remote Sensing, 25(24), pp. 5759–5770. doi: 10.1080/0143116042000274096.

Saxton KE, Rawls WJ (2006). Soil water characteristic estimates by texture and organic matter for hydrologic solutions. Soil Sci Soc Am J 70(5):1569–1578

Sazib, N., I. E. Mladenova, J.D. Bolten (2018). Leveraging the Google Earth Engine for Drought Assessment Using Global Soil Moisture Data. Remote Sensing, 10(8), p.1265. DOI 10.3390/rs10081265 Google Scholar

Scanlon, B. R., Healy, R. W. and Cook, P. G. (2002b). Choosing appropriate techniques for quantifying groundwater recharge. Hydrogeol. J., 10, 18–39.

Schilling JG (1973). Afar mantle plume: rare earth evidence. Nature 242:2–5

Selvam, S. et al. (2015). 'A GIS based identification of groundwater recharge potential zones using RS and IF technique: a case study in Ottapidaram taluk, Tuticorin district, Tamil Nadu', Environmental Earth Sciences, 73(7), pp. 3785–3799. doi: 10.1007/s12665-014-3664-0.

Senanayake, I. P. et al. (2016). 'An approach to delineate groundwater recharge potential sites in Ambalantota, Sri Lanka using GIS techniques', Geoscience Frontiers, 7(1), pp. 115–124. doi: 10.1016/j.gsf.2015.03.002.

Shiklomanov, I. A. and Rodda, J. C. (2003). World Water Resources at the Beginning of the Twenty-frst Century. Cambridge: Cambridge University Press.

Simmers, I. (ed.) (1997). Recharge of Phreatic Aquifers in (Semi-) Arid Areas. Rotterdam: A. A. Balkema.

Simmers, I. (1990). Aridity, groundwater recharge and water resources management. In Groundwater Recharge, A Guide to Understanding and Estimating Natural Recharge. International Contributions to Hydrogeology Vol. 8, ed. D. N. Lerner, A. S. Isaar and I. Simmers. Hanover: Verlag Heinz Heise, 3–22.

Simunek, J., Sejna, M., Saito, H., Sakai, M., and van Genuchten, M. T. (2008). The HYDRUS 1D software package for simulating the one-dimensional movement of water, heat, and multiple solutes in variability-saturated media, University of California Riverside, California, 281 pp., 2008.

Sloto, R.A., and Crouse, M.Y., (1996). HYSEP—A computer program for streamflow hydrograph separation and analysis: U.S. Geological Survey Water-Resources Investigations Report 96–4040, 46 p., http://pubs.er.usgs.gov/publication/wri964040

Smakhtin, V. U. (2001). Low flow hydrology: a review. J. Hydrol., 240, 147–186.

Stern RJ (1994). Neoproterozoic (900–550 Ma) arc assembly and continental collision in the East African Orogen. Ann Rev Earth Planet Sci 22:319–351

Sutanto SJ, Wenninger J, Coenders-Gerrits AMJ, Uhlenbrook S (2012). Partitioning of evaporation into transpiration, soil evaporation and interception: a comparison between isotope measurements and a HYDRUS-1D model. Hydrol Earth Syst Sc 16(8):2605–2616. doi:10.5194/hess-16-2605-2012

Swenson, S. C. and J. Wahr (2006). Post-processing removal of correlated errors in GRACE data, Geophys. Res. Lett., 33, L08402, doi:10.1029/2005GL025285.

Taddese Girma (2001). Land degradation: a challenge to Ethiopia. Environ Manage. 27:815–824.

Tibebu Kassawmar, Sandra Eckert, Kaspar Hurni, Gete Zeleke & Hans Hurni (2016). Reducing landscape heterogeneity for improved land use and land cover (LULC) classification across the large and complex Ethiopian highlands, Geocarto International, DOI: 10.1080/10106049.2016.1222637

Tilahun, K. and Merkel, B. J. (2009). 'Estimation of groundwater recharge using a GIS-based distributed water balance model in Dire Dawa, Ethiopia', Hydrogeology Journal, 17(6), pp. 1443–1457. doi: 10.1007/s10040-009-0455-x.

Thill, J. C. (Ed.). (1999). Multicriteria decision-making and analysis: A geographic information sciences approach. New York: Ashgate.

Turc L (1955). Le bilan de l'aue des sols. Relations entre les precipitations, l'evaporation et l'ecoulement, INRA, Paris

USDA-NRCS Soil Survey Division (1993). Soil survey manual. U.S. Department of Agriculture Handbook No. 18, U.S. Government Printing Office, Washington, DC, pp 437–1036

Wahl, K. L. and Wahl, T. L. (1988). Effects of regional ground water level declines on streamflow in the Oklahoma panhandle. In Proceedings of the Symposium on Water-Use Data for Water Resources Management, American Water Resources Association.

WAPCOS (1990). Preliminary water resources development master plan for Ethiopia. Ministry of Water Resoruces, Addis Ababa.

Wang, Y. et al. (2012). 'Monthly spatial distributed water resources assessment: a case study', Computers & Geosciences, 45, pp. 319–330. doi: 10.1016/j.cageo.2011.11.028.

Ward and Robinson, (1990). R.C. Ward, M. RobinsonPrinciples of Hydrology. McGraw-Hill, New York (1990)

Wolela A (2008). Sedimentation of the Triassic–Jurassic Adigrat sandstone formation, BlueNile (Abbai) basin, Ethiopia. J Afr Earth Sci 52:30–42

Wood, W. W. and Sanford, W. E. (1995). Chemical and isotopic methods for quantifying ground-water recharge in a regional, semiarid environment. Ground Water, 33, 458–468.

Woody Biomass Study Project (WBSP), (2000). A strategic plan for the sustainable development, construction, and management of the woody biomass resources in Oromiya Regional state. GIS and Remote Sensing (September 2000, Addis Ababa, Ethiopia).

Woody Biomass Study Project (WBSP), (2002). A strategic plan for the sustainable development, construction, and management of the woody biomass resources in Amhara regional state. GIS and Remote Sensing (June 2002, Addis Ababa, Ethiopia).

White RS, McKenzie DP (1989). Magmatism at rift zones: the generation of a continental margins and flood basalts. J Geoph Res 94:7685–7729

Yeh, H.-F. et al. (2009). 'GIS for the assessment of the groundwater recharge potential zone', Environmental Geology, 58(1), pp. 185–195. doi: 10.1007/s00254-008-1504-9.

Yenehun, A., Walraevens, K. and Batelaan, O. (2017). 'Spatial and temporal variability of groundwater recharge in Geba basin, Northern Ethiopia', Journal of African Earth Sciences, 134, pp. 198–212. doi: 10.1016/j.jafrearsci.2017.06.006.

Yimam, A. Y., Bekele, A. M., Nakawuka, P., Schmitter, P., Tilahun, S. A., (2019). 'Rainfall-Runoff Process and Groundwater Recharge in the Upper Blue Nile Basin: The Case of Dangishta Watershed', p. 14.

Zanettin B, Justin-Visentin E (1973). Serie di vulcaniti etiopiche: 1—La serie dell'altopiano etiopico centro-orientale. Boll Soc Geol It 92:313–327

Zarghami, M., & Szidarovszky, F. (2011). Multicriteria analysis applications to water and environment management. Berlin/Heidelberg: Springer.

Zhang X, Lindstrom G (1997). Development of an automatic calibration scheme for the HBV hydrological model. Hydrol Process 11(12):1671–1682

Zhang, Y. et al. (2017). 'WetSpass-Based Study of the Effects of Urbanization on the Water Balance Components at Regional and Quadrat Scales in Beijing, China', Water, 10(1), p. 5. doi: 10.3390/w10010005.